Cellular studies on the role of OGFOD1, a 2-oxoglutarate-dependent dioxygenase

Martin Attwood

St. Edmund Hall

University of Oxford

A thesis submitted for the degree of Doctor of Philosophy

Trinity Term 2017



Supervised by

Professor Sir Peter Ratcliffe

Dr. Matthew Cockman

Abstract

Cellular studies on the role of OGFOD1, a 2-oxoglutarate-dependent dioxygenase

Martin Attwood, St. Edmund Hall
Submitted for the degree of Doctor of Philosophy
Trinity Term 2017

2-Oxoglutarate (2-*OG*) and iron (Fe^{2+}) dependent *O*xygenase *D*omain containing protein *1* (OGFOD1) is an evolutionarily conserved prolyl hydroxylase enzyme in mammals, invertebrates (Sud1 in *D. melanogaster*) and yeast (TPA1 in *S. cerevisiae* and Ofd1 in *S. pombe*). This enzyme modifies a residue corresponding to Proline-62 in humans of the small ribosome protein S23 (RPS23) that occupies a critical site within the decoding centre of the eukaryotic ribosome. A number of cellular phenotypes have been reported following OGFOD1 inactivation, including altered ribosome decoding, activation of translational stress pathways and reduced proliferation. In addition, studies in *S. pombe* have assigned a novel signalling function for Ofd1 in the regulation of sterol response genes via the Sre1 transcription factor. Collectively, these studies indicated functions for OGFOD1 in both translation and transcription. However, it was not known whether these functions are conserved in mammalian cells or if they are linked.

To inform on OGFOD1-dependent cellular phenotypes, OGFOD1 defective cells were generated by genome editing using the CRISPR methodology. Clones re-expressing the OGFOD1 transgene under the control of a doxycycline regulable promoter were subsequently derived, facilitating comparison of OGFOD1 status within an isogenic setting. These cells were validated by the generation and use of antibodies specific to the modification site (Pro-62) in RPS23. Surprisingly, genetic inactivation of OGFOD1 did not mimic the reported phenotypes observed by RNA interference.

To improve understanding of OGFOD1 function, immunoprecipitations of ectopic and endogenous OGFOD1-containing protein complexes were analysed by proteomic methods. The transcriptional regulator, *Th*anatos *a*ssociated *p*rotein 11 (THAP11) was identified as a novel high stoichiometry OGFOD1-interacting protein across a range of cell lines. Analysis of the THAP11 transcriptional programme in SW620 cells defined a repressive action of OGFOD1 overexpression on THAP11 DNA binding and target gene expression. Reciprocal regulation of THAP11 signalling was not associated with OGFOD1 knockdown or genetic inactivation suggesting that THAP11 is not limiting in the steady state. Protein interaction studies revealed a direct association between the two proteins that was mediated by a region of THAP11 that shares sequence homology to the Ofd1-binding domain of Sre1. This, together with the observation that THAP11 forms a discrete association with the translational machinery, raises the interesting possibility that OGFOD1 performs an analogous regulatory function in mammalian cells to that described in *S. pombe*. These results provide a focus for future work dissecting the interrelationship between OGFOD1-dependent effects on transcription and translation.

Table of Contents

CHAPTER 1: INTRODUCTION 1

1.1 The 2-OG oxygenase superfamily 1
1.1.1 Overview 1
1.1.2 Catalytic mechanism of the 2-OG oxygenases 2
1.1.3 2-OG oxygenases catalyse hydroxylation and demethylation reactions in a range of substrates 3
1.1.4 2-OG oxygenases in oxygen sensing 6
1.2 Translational oxygenases 8
1.2.1 Ribosomal oxygenases (ROXs) 8
1.2.2 Translation factor hydroxylases 9
1.2.3 tRNA hydroxylases 10
1.3 2-Oxoglutarate and Fe^{2+} dependent Oxygenase Domain containing protein 1 (OGFOD1) 10
1.3.1 OGFOD1 is a prolyl hydroxylase enzyme targeting RPS23 11
1.3.2 OGFOD1 modulates protein translation and cellular growth 12
1.3.2.1 Modulation of translation fidelity 12
1.3.2.2 Regulation of translational stress phenotypes and cellular growth 14
1.3.3 An OGFOD1 homolog, Ofd1, functions outside of RPS23 hydroxylation 17
1.4 Hydroxylation as a signalling mechanism 20
1.5 Aims of this thesis 22

CHAPTER 2: PHENOTYPIC ANALYSIS OF OGFOD1 CRISPR-DERIVED KNOCKOUT CELLS 23

2.1 Introduction and aims of the chapter 23
2.2 Results 25
2.2.1 Cellular proliferation of OGFOD1 knockout cells 25
2.2.2 Regulation of eIF2α phosphorylation and G3BP1 stress granules in OGFOD1 knockout cells 27
2.2.3 Regulation of the DNA damage response in OGFOD1 knockout cells 32
2.3 Discussion 42

CHAPTER 3: CHARACTERISATION OF ACUTE OGFOD1 INTERVENTIONS 45

3.1 Introduction and aims of the chapter 45
3.2 Results 46
3.2.1 Generation of RPS23 hydroxylation specific antibodies 46
3.2.2 Characterisation of acute OGFOD1 suppression using an shRNA knockdown system. 48
3.2.3 Characterisation of acute OGFOD1 overexpression using the Tetracycline-Regulated expression (T-REx) system. 51
3.2.4 Characterisation of inducible OGFOD1 re-expression in OGFOD1 knockout cells. 53
3.2.5 Characterisation of inducible OGFOD1 re-expression under conditions of serum deprivation. 58
3.2.6 Characterisation of inducible OGFOD1 re-expression under conditions of glutamine deprivation. 63
3.2.7 Characterisation of inducible OGFOD1 re-expression under ischemia mimetic conditions. 66
3.3 Discussion 69

CHAPTER 4: INVESTIGATING THE EFFECT OF A DISEASE MUTATION ON RPS23 HYDROXYLATION 72

4.1 Introduction and aims of the chapter 72
4.2 Results 73
4.2.1 Characterisation of the R67K-RPS23 mutation. 73
4.2.2 R67K-RPS23 mutation affects RPS23 incorporation into the ribosome and native RPS23 hydroxylation. 77
4.3 Discussion 82

CHAPTER 5: PROTEOMIC SCREENS USING FLAG-OGFOD1 AND ENDOGENOUS OGFOD1 PULL DOWNS 85

5.1 Introduction and aims of the chapter 85
5.2 Results 86
5.2.1 Characterisation of the FLAG-OGFOD1 interactome 86
5.2.2 Characterisation of the endogenous OGFOD1 interactome 94
5.2.3 Identification of common OGFOD1 interacting proteins 100
5.2.4 Validation of THAP11 as a novel OGFOD1 interacting partner 101
5.2.5 Mapping the OGFOD1 binding domain in THAP11 103
5.2.6 The subcellular localisation of OGFOD1 and THAP11 105
5.3 Discussion 109

CHAPTER 6: CHARACTERISATION OF THAP11 CELLULAR COMPLEXES 112

6.1 Introduction and aims of the chapter 112
6.2 Results 113
6.2.1 The effect of OGFOD1 on THAP11 and RPS23 protein levels 113
6.2.2 The effect of OGFOD1 on the subcellular localisation of THAP11 and RPS23 116
6.2.3 The effect of OGFOD1 loss on the THAP11 interactome 120
6.2.4 The effect of OGFOD1 on THAP11 and RPS23 complexes 127
6.2.5 Investigating the role of THAP11 in translational control 133
6.3 Discussion 135

CHAPTER 7: INVESTIGATING A REGULATORY ROLE FOR OGFOD1 ON THE THAP11 TRANSCRIPTIONAL PROGRAMME 137

7.1 Introduction and aims of the chapter 137
7.2 Results 139
7.2.1 OGFOD1 does not associate with the THAP11 transcriptional co-activator HCF-1 139
7.2.2 Does OGFOD1 modulate the THAP11 transcriptional program in SW620 colon cancer cells? 140
7.2.3 Does OGFOD1 modulate the THAP11 transcriptional program in mouse embryonic stem (ES) cells? 155
7.3 Discussion 166

CHAPTER 8: FINAL DISCUSSION 169

8.1 Overview 169
8.2 Cellular phenotypes associated with genetic interventions on OGFOD1 171
8.3 Identification of novel OGFOD1 binding proteins by mass spectrometry 173
8.4 The transcriptional interaction between OGFOD1 and THAP11 175

CHAPTER 9: MATERIALS AND METHODS 179

9.1 Reagents and Solutions 179
9.2 Plasmids 180
9.3 Bacterial techniques 182
9.3.1 Transformation 182
9.3.2 Plasmid DNA purification 182
9.4 Nucleic acid techniques 182
9.4.1 Restriction enzyme digestion 182
9.4.2 Ligation 182
9.4.3 DNA sequencing 183
9.4.4 Agarose gel electrophoresis 183
9.4.5 Genomic DNA extraction 183
9.4.6 Polymerase chain reaction (PCR) 184
9.4.7 SURVEYOR mutation detection assay 184
9.4.8 RNA extraction using TRIzol 185

9.4.9 RNA extraction for microarray using mirVana isolation kit 185
9.4.10 Reverse transcription 186
9.4.11 Quantitative polymerase chain reaction (qPCR) 186
9.4.12 Chromatin immunoprecipitation (ChIP)- qPCR 187
9.4.13 Microarray 189
9.5 Tissue culture techniques 190
9.5.1 Cell lines 190
9.5.2 Plasmid transfection 192
9.5.3 Generation of OGFOD1 CRISPR-Cas9 knockout cells 192
9.5.4 Lentiviral production and creation of stable cell lines 193
9.5.5 siRNA transfection 194
9.5.6 Exposure of cells to test stimuli 195
9.5.7 Preparation of cell lysate 195
9.5.8 Cell proliferation assays 196
9.5.9 Colony survival assays 197
9.5.10 Immunofluorescence 197
9.5.11 Proximity ligation assays (PLA) 198
9.5.12 Microscopy 199
9.5.13 Polysome profile analysis 199
9.6 Protein techniques 200
9.6.1 Production of custom antibodies used in this study 200
9.6.2 Immunoblotting 201
9.6.3 Rate zonal centrifugation of protein complexes in sucrose gradients 202
9.6.4 Methanol chloroform precipitation of proteins 203
9.7 Proteomic techniques 203
9.7.1 Immunoprecipitation 203
9.7.2 In-solution tryptic digestion 204
9.7.3 Purification of ribosomal proteins 205
9.7.4 In-gel tryptic digestion 206
9.7.5 LC-MS/MS 207

APPENDIX 1: VALIDATION OF OGFOD1 CRISPR GUIDE SEQUENCES BY SURVEYOR MUTATION DETECTION ASSAY 209

APPENDIX 2: ABBREVIATIONS 210

APPENDIX 3: PUBLISHED MATERIAL 213

BIBLIOGRAPHY 214

ACKNOWLEDGEMENTS 226

Word count: 46,342

Chapter 1: Introduction

1.1 The 2-OG oxygenase superfamily

1.1.1 Overview

Cells constantly rely on the integration of external and internal signals to promote cellular growth and survival (Choudhary and Mann., 2010). To understand how cells promote these intricate molecular processes, an in-depth characterisation of the cellular components and their signalling events is required. Post-translational modifications of proteins represent an important mechanism in regulating the biological activity and function of a protein. The most ubiquitous and well-studied post-translational modifications include: phosphorylation, glycosylation, acetylation, and ubiquitination (Minguez et al., 2012). These modifications have the capacity to induce changes in a protein structure, subcellular localisation or modulate protein-protein interactions (Breker et al., 2014). Moreover, these modifications can be dynamic in nature and can alter their activities transiently to co-ordinate a complex signalling system. The characterisation of enzymes that mediate such modifications is important in understanding how the protein substrate functions and how it may be dysregulated in human disease.

Over 50 years ago, Hutton et al. reported that hydroxylation of a prolyl residue in collagen was catalysed by an enzyme termed the collagen prolyl hydroxylase, and required the presence of molecular oxygen, ferrous iron, and the Kreb's cycle intermediate 2-oxoglutarate (2-OG) (Hutton et al., 1967). Collagens consist of three polypeptide chains that each contain a repeat of the sequence Gly-Pro(X)-Pro(Y) that fold into a characteristic coiled triple helix (Myllyharju et al., 2004). The glycine residue is required for packing of the coiled

structure and the presence of 4-hydoxyproline (Y) plays an important function in maintaining its stability. Since this discovery, a large group of approximately 60 enzymes have been identified that comprise the evolutionarily conserved 2-OG oxygenase family, indicating that hydroxylation may exist as an important and widespread modification (Loenarz and Schofield, 2008).

1.1.2 Catalytic mechanism of the 2-OG oxygenases

The 2-OG oxygenases utilise 2-OG as a co-substrate and iron as a co-factor to couple substrate oxidation with the decarboxylation of 2-OG in a reaction that produces succinate and carbon dioxide (Loenarz and Schofield, 2008). Resolved crystal structures indicate that the 2-OG oxygenases share a conserved double-stranded β-helix (DSBH) fold that consists of two four-stranded β sheets that support the coordination of iron and 2-OG (Clifton et al., 2006; Aik et al., 2012). The 2-OG oxygenase reactions catalyse hydroxylation of C-H bonds or N-methyl group demethylation via hydroxylation (Loenarz and Schofield, 2011). In this catalytic reaction (Figure 1.1), 2-OG binds the oxygenase (1) enabling the substrate to bind (2), water is displaced enabling oxygen to bind (3) and decarboxylation of 2-OG results in the formation of a reactive Fe(IV)=O ferryl species, CO_2 and succinate (4). From molecular oxygen, one atom is transferred to succinate and the reactive Fe(IV)=O ferryl species oxidises the substrate, which is then released to complete the cycle (5).

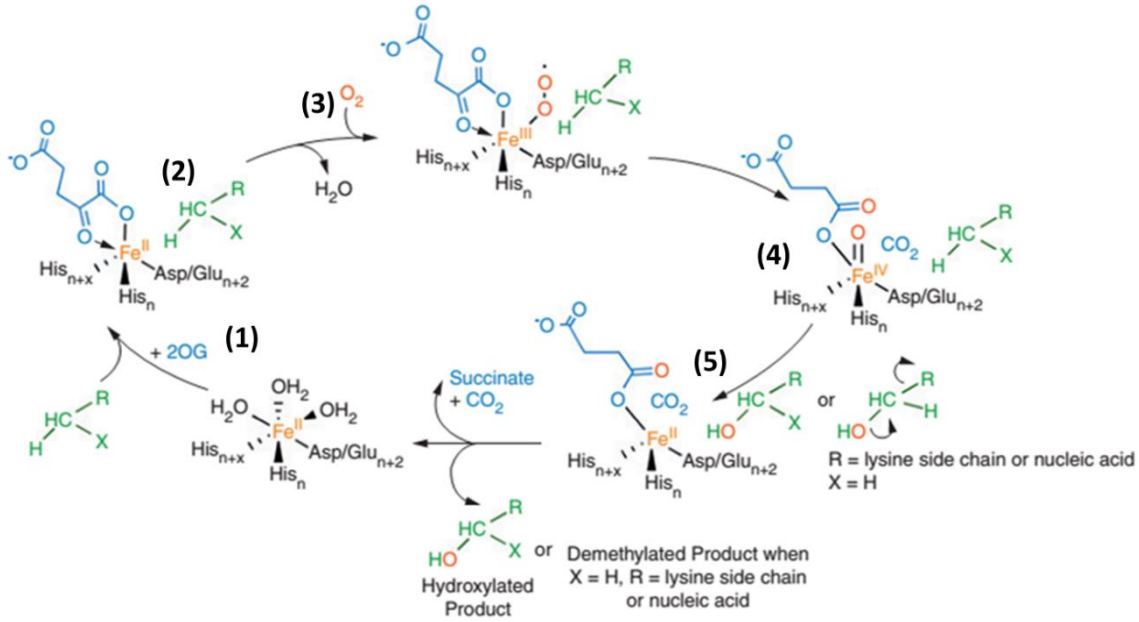


Figure 1.1: Outline of the catalytic mechanism for the 2-OG oxygenases. 2-OG binds the oxygenase (1) enabling the substrate to bind (2). Water is then displaced enabling oxygen to bind (3) and subsequent oxidative decarboxylation of 2-OG and the formation of a reactive Fe(IV)=O ferryl species (4). The Fe(IV)=O ferryl species then oxidises the substrate resulting in either a hydroxylated or demethylated product which is then released (5). Figure adapted from Aik et al., 2012.

1.1.3 2-OG oxygenases catalyse hydroxylation and demethylation reactions in a range of substrates

Biochemical studies on mammalian 2-OG oxygenases reveal broad substrate selectivity with 2-OG oxygenase-catalysed hydroxylations and associated demethylation detected on a variety of biological substrates including: small molecules, lipids, proteins and nucleic acids (Loenarz et al., 2011). The Jumonji-C (JmjC) histone lysine demethylases (KDM's) represent the largest subfamily within the 2-OG oxygenases with around 20 enzymes (Johannson et al., 2014). N-methylation of lysyl residues within the histone H3 tail is associated with regions of transcriptionally active (H3K4, H3K36 and H3K79) or transcriptionally silenced (H3K9, H3K27 and H4K20) chromatin (Klose et al., 2016). Genome-wide studies indicated that whilst demethylases may bind to a large number of genes, their inactivation results in

only a modest effect on the transcriptional output of a subset of genes, suggesting a broad regulatory function in fine-tuning the transcriptional response (Koonistra et al., 2012).

The AlkB protein in *E. coli* was originally identified as a DNA repair enzyme that could reverse 1-methyladenine (1mA) and 3-methylcytosine (3mC) DNA lesions via oxidative demethylation (Falnes et al., 2002; Trewick et al., 2002). The AlkB protein was identified as a member of the 2-OG oxygenase family and 8 AlkB mammalian homologs have been identified (ALKBH1-8) (Sedgwick et al., 2007). However, only ALKBH2 and ALKBH3 have been identified that possess demethylation activity for DNA.

These studies and numerous others (reviewed in Ploumakis et al., 2015), illustrate the biochemical and functional diversity of the 2-OG oxygenases which, via hydroxylation, have been implicated in distinct biological processes from transcriptional control, the DNA damage response to the control of protein stability. Given their requirement for molecular oxygen and 2-OG, the 2-OG oxygenases provide potential regulatory interfaces between oxygen, metabolism and gene expression that have yet to be fully explored. An overview of the 2-OG oxygenase family and their targets are summarised in Figure 1.2. Work relating to the regulation of the hypoxia inducible factor (HIF) transcription factors represented a major breakthrough in the field of the 2-OG oxygenases and their role in human physiology. An overview of the HIF system and related hydroxylases will be discussed in the following section. In addition to this, and of relevance to this thesis, I will provide an in-depth review of a functionally-related sub-class of 2-OG oxygenases that target the protein synthesis machinery.

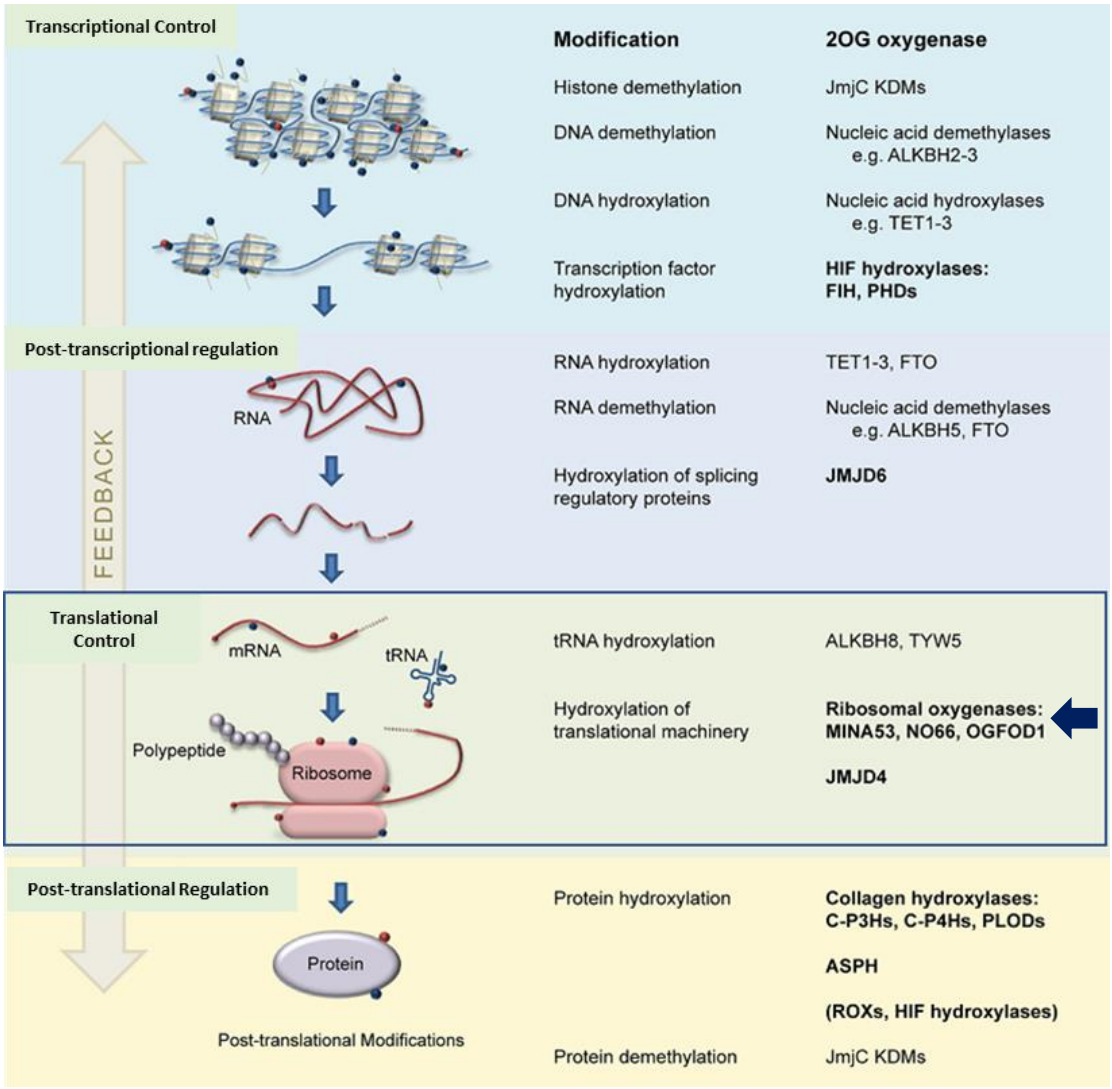


Figure 1.2: Diverse substrates are targeted by the 2-OG oxygenase family. The 2-OG oxygenases catalyse hydroxylation and demethylation reactions, and have the potential to modify a number of biomolecules including histones, DNA, RNA, transcription factors, splicing factors and proteins. The understanding of this diverse enzyme group is constantly evolving and work has highlighted the importance of these modifications in regulating transcriptional, post-transcriptional, translational and post-translational processes in normal physiology and disease. 2-OG oxygenases that target the translational machinery are highlighted by the box, and ribsosomal oxygenases (that include OGFOD1) are highlighted by the blue arrow. Figure adapted from Markolovic et al., 2015.

1.1.4 2-OG oxygenases in oxygen sensing

Hydroxylation of Hypoxia Inducible Factor (HIF) represents a key milestone in understanding the importance of this modification and its potential regulatory function (Jaakkola et al., 2001; Ivan et al., 2001). HIF is a heterodimeric basic-Helix-Loop-Helix Per/ARNT/Sim (bHLH-PAS) transcription factor composed of an α subunit (HIF-1α, 2α, or 3α) and a β subunit (Wang et al., 1995; Wang and Semenza, 1995; Tian et al., 1997; Gu et al., 1998). The β subunit is constitutively expressed, whilst the α subunits are subject to prolyl and asparaginyl hydroxylation that regulate expression and transcriptional activity (for review see Bishop and Ratcliffe., 2014).

HIF prolyl hydroxylation is catalysed by three related prolyl hydroxylase enzymes PHD (prolyl hydroxylase domain) 1-3 (Bruick and McKnight., 2001; Epstein et al., 2001). Evolutionary analysis has identified a functional HIF system in the simplest animal, *Trichoplax adhaerens* (Loenarz et al., 2011). In higher animals, two sites of prolyl hydroxylation have been identified (equivalent to Pro-402 and Pro-564 in HIF 1α) within an *N*-terminal transactivation domain (NAD). These hydroxyproline residues are specifically recognised by the von Hippel-Lindau protein (pVHL), the substrate recognition component of an E3 ubiquitin ligase (Maxwell et al., 1999; Masson et al., 2001). Consequently, HIF-α is polyubiquitinated and subjected to proteasomal degradation. Whilst the two sites can function independently to mediate pVHL recognition, sequential hydroxylation enhances HIF-α degradation (Chan et al., 2005). Suppression of PHD activity by hypoxia or in cells lacking a functional pVHL allows for the stabilisation of HIF-α which translocates to the nucleus to form a transcriptionally active complex with HIF-1β. An additional mechanism of HIF regulation occurs through asparaginyl hydroxylation (at Asp-803 in HIF1α) by factor inhibiting HIF (FIH), which prevents binding of the transcriptional co-activator p300/CBP to the *C*-terminal transactivation domain (CAD) (Mahon et al., 2001; Lando et al., 2002). FIH activity is less sensitive to

hypoxia than the PHD's, suggesting that subsequent inhibition of PHD and FIH activity under severe hypoxia allows for a graded response at the transcriptional level (Stolze et al., 2004; Tian et al., 2011). These findings indicate that other enzymes in the 2-OG oxygenase family may have similar regulatory functions. A summary of the HIF signalling system in response to hypoxia is highlighted in Figure 1.3.

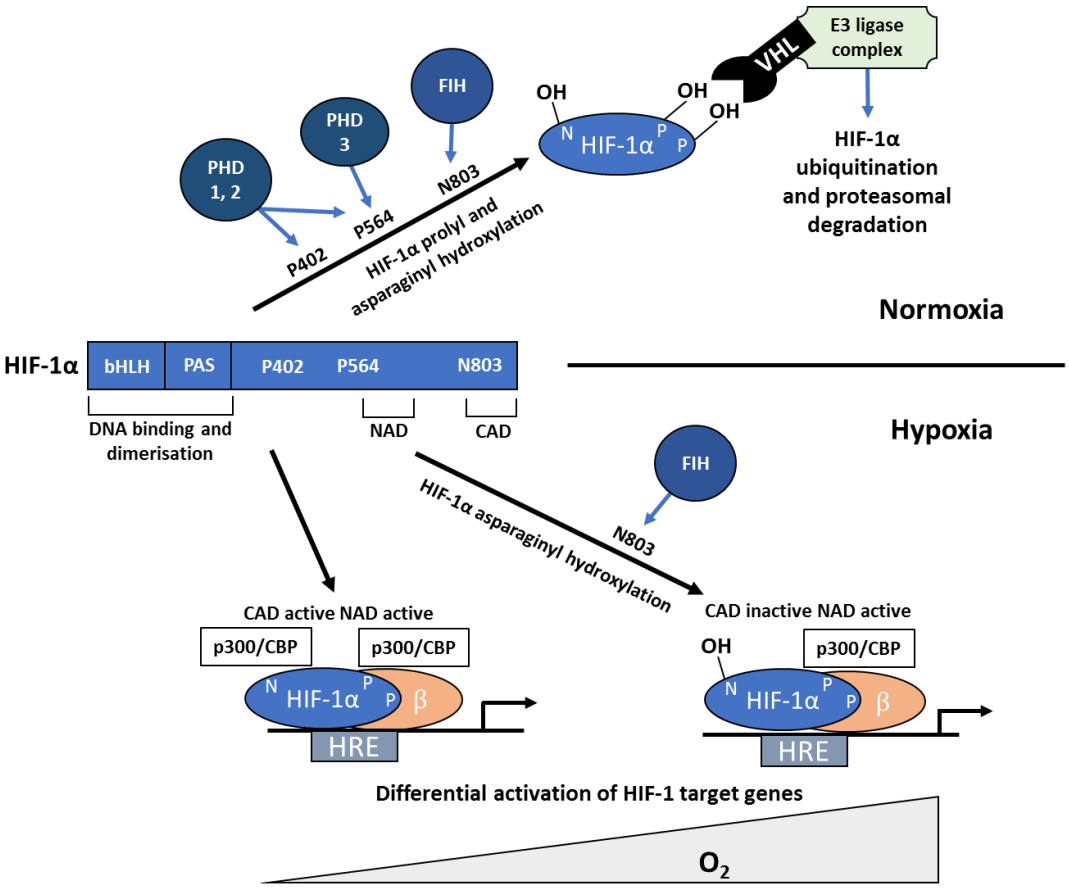


Figure 1.3: Regulation of HIF-1 by oxygen dependent prolyl and asparaginyl hydroxylation of HIF-1α. In normoxia, HIF-α is modified by prolyl hydroxylase enzymes PHD (prolyl hydroxylase domain) 1-3 which target HIF for proteasomal degradation by von Hippel-Lindau (pVHL), a component of the ubiquitin E3 ligase complex. Asparginyl hydroxylation (FIH) also prevents association with the transcriptional co-activators p300/CBP. Under limiting oxygen tensions, prolyl hydroxylation is limited and HIF is stabilised and can form a transcriptionally active complex with HIF-1β that binds to hypoxic response elements (HRE). FIH is suppressed under severe hypoxia and contributes to a fully activated transcriptional complex. Figure adapted from Masson and Ratcliffe., 2014.

1.2 Translational oxygenases

More recent studies have indicated that the protein synthesis machinery is also a major target for the 2-OG oxygenases via modifications to tRNA (ALKBH8; (Songe-Moller et al., 2010), TYW5; (Noma et al., 2010)), translation factors (JMJD4; (Feng et al., 2014)) and of relevance to this thesis, ribosomal proteins (MINA53 and NO66; (Ge et al., 2012), OGFOD1; (Singleton et al., 2014)).

1.2.1 Ribosomal oxygenases (ROXs)

MYC-induced nuclear antigen (MINA53) and its related homolog nucleolar protein 66 (NO66) were the first human 2-OG oxygenases to be assigned as ribosomal protein hydroxylases; termed the ribosomal oxygenases (ROXs) (Ge et al., 2012). MINA53 and NO66 share 36% amino acid sequence homology indicating that the proteins are evolutionary related (Eilbracht et al., 2004). MINA53 and NO66 catalyse histidinyl hydroxylation of 60S large subunit proteins RPL27a and RPL8, respectively (Ge et al., 2012). MINA53 catalyses hydroxylation at the carbon-3 position of histidinyl-39 in RPL27a and analysis from a range of mouse tissues and cell lines indicated that this modification is widespread and abundant. Similarly, RPL8 hydroxylation at the carbon-3 position of histidinyl-216, catalysed by NO66, was abundant in a range of tested cell lines. The target histidinyl residues project into the ribosome core and histidinyl-216 in RPL8 is positioned adjacent to the peptidyl transferase centre, indicating that hydroxylation could play a role in translational regulation. MINA53 and NO66 contain a conserved JmjC domain and were originally identified as histone demethylases targeting methylated lysine residues in histone H3 (Lu et al., 2009; Sinha et al., 2010). However, biochemical assignment supports their role as ribosomal hydroxylases (Ge et al., 2012; Chowdhury et al., 2014). The subcellular localisation of MINA53 and NO66

in the nucleolus supports a potential role in ribosomal biogenesis (Suzuki et al., 2007; Ge et al., 2012).

Reduced expression of MINA53 and NO66 is associated with suppression of cellular proliferation, however, the mechanism has not been linked to direct effects on translation or catalytic activity (Tsuneoka et al., 2002; Sinha et al., 2010; Ge et al., 2012). MINA53 and NO66 are orthologs of ycfD in *E. coli* and show considerable structural conservation (Chowdhury et al., 2014). YcfD catalyses arginine hydroxylation in the ribosomal protein RPL16 and interestingly a reduction in cell growth was observed under conditions of low nutrients, suggesting an important regulatory function under conditions of cellular stress (Ge et al., 2012). This finding is also of relevance to studies on OGFOD1, as highlighted in Section 1.3.2.2.

1.2.2 Translation factor hydroxylases

A more recent study has indicated that a translation termination factor, the eukaryotic release factor 1 (eRF1), is also a target for the 2-OG oxygenase family (Feng et al., 2014). eRF1 initiates translation termination when a stop codon in positioned in the ribosomal A-site (aminoacyl tRNA binding site) and stimulates peptidyl-tRNA hydrolysis at the ribosomal P-site (peptidyl tRNA binding site) to release the mature polypeptide (Song et al., 2000). JMJD4 has been reported to catalyse hydroxylation at the carbon-4 position of lysine 63 in eRF1. Analysis of several mouse tissues indicated that eRF1 hydroxylation is a widespread and abundant modification (Feng et al., 2014). Lysine 63 is embedded within a NIKS motif that was previously implicated in stop codon recognition (Chavatte et al., 2002). Inhibition of JMJD4 activity prevents eRF1 hydroxylation and promotes stop codon readthrough, indicating that this modification is required for optimal translation termination efficiency (Feng et al., 2014).

1.2.3 tRNA hydroxylases

In addition to the DNA demethylation reactions catalysed by the ALKBH proteins, ALKBH8 has recently been identified as a methyltransferase that was found to act on tRNA (Songe Moller et al., 2010; Fu et al., 2010). Unlike other AlkB homologs, ALKBH8 possesses additional annotated protein domains, including an RNA recognition motif and a methyl transferase domain which acts to catalyse methylation of 5-carbonylmethyluridine (cm^5U) at the wobble uridine position within the anti-codon loop of tRNA (glycine codon, UCC) (Songe Moller et al., 2010). Modifications of tRNA, including methylation, have been reported to facilitate folding of the tRNA molecule and help maintain structural stability (Helm et al., 2006).

Hydroxylation of the 5-methoxycarbonylmethyluridine (mcm^5U) into 5-methoxycarbonylhydroxymethyluridine ($mchm^5U$) is catalysed by ALKBH8, however, the direct effect on translation efficiency is yet to be determined (Fu et al., 2010; van den Born et al., 2011).

The JmjC protein, TYW5, catalyses hydroxylation of tRNA (Noma et al., 2010). Wybutosine (yW) is a modified guanosine found in phenylalanine tRNA that is hydroxylated by TYW5 to hydroxywybutosine (OHyW). Whilst yW has been implicated in maintaining the reading frame at phenylalanine codons, the effect from the OHyW modification remains unclear (Waas et al., 2007; Noma et al., 2010).

1.3 2-*O*xog*l*utarate and *F*e^{2+} dependent *O*xygenase *D*omain containing protein *1* (OGFOD1)

The aims of this thesis are to investigate the cellular processes and biochemical pathways that are regulated by OGFOD1, a protein hydroxylase that exists within the ribosomal oxygenase (ROX) subfamily.

1.3.1 OGFOD1 is a prolyl hydroxylase enzyme targeting RPS23

A collaborative effort between the Ratcliffe, Schofield and Wappner laboratories led to the identification of the small 40S ribosomal subunit protein RPS23 as an evolutionarily conserved substrate of OGFOD1 and its homologs Sudestada1 *(Drosophila melanogaster*), TPA1 (*Saccharomyces cerevisiae*) and Ofd1 *(Schizosaccharomyces pombe)* (Singleton et al, 2014; Katz et al., 2014; Loenarz et al., 2014).

Similar to the hydroxylation of RPL27a and RPL8, catalysed by MINA53 and NO66 respectively, RPS23 hydroxylation was observed across all model organisms studied and in a range of cell lines and mouse tissues (Singleton et al., 2014; Katz et al., 2014; Loenarz et al., 2014). The hydroxylation site, corresponding to Proline-62 in human RPS23, forms the apex of a conserved loop that projects into the decoding centre of the ribosome. RPS23 occupies the codon-anticodon interface that functions to maintain translational fidelity by ensuring complementarity between mRNA codons and the aminoacyl-tRNAs (Stark et al., 2002; Khatter et al., 2015).

OGFOD1 catalyses hydroxylation of Proline-62 at the carbon-3 position in RPS23 in *Drosophila melanogaster* and in mammalian cells (Singleton et al., 2014; Katz et al., 2014). By contrast, yeast homologs were shown to catalyse dihydroxylation of RPS23 at Proline-62, modifying the carbon-3 and carbon-4 position, although the biological relevance of this additional oxidation is not fully understood (Loenarz et al., 2014). Phylogenetic analysis has identified OGFOD1 homologs as far back as the unicellular organism *Naegleria gruberi*, which belongs to excavata group within the eukaryote domain (Scotti et al., 2014). The data indicate that OGFOD1 is an evolutionarily conserved enzyme and implies a functionally important role in some of the simplest forms of eukaryotes.

The crystal structure of OGFOD1 has been determined, indicating two distinct domains - an *N*-terminal domain (24-238) containing the iron binding catalytic site and a non-catalytic *C*-

terminal domain (270-542) that is separated by a linker region (239-269) (Horita et al., 2015). The *N*-terminal domain (NTD) of OGFOD1 and TPA1 are well conserved and the *C*-terminal domain (CTD) helices that support the major β sheet are conserved. Studies on TPA1 have indicated that it can form a homodimer in solution and a dimerization interface was proposed between two *C*-terminal domains (Kim et al., 2009; Henri et al., 2010). In contrast to TPA1, the linker region in OGFOD1 is shorter and the dimerization interface is not observed (Horita et al., 2015). Sequence comparisons have indicated that similar to OGFOD1, Ofd1 contains a shorter NTD to CTD linker region and therefore, OGFOD1 and Ofd1 are more similar with respect to this region.

1.3.2 OGFOD1 modulates protein translation and cellular growth

1.3.2.1 Modulation of translation fidelity

Studies on RPS12, the bacterial homolog of RPS23, have highlighted the importance of this protein in maintaining the accuracy of decoding within the ribosome (Sharma et al., 2007). Initial characterisation of RPS12 in *E. coli* demonstrated that strains with a deletion of RPS12 were not viable, indicating that the protein is essential for growth.

A new naming system for ribosomal proteins has been introduced to eliminate the confusion caused by use of identical names for ribosomal proteins from different species that are unrelated (Ban et al., 2014). In this system, ribosomal proteins found in ribosomes from all three domains (bacteria, yeast and humans) are given the prefix 'u' (for universal), which is followed by their *E. coli* names. Sequence alignment of universal S12 (uS12) (equivalent to human RPS23) from bacteria, archaea, mammals and plants indicate two regions of high conservation (Figure 1.4). These regions, termed 'PNSA' and 'PGVR' (62-65 and 116-119 in human RPS23) are located near the decoding centre. The PNSA loop

encompasses the Proline-62 hydroxylation site (proline-44 in *E. coli,* indicated by the red arrow). Mutational analysis by alanine substitution of this site resulted in a lethal growth phenotype, indicating the importance of this residue within the conserved region (Sharma et al., 2007).

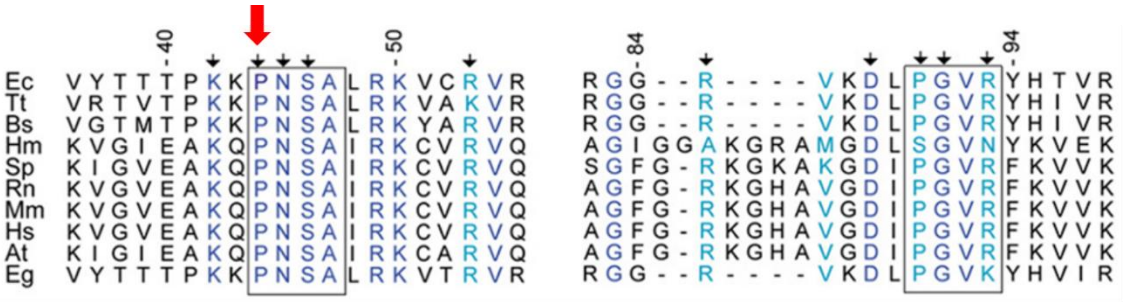


Figure 1.4: **Sequence alignment of conserved uS12 (RPS23 in humans) regions from bacteria, archaea and metazoans.** Dark and light blue residues indicate 100% and 80–90% conservation, respectively. The conserved PNSA and PGVR regions are highlighted in boxes. Arrowheads mark the sites chosen for alanine substitution mutations. Red arrowhead indicates the hydroxylation site equivalent to Proline-62 in human RPS23. Ec: *E. coli*; Tt: *T.thermophilus*; Bs: *Bacillussubtilis*; Hm: *Haloarculamarismortui*; Sp: *Schizosaccharomyces pombe* Rn: *Rattus norvegicus*; Ms: *Mus musculus*; Hs: *Homo sapiens*; At: *Arabidopsis thaliana*; Eg: *Euglenagracilis*. Figure adapted from Sharma et al., 2007.

Mutational analysis from other sites surrounding the two conserved regions (indicated by the arrowheads) resulted in milder growth defects. In a miscoding assay, these RPS12 variant ribosomes showed an increase in accuracy relative to wild-type ribosomes in selecting a near-cognate tRNA species containing an AUC codon for phenylalanine (Sharma et al., 2007). As a result, RPS12 variants surrounding the 'PNSA' and 'PGVR' regions display a hyper-accurate decoding phenotype and suggest a role in the tRNA selection process.

The effect of RPS23 hydroxylation at Proline-62 on decoding has been assessed in both yeast and mammalian cells (Keeling et al., 2006; Loenarz et al., 2014; Singleton et al., 2014). The loss of TPA1 in yeast was associated with both increased and decreased translational termination that was dependent on the context of the stop codon termination signal

(Keeling et al., 2006; Loenarz et al., 2014). In OGFOD1-defective mouse embryonic fibroblasts (MEFs), an increase in termination efficiency was observed with some but not all stop codon reporters (Singleton et al., 2014). Taken together, the data do not support generalised read-through or decoding defects following suppression of RPS23 hydroxylation.

1.3.2.2 Regulation of translational stress phenotypes and cellular growth

Prior to the identification of OGFOD1 as a ribosomal hydroxylase enzyme, Wehner et al., reported that OGFOD1 modulates phosphorylation of the eukaryotic translation initiation factor 2α (eIF2α) (Wehner et al., 2010). Phosphorylation of eIF2α inhibits translation initiation resulting in inhibition of cap-dependent translation (i.e., a global reduction in protein synthesis) and the formation of stress granules - dense cytoplasmic foci containing 48S preinitiation complexes (Kedersha et al., 2013; Pakos-Zebruck et al., 2016). The phosphorylation of eIF2α mediates the Integrated Stress Response (ISR) – a signalling system that functions to maintain cellular homeostasis in response to cellular stress (for review see Pakos-Zebruck et al., 2016). The system is co-ordinated through four kinases (PKR-like ER kinase (PERK), double-stranded RNA-dependent protein kinase (PKR), heme-regulated eIF2α kinase (HRI), and general control nonderepressible 2 (GCN2)) which are activated in response to a range of physiological changes, including amino acid deprivation, viral infection, heme deprivation and ER stress (Figure 1.5). Whilst phosphorylation of eIF2α inhibits global protein synthesis, select genes including activating transcription factor 4 (ATF4) are translated to support cell survival and recovery. Long term stress induces ATF4 stimulation of CCAAT enhancer-binding protein homologous protein (CHOP), resulting in the initiation of apoptosis (Rozpędek et al., 2016).

Wehner et al., reported that OGFOD1 co-localised with Ras GTPase-activating protein-binding protein 1 (G3BP1) in stress granules following treatment with sodium arsenite. In

addition, a modest reduction in eIF2α phosphorylation was described following OGFOD1 suppression by RNA interference (RNAi) after treatment with sodium arsenite (Wehner et al., 2010).

Subsequent studies indicated that suppression of OGFOD1 by RNAi is associated with marked translational stress phenotypes including: reduced protein synthesis, increased eIF2a phosphorylation, stress granule formation, autophagy and inhibition of proliferation (Singleton et al., 2014). In *Drosophila melanogaster* suppression of the OGFOD1 homolog, Sud1, resulted in similar effects on growth inhibition, including a reduction in larvae size and an impairment in wing growth (Katz et al., 2014). In addition to the induction of eIF2α phosphorylation, and stress granule formation, suppression of Sud1 resulted in the induction of the unfolded protein response (UPR). The UPR is activated in the endoplasmic reticulum to cope with protein folding alterations, indicating that OGFOD1 can regulate various homeostatic signalling networks in different organisms (Hetz., 2012; Katz et al., 2014).

OGFOD1 knockdown by siRNA and shRNA impeded proliferation in various cell types including HEK293, SW620, U2OS, HCT116 (Singleton et al., 2014). These observations have been further characterised by other groups. Kustatscher et al. demonstrated that depletion of OGFOD1 by siRNA in retinal pigment epithelial (RPE) cells resulted in a reduction of cells in the S-phase of the cell-cycle, which was indicative of activation of G1 or G2 checkpoints, or inhibition of replication initiation (Kustatscher et al., 2014). Similarly, Kim et al. demonstrated that OGFOD1 shRNA in MDA-MB-231 significantly impeded cell proliferation and resulted in an accumulation of cells at G1 and G2/M phases of the cell-cycle (Kim et al., 2015). Furthermore, Kustatscher et al. indicated that OGFOD1 was a chromatin associating protein as identified through a technique termed chromatin enrichment for proteomics (ChEP) (Kustatscher et al., 2014). Together with its predominant nuclear localisation, these

studies have raised the possibility that OGFOD1 has a nuclear in addition to ribosomal functions.

In the reports relating to the effect of OGFOD1 on the cell-cycle, no correlation between suppression of OGFOD1 and the effect on RPS23 hydroxylation was discussed, and therefore how these observations are linked to RPS23 is unclear. Furthermore, some cell types including HeLa and NCI-H727 are relatively insensitive to OGFOD1 siRNA or shRNA, suggesting that there are cell type contextual effects (Singleton et al., 2014). Interestingly, RPS23 hydroxylation is supressed following OGFOD1 knockdown in cells that manifest a proliferation defect and in those that do not, suggesting that loss of RPS23 hydroxylation is not directly linked to the associated growth phenotype.

Finally, Saito et al. reported that OGFOD1 suppression resulted in increased cell viability under conditions of ischaemic stress (low glucose and hypoxia) (Saito et al., 2010). This supports the possibility that, similar to ycfD (Section 1.2.1), OGFOD1 or other ribosomal hydroxylases may have an important regulatory function under conditions of cellular stress.

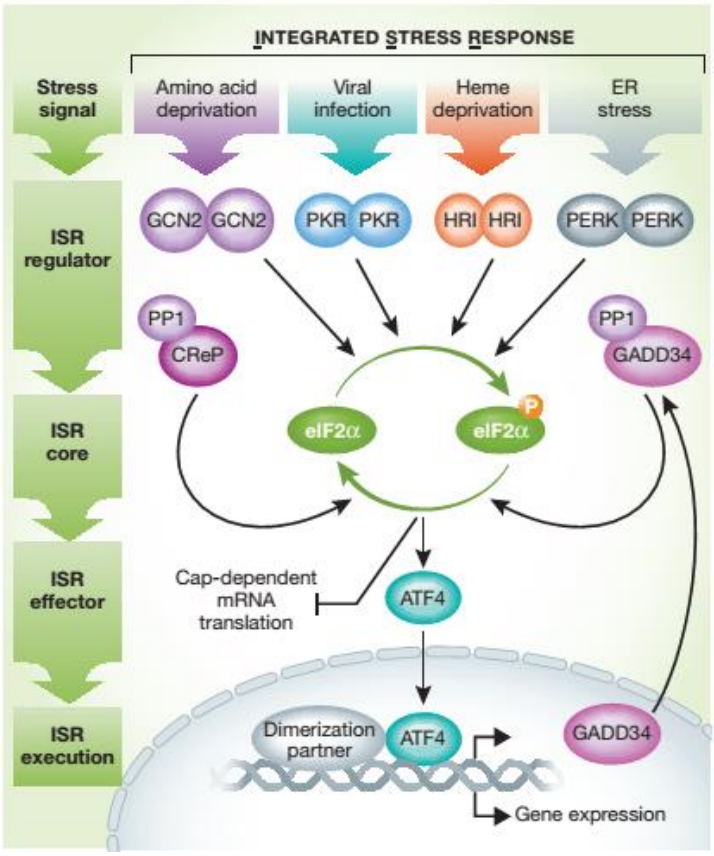


Figure 1.5: The integrated stress response (ISR): signalling via eIF2α phosphorylation. Activation of GCN2, PKR, HRI, or PERK serine/threonine kinases through distinct stress stimuli will result in the phosphorylation of eIF2α and the initiation of the integrated stress response (ISR). Phosphorylation of eIF2α results in the inhibition of cap-dependent translation whilst preserving translation of pro-survival genes such as activating transcription factor 4 (ATF4). ATF4 activates a transcriptional program to promote cellular recovery during stress. Continued activation of the ISR can result in cell death when cellular homeostasis cannot be restored. Dephosphorylation of eIF2α and termination of the ISR is mediated through protein phosphatase 1 (PP1). PP1 phosphatase activity is regulated through either Growth Arrest and DNA Damage-inducible protein (GADD34), which is induced as part of the ISR, or by the Constitutive Repressor of eIF2a Phosphorylation (CReP) which is constitutively expressed and targets PP1 to eIF2α. Figure from Pakos-Zebruck et al., 2016.

1.3.3 An OGFOD1 homolog, Ofd1, functions outside of RPS23 hydroxylation

The hypothesis that OGFOD1 might have a nuclear function in response to cellular stress is supported by studies from Espenshade and colleagues who reported that Ofd1, the OGFOD1 homolog in *S. pombe*, performs a key role in the oxygen-dependent control of the sterol response through its own oxygen sensitivity (Lee et al., 2009). Sre1 is an endoplasmic

reticulum (ER) membrane-bound protein that is proteolytically processed in response to reduced cholesterol levels in hypoxia. This processing takes place in the Golgi and liberates the transcriptionally-active *N*-terminus, Sre1N, which can then enter the nucleus and bind sterol response elements to activate genes required for survival under hypoxic conditions (Todd et al., 2006; Stewart et al., 2011). Transcriptional profiling experiments have indicated that Sre1N controls around 68% of genes induced under anaerobic conditions, including targets of ergosterol, heme, sphingolipid, and ubiquinone pathways (Todd et al., 2006). In mammals, lipid homeostasis is regulated by two closely related sterol regulatory element binding protein (SREBP1 and 2) transcription factors (Brown et al., 2000; Bien at al., 2010). Under sterol replete conditions, SREBP is retained in the ER by SREBP cleavage activating protein (Scap). Under low sterol conditions, SREBP is transported to the Golgi and cleaved to release the *N*-terminal SREBP transcription factor that upregulates genes required for lipid synthesis. The increased levels of sterol prevent the Golgi transport of Scap and supresses SREBP transcriptional activity. Although the oxygen sensitivity of mammalian SREBP stability has not been demonstrated, DEC1 and DEC2, which are HIF target genes, transcriptionally repress SREBP-1 (Choi et al., 2008). This suggests an indirect oxygen-dependent mechanism of SREBP-1 regulation in mammalian cells.

Yeast two-hybrid experiments indicated that the *C*-terminal domain (215-515) of Ofd1 interacts with Sre1N transcription factor in *S. pombe* in the presence of oxygen to prevent its DNA binding (Lee et al., 2011). The minimal Ofd1 binding site was mapped to a region that encompasses the basic helix-loop-helix domain of the Sre1N transcription factor (271-340) indicating that Ofd1 exerts its regulation through the DNA binding domain of Sre1N. Ofd1 also functions to regulate Sre1N through accelerating its degradation in normoxia (Lee et al., 2009). Mathematical models predict that accelerating Sre1N degradation is necessary for the yeast to switch off the hypoxic response when oxygen is restored (Porter et al.,

2012). The E3 ubiquitin ligase Ubr1 is required for Sre1N degradation, and Ofd1 has been shown to act upstream of Ubr1, as deletion of Ofd1 in Ubr1 mutant cells does not alter Sre1N levels (Lee et al., 2011). It is unclear whether Ofd1 acts directly on Sre1N to accelerate its degradation or if Ofd1 alters Ubr1 activity.

Interestingly, in contrast to the HIF system (Figure 1.3), hydroxylase activity is not required for Ofd1 to inhibit Sre1N DNA binding or accelerate Sre1N degradation (Hughes and Espenshade, 2008; Lee et al., 2011). Instead, a competitive system operates in which Sre1N competes with a helical repeat protein, termed Nro1 (Negative regulator of Ofd1) for binding to Ofd1. Interestingly, the association between Ofd1 and Nro1 is regulated in an oxygen-dependent manner (Lee et al., 2009). In the absence of oxygen, Nro1 preferentially binds to the *C*-terminal domain of Ofd1 blocking Sre1N binding and turnover and resulting in Sre1N accumulation and hypoxic gene expression. An overview of Sre1N regulation is highlighted in Figure 1.6.

An ortholog of Nro1 exists in *S. cerevisiae*, termed ETT1 (Enhancer of translation termination 1), and was originally identified as an interacting partner with TPA1 (*S. cerevisiae* Ofd1 ortholog) using tandem affinity purification and mass spectrometry (Krogan et al., 2006). ETT1 deletion alters stop-codon readthrough, a phenotype that is similarly observed with TPA1 deletion (Keeling et al., 2006; Henri et al., 2010; Loenarz et al., 2014). Although no clear ortholog of the Sre1 protein has been found in *S. cerevisiae*, TPA1 has also been shown to represses the activity of the HAP1 transcription factor, that regulates gene expression in response to levels of heme and oxygen (Henri et al., 2010). However, whether TPA1 regulation of HAP1 requires ETT1 and whether an interface with oxygen exists remains unclear. Given that RPS23 hydroxylation is evolutionary conserved as far back as yeast, the possibility that OGFOD1 has additional nuclear signalling function(s), analogous to Ofd1 regulation of Sre1N, is of significant interest.

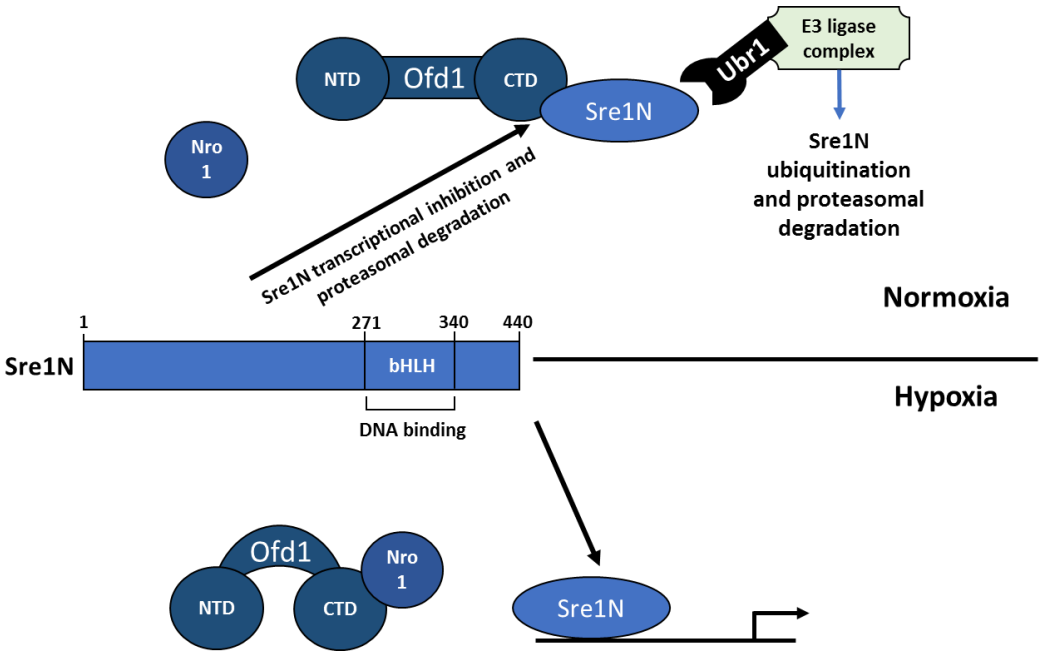


Figure 1.6: Regulation of the sterol response by Ofd1, the OGFOD1 homolog in *S. pombe*. The proteolytically-processed Sre1 transcription factor (Sre1N) enters the nucleus with different consequences depending on the oxygen-regulated activity of Ofd1. In oxygen-replete conditions, the *C*-terminal degradation domain (CTD) of Ofd1 inhibits Sre1N activity at two levels: (i) potentiation of Ubr1-dependent proteasomal degradation (ii) direct inhibition of Sre1N DNA binding. At limiting levels of oxygen, the *N*-terminal hydroxylase domain is inhibited permitting the binding of an inhibitory factor, Nro1 (Negative regulator of Ofd1), to the CTD of Ofd1. This leads to the stabilisation of Sre1N and transcription of genes required for hypoxic growth. Figure modified from Lee et al., 2011.

1.4 Hydroxylation as a signalling mechanism

The catalytic dependence of the 2-OG oxygenases on molecular oxygen, 2-OG as a co-substrate, and iron as a co-factor indicate that they may be subject to regulation by a complex interplay between oxygen and metabolic signals (Loenarz et al., 2011). Regulation of the HIF system provides the best evidence that hydroxylation functions as a signalling process. Although there is no evidence for reversal of hydroxylation, HIF hydroxylation is coupled to proteasomal degradation which enables the system to be 'reset' (Schofield and Ratcliffe, 2004). The proteasomal degradation of HIF is signalled via the oxygen-sensitivities of the PHD enzymes (Tian et al., 2011). Hydroxylation that is catalysed by MINA53, NO66

and OGFOD1 appears to be relatively insensitive to oxygen deprivation (Ge et al., 2012; Singleton et al., 2014). Furthermore, hydroxylation reactions catalysed by the ribosomal oxygenases appear complete at least in proteins assembled into the mature ribosome in a range of cell lines and tissues. This contrasts with the HIF system in which reversal of hydroxylation occurs through proteolysis which, in turn, creates a signalling system. This suggests that modifications catalysed by the ribosomal oxygenases may play a 'housekeeping' role as opposed to a signalling function. However, studies on ycfD, which catalyses arginine hydroxylation of RPL16 in *E. coli*, have reported a growth defect that was induced under conditions of nutrient deprivation (Ge et al., 2012). Although effects on growth have not been directly linked to RPL16 hydroxylation, this suggests that the ribosomal modifications may have an important signalling role under conditions of cellular stress. This is also exemplified for the OGFOD1 homolog, Ofd1, in which a transcriptional programme is signalled via Ofd1 under conditions of low oxygen and reduced sterol synthesis (Lee et al., 2009). Although the exact role for RPS23 hydroxylation in this system is unclear, the study implies that hydroxylation may serve as regulator of a signalling pathway under conditions of nutrient deprivation. In relation to OGFOD1, it is also interesting to consider that whilst RPS23 is evolutionary conserved from bacteria, OGFOD1 homologs have only been identified as far back as eukaryotes, suggesting a distinct signalling role or extra-ribosomal function for hydroxylated RPS23 that only occurs in higher organisms (Sharma et al., 2007; Scotti et al., 2014).

1.5 Aims of this thesis

This thesis aims to better characterise the cellular role of OGFOD1, a ribosomal hydroxylase enzyme within the 2-OG oxygenase superfamily. The work aims to define the link between the associated OGFOD1 cellular proliferation defects and RPS23 hydroxylation. The work also aims to determine the existence of a nuclear signalling function for OGFOD1 that is analogous to Ofd1-mediated regulation of the Sre1N transcription factor in *S. pombe.* It is also hoped that functional analysis of OGFOD1 may help to better inform on the role of other described 2-OG oxygenases that target ribosomal proteins and for those that may be identified in future studies.

Chapter 2: Phenotypic analysis of OGFOD1 CRISPR-derived knockout cells

2.1 Introduction and aims of the chapter

OGFOD1-dependent cellular phenotypes have been reported by independent groups. These phenotypes were principally defined in response to OGFOD1 inhibition by RNA interference (RNAi). In proliferation and viability screens, OGFOD1 knockdown had marked effects on the proliferation of a range of cell lines, including: HEK293, SW620, U2OS, HCT116, retinal pigment epithelial (RPE) and MDA-MB-231 (Singleton et al., 2014; Katz et al., 2014; Kustatscher et al., 2014; Kim et al., 2015). The severity of the proliferative defect varied considerably however, as some cell lines including HeLa and NCI-H727 were relatively insensitive to OGFOD1 knockdown indicating cell context-dependent effects. Importantly, OGFOD1 siRNA suppressed RPS23 hydroxylation in cells that manifest a cell proliferation defect and in those that did not. This suggests that the loss of RPS23 hydroxylation may not directly cause the associated growth phenotype.

In characterising the role of OGFOD1 in cellular proliferation, other groups have reported inhibitory effects of OGFOD1 knockdown on cell-cycle progression. The Rappsilber laboratory identified OGFOD1 as a cell-cycle regulated chromatin-associating protein using a novel chromatin enrichment procedure for proteomics (Kustatscher et al., 2014). Consistent with this observation, the authors also demonstrated that siRNA-mediated knockdown of OGFOD1 suppressed S-phase entry and progression of RPE cells. Further mechanistic dissection of the cell-cycle defect was not undertaken, though similar findings have been independently corroborated by Kim et al. who noted a similar reduction in the proportion of

MDA-MB-231 cells in S-phase with shRNA-mediated OGFOD1 knockdown (Kim et al., 2015). In these reports relating to OGFOD1 and the cell-cycle, no correlation between suppression of OGFOD1 and the effect on RPS23 hydroxylation was discussed, and therefore how these observations are linked to RPS23 is unclear.

Reports have also linked OGFOD1 to post-transcriptional stress response pathways, although caveats surround the mechanism and robustness of this phenotype. Mammalian OGFOD1 was initially characterised as a stress granule component that regulates the resumption of protein synthesis in cells recovering from arsenite-induced stress (Wehner et al., 2010). Specifically, OGFOD1 knockdown was associated with reduced levels of eIF2α phosphorylation (and consequently enhanced accumulation of translating ribosomes) in HeLa cells treated with sodium arsenite. eIF2α phosphorylation acts to inhibit translation initiation and occurs following activation of the integrated stress response, a signalling pathway that functions to maintain homeostasis in response to cellular stress (Pakos-Zebruck et al., 2016). Four kinases: PERK, PKR, HRI, and GCN2 converge on eIF2α and are activated in response to specific stresses (chapter 1: Figure 1.5). Sodium arsenite-mediated eIF2α phosphorylation and inhibition of protein synthesis requires the HRI kinase (McEwen et al., 2005; Lu et al., 2001). In contrast to Wehner et al., Singleton et al. reported no effect of OGFOD1 intervention on eIF2α phosphorylation in HeLa cells under similar conditions, but described marked translational stress phenotypes including: reduced protein synthesis, increased eIF2α phosphorylation and G3BP1 stress granule formation, in U2OS cells in the absence of an exogenous stress (Singleton et al., 2014). Overall, the effect of OGFOD1 loss in different cell types on cellular proliferation, translational stress phenotypes and RPS23 hydroxylation have not been fully addressed and remain largely unexplained.

Outside of the human cancer cell setting, a phenotype in response to DNA damage has been reported in yeast defective for TPA1, the OGFOD1 homolog in *S. cerevisiae.* TPA1 deletion

was reported to sensitize yeast to the DNA alkylating agent methyl methane sulfonate (MMS), suggesting a role for the OGFOD1 homolog in DNA alkylation repair (Shivange et al., 2014). Given that OGFOD1 has been reported as a chromatin associated protein (Kustatscher et al., 2014), one possibility is that OGFOD1 possesses a novel role in DNA repair similar to that of TPA1.

This chapter aims to explore OGFOD1-dependent cellular phenotypes using knockout cell lines derived through the CRISPR methodology. It was hypothesised that the variability reported in proliferation defects and translational stress responses between different cell lines might in part be due to the incomplete and variable reduction in OGFOD1. I postulated that OGFOD1 knockout cell lines would provide a better setting in which to explore complex OGFOD1-dependent phenotypes. In this chapter, to enable a comparison with the effects from OGFOD1 RNAi on cellular proliferation, the growth rates of OGFOD1 knockout cell lines were assessed. The regulation of eIF2α phosphorylation was addressed in OGFOD1 knockout cells in relation to the reported translational stress phenotypes. Finally, based on the role of TPA1 in DNA alkylation repair, OGFOD1 knockout cells were subject to MMS treatment and markers for DNA damage and effects on cellular growth were assessed.

2.2 Results

2.2.1 Cellular proliferation of OGFOD1 knockout cells

The phenotypic characterisation of OGFOD1 was performed in HEK293 cells in which a number of independent OGFOD1 CRISPR clones had been derived. HEK293 cells were chosen as the model cell line for these studies as significant effects of OGFOD1 knockdown on cellular proliferation had been reported in this cell background (Singleton et al., 2014). Two independent OGFOD1 knockout clonal sublines were derived in HEK293 cells using the CRISPR-Cas9 double-nickase strategy; a method that combines a Cas9 nickase mutant with

paired guide RNAs to enhance target specificity (Ran et al., 2013). OGFOD1 knockout clones that were derived in HEK293 cells using the double-nickase strategy are hereafter termed 'DN2' and 'DN9'. In addition to this, an OGFOD1 knockout clonal cell line was also derived using wild-type Cas9 with a single guide RNA and is hereafter referred to as 'DSB' (double-strand break). To complete this cell panel, parental HEK293 cells, and a clonal subline derived from transfection with a corresponding empty vector CRISPR plasmid (EV) served as the controls. Details regarding the derivation of OGFOD1 knockout sublines is described in chapter 9: Table 9.2-9.3; Section 9.4.7; Section 9.5.3; and Appendix I. Immunoblotting using anti-OGFOD1 antibody confirmed loss of OGFOD1 in the CRISPR derived HEK293 cells (Figure 2.1A). To note, further validation of OGFOD1 knockout cell lines can be found in chapter 3, which describes the generation and validation of RPS23 Pro-62 modification-specific antibodies (chapter 3: Figure 3.1).

To determine the effect of OGFOD1 inactivation on cell growth, HEK293 CRISPR clones were seeded into 96-well plates for an MTS [3-(4,5-dimethylthiazol-2-yl)-5-(3-carboxymethoxyphenyl)-2-(4-sulfophenyl)-2H-tetrazolium) cell proliferation assay. MTS is reduced by metabolically active cells into a formazan product that can be measured by absorbance at 490 nm and is presumed to be directly proportional to the number of living cells in culture. The effect of OGFOD1 loss on cell growth was assessed by the MTS assay (Figure 2.1B).

The results indicate that OGFOD1 loss does not result in a proliferation defect as measured over a 5-day time course. In fact, the 'DSB' clone appeared to display a moderate increase in cell growth at day 4 and 5 relative to the other clones. These results are in contrast to the reported growth phenotypes associated with acute OGFOD1 inactivation by siRNA and shRNA. One possibility is that rapid (acute) suppression of OGFOD1 is 'sensed' by the cells resulting in a short-term growth defect. In contrast, the OGFOD1 knockout cells have been

selected over time based on their ability to grow. As a result, the cells may have developed a compensatory mechanism that restores their normal growth rates.

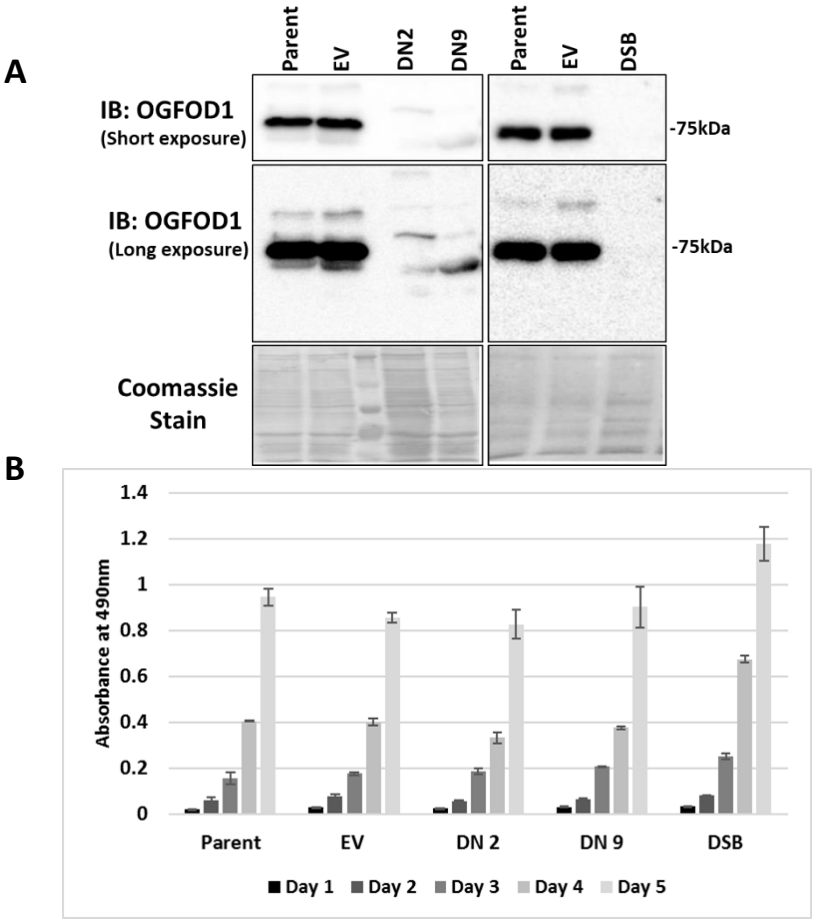


Figure 2.1: OGFOD1 loss does not confer a growth disadvantage. A) Immunoblot of wild-type (parent), empty vector CRISPR (EV), and OGFOD1 knockout (DN2, DN9 and DSB) HEK293 cells. Loss of OGFOD1 protein is observed in the three independent OGFOD1 clones. A short and long (uncropped) exposure is presented. **B)** Growth curves of HEK293 parental, EV and OGFOD1 knockout clones (DN2, DN9 and DSB) over 5 days as measured by MTS cell proliferation assay. Data (n=4) represent the mean; error bars ± standard deviation.

2.2.2 Regulation of eIF2α phosphorylation and G3BP1 stress granules in OGFOD1 knockout cells

The effect of OGFOD1 loss on cellular proliferation was noted under steady state conditions, however, OGFOD1 dependent phenotypes have also been reported in the context of translational stress, exemplified by alterations in the expression of phosphorylated eIF2α

and the abundance of G3BP1-dependent stress granules (Wehner et al., 2010). Based on these data, it was hypothesised that subjecting OGFOD1 knockout cells to a translational stress may induce an OGFOD1 dependent phenotype. Consequently, I examined the effect of sodium arsenite on eIF2α phosphorylation and G3BP1-containing stress granule formation in wild-type and OGFOD1 knockout cells.

Wehner et al. observed an OGFOD1 phenotype in the recovery to arsenite stress, and both the induction and resolution of eIF2α phosphorylation were examined (Wehner et al., 2010). A pilot experiment was performed in parental HEK293 cells to assess the dose response relationship to arsenite treatment and recovery (Figure 2.2A). HEK293 cells were treated with up to 1 mM arsenite for 30 minutes before harvesting. Immunoblotting demonstrated an induction of phosphorylated eIF2α consistent with the dose titration, with maximal induction at 0.5 mM. Paralleling the approach of Wehner et al., I assessed the recovery phase by pulsing HEK293 cells with arsenite for 30 minutes prior to harvesting in normal media at the indicated times. Phosphorylated eIF2α had returned to basal levels (untreated) after 240 minutes with no obvious relationship to dose at the 90-minute intermediate timepoint.

To monitor phosphorylated eIF2α induction kinetics between wild-type and OGFOD1 knockout clones, a sub-maximal dose of 0.1 mM arsenite was employed. Immunoblotting revealed similar levels and timing of eIF2α phosphorylation between wild-type and OGFOD1 knockout clones, indicating that OGFOD1 was not impacting on the induction of eIF2α phosphorylation following treatment with sodium arsenite (Figure 2.2B). The results also contrast with published work, in which OGFOD1 knockdown (by shRNA) resulted in a marked induction of eIF2α phosphorylation in the absence of an exogenous stress in U2OS cells (Singleton et al., 2014). In order to track the recovery phase over time, wild-type and knockout clones were subjected to 30 minutes of treatment with a dose of 0.5 mM arsenite

(Figure 2.2C). Consistent with previous observations (Figure 2.2B), induced levels of phosphorylated eIF2α at 0.5 mM arsenite were similar between wild-type and OGFOD1 variant HEK293 cells (Figure 2.2C; recovery time 0). Moreover, in contrast to published findings (with siRNA) in HeLa cells (Wehner et al., 2010), HEK293 cells defective for OGFOD1 did not show enhanced recovery to arsenite stress as determined by phosphorylated eIF2α blotting (Figure 2.2C). Overall, the results do not support large effects from OGFOD1 loss on the induction or resolution of eIF2α phosphorylation in response to arsenite treatment.

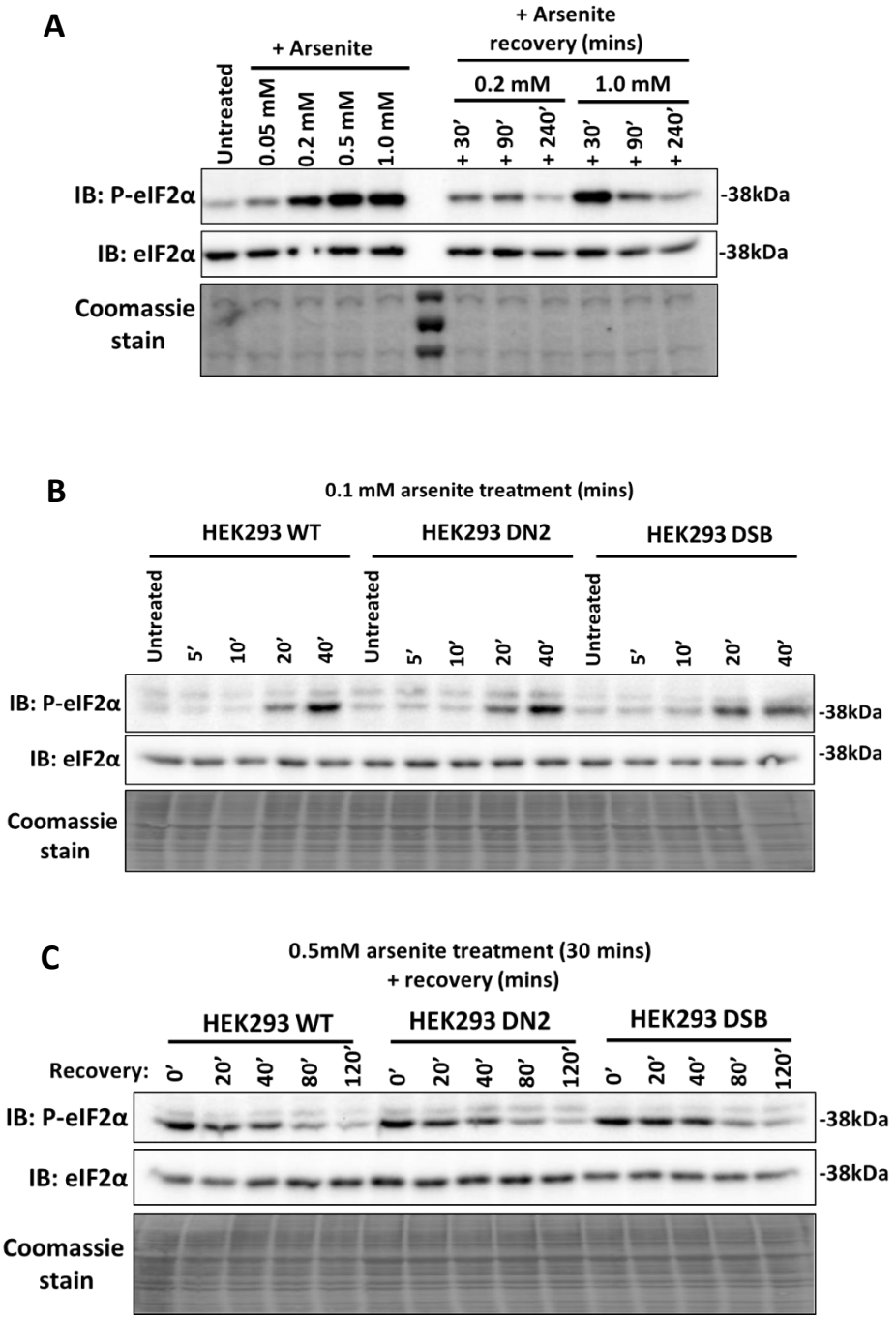


Figure 2.2: eIF2α phosphorylation is equivalent in wild-type and OGFOD1 knockout HEK293 cells under arsenite induced translational stress. A) Immunoblot of total and phosphorylated eIF2α following a dose titration of sodium arsenite in HEK293 cells. Induction and recovery of P-eIF2α was assessed following treatment for 30 minutes. **B)** Immunoblot of total and phosphorylated eIF2α in wild-type and OGFOD1 knockout HEK293 cells (clones: DN2 and DSB) treated with sodium arsenite at 0.1 mM for the indicated times. **C)** Immunoblot of total and phosphorylated eIF2α in wild-type and OGFOD1 knockout HEK293 cells following recovery from 0.5 mM arsenite treatment for 30 minutes.

Phosphorylation of eIF2α also leads to the formation of stress granules; dense cytoplasmic foci that contain stalled 48S pre-initiation complexes and translationally repressed mRNAs (Anderson et al., 2015). Stress granules can form in response to inhibition of translation and act to determine the fate of the mRNAs they contain and, therefore, stress granule assembly and disassembly is linked to translational control (Aulas et al., 2017).

The inhibition of eIF4A, a DEAD-box helicase that enables the 48S pre-initiation complex to reach the start codon, results in the assembly of stress granules independent of eIF2α phosphorylation (Dang et al., 2006; Bordeleau et al., 2015). It has been reported that G3BP1 is essential for stress granule condensation initiated by eIF2α phosphorylation or eIF4A inhibition (Kedersha et al., 2016). Given that the levels of eIF2α phosphorylation appear comparable between wild-type and OGFOD1 knockout cells (Figure 2.2), one possibility is that OGFOD1 loss mediates an eIF2α independent mechanism of stress granule assembly. To assess downstream effects of OGFOD1 loss on stress granule formation, staining of G3BP1 by confocal immunofluorescence was performed in wild-type and OGFOD1 knockout cells. In the steady state, G3BP1 displays diffuse a cytoplasmic stain (Figure 2.3). To demonstrate antibody specificity and to induce G3BP1 stress granule condensation, cells were treated with 1 mM arsenite for 30 minutes. Immunostaining did not reveal any evidence for condensation of G3BP1 in the untreated OGFOD1 knockout cells relative to wild-type cells. G3BP1 condensation was observed in wild-type cells following arsenite treatment. However, the number and intensity of G3BP1 stress granules were broadly comparable between wild-type and OGFOD1 knockout cells. Therefore, the results do not support large effects from OGFOD1 loss on G3BP1 stress granule condensation in steady state and arsenite treated cells.

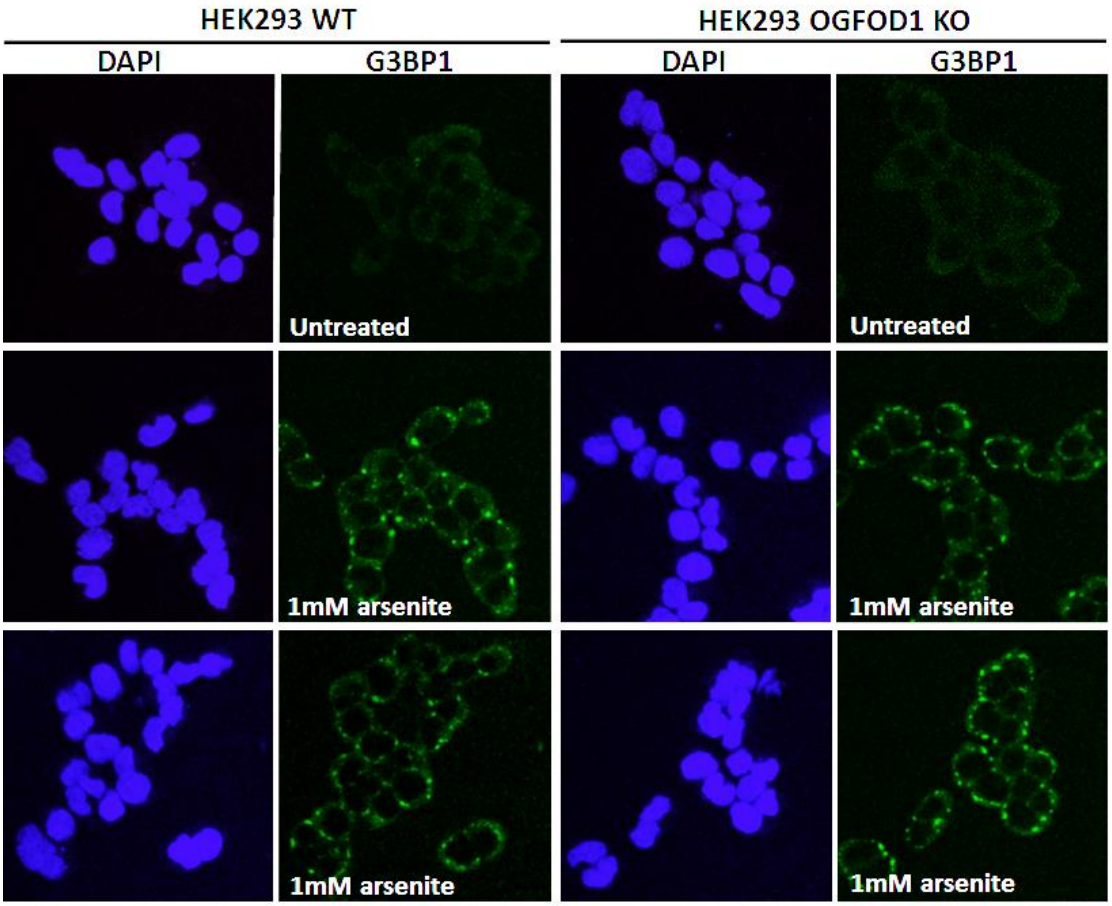


Figure 2.3: G3BP1 stress granule formation is not altered in OGFOD1 knockout (clone DN2) HEK293 cells. Confocal immunofluorescence of G3BP1 (green) in wild-type and OGFOD1 knockout (KO) HEK393 cells untreated or treated with 1 mM sodium arsenite for 30 minutes. G3BP1 shows diffuse cytoplasmic staining in untreated conditions in both wild-type and OGFOD1 knockout cells. Sodium arsenite induces stress granule assembly resulting in G3BP1 foci around the nuclei. G3BP1 foci were comparable between wild-type and OGFOD1 knockout cells. Nuclei are counterstained with DAPI (blue).

2.2.3 Regulation of the DNA damage response in OGFOD1 knockout cells

Aside from the reported growth and translational stress phenotypes associated with acute OGFOD1 inactivation in mammalian cells, a recent study implicated the OGFOD1 ortholog in *S. cerevisiae* in DNA alkylation repair (Shivange et al., 2014). This work was derived from a screen that identified TPA1-defective yeast as being sensitive to the DNA alkylating agent, methyl methane sulfonate (MMS) (Hanway et al., 2002).

Shivange et al. demonstrated that mutation of residues in TPA1 that are required for iron and 2-OG binding inhibited DNA repair activity, implying a catalytic action of TPA1 in alkylation repair. Based on the report that TPA1 null yeast cells showed susceptibility to methylation induced toxicity and given that OGFOD1 was reported as a chromatin associating protein, it was hypothesised that OGFOD1-defective cells might also display a DNA damage hypersensitivity phenotype (Kustatscher et al., 2014; Shivange et al., 2015). To test this, wild-type and OGFOD1 knockout cells were treated with MMS.

The cellular response to DNA damage in mammalian cells is coordinated by two distinct kinase signalling cascades, the ATM-Chk2 and ATR-Chk1 pathways, which can be activated by alkylating agents (Jackson et al., 2009). KRAB-associated protein 1 (KAP1) is an ATM target that is rapidly phosphorylated on serine 824 in response to DNA damage and leads to decondensation of global chromatin for an efficient repair process (Ziv et al., 2006). Similarly, the phosphorylation of histone H2AX (termed γ-H2AX) provides a marker for DNA damage as it functions in the recruitment of repair factors (Burma et al., 2001; Ward et al., 2001). I hypothesised that the phosphorylation of KAP-1 and H2AX would serve as markers for DNA damage following MMS treatment. These markers were used to determine that a robust DNA damage response had been achieved. Concomitantly, they could also inform on whether there were any defects in signalling DNA damage via these pathways in OGFOD1 knockout cells.

The initial dosage for MMS treatment was based on studies examining the mechanism and survival of mammalian cells in response to alkylating agents following a dose of 1.5 mM MMS for 30 minutes (Lundin et al., 2005). Immunoblotting using anti-P-KAP-1 demonstrated a clear induction of the phosphorylated form of this protein in response to MMS after 30 minutes of treatment in wild-type and OGFOD1 knockout HEK293 cells (Figure 2.4).

However, the induction of phosphorylated H2AX was not observed at this timepoint and dosage (3 mM).

To validate the efficacy of the antibodies against DNA damage pathways, lysates were obtained as a kind gift from Dr. Shaliny Ramachandran (E. Hammond laboratory, University of Oxford). Colon carcinoma cells (RKO) had been placed under anoxia (6 hours at <0.1% oxygen), a condition which has been reported to induce replication stress, resulting in the activation of the DNA damage response (Olcina et al., 2013). These samples demonstrated a clear induction of phosphorylated KAP-1. Treatment of cells with siRNA to KAP-1 before anoxia resulted in loss of the phosphorylated KAP-1 and confirmed specificity of the antibodies. In contrast to the MMS treatment, anoxia also appeared to induce phosphorylation of H2AX.

When responses in OGFOD1 knockout and wild-type cells were directly compared, it was clear that levels of KAP-1 phosphorylation were similar between the two genotypes, indicating no apparent difference in the initiation of the DNA damage response, at least in respect to activation of this pathway at this dosage and timepoint (Figure 2.4)

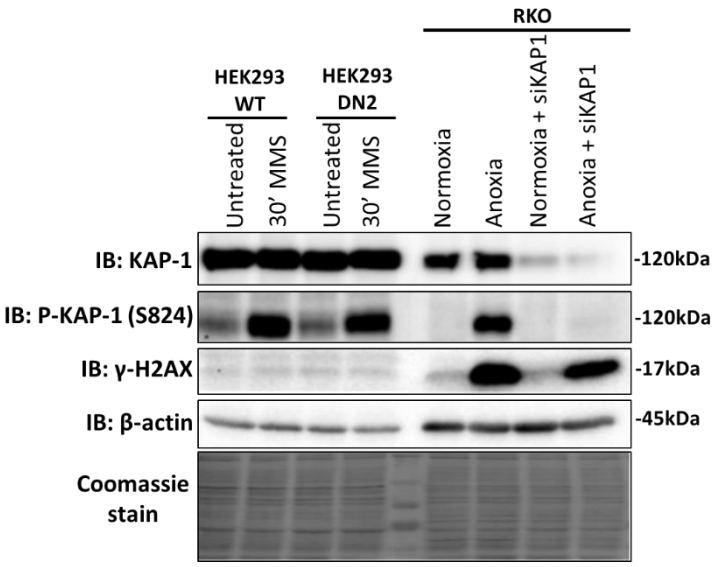


Figure 2.4: Induction of the DNA damage response by methyl methane sulfonate (MMS) is equivalent in wild-type and OGFOD1 knockout HE293 cells. Immunoblot of DNA damage markers (total and phosphorylated KAP-1 and phosphorylated (γ)-H2AX) in wild-type and OGFOD1 knockout HEK293 cells following treatment with 3 mM MMS for 30 minutes. RKO cells had been placed under conditions of anoxia (6 hours at <0.1% oxygen).

To further consider whether inactivation of OGFOD1 enhanced the sensitivity of cells to DNA damage induced by MMS a dose titration was performed. The dose response was guided by Gu et al., 2014, who assayed the level of H2AX phosphorylation in response to MMS treatment in HEK293 cells. Wild-type and OGFOD1 knockout HEK293 cells were exposed to different concentrations of MMS for 6 hours and 24 hours (Figure 2.5A and B, respectively). Induction of phosphorylated KAP-1 was observed in wild-type cells after 6 hours treatment at 0.5 mM MMS. Interestingly, no induction of phosphorylated KAP1 was observed in the knockout cells at the same dosage. However, it was also noted that total KAP-1 levels were markedly reduced in this sample. H2AX phosphorylation appeared equivalent between wild-type and OGFOD1 knockout cells with a modest induction following treatment at 0.5 mM MMS. Extending these observations to a 24 hour timepoint, the induction of phosphorylated KAP1 and H2AX appeared equivalent between wild-type and OGFOD1 knockout cells across the dose titration, with an induction of DNA damage markers observed following a 24-hour treatment of MMS at concentrations of 0.25 and 0.5 mM (Figure 2.5B).

To determine if the differences observed at the 6-hour timepoint between wild-type and knockout cells could be replicated, independent OGFOD1 knockout clones (DSB and DN2) were treated with 0.6 mM MMS at 2 hours and 6 hours (Figure 2.6A). However, no consistent differences were observed between wild-type and OGFOD1 knockout cells. Furthermore, the effects across three independent OGFOD1 knockout clones (DSB, DN2, and DN9) following a 24-hour treatment of MMS at 0.4 mM and 0.6 mM appeared to correlate with that of the wild-type cells (Figure 2.6B). Overall, it was concluded that genetic inactivation of OGFOD1 did not alter the phosphorylation kinetics of the DNA damage pathway markers, KAP1 or histone H2AX, in response to MMS.

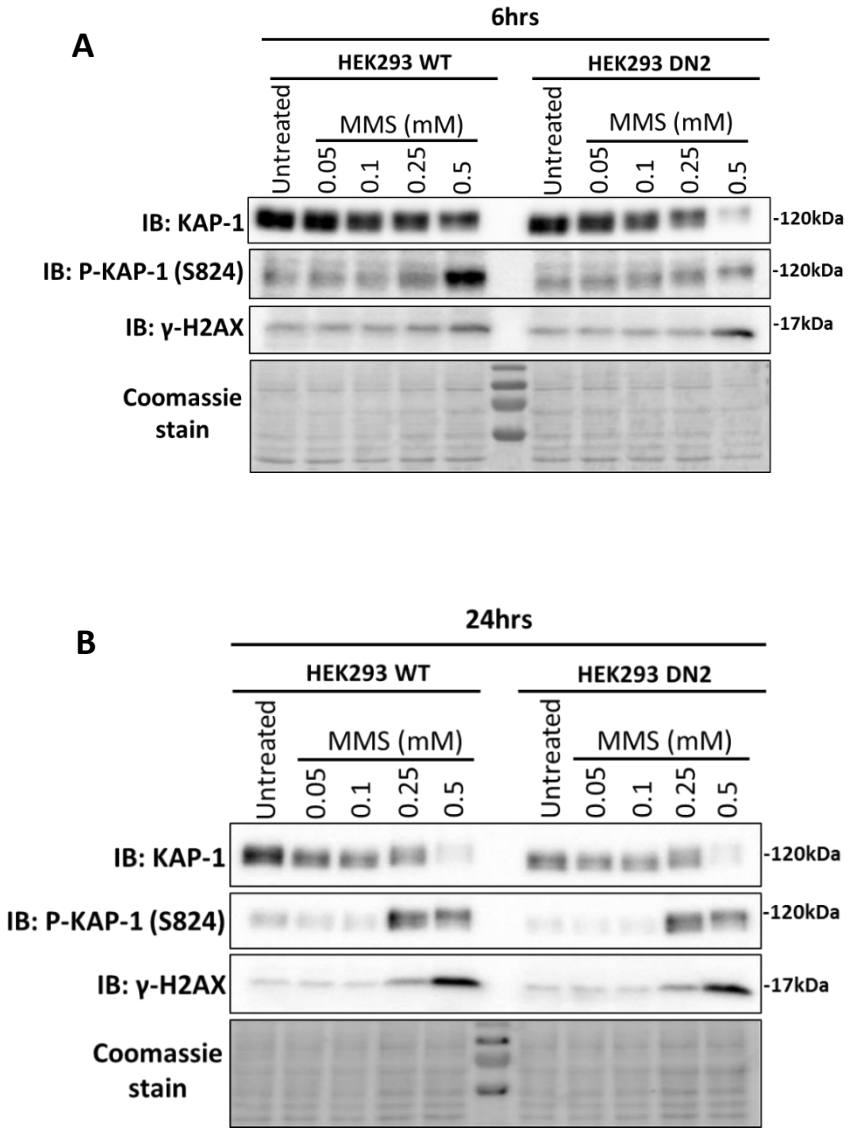


Figure 2.5: Induction of the DNA damage response following a dose and time course of MMS is equivalent in wild-type and OGFOD1 knockout HEK293 cells. Wild-type and OGFOD1 knockout (clone DN2) HEK293 cells were treated with a dose titration of MMS for 6 hours **(A)** or 24 hours **(B)**. Immunoblot of the DNA damage markers: P-KAP1 and P-H2AX, showing induction at the indicated timepoints and concentrations.

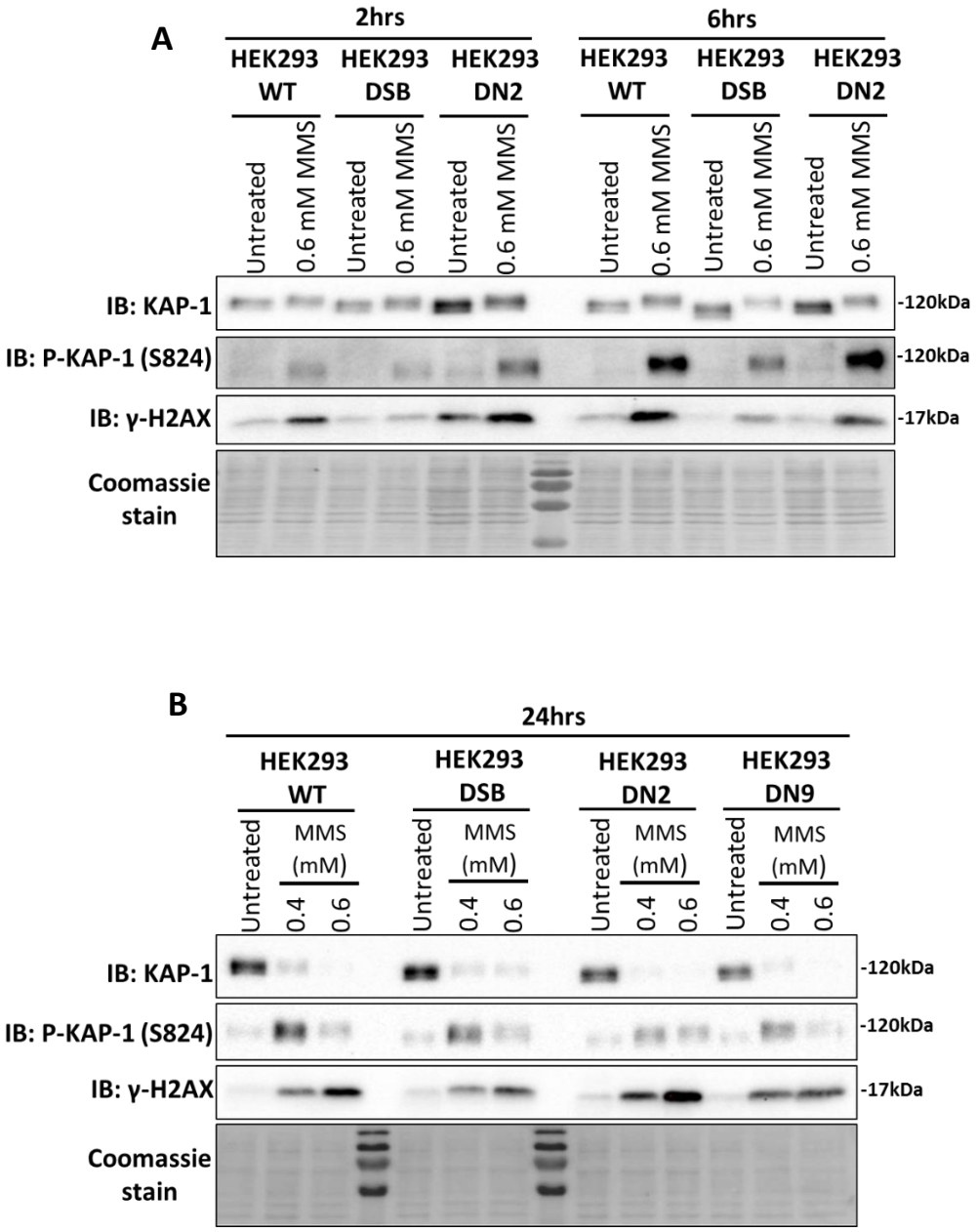


Figure 2.6: Induction of the DNA damage response following a dose and time course of MMS treatment in independent OGFOD1 knockout HEK293 clones is equivalent to wild-type HEK293 cells. Wild-type and OGFOD1 knockout (DSB, DN2 or DN9) HEK293 cells were treated with a dose titration of MMS for 2 hours, 6 hours **(A)** or 24 hours **(B)**. Immunoblot of the DNA damage markers: P-KAP1 and P-H2AX, showing induction at the indicated timepoints and concentrations.

The sensitivity of TPA1-defective yeast to MMS-induced DNA damage was notable as a growth defect (Shivange et al., 2014). Whilst activation of the pathway markers that I tested were unchanged, it remained possible that OGFOD1-defective were also differentially sensitive to MMS. To assay this integrated response I performed cell viability and colony survival assays. In the first instance, viability assays using MTS reagent (as described in Figure 2.1B), were used to assess short-term effects on cell growth over a 48-hour period following a dose titration of MMS (Figure 2.7). The growth rates appeared comparable between wild-type and OGFOD1 knockout cells in the untreated state over 48 hours, supporting the absence of a growth phenotype in the OGFOD1 knockout cells (Figure 2.1B). It was evident that after 48 hours of treatment with dosages of 0.4 mM MMS or higher resulted in a severe growth phenotype in both wild-type and OGFOD1 knockout cells. However, no sensitisation from OGFOD1 loss was observed in response to the MMS dose titration over the time course (Figure 2.7).

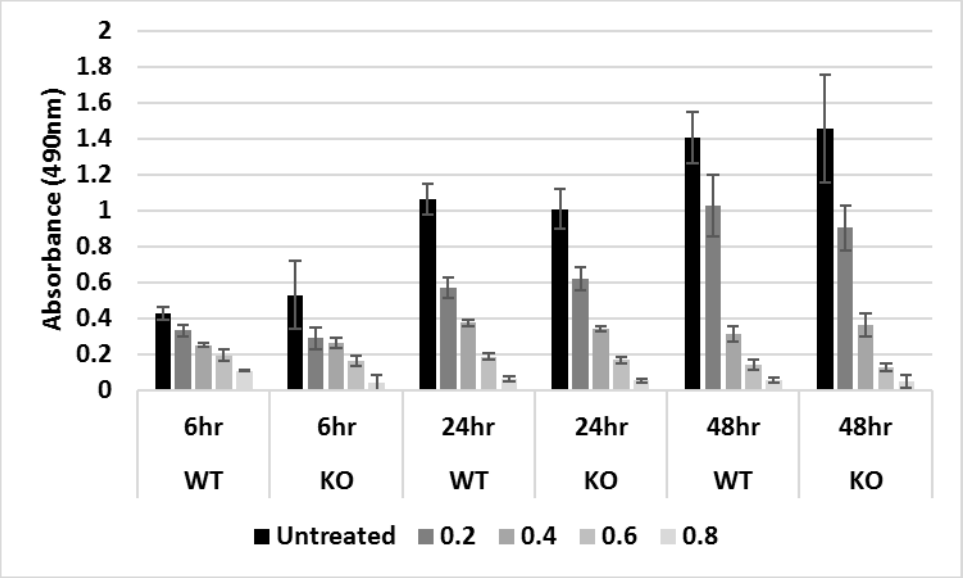


Figure 2.7: OGFOD1 loss does not confer a growth disadvantage in response to a dose titration of MMS. The growth of wild-type and OGFOD1 KO (clone DN2) HEK293 cells was assessed by MTS cell proliferation assay following no treatment or treatment with MMS (0.2 mM, 0.4 mM, 0.6 mM or 0.8 mM) for the indicated times (6 hours, 24 hours and 48 hours). Data (n=4) represent the mean; error bars ± standard deviation.

To monitor the long-term consequences of MMS treatment in OGFOD1 knockout cells, I performed colony survival assays. Initial optimisation of the colony survival assay indicated that treatment of HEK293 cells with 0.4 mM MMS for 3 hours had a marked effect on cell viability (data not shown). In light of these findings, cells were treated with a reduced dose of 0.25 mM MMS for 3 hours before plating into 6-well plates at 150 cells per well. The number of colonies were assessed by crystal violet staining approximately 10 days after plating (Figure 2.8). A reduction in colony survival was observed in MMS treated cells relative to control. However, no apparent sensitisation to MMS was observed in OGFOD1-defective clones. Interestingly, it was noted that the colony size of the OGFOD1 knockout clones appeared larger relative to the wild-type cells. This effect was observed across independent knockout clones suggesting that this phenotype was consistent with the OGFOD1 genotype. In contrast to the cell growth rates observed by MTS proliferation assay

which appear broadly similar (with the exception of the DSB clone, Figure 2.1B), the results indicate that OGFOD1 loss may provide a growth advantage when the cells are cultured in isolation.

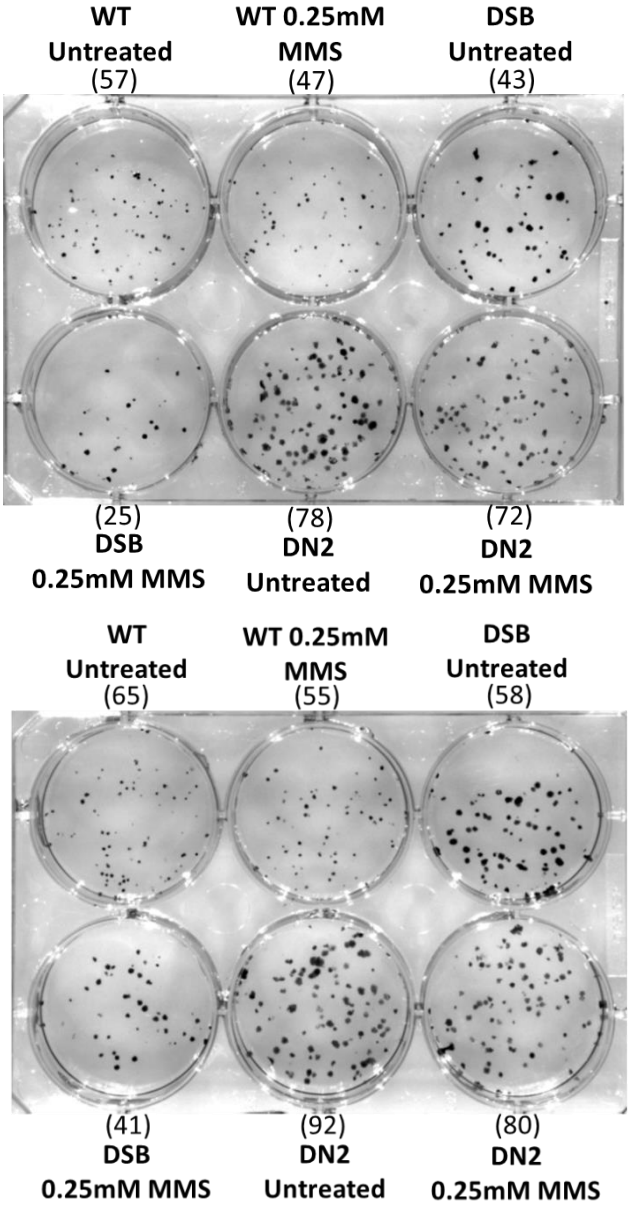


Figure 2.8: OGFOD1 loss does not confer a clear growth disadvantage in response to long-term recovery from MMS treatment. Colony survival assay of wild-type and OGFOD1 knockout (clones: DN2, DSB) HEK293 cells following treatment with MMS. Wild-type and OGFOD1 knockout cells were treated with 0.25 mM MMS for 3 hours before seeding into 6-well plates at 150 cell/well. The number of colonies were assessed by crystal violet staining approximately 10 days after plating, colonies numbers are indicated in brackets and were counted using ImageJ software. Two representative 6-well plates are shown.

2.3 Discussion

Work presented in this chapter concerns the creation, validation and phenotyping of a set of OGFOD1-defective clonal lines, in the HEK293 cell background. These lines were created by the CRISPR methodology. Independent clones were selected from cells transfected with different CRISPR guides and phenotyping was typically performed with two defective clones (referenced to wild-type) to help distinguish between clonal artefacts. The rationale for this work was that a genetically inactivated cell line would provide a more tractable setting in which to dissect OGFOD1-regulated pathways. HEK293 cells were considered an appropriate background for this work, as Singleton et al. had described a large proliferative defect in this cell line following RNAi-mediated knockdown (Singleton et al., 2014).

In contrast to the reported RNAi-associated phenotypes, there was no evidence of a proliferative defect in OGFOD1-defective cells as determined by MTS assay over a 5 day time course (Figure 2.1). Similarly, there was no appreciable difference in other reported phenomena pertaining to translational stress pathways, including the activation and resolution of eIF2 phosphorylation (Figure 2.2) and the formation of G3BP1 stress granules (Figure 2.3).

A more speculative link between OGFOD1 and the DNA damage response was explored using OGFOD1-defective HEK293 cells. The response to MMS treatment was independent of OGFOD1 status in terms of pathway marker activation profiles (P-KAP1 and P-H2AX; Figures 2.4-2.6) and cell proliferation/survival outcomes (Figures 2.7-2.8). The colony size of the OGFOD1 knockout clones appeared moderately larger in size relative to the wild-type cells, suggesting that OGFOD1 loss may provide a growth advantage when the cells are cultured in isolation (Figure 2.8). However, the observed phenotype was only relatively modest and

contrasts with the reported proliferative defects associated with RNAi-mediated knockdown of OGFOD1 in this cell background.

Overall, the findings were unexpected and did not concord with the literature describing OGFOD1-dependent phenotypes in either yeast or mammalian cells (Wehner et al., 2010; Singleton et al., 2014; Katz et al., 2014; Kustatscher et al., 2014; Kim et al., 2015; Shivange et al., 2014). It is possible that for some of the reported phenotypes differences exist due to the cellular context. For example, in humans several alkylation repair proteins exist (ALKBH2 and 3), whereas in *S. cerevisiae* alkylation repair proteins have not been identified (Sedgwick et al., 2007; Shivange et al., 2014). It is conceivable therefore, that TPA1 may be functioning to compensate for the absence of AlkB homologs in this context.

Variable responses and cell context-dependent effects have been described in response to OGFOD1 knockdown. Wehner et al. reported that siRNA-mediated knockdown of OGFOD1 resulted in the reduction of eIF2α phosphorylation in HeLa cells recovering from arsenite-induced stress (Wehner et al., 2010). Whereas, Singleton et al. reported a steady-state increase in eIF2α phosphorylation following shRNA-mediated knockdown of OGFOD1 in U2OS cells but not HeLa cells (Singleton et al., 2014). In addition, and in contrast to the work of Wehner et al., there was no measurable effect of OGFOD1 knockdown on phosphorylated eIF2a levels during the recovery period following arsenite stress (Singleton et al., 2014). These studies highlight the variable responses to OGFOD1 RNAi in different cell settings, which may be due to incomplete reduction in OGFOD1 levels.

As a result, considerable effort was made to examine basal growth and translational stress markers in OGFOD1 knockout cells, where the effects cannot be attributed to incomplete suppression of OGFOD1. Although it is possible that other conditions could have brought out differences, this work remains the most thorough examination to date. A caveat of the work remains in that the phenotypes were explored only in the HEK293 cell background

and, therefore, it is possible that phenotypes may be observed in other cell settings. However, given that a number of independent OGFOD1 knockout clones were derived, I can conclude that the results do not support a general difference with respect to OGFOD1 loss using the HEK293 cells as the model cell line. To note, analyses of OGFOD1-defective cells generated in HeLa, SW620 and mouse embryonic stem cells using CRISPR-Cas9 is performed in later chapters (HeLa and SW620 cells (chapter 6 and 7); mouse ES cells (chapter 7)).

OGFOD1 cellular phenotypes have largely been reported in response to acute inactivation through OGFOD1 siRNA or shRNA (Wehner et al., 2010; Singleton et al., 2014; Kustatscher et al., 2014; Kim et al., 2015). Therefore, the studies have only examined relatively rapid suppression without a period for adaptation. The data obtained using OGFOD1 CRISPR-derived knockout cells appear to contrast significantly with the OGFOD1 knockdown phenotypes (Singleton et al., 2014; Kim et al., 2015). One possible explanation is that the OGFOD1 knockout cells have compensated to restore normal growth rates. The cells were derived from clones that had been cultured over a two-week period and selected for based on their ability to grow. Therefore, it remains a possibility that acute loss of OGFOD1 is 'sensed' and manifests as a short-term growth inhibitory effect which is mediated through translational stress pathways.

The mechanism in which acute loss of OGFOD1 exerts regulation on cell proliferation in different contexts has not been fully addressed, especially with respect to effects on RPS23 hydroxylation. I hypothesised that OGFOD1 re-expression in the generated knockout cell lines may provide a setting in which rapid shifts in OGFOD1 expression, independent of RNAi, can be correlated with effects on cell growth and RPS23 hydroxylation.

Chapter 3: Characterisation of acute OGFOD1 interventions

3.1 Introduction and aims of the chapter

Chapter 2 sought to define a robust OGFOD1-dependent phenotype using CRISPR engineered OGFOD1-defective cells. These findings, however, did not support clear phenotypic differences between wild-type and OGFOD1 knockout cells and contrasted with reported phenotypes observed with acute suppression of OGFOD1 (Wehner et al., 2010; Singleton et al., 2014; Kustatscher et al., 2014; Kim et al., 2015).

Failure to recapitulate knockdown phenotypes in a stable genetic background is compatible with the aforementioned possibility that OGFOD1-defective cells undergo selection during clonal outgrowth that invokes compensatory mechanisms (Section 2.3). An alternate hypothesis is that OGFOD1 acts a cellular rheostat in which acute loss or acute overexpression of OGFOD1 may be 'sensed', resulting in a growth or translational stress response. In this model, it is the change in OGFOD1 protein level that elicits the phenotype. I hypothesised that it would be of interest to determine how short-term changes in OGFOD1 levels impact on cell growth and whether this persists over time.

In this chapter I also sought a means to define links between RPS23 hydroxylation and (any) cellular phenotype more clearly. For instance, it is possible that OGFOD1 mediates an effect on proliferation only under conditions of cellular stress and that some of these stresses affect catalysis of RPS23 hydroxylation. If the catalytic activity of OGFOD1 was inhibited or the production of RPS23 was altered under certain conditions, then signalling via the OGFOD1 and RPS23 complex might also be perturbed. Consistent with this, OGFOD1

suppression resulted in increased cell viability under conditions of ischaemic stress (low glucose and hypoxia), which might limit rates of OGFOD1-dependent catalysis (Saito et al., 2010).

This chapter aims to explore the cellular phenotypes mediated through acute changes to OGFOD1 levels. In an attempt to correlate changes in cellular growth with effects on RPS23 hydroxylation, antibodies were generated that were raised against hydroxylated and non-hydroxylated forms of RPS23. To corroborate findings from published reports, initial characterisation of acute OGFOD1 loss was performed using shRNA in HEK293 cells. To investigate the effect of OGFOD1 overexpression a tetracycline-regulated expression system (T-REx) was used in HEK293 cells. Furthermore, OGFOD1 re-expression was performed in a HEK293 OGFOD1 knockout cell line, and OGFOD1 expression levels were correlated with effects on cellular growth under steady state conditions and in conditions of cellular stress. A number of cellular stresses were investigated, including: serum starvation, low glutamine, and ischaemic stress (low glucose and hypoxia).

3.2 Results

3.2.1 Generation of RPS23 hydroxylation specific antibodies

Existing methods to measure endogenous RPS23 hydroxylation rely upon ribosomal purification coupled with mass spectrometry, as described by Singleton et al., 2014. Although this method provides an accurate quantitation of RPS23 hydroxylation, technical caveats exist with regards to experimental scalability. As a result, antibodies were sought that could be used to measure RPS23 hydroxylation more easily. The antibodies would help to further define the effect of OGFOD1 manipulation on RPS23 hydroxylation and help to establish whether there is a correlation between the reported effects on cellular

proliferation and OGFOD1 that is linked to catalysis (Singleton et al., 2014; Kustatscher et al., 2014; Kim et al., 2015). A custom antibody project was initiated with Dundee Cell Products and peptide immunogens were generated to hydroxylated and non-hydroxylated forms of RPS23. Sera from rabbits immunised with the non-hydroxylated peptide or hydroxylated peptide was purified through immunoaffinity chromatography to isolate polyclonal antibodies. Fractions from the affinity purification were obtained to test for specificity. Further details of the antibody generation from Dundee Cell Products is described in Chapter 9: Section 9.6.1

Validation of RPS23 hydroxylation-specific antibodies was performed by immunoblot, comparing the affinity of the different antibody fractions to cell lysate derived from either wild-type HEK293 cells or a derivative OGFOD1-defective clone (DN2) engineered by CRISPR. Given that ribosomal RPS23 is fully hydroxylated in HEK293 cells in the steady-state and that this modification is a non-redundant function of OGFOD1, this binary comparison provided a setting in which to test the efficacy of the different antibodies (Singleton et al., 2014). Signal was referenced to a control immunoblot performed with a pre-validated commercial antibody to RPS23 (pan-RPS23). Accordingly, when immunoblots were probed with antibodies raised to the unmodified form of RPS23 (‘14’ refers to sera from a rabbit immunised with non-hydroxylated RPS23 peptide), a signal of the expected mobility was highly enriched in lysates derived from OGFOD1-defective cells (Figure 3.1A). Immunoreactivity was observed in all 5 fractions with the highest affinity noted in fractions 1.4-1.6. A reciprocal relationship was observed with antibodies raised to the hydroxylated form (‘15’ refers to sera from a rabbit immunised with hydroxylated RPS23 peptide), which demonstrated signal enrichment in wild-type lysates (Figure 3.1B). Although the affinity of this antibody was weaker, specific signal was clearly discernible in fractions 1.3-1.5 with fraction 1.4 having the highest affinity. Antibody fractions with the highest affinity for non-

hydroxylated RPS23 (14.1.6) and hydroxylated RPS23 (15.1.4) were used for further characterisation.

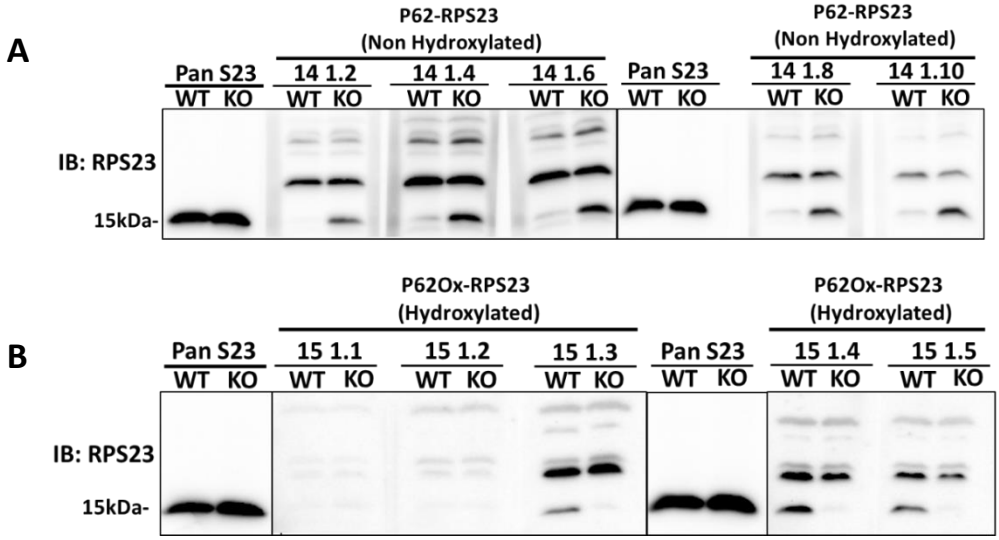


Figure 3.1: Validation of RPS23 hydroxylation specific antibodies and confirmation of OGFOD1 defective (clone DN2) HEK293 cells. A) Immunoblot of pan-RPS23 and non-hydroxylated RPS23 in wild-type (WT) and OGFOD1 knockout (KO) HEK293 cells. A range of fractions for the non-hydroxylated form of RPS23 were tested (14.1.2, 14.1.4, 14.1.6, 14.1.8, 14.1.10). Appearance of the non-hydroxylated form of RPS23 was evident in OGFOD1 knockout HEK293 cells. **B)** Immunoblot of pan-RPS23 and hydroxylated RPS23 in wild-type and OGFOD1 knockout HEK293 cells. A range of fractions for the hydroxylated form of RPS23 were similarly tested (15.1.1, 15.1.2, 15.1.3, 15.1.4, 15.1.5). Hydroxylated RPS23 was detected in wild-type cells but not OGFOD1 knockout cells for fractions 15.1.3-15.1.5.

3.2.2 Characterisation of acute OGFOD1 suppression using an shRNA knockdown system.

Defects in cellular proliferation have been reported in response to acute suppression of OGFOD1 by RNA interference (Singleton et al., 2014; Kustatscher et al., 2014; Kim et al., 2015). Cell type specific differences in sensitisation to OGFOD1 siRNA or shRNA have been described, which could reflect variation in the level of OGFOD1 knockdown. In order to corroborate reported RNAi phenotypes and provide a basis for mechanistic dissection, a new generation of shRNA vectors (shERWOOD Ultramir; Transomic technologies) were

utilised that reportedly offer greater potency and specificity (Auyeung et al., 2013; Knott et al., 2014) and, in addition, expand on the repertoire of RNAi guide sequences targeting OGFOD1.

Three independent OGFOD1-targeting short hairpin guide sequences, termed '88', '89' and '90', were lentivirally transduced into HEK293 cells and selected with puromycin. The level of OGFOD1 knockdown in puromycin-resistant cells was determined by anti-OGFOD1 immunoblot (Figure 3.2A). The efficacy of OGFOD1 knockdown varied across the three vectors, with guide '90' providing the most efficient knockdown relative to a non-targeting (NT) shRNA vector. A concomitant increase in non-hydroxylated RPS23 was observed in HEK293 cells transduced with this guide sequence. In contrast, the level of OGFOD1 knockdown achieved with guides "88" and "89" was not sufficient to demonstrably inhibit RPS23 hydroxylation. This finding was rather surprising, given the level of knockdown observed in cells transduced with short hairpin guide 89. Taken together, the data indicate that the basal expression of OGFOD1 in HEK293 cells is significantly above the level required for the maintenance of RPS23 hydroxylation in the assembled ribosome.

I next sought to determine if there was a correlation between OGFOD1 knockdown (and inhibition of RPS23 catalysis) and proliferative capacity by MTS assay in these cells over a 5-day period. Surprisingly, I did not observe a correlation between OGFOD1 knockdown and effects on cellular growth rate (Figure 3.2B). Cells reporting the greatest level of knockdown (i.e., those transduced with guide "90") showed no measurable growth defect and tracked the proliferative rate of control cells transduced with a non-targeting (NT) guide shRNA. Cells transduced with short hairpin guide "89", which displayed intermediate knockdown, showed a growth-defect. However, taken in context with the other guide sequences, I decided to end this line of inquiry. These results contrast with the significant growth defects observed with OGFOD1 siRNA in HEK293 cells (Singleton et al., 2014), and contrast with the

effect of OGFOD1 shRNA in other cell types, including MDA-MB-231 cells (Kim et al., 2015). The reason(s) for these discrepant and inconsistent findings are currently not clear.

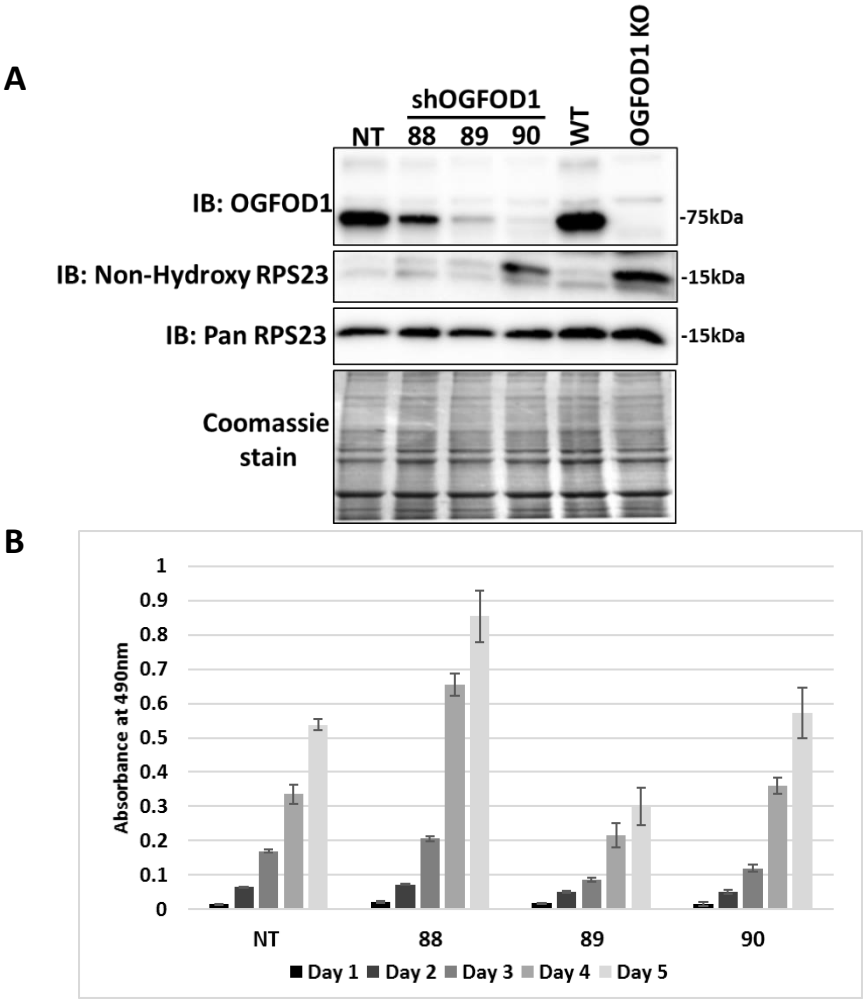


Figure 3.2: Suppression of OGFOD1 by shRNA in HEK293 cells does not correlate with effects on cell proliferation. A) HEK293 cells stably expressing pZIP shERWOOD-UltramiR vectors against non-targeting (NT) or OGFOD1 (88, 89, 90) sequences. Cells were selected for 10 days using puromycin. Immunoblot using anti-OGFOD1 antibody shows suppression of OGFOD1 using the targeted sequences (88, 89, 90). Immunoblot using anti-non-hydroxylated RPS23 antibody indicates that suppression of OGFOD1 with sequence '90' correlates with the induction of non-hydroxylated RPS23. Parental (WT) and OGFOD1 CRISPR-derived knockout (OGFOD1 KO) HEK293 cells were used to define the specificity of the anti-OGFOD1 and anti-non-hydroxylated RPS23 antibody. **B)** An MTS proliferation assay was performed on HEK293 cells transduced with shERWOOD UltramiR vectors. Neither the level of OGFOD1 nor the extent of OGFOD1 expression correlated with inhibitory effects on cell growth over the 5-day time course experiment.

3.2.3 Characterisation of acute OGFOD1 overexpression using the Tetracycline-Regulated expression (T-REx) system.

The aforementioned inconsistencies with shRNA-mediated knockdown of OGFOD1 led me to consider an alternative system in which I could rapidly manipulate cellular levels of OGFOD1. The Flp-In Tetracycline-Regulated expression (T-REx) system in HEK293 cells (Thermo Fisher) was selected as a convenient method for generating tetracycline-regulated stable cell lines via the efficient process of Flp-mediated recombination (O'Gorman et al., 1991). In this system, cells containing a single stably integrated FRT site were co-transfected with a FLAG-OGFOD1 expression vector harbouring an FRT site and a Flp recombinase expression plasmid. The integrated vector contains Tet operator sequences enabling tetracycline (doxycycline)-regulable expression of FLAG-OGFOD1.

To determine the effect of OGFOD1 overexpression on cell proliferation in HEK293 T-REx cells, cultures of empty vector (EV) or FLAG-OGFOD1 T-REx cells were treated in the presence or absence of doxycycline for 4 days and proliferation was assayed by MTS reagent (Figure 3.3). No measurable effect of doxycycline on the proliferation of inducible FLAG-OGFOD1 expressing cells was noted (Figure 3.3B). Control anti-OGFOD1 immunoblots confirmed the regulated induction of FLAG-OGFOD1 at mid (day 2) and endpoint (day 4) of the proliferation assay (Figure 3.3A). The FLAG-OGFOD1 species was discernible at slightly reduced mobility (~80 kDa) relative to the endogenous protein (~75 kDa) following SDS-PAGE and OGFOD1 immunoblotting. The previously characterised OGFOD1:RPS23 100 kDa complex was also clearly observed following doxycycline treatment of inducible FLAG-OGFOD1 expressing cells (Singleton et al., 2014). Untreated cells were cultured in tetracycline-free media, suggesting that the low level of FLAG-OGFOD1 expression detected in the uninduced state represented low level constitutive "leaky" expression. Imperfections

in the "leaky" expression of FLAG-OGFOD1 in T-REx HEK293 cells and limitations in the dynamic range of OGFOD1 expression within this context led me to consider an alternate strategy in which an OGFOD1 knockout cell line was engineered to re-express OGFOD1 in an inducible fashion.

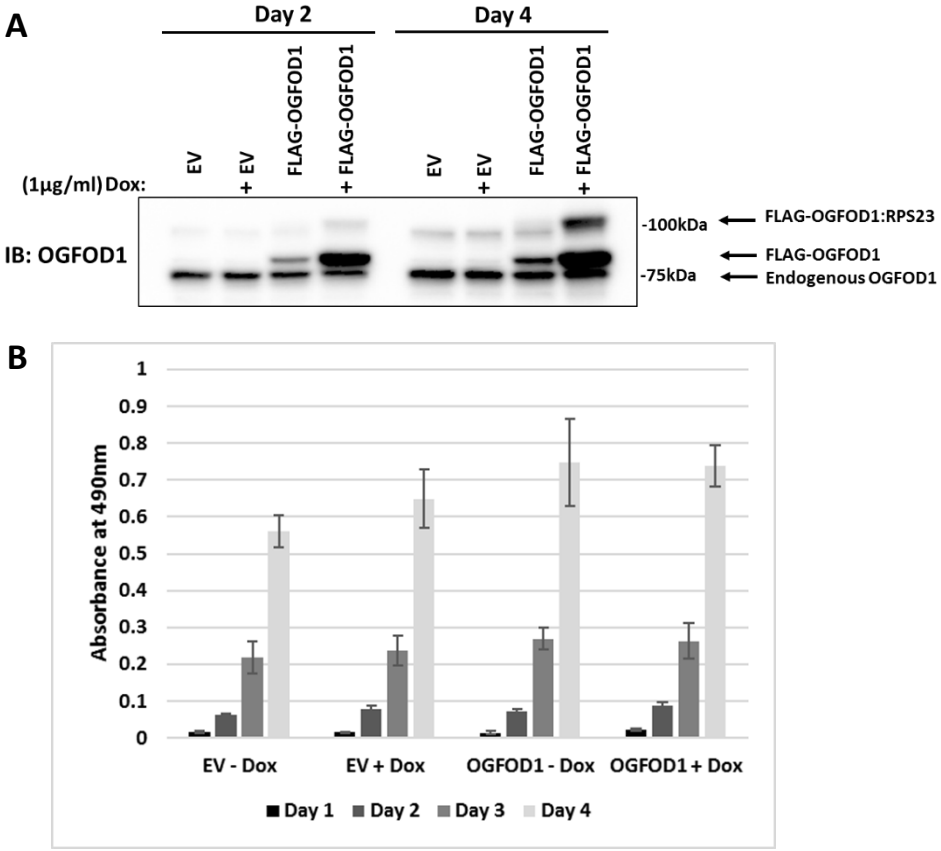


Figure 3.3: Cell proliferation in HEK293 cells is not affected by acute OGFOD1 overexpression. A) HEK293 T-REx cells expressing either empty vector (EV) or FLAG-OGFOD1 were treated with doxycycline (1 µg/ml) for the indicated times. Immunoblot using anti-OGFOD1 antibody indicates induction of FLAG-OGFOD1 (~80 kDa) relative to endogenous OGFOD1 (75 kDa) in the presence of doxycycline. OGFOD1:RPS23 100 kDa complex was observed in doxycycline treated inducible FLAG-OGFOD1 expressing cells. Presence of FLAG-OGFOD1 expression in the absence of doxycycline indicates some "leaky" expression in this system. **B)** HEK293 T-REx cells expressing either empty vector (EV) or FLAG-OGFOD1 were treated with doxycycline (1 µg/ml) and an MTS cell proliferation assay was performed. No clear effect was observed on cell growth over the 4-day time course in response to OGFOD1 overexpression, and no effect was observed in the empty vector expressing cells following doxycycline treatment.

3.2.4 Characterisation of inducible OGFOD1 re-expression in OGFOD1 knockout cells.

To consider the effect of inducible ectopic OGFOD1 re-expression on cellular growth, HEK293 OGFOD1 CRISPR-derived knockout cells (clone 'DSB' from chapter 2) were lentivirally transduced with a tetracycline-inducible transfer vector (pTRIBZ) encoding FLAG-OGFOD1. Transduced cells were selected with blasticidin and clones were isolated by serial dilution prior to screening for clones with tight regulated re-expression. For the screening procedure, 6 different clones ("a-f") were incubated in the presence or absence of doxycycline for 3 days. Immunoblotting cell lysates with anti-OGFOD1 antibody demonstrated that not all of the clones re-expressed FLAG-OGFOD1 (Figure 3.4A). Despite this, a number of FLAG-OGFOD1 re-expressing clones were obtained and, in contrast to the T-REx system (Figure 3.3A), no evidence for "leaky" FLAG-OGFOD1 expression was observed in the absence of doxycycline (Figure 3.4A). Clone 'f' was selected for further characterisation and phenotypic analysis based on the high re-expression level of FLAG-OGFOD1 relative to other clones.

Before assaying for effects of OGFOD1 re-expression on proliferation, I sought to better characterise clonal subline "f". Two related experiments were performed. In the first, I assessed the heterogeneity of FLAG-OGFOD1 re-expression within the clonal population by anti-OGFOD1 immunofluorescent staining. Cells were incubated in the presence or absence of doxycycline for 3 days prior to fixation and confocal immunofluorescence-based imaging. Consistent with the immunoblot data, OGFOD1 was not detected in untreated (-Dox) cells (Figure 3.4B). In the presence of doxycycline (+Dox) a robust induction of nuclear OGFOD1 expression was observed in the vast majority of cells, though clusters of DAPI positive nuclei that showed no appreciable OGFOD1 signal were observed (as indicated by arrow; Figure

3.4B, bottom right panel). In the second, I sought to confirm that OGFOD1 re-expression restored RPS23 hydroxylation. I harvested cells at timed intervals of up to 1 week following exposure to doxycycline and performed RPS23 immunoblots comparing the ratio of non-hydroxylated RPS23 to total levels (pan-RPS23). Lysates derived from wild-type (parental) and OGFOD1 CRISPR-derived knockout HEK293 cells served as reference controls. Despite some variability in protein loading as determined by Coomassie staining, comparative immunoblotting revealed that 3 days of doxycycline treatment in FLAG-OGFOD1 re-expressing cells resulted in near complete suppression of non-hydroxylated RPS23 which persisted over the duration of the experiment (Figure 3.4C). At the 3-day interval, the ratio of non-hydroxylated RPS23 signal to total RPS23 signal in the re-expressing cells was comparable to that observed in parental (wild-type) HEK293 cells and indicates that if, as suggested by the immunofluorescence (Figure 3.4B), some cells within the population are not expressing FLAG-OGFOD1 then it is a relatively minor fraction. An additional and notable point is that re-expressed levels of FLAG-OGFOD1 in clone 'f' were significantly higher than endogenous OGFOD1 in wild-type (parental) cells, indicating that this model provides a setting in which the dynamic range of OGFOD1 expression is at its largest.

This system enabled the controlled regulation of OGFOD1 expression and therefore, effects on RPS23 hydroxylation and cellular proliferation could now be correlated within an isogenic context. To control for an effect of doxycycline, OGFOD1 knockout cells were transduced with pTRIBZ empty vector (EV) and clones were selected using blasticidin in a similar method. One population of cells were placed into doxycycline-containing medium whilst the other remained untreated. The effect of OGFOD1 re-expression on cell growth was assessed by MTS assay using different intervals of doxycycline (pre)-treatment. The starting point of the MTS assay was either immediately following administration of doxycycline (+) or after three-days pre-treatment in doxycycline (PT) (Figure 3.5). The assay was designed in this

way to capture effects of acute OGFOD1 re-expression and, in addition, uncover signals that are dependent upon the restoration of RPS23 hydroxylation.

Immunoblotting for FLAG-OGFOD1 using anti-FLAG antibody demonstrated robust induction of FLAG-OGFOD1 in clone "f" cells exposed to doxycycline (Figure 3.5A). Suppression of non-hydroxylated RPS23 was observed in OGFOD1 re-expressing cells by the MTS day 1 timepoint in cells that had been exposed to doxycycline for 3 days. For OGFOD1 re-expressing cells immediately exposed to doxycycline, suppression of non-hydroxylated RPS23 was observed at the day 4 timepoint. The MTS assay revealed that there was no doxycycline-dependent effect on cell growth over the time course in the empty vector expressing cells (Figure 3.5B). No effect from OGFOD1 re-expression on cell growth was observed over the 4 days in cells that had been treated for three days with doxycycline or immediately exposed to doxycycline (Figure 3.5C). The results indicate that OGFOD1 re-expression and effects on RPS23 hydroxylation do not alter the proliferative capacity in this cell context or at these timepoints.

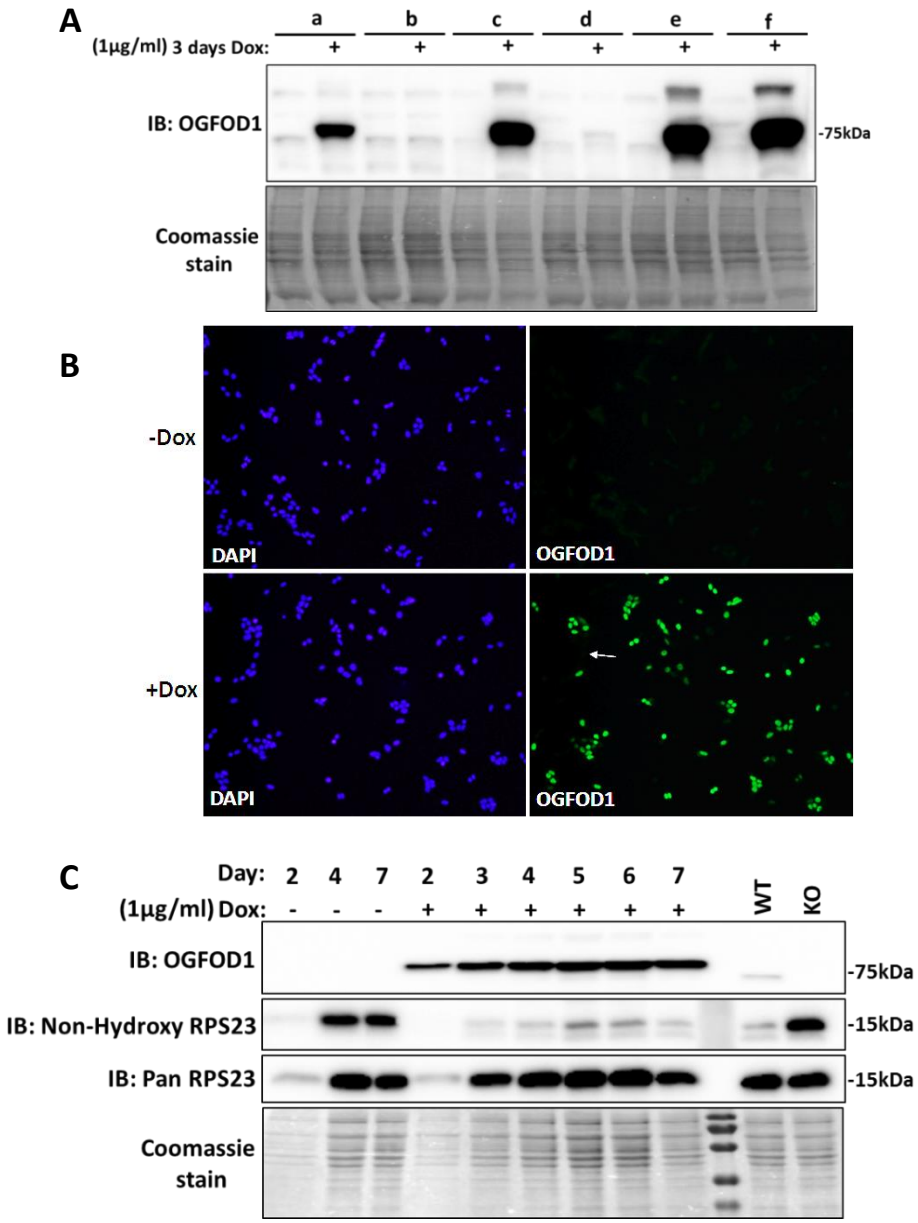


Figure 3.4: Generation of an inducible OGFOD1 re-expressing HEK293 cell line. A) OGFOD1 CRISPR-derived knockout cells were transduced with pTRIBZ FLAG-OGFOD1, selected with blasticidin and clones were isolated by serial dilution. Immunoblotting using anti-OGFOD1 antibody revealed induction of OGFOD1 in clones 'a', 'c', 'e', and 'f' following treatment with doxycycline for 3 days. No evidence for "leaky" expression was observed in the absence of doxycycline. **B)** Clone 'f' was subject to confocal immunofluorescence using anti-OGFOD1 antibody following treatment with doxycycline for 3 days. Immunofluorescence indicates a relatively homogeneous population of re-expressing cells although a number of cells that did not measurably re-express OGFOD1 in the presence of doxycycline were observed (indicated by arrow). **C)** Immunoblots following a doxycycline time course in OGFOD1 re-expressing cells (clone 'f'). Anti-OGFOD1 antibody indicates re-expression of OGFOD1 following 2 days of doxycycline treatment. Anti-non-hydroxylated RPS23 antibody demonstrates suppression of non-hydroxylated RPS23 in response to OGFDO1 re-expression by day 3.

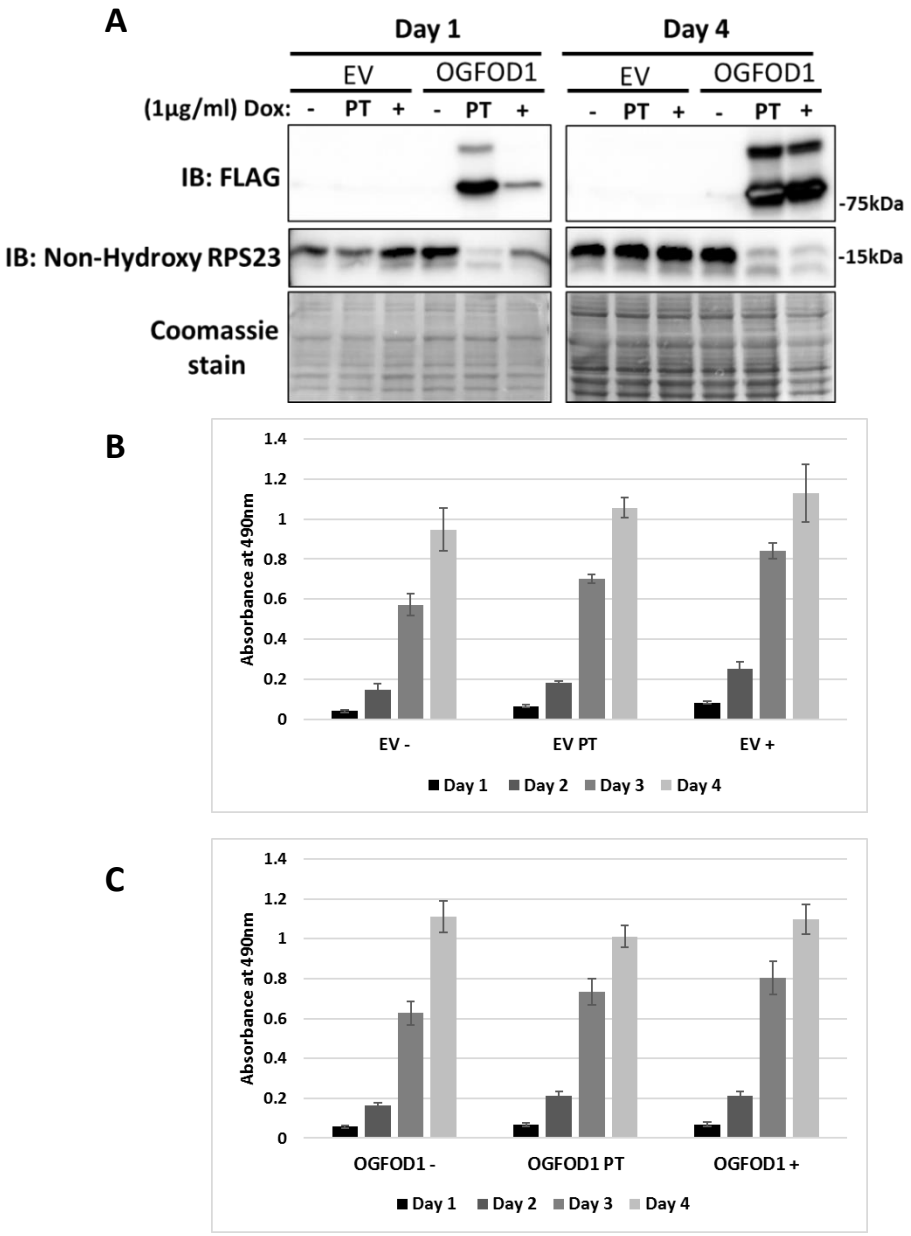


Figure 3.5: OGFOD1 re-expression in HEK293 cells does not confer a proliferation advantage or disadvantage. OGFOD1 knockout cells were transduced with either empty vector (EV) or OGFOD1 (clone 'f') following doxycycline treatment (1 µg/ml) for the indicated times. Cells were either untreated (-), treated at the time of plating (+) or pre-treated with doxycycline for 3 days (PT). Immunoblot using anti-FLAG antibody indicates OGFOD1 re-expression in the pre-treated and treated OGFOD1 re-expressing cells. Anti-non-hydroxylated RPS23 antibody indicates inhibition of non-hydroxylated RPS23 at the day 1 and day 4 timepoints for pre-treated and treated OGFOD1 re-expressing cells. **B)** MTS cell proliferation assay of empty vector re-expressing cells indicates no evidence for a growth effect in the OGFOD1 knockout cells in response to doxycycline treatment over the 4-day time course. **C)** MTS cell proliferation assay of OGFOD1 re-expressing cells indicates no clear growth effect in response to OGFOD1 re-expression over the 4-day time course.

3.2.5 Characterisation of inducible OGFOD1 re-expression under conditions of serum deprivation.

The effect of OGFOD1 expression on cellular growth has thus far been performed under steady state nutrient replete conditions. One possibility is that OGFOD1 may serve as a regulator of proliferation under conditions of cellular stress. In support of this hypothesis, Saito et al., reported that OGFOD1 loss resulted in increased cell viability under conditions of ischaemic stress (low glucose and hypoxia) (Saito et al., 2010). To explore the role of OGFOD1 in the maintenance of cell growth under conditions of cellular stress, OGFOD1 inducible re-expressing HEK293 cells were subject to conditions of combined low glucose and hypoxia, amino acid deprivation or serum starvation.

For the majority of cell lines, fetal bovine serum is a supplement to normal cell culture media, and acts to provide optimal conditions to support cellular growth. It is a complex mixture that contains various components including: growth factors, proteins, trace elements, vitamins, amino acids, lipids, and hormones (van der Valk et al., 2010). Protein synthesis is co-ordinated by the mammalian target of rapamycin (mTOR) pathway which is regulated by the abundance of nutrients and growth factors. As a result, serum starvation suppresses the mTOR pathway that leads to inhibitory effects on protein synthesis (Pirkmajer et al., 2011).

It was hypothesised that OGFOD1 expression may have an important regulatory role that is directed though RPS23 under conditions in which protein synthesis is reduced. Therefore, to determine whether OGFOD1 status alters the proliferative capacity under conditions of serum starvation, an MTS assay was performed in the HEK293 knockout inducible re-expression system. To investigate the effect of serum deprivation, the pre-treatment protocol was used in which OGFOD1 inducible re-expressing HEK293 cells (Clone ‘f’: Figure

3.4A) were exposed to doxycycline for 3 days before plating into media containing different concentrations of serum. To consider the possibility that an OGFOD1-dependent phenotype could be exacerbated in conditions of severe serum starvation, different concentrations of both complete (but tetracycline-free) serum and dialysed serum (providing a 10 kDa molecular weight cut-off) were compared in parallel. No doxycycline-dependent growth effects were observed in OGFOD1 knockout cells transduced with pTRIBZ empty vector (Figure 3.5) and, therefore, these cells were omitted for subsequent analyses. OGFOD1 re-expressing cells were harvested at the start (day 1) and end (day 4) of the MTS assay (Figure 3.6A and 3.6B, respectively) and immunoblotting with anti-FLAG antibody revealed consistent induction of OGFOD1 in the presence of doxycycline at the differing serum percentages. Immunoblotting with an anti-non-hydroxylated RPS23 antibody indicated that RPS23 hydroxylation was restored by the day 1 timepoint (4 days in doxycycline) and remained hydroxylated by the day 4 timepoint (7 days in doxycycline). Immunoblotting with an anti-RPS23 antibody indicated that total RPS23 levels broadly correlated with changes in protein loading as assessed by Coomassie staining (Figure 3.6A and 3.6B). Marked inhibitory effects on cell growth were observed by the day 4 timepoint with 0.5% serum and it was noted this was reflected in the reduced protein loading (Figure 3.6B). Furthermore, protein lysates were not obtained for 'no serum' conditions at the day 4 timepoint due to spontaneous detachment of the cells, which could therefore not be harvested.

The MTS proliferation assay was performed across a range of serum concentrations with either tetracycline-free serum or dialysed serum (Figure 3.6C and 3.6D, respectively). OGFOD1 knockout and re-expressing cells failed to grow over the 4-day time course in 'no serum' conditions. As anticipated, cell proliferation rates increased with increasing concentrations of serum (Figure 3.6C and 3.6D). As expected, cell proliferation appeared suppressed in the dialysed serum relative to the tetracycline free serum. No clear and

consistent differences were observed between untreated and doxycycline-treated cells (OGFOD1 knockout and OGFOD1 re-expression) in media containing differing concentrations of tetracycline-free serum or dialysed serum. Therefore, the results indicate that OGFOD1 expression does not mediate a proliferative effect under conditions that alter protein translation. It was noted that cell proliferation was moderately reduced in the presence of doxycycline at the day 4 timepoint (7 days in doxycycline) in both tetracycline-free serum and dialysed serum at 10%. However, the initial MTS assay performed with 10% tetracycline-free serum under replicate conditions did not result in clear growth inhibitory effects so any such effect appeared to be inconsistent (Figure 3.5).

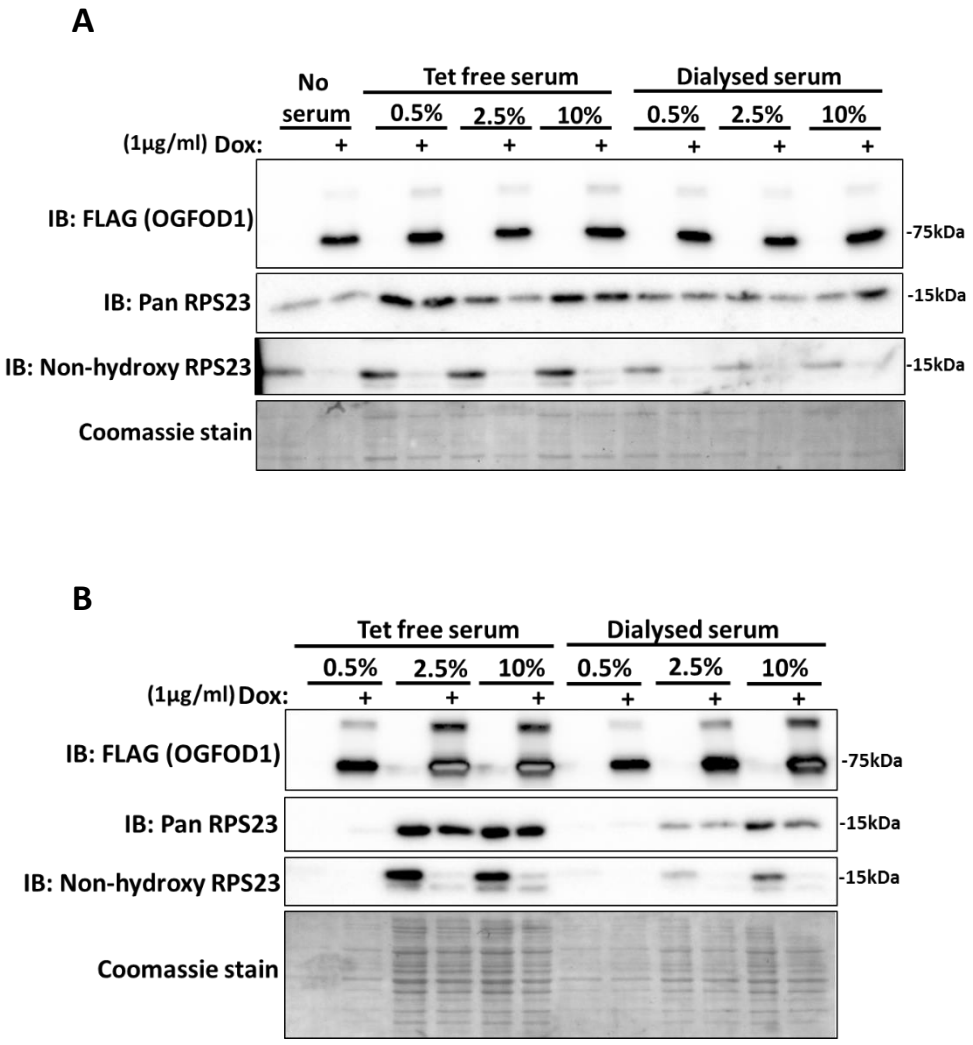


Figure 3.6: Proliferation of HEK293 cells is not affected by OGFOD1 expression under conditions of serum starvation. OGFOD1 re-expressing HEK293 cells (clone 'f') were pre-treated with doxycycline for 3 days before plating into media containing differing percentages of tetracycline-free (Tet free) serum or dialysed serum. Lysates were harvested at day 1 **(A)** and day 4 **(B)** following doxycycline pre-treatment. Anti-FLAG antibody indicates induction of OGFOD1 in the doxycycline treated cells and suppression of non-hydroxylated RPS23 using anti-non-hydroxylated RPS23 antibody.

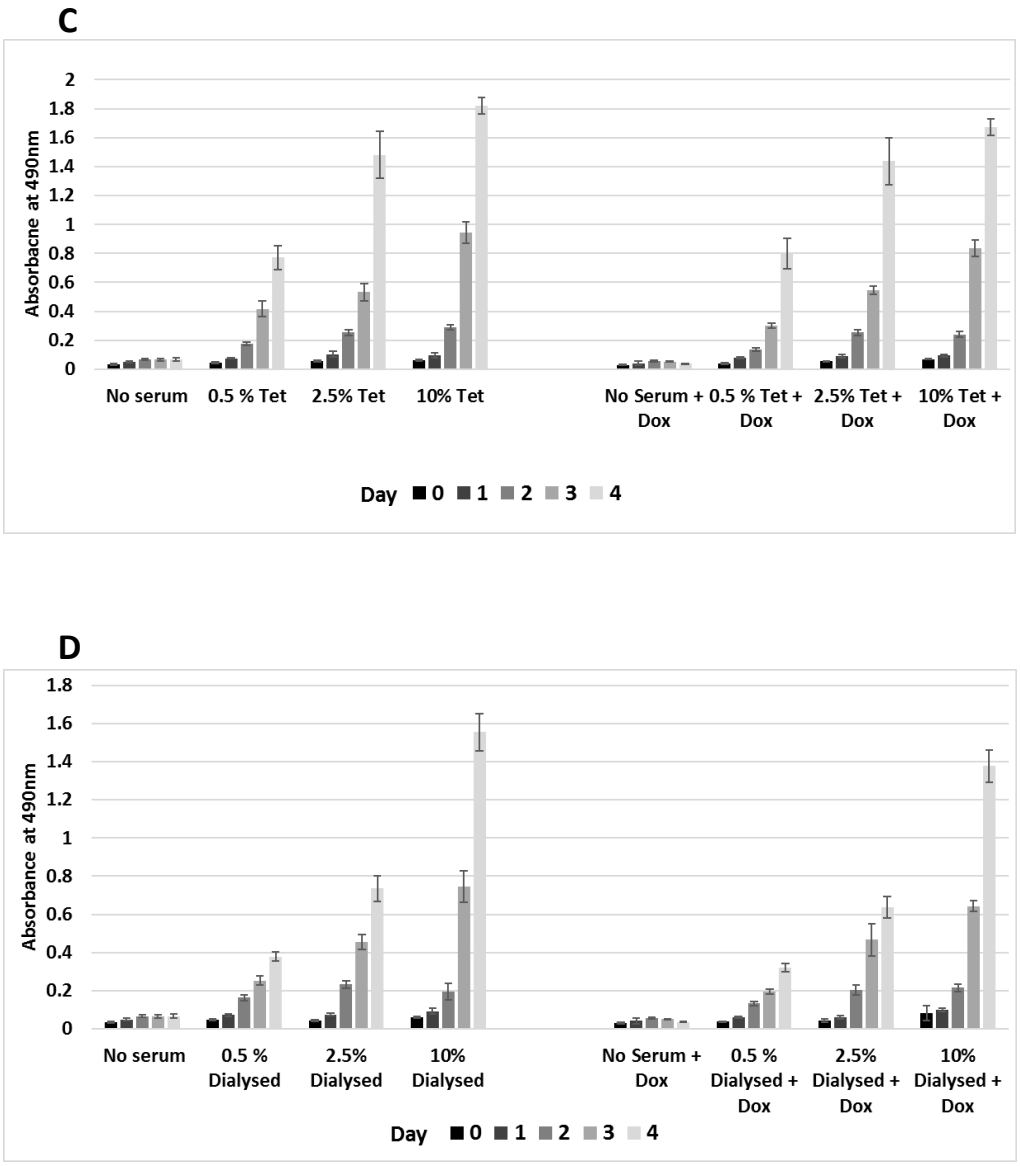


Figure 3.6 (Continued): Proliferation of HEK293 cells is not affected by OGFOD1 expression under conditions of serum starvation. MTS cell proliferation assay of OGFOD1 knockout or re-expressing cells (+Dox) indicates no clear growth effect in response to OGFOD1 re-expression under conditions of tetracycline-free 'tet' serum starvation **(C)** or dialysed serum starvation **(D)** over the 4-day time course. A moderate inhibition of cell proliferation is apparent in OGFOD1 re-expressing cells under standard serum conditions (10%) at day 4 for both tetracycline-free and dialysed serum.

3.2.6 Characterisation of inducible OGFOD1 re-expression under conditions of glutamine deprivation.

Proliferating cells place a demand on metabolic pathways to provide sufficient biosynthetic precursors that can be used for anabolic processes (Shanware et al., 2014). Among these metabolic dependencies is the increased use of the amino acid glutamine, which provides a carbon source for the tricarboxylic acid (TCA) cycle (Son et al., 2013). Glutamine is converted to glutamate by glutaminase, and to 2-oxoglutarate by glutamate dehydrogenase. Although glutamine can be synthesised *de novo* from glucose, many cells require exogenous supply. Glutamine starvation has also been reported to mediate eIF2α phosphorylation through activation of the GCN2 kinase with consequent inhibition of protein translation (Harding et al., 2003; Boukhettala et al., 2012). Therefore, glutamine starvation would provide an independent translational stress that would help to determine whether the cells show any sensitisation to eIF2α phosphorylation in an OGFOD1-dependent manner.

To determine whether OGFOD1 status modulates cellular proliferation under glutamine starvation an MTS assay was performed using established doxycycline treatment protocols. OGFOD1 inducible re-expressing HEK293 cells (Clone 'f': Figure 3.4B) were treated in the presence or absence of doxycycline for 3 days before plating into media containing different concentrations of glutamine. The recommended concentration of glutamine for optimal growth of HEK293 cells is 4 mM (www.atcc.org). Therefore, a dose titration of glutamine from nil to 12 mM was investigated. Protein lysates were prepared at the start (day 1) and end (day 4) of the MTS assay, and immunoblotting with anti-FLAG antibody was performed to confirm OGFOD1 induction in the doxycycline-treated cells across the dose titration of glutamine (Figure 3.7A and 3.7B, respectively). Culturing cells in the absence of glutamine

was highly cytotoxic as reflected by the reduced protein loading that was determined by Coomassie staining. Results from the MTS assay indicated that reduction of glutamine below 1 mM inhibited cell proliferation independent of OGFOD1 status. Modest differences in growth at higher concentrations of glutamine (1 mM and above) were observed with doxycycline-treated (OGFOD1 re-expressing) cells displaying reduced MTS signal at the final day 4 timepoint. However, the response was variable across the concentration range. Moreover, as similar variability was seen at 4 mM glutamine between replicate experiments (Figures 3.5-3.6), I decided not to pursue the phenotypic response to modulation of glutamine levels any further.

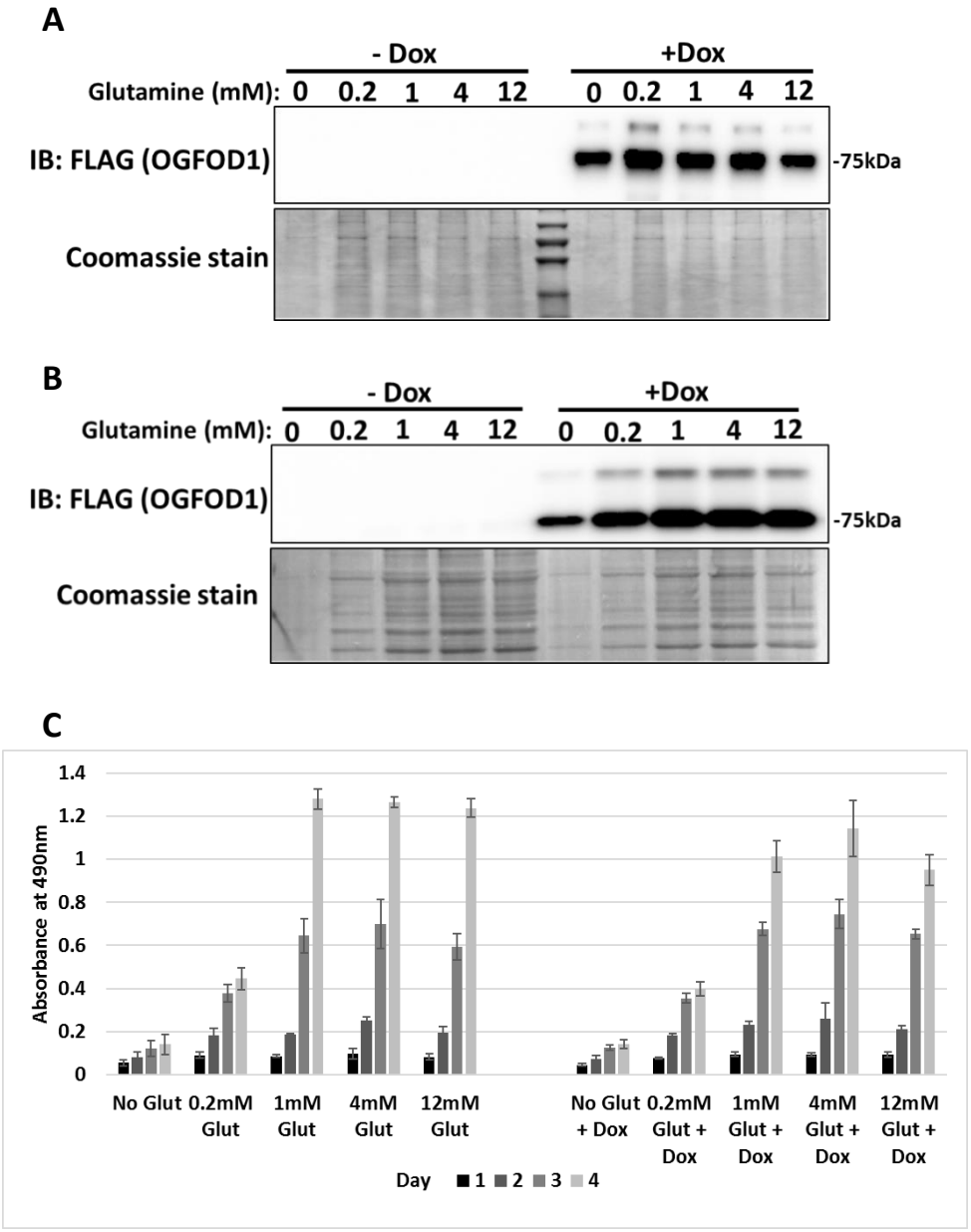


Figure 3.7: Proliferation of HEK293 cells is not affected by OGFOD1 expression under conditions of glutamine deprivation. OGFOD1 re-expressing HEK293 cells (clone 'f') were pre-treated with doxycycline for 3 days before plating into media containing differing concentrations of glutamine. 4 mM of glutamine is the recommended concentration for optimal growth of HEK293 cells. Lysates were harvested at day 1 **(A)** and day 4 **(B)** following doxycycline pre-treatment. Anti-FLAG antibody indicates induction of OGFOD1 in the glutamine deprived cells. **C)** MTS cell proliferation assay of OGFOD1 knockout versus OGFOD1 re-expressing cells (+Dox). No clear growth effect was observed in response to OGFOD1 expression under conditions of severe glutamine starvation over the 4-day time course. A moderate inhibitory effect on cell proliferation at day 4 is apparent in OGFOD1 re-expressing cells at higher concentrations of glutamine (1 mM, 4 mM and 12 mM).

3.2.7 Characterisation of inducible OGFOD1 re-expression under ischemia mimetic conditions.

Mammalian cells have an ongoing requirement to maintain oxygen homeostasis to support aerobic metabolism for energy production (Shohet et al., 2007). Restriction of tissue blood flow causes a reduction in cellular oxygen levels and deprivation of metabolic nutrients, including glucose, resulting in a stress known as ischaemia. A study by Saito et al. reported that OGFOD1 loss resulted in significant resistance to cell death under ischemic conditions (Saito et al., 2010). The authors performed OGFOD1 knockdown by siRNA in HeLa cells and generated OGFOD1-defective cells by genetic mutation in Nalm6 cells. For genetic mutation, exons 5-8 in OGFOD1 were disrupted by substitution with hygromycin and puromycin resistance genes through homologous recombination (Saito et al., 2010). In both systems OGFOD1 loss was associated with an increase in cell viability as assessed by an MTS cell proliferation assay. Given that the effects from OGFOD1 loss by genetic inactivation or siRNA are consistent across different cell types, it was hypothesised that the OGFOD1 knockout cells derived through the CRISPR methodology with inducible re-expression would enable greater dynamic range of OGFOD1 expression that would help to explore this phenotype.

To investigate the role of OGFOD1 in regulating proliferation and viability under conditions of ischaemic stress, OGFOD1 inducible re-expressing HEK293 cells were utilised. Cells were pre-treated with doxycycline for 3 days to ensure restoration of RPS23 hydroxylation, prior to the commencement of the MTS cell proliferation assay. I compared the response to varying glucose levels (low, 1 g/L; high 4.5 g/L), hypoxia (1% oxygen, 0.1% oxygen) or a combination of both over 4 days. Of note, the combination of 0.1% hypoxia and 1 g/L low

glucose replicates ischaemic conditions that elicited a protective response in OGFOD1 defective cells (Saito et al., 2010).

In normoxic (21%) conditions and using standard high glucose medium (4.5 g/L glucose) cell proliferation increased over the 4-day time course, with no discernible effect from OGFOD1 re-expression (Figure 3.8A). As anticipated glucose starvation was associated with reduced cell growth in normoxia (Figure 3.8A). Interestingly, an effect from OGFOD1 re-expression was observed at day 4 in low glucose and normoxic conditions with a moderate decrease in growth relative to cells which were not treated with doxycycline. Combined glucose starvation and oxygen deprivation was associated with a further reduction in cell growth relative to normoxic conditions (Figure 3.8B and 3.8C relative to Figure 3.8A). A moderate decrease in cell proliferation was observed in the OGFOD1 re-expressing cells at day 4 in high glucose and 1% hypoxia (Figure 3.8B), however, this was not replicated at 0.1% hypoxia (Figure 3.8C). In contrast to Saito et al., OGFOD1 re-expression did not appear to have a clear effect on the proliferation of cells under similar conditions of ischemic stress. Saito et al., reported a modest increase in cell viability in response to OGFOD1 loss under conditions of low glucose and 0.1% hypoxia. It was predicted that the OGFOD1 re-expression model would induce a much greater phenotypic response given that OGFOD1 is highly expressed in this system, however the results were not consistent with this hypothesis. Overall, the results have highlighted the complexities in defining a robust phenotype in response to acute changes in OGFOD1 expression.

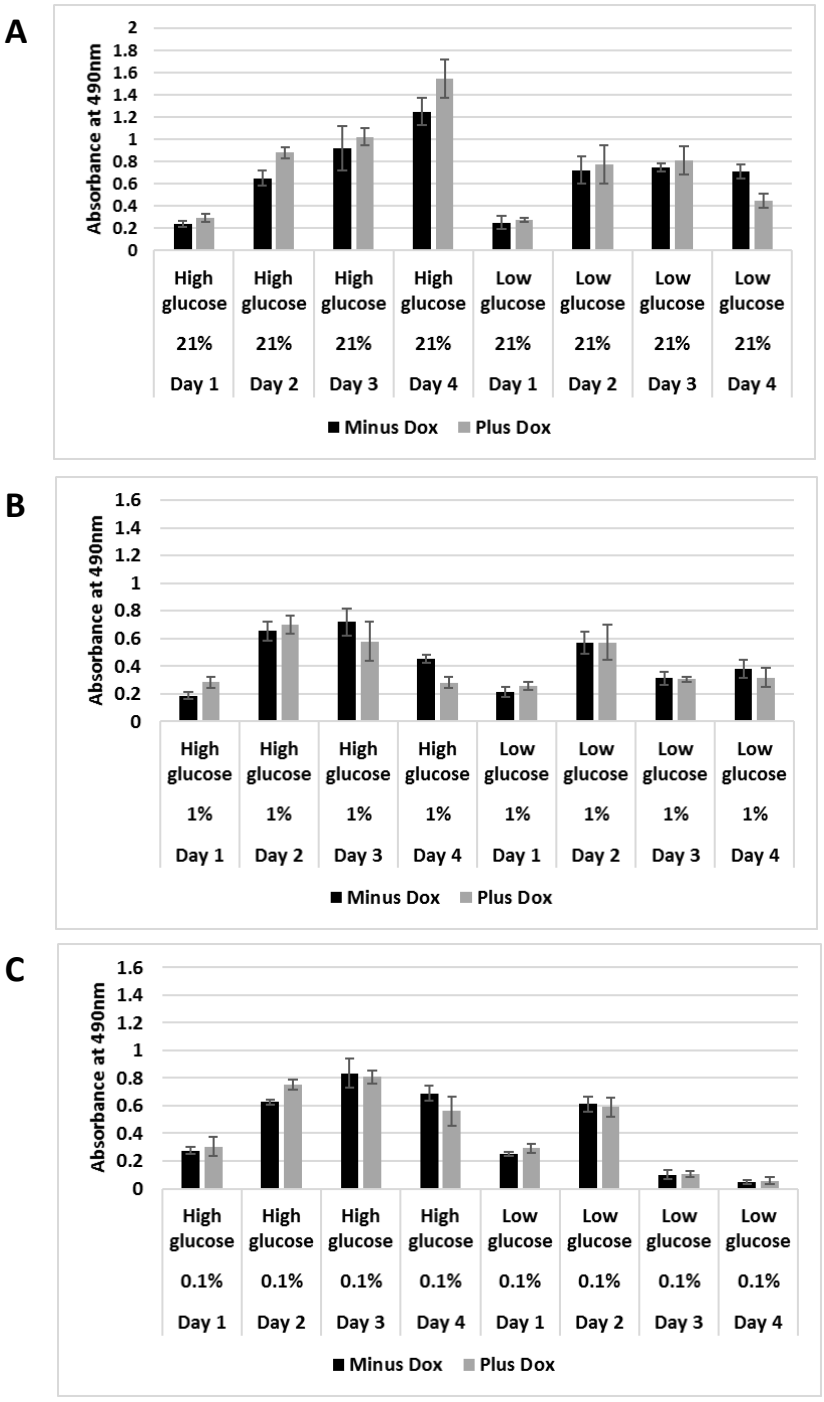


Figure 3.8: Proliferation of HEK293 cells is not affected by OGFOD1 expression under conditions of ischemic stress. OGFOD1 re-expressing HEK293 cells (clone 'f') were pre-treated with doxycycline for 3 days before plating into high glucose (4.5 g/L) or low glucose (1 g/L) containing media. Cells were placed under conditions of normoxia: 21% oxygen, **(A)**, or hypoxia: 1% oxygen **(B)**; 0.1% oxygen **(C)**. Cell proliferation was assessed using the MTS assay. No clear growth effect was observed in response to OGFOD1 levels under ischemic (low glucose and hypoxic) conditions.

3.3 Discussion

Work described in this chapter sought to determine if rapid changes in OGFOD1 status provoked alterations in cell proliferation under basal and stressed conditions. The rationale for this was based on the findings from independent groups who have reported large reductions in cell proliferation following suppression of OGFOD1 by RNAi (Wehner et al., 2010; Singleton et al., 2014; Katz et al., 2014; Kustatscher et al., 2014; Kim et al., 2015). As described in chapter 2, these data appeared inconsistent with my findings in sublines of OGFOD1 knockout cells that were derived by CRISPR methodology. This led to the proposal that the cells were responding to change, and that it was a change in OGFOD1 level that was responsible for the reported proliferative defects.

To explore this possibility, a variety of systems were developed to enable both suppression of OGFOD1 by shRNA and rapid upregulation from physiological levels or from a knockout cell line, using tetracycline-inducible vectors expressing OGFOD1. These interventions were tested in cells either in normal culture conditions or under stress conditions through nutrient deprivation. The central hypothesis underpinning this work was that modulation of nutrient sensitive and/or translation stress pathways would interface with OGFOD1 signalling and elicit a robust proliferative phenotype. In support of this, Saito et al. reported a protective action of OGFOD1 inhibition in response to ischaemic stress (Saito et al., 2010).

Unexpectedly, there appeared to be no correlation between OGFOD1 suppression by three lentiviral shRNA vectors and effects on cellular proliferation as assessed by an MTS proliferation assay (Figure 3.2). Suppression of RPS23 hydroxylation, as determined using the generated anti-non-hydroxylated RPS23 antibody (Figure 3.1), did not correlate with effects on growth. Similarly, no effect from acute OGFOD1 overexpression or OGFOD1 re-expression on cellular proliferation was observed (Figure 3.3 and 3.5). Finally, I observed no

clear effect of OGFOD1 status on cellular proliferation under conditions of cellular stress including: serum deprivation (Figure 3.6), glutamine deprivation (Figure 3.7) or using an ischaemic cell culture model (Figure 3.8). Overall, these findings did not generate a coherent picture of an action of OGFOD1 on the control of cell proliferation. Saito et al., reported that OGFOD1 loss increased cell viability using a cell culture model of ischaemia (Saito et al., 2010). However, the OGFOD1-inducible re-expressing HEK293 cells, which provided a greater dynamic range of OGFOD1 expression within an isogenic context, did not recapitulate these findings.

A modest decrease in proliferation irrespective of cellular stress was observed at day 4 when OGFOD1 was overexpressed: Figure 3.6C (10% tetracycline-free serum), Figure 3.6D (10% dialysed serum), Figure 3.7C (12 mM glutamine), Figure 3.8A (low glucose, 21% O_2) and Figure 3.8B (high glucose, 1% O_2). The mild phenotypic differences observed following OGFOD1 overexpression may in part be linked to increased sequestration of RPS23 by OGFOD1. Therefore, one possibility is that the growth phenotype could become more severe if, for example, RPS23 biogenesis was progressively reduced.

It is possible that further exploration of specific conditions would reveal an OGFOD1-dependent phenotype. However, the conditions explored were diverse and only very small effects were observed. It seems therefore unlikely that OGFOD1 plays a direct role in the control of cell proliferation. One possibility is that the effects previously observed had been generated by indirect actions that are highly context specific. RNAi has been reported to induce a broad spectrum of off-target activity through interacting with unintended mRNAs through partial sequence complementarity (Jackson et al., 2010). Certain siRNA or shRNA sequences have been shown to induce cytotoxicity through an unknown mechanism or trigger immune responses via binding to toll like receptors (Fedorov et al., 2006; Hornung et al., 2005). To investigate the potential for off-target mediated effects, further work to test a

spectrum of individual OGFOD1 siRNA or shRNA targeting sequences may be warranted. However, results from the various studies were obtained using several different individual and pooled siRNA sequences or shRNA sequences (Wehner et al., 2010; Singleton et al., 2014; Katz et al., 2014; Kustatscher et al., 2014; Kim et al., 2015).

A second possibility is that the cells used in the described assays had somehow lost the ability to respond to the signals that OGFOD1 may be generating. OGFOD1-defective cells that were generated through the CRISPR methodology had been selected after a two-week period during which compensatory mechanisms may have occurred. An inducible OGFOD1 expressing cell line generated in OGFOD1 wild-type cells could be used to overcome potential compensatory mechanisms. In this strategy, the inducible OGFOD1 expressing cell line would be maintained in the presence of doxycycline during the process of CRISPR-Cas9 gene editing of OGFOD1. The removal of doxycycline after clonal isolation would then provide rapid loss of OGFOD1 in the absence of a selection period.

Overall, the strategies utilised in this chapter did not capture a clear OGFOD1-dependent function. Therefore, a different approach was considered and the role of OGFOD1 in a clinically relevant setting was investigated to provide further insight into OGFOD1 function on RPS23.

Chapter 4: Investigating the effect of a disease mutation on RPS23 hydroxylation

4.1 Introduction and aims of the chapter

The cellular studies described in chapters 2 and 3 did not provide clear insights into OGFOD1 function. The striking evolutionary conservation of OGFOD1 supports an important non-redundant function that might not have been captured in HEK293 cells, a transformed cell line which might have lost the ability to respond to OGFOD1-dependent signals. During the course of this work, a heterozygous mutation in RPS23 was identified in a child presenting with numerous dysmorphic features including: a small skull, short stature, thin brittle hair and a developmental delay. Exome sequencing identified a *de novo* missense mutation (arginine-lysine, R67K) in RPS23 in the child, that was absent from both parents. The mutation occurs 5 residues from the Proline-62 hydroxylation site and so it was postulated that the child's mutation might affect RPS23 hydroxylation and potentially provide insights into OGFOD1 and RPS23 functions.

To date, mutations in RPS23 have not been implicated in human disease, however, ribosomopathies have been widely described. Ribosomopathies represent a group of disorders caused by mutations in ribosomal genes, including those involved in ribosomal biogenesis or in the ribosomal proteins themselves (Nakhoul et al., 2014). Diamond-Black fan anaemia (DBA) was the first human ribosomopathy identified, and is typically characterised as an inherited bone marrow failure disorder presenting with reduced erythroid precursors and a macrocytic anaemia (Campagnoli et al., 2008). Around one third of patients also present with craniofacial abnormalities, or malformations in the upper limb, heart or urogenital system. Some of these clinical features are overlapping with clinical

features described in the patient bearing the R67K-RPS23 mutation. However, distinct from DBA, no abnormal haematology results were observed.

An opportunity was presented to work on cells derived from the patient to investigate the effect of the R67K-RPS23 mutation on RPS23 hydroxylation. OGFOD1 retains a high affinity association with hydroxylated RPS23 - forming an SDS-resistant complex at 100 kDa (Singleton et al., 2014). The OGFOD1:RPS23 100 kDa adduct is inhibited by hydroxylase inhibitors, such as dimethyloxalylglycine (DMOG) and can be used as a surrogate for effects on RPS23 hydroxylation. The effect on the OGFOD1:RPS23 100 kDa adduct will be assessed in the mutant RPS23 patient cells. Using cells derived from the patient carrying the R67K-RPS23 mutation, together with an overexpression model, this chapter aims to determine the effect of OGFOD1 binding to mutant RPS23 and the consequence on RPS23 hydroxylation.

4.2 Results

4.2.1 Characterisation of the R67K-RPS23 mutation

The patient RPS23 mutation occurs on Arginine-67 which, as indicated in chapter 1 (Figure 1.4), lies within a highly conserved functional domain of RPS23 that includes the target (Proline-62) hydroxylation site. To test the hypothesis that this mutation alters the ability of OGFOD1 to hydroxylate RPS23, I characterised an EBV-transformed lymphoblastoid cell line (LCL) isolated from patient blood, which was provided by our collaborators. A facile method for assessing OGFOD1 activity is to probe for the presence of the 100 kDa OGFOD1:RPS23 adduct in cells. To this end, I performed parallel OGFOD1 immunoprecipitations in cell lysate derived from patient LCLs carrying the R67K RS23 mutation or related (parent) healthy control cells. Immunoblotting OGFOD1 immunoprecipitates in healthy control LCLs with an OGFOD1 antibody demonstrated efficient capture of endogenous OGFOD1 at 75 kDa in

addition to the high molecular weight OGFOD1:RPS23 adduct at 100 kDa (Figure 4.1A). Strikingly, despite similar capture of OGFOD1 at 75 kDa in the patient cell lysate, a significant inhibition of the 100 kDa adduct was observed. Reduced binding at the 100 kDa adduct could reflect differences in the ability of OGFOD1 to bind and hydroxylate wild-type and mutant RPS23 in the context of the heterozygous RPS23 mutation. Reduced formation of the 100 kDa adduct in patient LCLs occurred in the absence of an inhibitory effect on binding to RPS23 at its native molecular weight of 15 kDa. In fact, a moderate increase in OGFOD1 binding to native RPS23 was observed in the patient LCLs. Overall, this suggests that OGFOD1 is capable of binding mutant RPS23, yet hydroxylation is significantly impaired. To confirm these observations and to assay the effect of the disease-associated mutation on RPS23 binding to OGFOD1 in a discrete cell context, HA-tagged wild-type and R67K RPS23 constructs were co-transfected with FLAG-OGFOD1 into HEK293 cells. FLAG (OGFOD1) immunoprecipitation and immunoblot demonstrated equivalent capture of uncomplexed (~75 kDa) OGFOD1 from cells co-transfected with HA-RPS23 and empty vector (Figure 4.1B). A FLAG-OGFOD1: endogenous RPS23 adduct, which migrates at ~100 kDa by SDS-PAGE, was observed in all FLAG-OGFOD1 immunoprecipitates. In contrast, only wild-type HA-RPS23 co-transfectants displayed an additional (unique) co-precipitating species of slightly reduced mobility by SDS-PAGE (~100 kDa: lane 9 versus lane 8 and 10). HA Immunoblot confirmed the assignment of this species as ectopic HA-RPS23. Importantly, this species was not detected in cells co-transfected with HA-(R67K) RPS23, indicating that the R67K mutation did not support adduct formation in this setting. Consistent with endogenous OGFOD1 immunoprecipitations in patient and control LCLs (Figure 4.1A) capture of the native 15 kDa RPS23 species appeared equivalent between wild-type and R67K RPS23 transfected cells raising the interesting possibility that patient mutation selectively inhibits OGFOD1 dependent catalysis (Figure 4.1B). An unrelated though interesting finding of the work is

that co-transfection of FLAG-OGFOD1 stabilised ectopic HA-RPS23 (both wild-type and R67K variants) (15 kDa: (lanes 4 and 5 versus lanes 1 and 2).

In the process of characterising the effect of the R67K RPS23 mutation on OGFOD1-dependent catalysis, a second unrelated patient was identified that possessed an independent *de novo* mutation in RPS23 corresponding to Phe120Ile (F120I) in human RPS23. The patient presented with a number of overlapping clinical features with that of the R67K patient, including small skull and short stature. Although the F120I mutation is more distally sited, it was postulated that alterations in this residue might similarly alter RPS23 hydroxylation. Patient F120I lymphocytes were not available, so attempts to link the F120I mutation to OGFOD1-dependent catalysis were limited to analysing FLAG-OGFOD1: RPS23 adduct formation with different disease-associated HA-RPS23 variants by co-transfection in HEK293 cells as described previously (Figure 4.1B). In this experiment HA-RPS23 pulldowns were performed, which provided a clearer setting to view the interaction in the absence of competing endogenous RPS23 (Figure 4.1C). In comparing the effect(s) of the different disease-associated mutations on OGFOD1 binding, some differences were apparent. In contrast to R67K, the F120I mutation did not completely inhibit OGFOD1 adduct formation. An appreciable reduction in the amount of F120I adduct co-purifying with FLAG-OGFOD1 was noted when compared to wild-type. However, it is unclear if this effect is secondary to the reduced expression (and associated capture) of HA-tagged F120I mutant. The destabilising effect of the F120I mutant was subsequently attributed to an inhibitory action on ribosome complex assembly (Paolini et al., 2017).

Overall, the data indicate different actions of the disease-associated mutations with respect to OGFOD1 binding and presumably (based on the abundance of the OGFOD1: RPS23 adduct) catalytic activity. An opportunity was presented to work on cells derived from the

patient bearing the R67K mutation, and so efforts were made to directly measure RPS23 hydroxylation by mass spectrometry in this context.

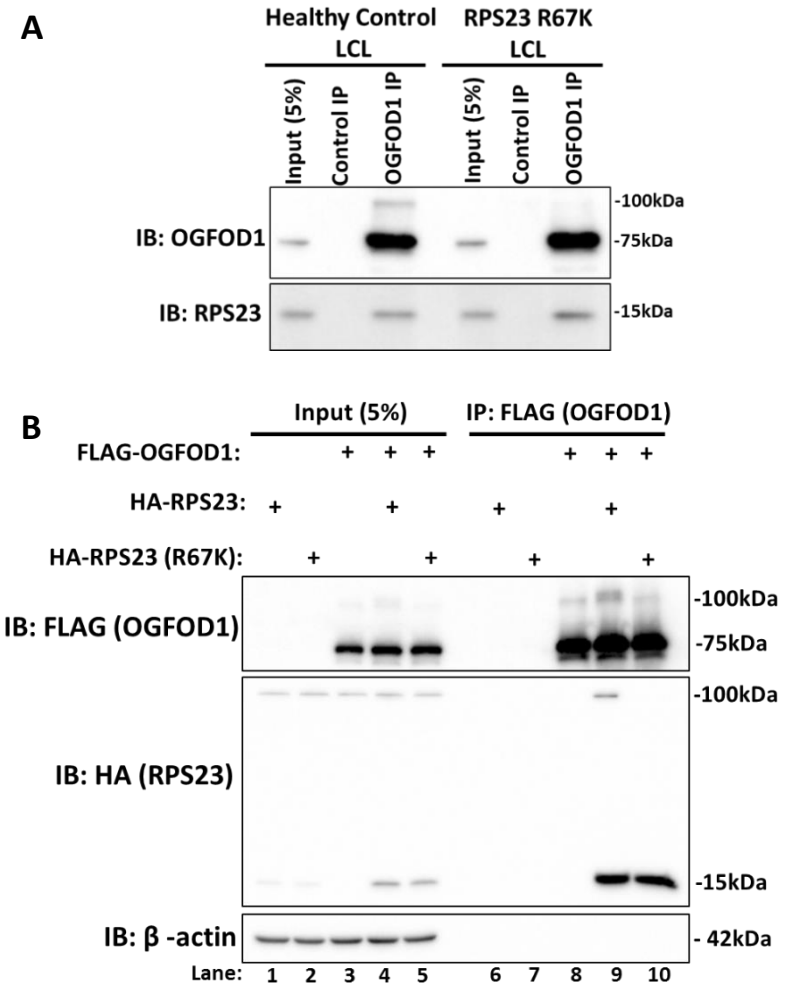


Figure 4.1: RPS23 mutant (R67K) suppresses OGFOD1:RPS23 100 kDa cross-link formation. **A)** Immunoprecipitation using anti-OGFOD1 antibody in healthy control (parent) and R67K-RPS23 patient LCLs. Immunoblotting for OGFOD1 demonstrates capture of OGFOD1 at 75 kDa and presence of the 100 kDa OGFOD1:RPS23 cross link in the healthy control (parent) cells. Capture of OGFOD1 at 75 kDa is observed in the R67K cells, however, the 100 kDa OGFOD1:RPS23 cross link is impaired. Immunoblotting for native RPS23 at 15 kDa indicates equivalent capture between healthy control and R67K cells. **B)** FLAG IP of FLAG-OGFOD1 co-transfected with HA-WT RPS23 or HA-R67K RPS23 in HEK293 cells. Results confirm inhibition of R67K-RPS23 binding at the 100 kDa OGFOD1:RPS23 cross link.

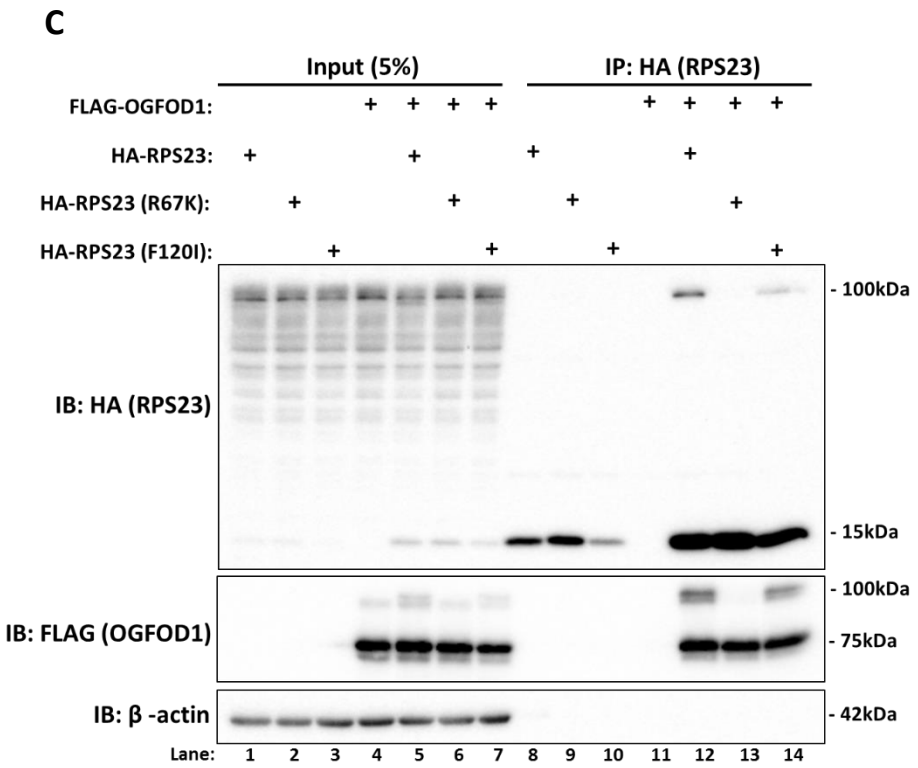


Figure 4.1 (continued): RPS23 mutant (R67K) suppresses OGFOD1:RPS23 100 kDa cross-link formation. C) HA IP of HA-WT-RPS23, HA-R67K-RPS23 or HA-F120I-RPS23 co-transfected with FLAG-OGFOD1 into HEK293 cells. Results support the absence of R67K-RPS23 binding at the 100 kDa cross link and support inhibition of F120I-RPS23 binding at the 100 kDa cross link.

4.2.2 R67K-RPS23 mutation affects RPS23 incorporation into the ribosome and native RPS23 hydroxylation.

To determine the precise effect of the R67K mutation on RPS23 hydroxylation and to assay its ability to be incorporated into the ribosome, endogenous RPS23 was isolated from the ribosomes derived from healthy control (parent) and patient R67K lymphocytes and subject to liquid chromatography-tandem mass spectrometry (LC-MS/MS) analysis. Ribosomes were purified using established protocols from Ge et al., 2012. LCLs were harvested and ribosomes purified by sedimentation through a 25% sucrose cushion. Ribosomal proteins were isolated using reverse phase high-performance liquid chromatography (HPLC) separation; exemplar traces from control and patient lymphocytes are highlighted in Figure

4.2A. Fractions containing RPS23 were identified and corresponding Coomassie stained gel slices were digested with trypsin and analysed by LC-MS/MS (Figure 4.2B).

LC-MS/MS data processing and analysis was performed by Dr. Matthew Cockman and Dr. Roman Fisher (Head of Advanced Proteomics Facility, TDI). The abundance of the mutant peptide in the ribosome was determined by measuring the peak intensities of equivalent wild -type and mutant precursor ions in the patient lymphocytes (Table 4.1). Ion intensities were summed and presented as a percentage relative to wild-type peptides. Interestingly, the results from 5 independent experiments revealed that R67K peptides were far less abundant in the ribosome, with less than 10% of the peptides isolated carrying the R67K mutation (Figure 4.3A). Importantly, RNA sequencing from the LCLs indicated that wild-type and mutant alleles were equally expressed (Paolini et al., 2017). As a result, a mechanism may exist to prevent incorporation of the mutant RPS23 into the ribosome.

In order to extend the observations that R67K impairs the ability to form the OGFOD1:RPS23 100 kDa adduct, mass spectrometry was used to directly quantify the relative level of hydroxylation in R67K mutant RPS23 that is incorporated into the ribosome. Trypsin cleaves both arginine (R) and lysine (K) residues, therefore the R67K mutant preserves trypsin cleavage and is present on all peptides containing the Proline-62 hydroxylation site. This enabled direct measurement of the effect of R67K on RPS23 hydroxylation at the peptide level. Interestingly, quantification of hydroxylation in the patient cells revealed that less than 40% of R67K peptides recovered from the ribosome were hydroxylated (Table 4.1 and Figure 4.3B). In contrast, wild-type peptides from both patient cells and healthy control cells were nearly fully hydroxylated (>95%). In relation to the binding data demonstrating that mutant RPS23 captures equivalent amounts of OGFOD1 relative to wild-type RPS23 (Figure 4.1C), it was noted that wild-type peptides in the patient cells remain hydroxylated.

Therefore, mutant RPS23 is not causing an inhibitory effect on the hydroxylation of wild-type RPS23 peptides.

Overall, the data suggests that the R67K-RPS23 mutation causes an inhibitory effect on hydroxylation and that a mechanism exists to prevent mutant R67K-RPS23 ribosomes from being incorporated into assembled ribosomes.

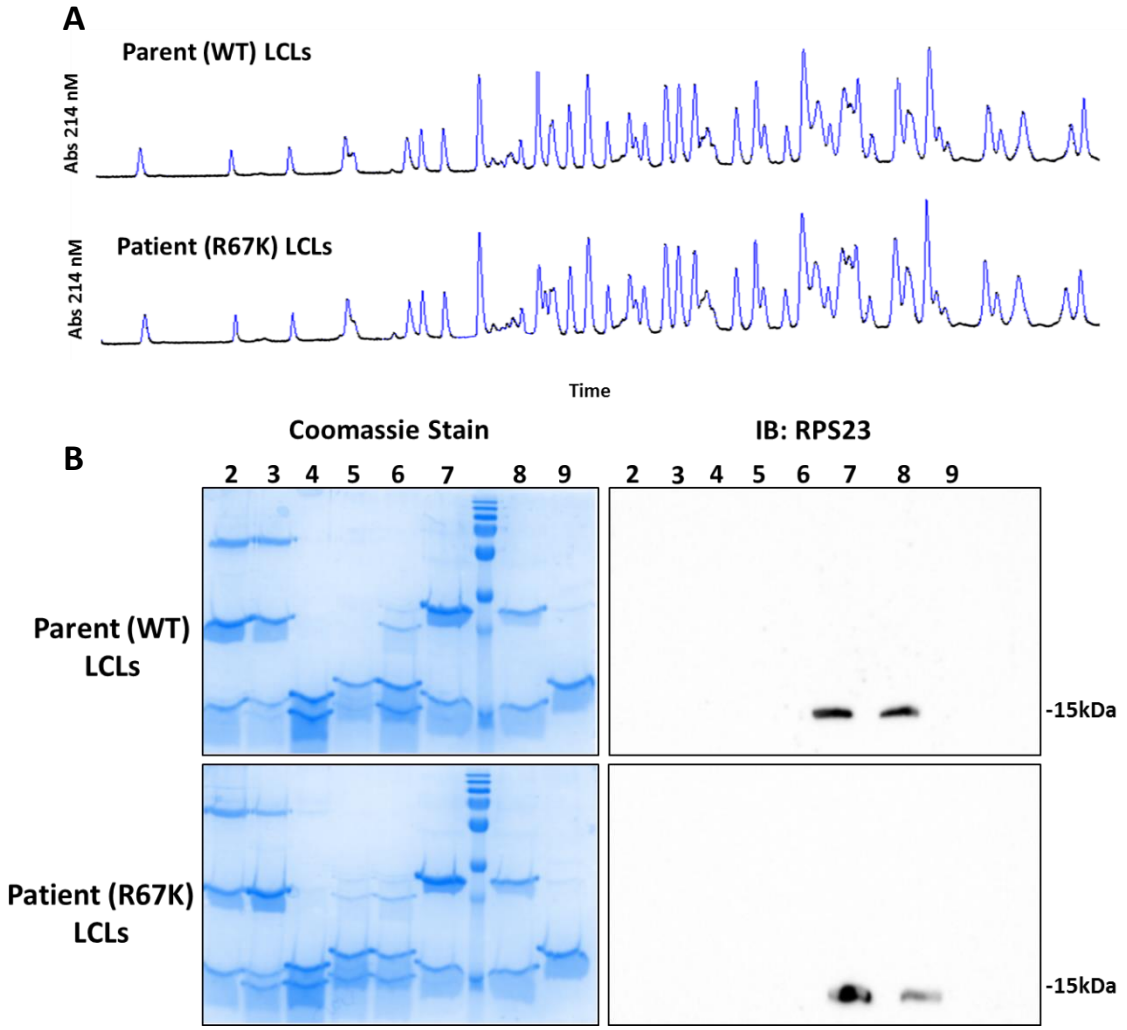


Figure 4.2: Isolation of RPS23 in parent and patient (R67K) LCLs by reverse phase HPLC. A) RPS23 isolation was performed by sucrose sedimentation (25%) and reverse phase HPLC analysis of ribosome isolates (n=3 Parent, n=5 R67K patient). Representative HPLC traces from parent (WT) and patient (R67K) LCLs are shown. **B)** Fractions 2-9 from the HPLC were lyophilised by vacuum centrifugation prior to solubilisation in Laemmli sample buffer and subject to SDS-PAGE followed by Coomassie blue staining. Species corresponding to RPS23 from the fractions were identified by immunoblotting with anti-RPS23 antibody. Fractions containing RPS23 were subject to in-gel proteolysis with trypsin. Representative Coomassie stain and immunoblot from parent and patient (R67K) LCLs is shown.

			Patient #1		Patient #2		Patient #3		Patient #4		Patient #5		Parent #1		Parent #2		Parent #3	
Peptide	PTM		XIC	% OH	XIC	% OH	XIC	% OH	XIC	% OH	XIC	%OH	XIC	%OH	XIC	%OH	XIC	%OH
R67K$_{(61-67)}$: QPNSAIK	N/A	P62	43710931	23.76	16557336	7.75	42539525	16.22	3432651	56.18	2841690	30.00	ND		ND		ND	
		P62(OH)	13619663		1390513		8238296		4401210		1217624		ND		ND		ND	
WT$_{(61-67)}$: QPNSAIR		P62	1.55E+08	97.62	1.8E+08	91.74	110092347	93.64	8876145	96.43	4011135	95.42	7410932	99.57	20995386	99.37	5004462	99.36
		P62(OH)	6.38E+09		2E+09		1621792355		2.4E+08		83597669		1.71E+09		3.32E+09		7.72E+08	
R67K$_{(61-67)}$: QPN(+.98)SAIK	Deamida-tion	P62	8461976		1116866		4067786		<LOD		<LOD		ND		ND		ND	
		P62(OH)	<LOD		<LOD		<LOD		<LOD		<LOD		ND		ND		ND	
WT$_{(61-67)}$: QPN(+.98)SAIR		P62	12451597	98.66	15532138	93.92	12147260	95.22	113152	99.59	<LOD		236018	99.83	508146	99.84	126235	99.89
		P62(OH)	9.18E+08		2.4E+08		242085969		27554399		<LOD		1.38E+08		3.22E+08		1.17E+08	
R67K$_{(61-68)}$: QPNSAIKK	N/A	P62	18054246	51.36	6378251	32.62	27148278	33.91	3310932	49.19	4052663	29.85	ND		ND		ND	
		P62(OH)	19066352		3087923		13930364		3204752		1724121		ND		ND		ND	
WT$_{(61-68)}$: QPNSAIRK		P62	2035855	99.41	21509799	96.19	12728671	97.01	1083592	98.75	1332118	97.25	114308	99.72	1012827	99.60	<LOD	
		P62(OH)	3.43E+08		5.44E+08		412845273		85335560		47078646		40297438		2.52E+08		77266509	
R67K$_{(61-68)}$: QPN(+.98)SAIKK	Deamida-tion	P62	6863261	43.93	1506523	17.70	7019949	24.06	730093	34.45	<LOD		ND		ND		ND	
		P62(OH)	5377766		323901		2223805		383653		<LOD		ND		ND		ND	
WT$_{(61-68)}$: QPN(+.98)SAIRK		P62	2035855	99.41	21509799	96.19	12728671	97.01	1083592	98.75	1332118	97.25	96635	99.76	1012827	99.60	<LOD	
		P62(OH)	3.43E+08		5.44E+08		412845273		85335560		47078646		40297438		2.52E+08		77266509	
R67K$_{(61-68)}$: Q(-17.03)PNSAIKK	Pyro Glu	P62	56287466	45.27	25784318	48.09	362087990	18.21	20336564	40.68	27732217	19.18	ND		ND		ND	
		P62(OH)	46553920		23883498		80596225		13943833		6582410		ND		ND		ND	
WT$_{(61-68)}$: Q(-17.03)PNSAIRK		P62	4004904	99.56	47677962	96.42	80472036	96.76	4198473	98.91	6709067	98.57	1480482	99.23	3543114	99.57	670062	99.77
		P62(OH)	9E+08		1.29E+09		2405777488		3.82E+08		461256756		1.9E+08		8.16E+08		2.95E+08	
R67K$_{(61-68)}$: Q(-17.03)PN(+.98)SAIKK	Pyro Glu & Deamida-tion	P62	10695781	23.28	5083444	46.59	52401445	18.08	3821057	33.58	4432627	14.92	ND		ND		ND	
		P62(OH)	3245022		4433705		11562312		1931990		777557		ND		ND		ND	
WT$_{(61-68)}$: Q(-17.03)PN(+.98)SAIRK		P62	1779982	99.36	13967779	95.42	13864112	96.60	861952	98.54	994880	97.96	248344	99.53	1383368	99.33	404872	99.36
		P62(OH)	2.75E+08		2.91E+08		394466817		58032498		47787081		52363349		2.06E+08		63077048	
R67K$_{(55-67)}$: VGVEAKQPNSAIK	N/A	P62	1148285		<LOD		759023	12.21	<LOD		<LOD		ND		ND		ND	
		P62(OH)	<LOD		<LOD		105591		<LOD		<LOD		ND		ND		ND	
WT$_{(55-67)}$: VGVEAKQPNSAIR		P62	318715	98.17	992445	95.47	1411038	95.51	65955	98.68	59391	99.37	286211	99.36	57382	99.62	59215	99.44
		P62(OH)	17125658		20921637		30017075		4919490		9314962		44151482		15116848		10508507	
R67K$_{(55-67)}$: VGVEAK(+43.01)QPNSAIK	Carbamyl-ation	P62	3155705	44.90	<LOD		<LOD		<LOD		<LOD		ND		ND		ND	
		P62(OH)	2571126		<LOD		<LOD		<LOD		<LOD		ND		ND		ND	
WT$_{(55-67)}$: VGVEAK(+43.01)QPNSAIR		P62	7128477	97.64	1601598	92.92	173019	95.47	<LOD		<LOD		750421	99.56	228580	99.27	49637	96.38
		P62(OH)	2.95E+08		21019762		3649853		460697		1310486		1.7E+08		30966284		1321823	
R67K$_{(55-67)}$: VGVEAK(+57.02)QPNSAIK	Carbamido-methylation	P62	778214		<LOD		755837		<LOD		<LOD		ND		ND		ND	
		P62(OH)	<LOD		<LOD		<LOD		<LOD		<LOD		ND		ND		ND	
WT$_{(55-67)}$: VGVEAK(+57.02)QPNSAIR		P62	537147	97.16	1813552	59.20	244322	95.93	253107	82.59	117120	74.80	481721	93.85	901566	71.39	215379	90.94
		P62(OH)	18387771		2631195		5761836		1200886		347604		7348169		2249969		2162443	
R67K	TOTAL XIC P62		1.49E+08	37.75	56426738	36.99	496779833	19.02	31631297	43.00	39059197	20.87						
	TOTAL XIC P62(OH)		90433849		33119540		116656593		23865438		10301712							
WT	TOTAL XIC P62		1.86E+08	98.08	3.05E+08	94.20	243861476	95.78	16535968	98.17	14555829	97.96	11105072	99.54	29643196	99.44	6529862	99.54
	TOTAL XIC P62(OH)		9.49E+09		4.95E+09		5529241939		8.85E+08		697771850		2.4E+09		5.22E+09		1.42E+09	
	% R67K Incorportaion		2.42		1.68		9.61		5.80		6.48							

Table 4.1: RPS23 R67K peptides are less abundant in the polysomal ribosomes and show reduced hydroxylation relative to equivalent wild-type RPS23 peptides. RPS23 peptides were quantified from parent and mutant R67K LCLs by mass spectrometry. Key: XIC: Extracted ion chromatogram counts; ND: Not Detected – Arg67Lys Peptide not assigned by MS/MS in healthy control; <LOD: Below limit of detection or confounding co-eluting peptide interfering with quantitation; Post-translationally modified peptides: N(+.98) deamidation, Q(-17.03) pyroGlu, K(+43.01) carbamylation, K(+57.02) carbamidomethylation.

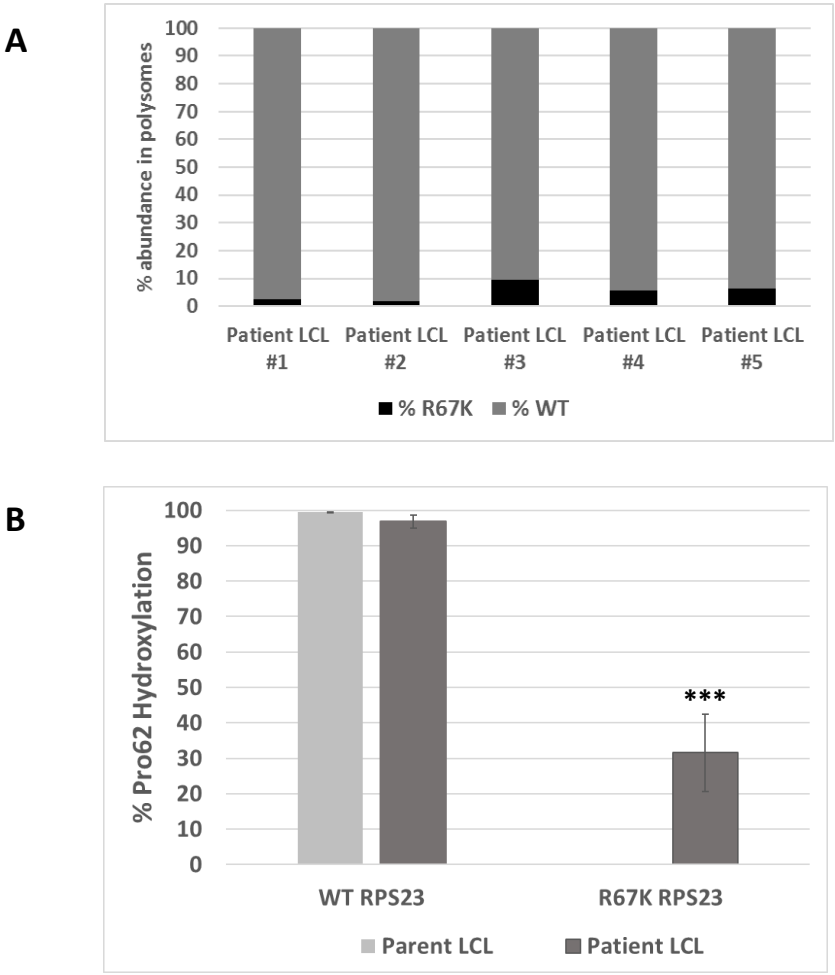


Figure 4.3: RPS23 R67K peptides are less abundant in the polysomal ribosomes and show reduced hydroxylation relative to equivalent wild-type RPS23 peptides. A) Relative quantitation of wild-type and mutant RPS23 peptides by mass spectrometry in ribosomes isolated from R67K patient LCLs. The results indicate that mutant R67K RPS23 is prevented from entering the polysome pool. **B)** Relative quantitation of RPS23 hydroxylation indicates a deleterious effect of the R67K mutation on Pro-62 hydroxylation with <40% of the mutant R67K-bearing peptides recovered from ribosomes hydroxylated. Data represent aggregate counts from biological replicates (parent LCLs n=3; patient R67K LCLs n=5); error bars represent ± standard deviation *** $P < 0.001$.

4.3 Discussion

This chapter sought to further explore the association between OGFOD1 and RPS23 and assess the effects on RPS23 hydroxylation in the context of a disease associated mutation. From investigating the effect of R67K-RPS23 mutation in patient derived cells and in co-transfection experiments, it was evident that R67K-RPS23 causes an inhibitory effect on the formation of the 100 kDa OGFOD1:RPS23 adduct (Figure 4.1A-4.1B). Although the exact nature and function of this adduct is unclear, work in this chapter has established that a clinically relevant mutation in RPS23 can impair the stable OGFOD1:RPS23 complex. Furthermore, an inhibitory effect on endogenous RPS23 hydroxylation was observed with less than 40% of R67K peptides hydroxylated (Table 4.1 and Figure 4.3B). Therefore, some components of the clinical syndrome might be generated directly by effects of impaired RPS23 hydroxylation, or by effects on the OGFOD1-RPS23 complex itself.

A second unrelated patient was identified that possessed a *de novo* mutation in RPS23, Phe120Ile (F120I), and who presented with overlapping clinical features. Patient lymphocytes were not available from the individual with the F120I mutation, which precluded further biochemical dissection of the effect on RPS23 hydroxylation. Co-transfection experiments revealed an inhibitory effect on the 100 kDa adduct (Figure 4.1C). The reduced expression of HA-RPS23 (F120I) was observed at both its native molecular weight of 15 kDa and in adduct form at 100 kDa, and suggest that this mutation could impair RPS23 stability that in turn reduces hydroxylation. However, further work would be required to confirm the effect of the F120I mutation on native RPS23 hydroxylation.

Quantification of equivalent wild-type and mutant RPS23 peptides from cells bearing the R67K mutation indicated that R67K-RPS23 is very rarely found in the assembled ribosome (Figure 4.3A), despite equivalent mRNA expression of wild-type and mutant alleles (Paolini

et al., 2017). This indicates that a mechanism exists to prevent the incorporation of the R67K-RPS23 protein into the ribosome. Although reduced incorporation of mutant RPS23 is observed in cells from the affected patient, it is difficult to know to what extent they derived from impaired OGFOD1 function as opposed to the direct effect of the mutation itself in the ribosome.

The results presented in this chapter form part of a larger dataset that have recently been published in collaboration with three other groups (Paolini et al., 2017). The paper explores the molecular mechanisms driving growth and translational fidelity defects in both yeast and mammalian cells bearing the RPS23 mutations.

In contrast to lymphocytes derived from patients with DBA, no impairment in proliferation or *de novo* protein synthesis was observed in lymphocytes bearing the R67K mutation (Paolini et al., 2017). The results suggest that reduced RPS23 hydroxylation does not alter cell proliferation in this context as was observed following OGFOD1 interventions in chapters 2 and 3. The R67K mutation was shown to increase the rate of stop codon readthrough in the context of the UAA and UAG termination signals. In contrast OGFOD1 -/- MEFs were reported to show an increase in termination fidelity, and adding further complexity, bidirectional effects on stop codon readthrough were reported in response to TPA1 loss in *S. cerevisiae* (Singleton et al., 2014; Loenarz et al., 2014). Overall, the differences between the effects of OGFOD1 loss in both yeast and mammalian cells make it difficult to distinguish whether the effects on miscoding in the R67K cells are likely due to the mutation or inhibition of hydroxylation.

Further insight into the effect of the R67K mutation on translation could be assessed using genome-wide ribosome profiling; a technique that identifies the position of active ribosomes bound to the target mRNA by measuring the ribosome protected fragments (RPF) (Ingolia et al., 2013). Differences in translation efficiencies between mRNA transcripts could

be investigated to help extend the observations that the mutation impairs general stop codon readthrough. In addition, ribosome profiling in wild-type and OGFOD1-defective cells would help to assess the correlation between inhibition of RPS23 hydroxylation and effects from the R67K mutation on translation.

Although some aspects of the affected patient's clinical features bear similarities to the reported phenotypes observed in OGFOD1 knockout mice, including skeletal phenotypes reported by the International Mouse Phenotyping Consortium, the links remain unclear. These studies suggest that OGFOD1 catalysed hydroxylation might have functions that had not been observed in the cellular work described in chapters 2 and 3. However, this was difficult to prove given the potential direct effect of the mutation in the ribosome, together with limitations implicit in working on clinical material. Therefore, it was decided to refocus on the biochemistry of OGFOD1, on the basis that this might better focus subsequent physiological and pathophysiological analyses.

Chapter 5: Proteomic screens using FLAG-OGFOD1 and endogenous OGFOD1 pull downs

5.1 Introduction and aims of the chapter

In the preceding chapters, I sought to define a robust cellular phenotype that was associated with modulation of OGFOD1 expression levels that would in turn provide a focus for mechanistic dissection. Despite considerable effort, however, a clear and consistent phenotype was not forthcoming. At a basic level some of my findings are in conflict with the published reports, though inconsistent findings have also been documented in the literature - exemplified by the contrasting effect of OGFOD1 suppression on the regulation of eIF2α phosphorylation (Wehner et al., 2010; Singleton et al., 2014). Collectively, these findings raise the possibility that some of the reported OGFOD1 phenotypes are indirect and hence highly context specific. To better define OGFOD1 functions a more direct biochemical approach was taken. This was in part directed by an established function of the OGFOD1 ortholog, Ofd1, in regulating the oxygen-dependent sterol response in fission yeast (Lee et al., 2009). In this system, which is outlined in chapter 1, Ofd1 binds to and regulates the Sre1N transcription factor by preventing its DNA binding ability and accelerating its proteasomal degradation (Lee et al., 2011). A similar though less well-defined role for the OGFOD1 ortholog, TPA1, in repressing the activity of the HAP1 transcription factor has also been documented in budding yeast (Henri et al., 2010). Recognition that RPS23 hydroxylation is a conserved action of OGFOD1 led me to consider the possibility that additional functional homology might exist (Loenarz et al., 2014; Singleton et al., 2014).

Proteomic screens that couple affinity purification of bait protein with mass spectrometry provide an unbiased approach for identifying novel interacting partners. Indeed, this methodology led to the identification and discovery of RPS23 as a substrate for OGFOD1 (Singleton et al., 2014). This chapter seeks to define the OGFOD1 interactome at an unprecedented depth in an attempt to define an OGFOD1-dependent signalling function analogous to Ofd1 and TPA1.

5.2 Results

5.2.1 Characterisation of the FLAG-OGFOD1 interactome

To establish robust OGFOD1 protein associations, the OGFOD1 interactome was defined in two different cell backgrounds. HEK293 and SW620 cells were generated that overexpressed OGFOD1 possessing an *N*-terminal FLAG tag. The stably-expressing FLAG-OGFOD1 HEK293 cell line was derived by neomycin selection and standard clonal isolation procedures; henceforth these cells are referred to as HEK293 FLAG-OGFOD1 cells. Untransfected HEK293 cells were used to control for non-specific FLAG immunoprecipitation and will be referred to as HEK293 control cells throughout. One caveat of a cell line generated through the transient expression of a transgene is that the level of expression of the protein is often higher than its endogenous level, which can result in artefactual interactions. However, tagging of the bait protein can be advantageous if the antibody raised against the bait protein is not effective in immunoprecipitation or if it lacks specificity. A second cell line was used to facilitate expression of FLAG-OGFOD1 within the physiological range. SW620 cells were transduced with lentiviral plasmids encoding FLAG-OGFOD1 or empty vector (EV) upstream of an IRES-driven GFP reporter. This enabled the cells to be sorted into populations representing the lowest 20% of GFP-positive cells, the resultant SW620 cells transduced with FLAG-OGFOD1 transgene will be termed SW620 FLAG-OGFOD1 cells

throughout. The empty vector transduced cells were similarly sorted and will be termed SW620 control cells throughout.

Preparative-scale immunoprecipitations were performed in HEK293 FLAG-OGFOD1 and SW620 FLAG-OGFOD1 cells and their respective control cells using FLAG affinity magnetic beads. Immunoprecipitated proteins were eluted off the beads with FLAG peptide and a small volume was retained for immunoblotting. Immunoblotting the lysates with anti-FLAG antibody indicated presence of FLAG-OGFOD1 at the expected molecular weight (~80 kDa) in the input and following FLAG immunoprecipitation in the HEK293 FLAG-OGFOD1 cells (Figure 5.1A). As expected this species was absent from the HEK293 control cells. Immunoblotting with an anti-RPS23 antibody indicated clear co-immunoprecipitation of the substrate, RPS23, in the FLAG-OGFOD1 expressing cells, indicating that this cell line would be suitable to identify established OGFOD1 interacting proteins.

Immunoblotting the SW620 cell lysates with anti-OGFOD1 enabled a comparison between endogenous OGFOD1 and the FLAG-OGFOD1 species (Figure 5.1B). Endogenous OGFOD1 was detected at 75 kDa in the SW620 control and FLAG-OGFOD1 cells. The FLAG-OGFOD1 species was detected by immunoblotting using an anti-OGFOD1 antibody in the input and following FLAG immunoprecipitation in the SW620 FLAG-OGFOD1 cells. The level of FLAG-OGFOD1 appeared lower relative to endogenous OGFOD1 in the SW620 control cells, indicating that the SW620 FLAG-OGFOD1 cells reflect OGFOD1 expression that is similar to physiological levels (Figure 5.1B). The level of FLAG-OGFOD1 capture following FLAG immunoprecipitation appeared relatively high, indicating that co-immunoprecipitation of other interacting factors would be possible with this cell line despite the apparent reduction in FLAG-OGFOD1 expression in the input relative to endogenous levels.

The OGFOD1:RPS23 complex at ~100 kDa that was previously characterised by Singleton et al., and described in chapter 4 was similarly observed in the HEK293 and SW620 FLAG-OGFOD1 cells (Figure 5.1A and B) (Singleton et al., 2014).

Following FLAG immunoprecipitation in the HEK293 and SW620 control and FLAG-OGFOD1 cells, proteins were eluted using FLAG peptide and the remaining volume that was not used for immunoblotting was subject to in-solution digestion with trypsin for proteomic analysis. Samples were submitted for liquid chromatography tandem mass spectrometry (LC-MS/MS) (Target Discovery Institute, University of Oxford) and data processing and analysis was performed by Dr. Matthew Cockman. OGFOD1-interacting proteins were identified using the PEAKS software package (Bioinformatics Solutions Inc.) which uses probability based algorithms to interpret and assign peptide fragmentation data. Relative label-free quantification was performed on two unique peptides, measuring the average peak ion intensity. A normalisation factor was applied using Total Ion Current (TIC) which accounts for the amount of material injected into the spectrophotometer. The abundance of the peptides can then be used as a reference to assess the stoichiometry of the interacting proteins. See chapter 9 (section 9.7.5) for further details on mass spectometry data processing.

A summary of OGFOD1-interacting proteins dervied from HEK293 and SW620 FLAG-OGFOD1 screens is provided in Table 5.1 and Table 5.2, respectively. Interacting proteins were ranked according to peptide level abundance ('IP area') and their respective enrichment ratio in OGFOD1 immunoprecipitates ('Ratio: OGF/CON'). These tables include a list of all OGFOD1-interacting proteins that showed a 3-fold enrichment. As expected, OGFOD1 was identified as the most highly enriched protein in both HEK293 and SW620 FLAG-OGFOD1 cells, being undetected in the control cells. RPS23 was also identifed as a top interacting protein and its abundance was significantly higher than other associating factors. Reflecting

the abundance of RPS23 in the cell lysate, contaminating RPS23 peptides were detected in the control cells which resulted in a reduced enrichment ratio. Nevertheless, RPS23 was consistently enriched by ~50-fold and 10-fold in HEK293 and SW620 FLAG-OGFOD1 cells, respectively (Table 5.1 and Table 5.2).

A number of other associating proteins were identified in both HEK293 and SW620 FLAG-OGFOD1 cells that were absent in the control cells. In addition to RPS23, 14 interacting proteins were identfied in the HEK293 FLAG-OGFOD1 cells that showed an enrichment of 3-fold (Table 5.1). In the SW620 FLAG-OGFOD1 cells, 7 interacting proteins were identified in addition to RPS23 that showed an enrichment of 3-fold (Table 5.2).

.

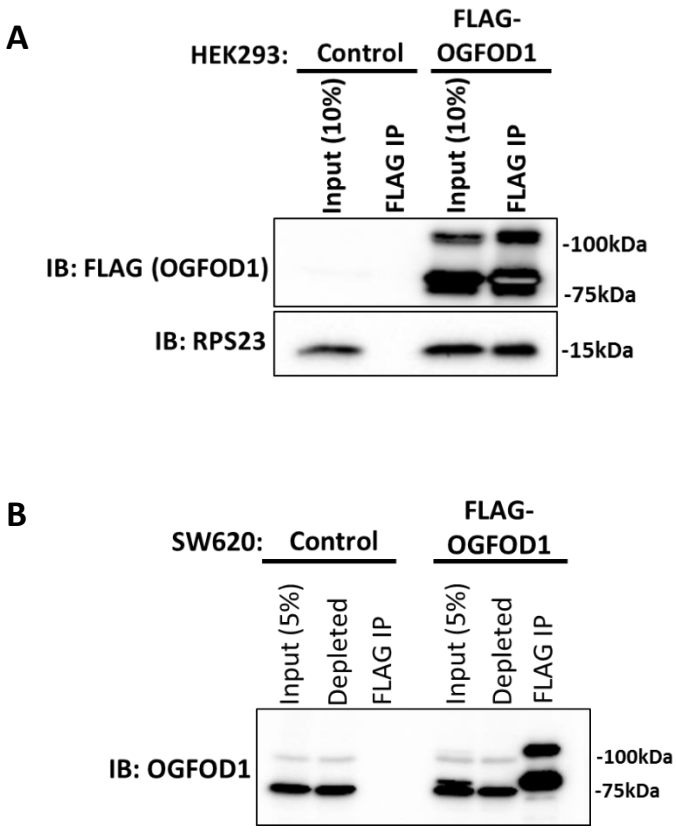


Figure 5.1: Validation of FLAG-OGFOD1 immunoprecipitation in HEK293 and SW620 FLAG-OGFOD1 cells. A) Immunoblot demonstrating immunoprecipitation of FLAG-OGFOD1 at ~80 kDa by anti-FLAG affinity in HEK293 FLAG-OGFOD1 cells. The previously characterised 100 kDa OGFOD1:RPS23 adduct was also observed in FLAG-OGFOD1 immunoprecipitates. Co-immunoprecipitation of RPS23 at its native molecular weight of 15 kDa is specifically observed with capture of FLAG-OGFOD1. HEK293 control cells represent the parental cell line and input corresponds to 10% of cell extract before immunoprecipitation. **B)** Immunoblot demonstrating immunoprecipitation of FLAG-OGFOD1 using anti-FLAG affinity in SW620 FLAG-OGFOD1 cells. SW620 control cells represent empty vector transduced SW620 cells. Endogenous OGFOD1 is detected in the control and FLAG-OGFOD1 cells at 75 kDa. The FLAG-OGFOD1 species was detected at ~80 kDa in the FLAG-OGFOD1 cells and was enriched following FLAG immunoprecipitation. The OGFOD1:RPS23 complex at 100 kDa was observed following immunoprecipitation in the FLAG-OGFOD1 cells. Depleted fractions correspond to the cell extract after immunoprecipitation and confirm depletion of FLAG-OGFOD1 from the lysate. Inputs corresponds to 5% cell extract before immunoprecipitation.

Gene ID	Significance	Coverage (%)	#Unique	HEK293 Control FLAG IP Area	HEK293 OGFOD1 FLAG IP Area	Ratio: OGF/Con	Description
OGFOD1	**200**	**96**	**243**	**0**	**2170000000**	**DIV/0**	**Prolyl 3-hydroxylase OGFOD1**
THAP11	200	38	9	0	16300000	DIV/0	THAP domain-containing protein 11
PKMYT1	200	32	10	0	4770000	DIV/0	Membrane-associated tyrosine- and threonine-specific cdc2-inhibitory kinase
C2CD2L	200	42	20	0	4540000	DIV/0	Phospholipid transfer protein C2CD2L
FAM207A	200	38	6	0	2610000	DIV/0	Protein FAM207A
PURB	200	28	4	0	1330000	DIV/0	Transcriptional activator protein Pur-beta
EXD2	200	35	15	0	1010000	DIV/0	Exonuclease 3'-5' domain-containing protein 2
NET1	142.06	10	2	0	396000	DIV/0	Neuroepithelial cell-transforming gene 1 protein
PTPN14	200	5	3	0	345000	DIV/0	Tyrosine-protein phosphatase non-receptor type 14
PHLPP2	200	7	5	0	275000	DIV/0	PH domain leucine-rich repeat-containing protein phosphatase 2
SP4	200	12	3	0	238000	DIV/0	Transcription factor Sp4
MRPL11	127.32	15	2	0	215000	DIV/0	39S ribosomal protein L11 mitochondrial
RPS23	200	65	39	7310000	358000000	48.97	40S ribosomal protein S23
MRPS9	52.27	8	2	51400	403000	7.84	28S ribosomal protein S9 mitochondrial
KRT9	200	22	9	261000	908000	3.48	Keratin type I cytoskeletal 9
RBM27	153.53	14	7	246000	755000	3.07	RNA-binding protein 27

Table 5.1: The OGFOD1 interactome in HEK293 FLAG-OGFOD1 cells. FLAG immunoprecipitation was performed with anti-FLAG affinity in parental HEK293 cells or HEK293 cells stably expressing FLAG-OGFOD1. To identify OGFOD1 interacting proteins, FLAG affinity beads were eluted using FLAG peptide and subject to in-solution tryptic digestion and analysis using LC-MS/MS. Interacting proteins were identified using PEAKS software. Targets are ranked according to enrichment ratio and peptide level abundance; the average intensity of two uniquely assigned peptides in the FLAG-OGFOD1 cells (HEK293 OGFOD1 FLAG IP area) relative to the control cells (HEK293 Control FLAG IP area); enrichment ratio (Ratio: OGF/CON). The tables include a list of OGFOD1 interacting proteins that showed a 3-fold enrichment following FLAG immunoprecipitation in HEK293 FLAG-OGFOD1 cells relative to HEK293 control cells. The “Significance” column refers to the strength of the protein assignment; a peaks -10lgP significance score above 20 is equivalent to a false discovery rate of <1%. “Coverage” refers to the percentage of the protein sequences covered by the peptides and “Unique" refers to the number of high-confidence peptides that are unique to that protein.

Gene ID	Significance	Coverage (%)	#Unique	SW620 Control FLAG IP Area	SW620 OGFOD1 FLAG IP Area	Ratio: OGF/Con	Description
OGFOD1	**200**	**93**	**170**	**0**	**830000000**	**DIV/0**	**Prolyl 3-hydroxylase OGFOD1**
PKMYT1	45.21	35	11	0	3550000	DIV/0	Membrane-associated tyrosine- and threonine-specific cdc2-inhibitory kinase
THAP11	41.9	14	4	0	1820000	DIV/0	THAP domain-containing protein 11
C2CD2L	39.24	32	11	0	1040000	DIV/0	Phospholipid transfer protein C2CD2L
MORC3	38.7	31	17	0	892000	DIV/0	MORC family CW-type zinc finger protein 3
FAM207A	40.08	17	3	0	881000	DIV/0	Protein FAM207A
MEST	36.2	19	4	0	455000	DIV/0	Mesoderm-specific transcript homolog protein
KRT2	34.93	11	2	0	303000	DIV/0	Keratin type II cytoskeletal 2 epidermal
RPS23	51.35	55	14	8720000	91700000	10.52	40S ribosomal protein S23

Table 5.2: The OGFOD1 interactome in SW620 FLAG-OGFOD1 cells. FLAG immunoprecipitation was performed using anti-FLAG affinity beads in empty vector (EV) transduced or FLAG-OGFOD1 transduced SW620 cells. FLAG affinity beads were eluted using FLAG peptide and subject to in-solution tryptic digestion and analysis using LC-MS/MS. Interacting proteins were identified using PEAKS software and were ranked according to enrichment ratio and peptide level abundance; the average intensity of two uniquely assigned peptides in the SW620 FLAG-OGFOD1 cells (SW620 OGFOD1 FLAG IP area) relative to the SW620 control cells (SW620 Control FLAG IP area) and expressed as a ratio (Ratio: OGF/CON). The tables include a list of OGFOD1 interacting proteins that showed a 3-fold enrichment following FLAG immunuoprecipitation in the SW620 FLAG-OGFOD1 cells relative to SW620 control cells. “Significance”, “Coverage” and “Unique”are as described in Table 5.1.

To identify robust OGFOD1 interacting proteins, a comparison was made between proteins that were enriched by 3-fold following FLAG immunoprecipitation in the HEK293 and SW620 FLAG-OGFOD1 cells relative to their control cells (Figure 5.2). A shortlist of 5 common OGFOD1 interacting proteins were identified between the two cell types including RPS23. Therefore, a refined list comprising of 4 novel OGFOD1 interacting proteins, namely: THAP11, PKMYT1, C2CD2L and FAM207A was established.

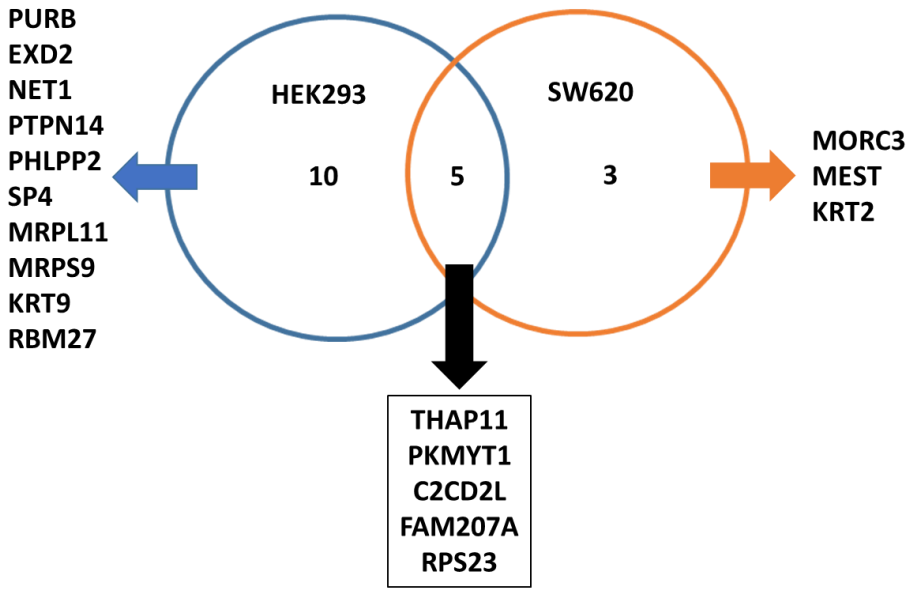


Figure 5.2: Overlap between OGFOD1 interacting proteins in HEK293 and SW620 FLAG-OGFOD1 cells. A list of 10 unique OGFOD1 interacting proteins that are enriched by over 3-fold in the HEK293 FLAG-OGFOD1 cells relative to the HEK293 control cells are shown. Similarly, a list of 3 unique OGFOD1 interacting proteins that are enriched by over 3-fold in the SW620 FLAG-OGFOD1 cells relative to the SW620 control cells is shown. 5 interacting proteins were enriched by over 3- fold in both HEK293 and SW620 FLAG-OGFOD1 cells relative to their control cells.

5.2.2 Characterisation of the endogenous OGFOD1 interactome

In an attempt to corroborate data from the FLAG-OGFOD1 interactome and confirm robust protein associations, the endogenous OGFOD1 interactome was investigated in HEK293 cells using an affinity-purified anti-OGFOD1 antibody raised against full-length human OGFOD1. This antibody was generated in a custom antibody project with Generon; see chapter 9: section: 9.6.1 for details on antibody production. The OGFOD1 antibody was covalently coupled to the magnetic beads to avoid co-elution of the antibody in the final eluate.

Preparative-scale anti-OGFOD1 immunoprecipitations were performed in biological replicate. Proteins were eluted under conditions of high pH and a fraction of the eluate (corresponding to 5% of the total lysate) was set aside in order to validate the OGFOD1 pulldown. Confirming the efficacy of the immunoprecipitations, immunoblotting using a commercially available anti-OGFOD1 antibody (from Sigma; raised against the *C*-terminus) indicated specific capture of OGFOD1 equivalent to ~10% of the total cellular lysate, which was absent from control (Rabbit IgG) immunoprecipitations (Figure 5.3). A caveat of unknown significance is that this antibody has reduced reactivity to the 100 kDa OGFOD1:RPS23 adduct. In contrast to the FLAG-OGFOD1 pulldowns, a weak signal corresponding to this stable complex was noted in replicate 1, which was not observed in replicate 2.

The remaining eluate was subject to in-solution tryptic digestion for proteomic analysis using LC-MS/MS. Sample normalisation and protein level quantitation was performed using the PEAKS software package as described in section 5.2.1. Interacting proteins that were detected in biological replicates following OGFOD1 immunoprecipitation were ranked according to the average intensity of two unique peptides relative to control immunopecipitation. In tabulating these data it was clear that many more proteins were identified in the endogenous OGFOD1 pulldowns. Over 150 proteins met the siginificance

criteria at an arbitrary threshold of 10-fold enrichment in OGFOD1 specific immunoprecipitates. These results contrast with the FLAG-OGFOD1 interactome data which identified only 15 proteins enriched by 3-fold in the HEK293 FLAG-OGFOD1 cells, and 8 proteins enriched by 3-fold in the SW620 FLAG-OGFOD1 cells (Table 5.1 and Table 5.2).

To determine whether there was a functional link between the large number of endogenous OGFOD1 associations, the top 100 enriched proteins were subject to STRING analysis (Figure 5.4). The STRING database provides information on known and predicted protein-protein interactions which can be used to group proteins into functionally associated networks. (https://string-db.org). The data is derived from a number of sources including: high throughput assays, conserved co-expression and automated text mining from published reports, and includes both direct (physical) and indirect (functional) interactions. STRING analysis indicated that endogenous OGFOD1 was associating with a large cluster of ribosomal proteins. Of the top 100 endogenous OGFOD1 associating proteins, 37 ribosomal proteins showed an enrichment of over 30-fold relative to the control immunoprecipitate. The ribosomal proteins included 21 large subunits and 16 small subunits, RPS23 was also enriched by over 60-fold relative to the control immunoprecipitate. However, in contrast to the FLAG-OGFOD1 interactome in HEK293 and SW620 cells, in which RPS23 was highly enriched (Table 5.1 and 5.2), RPS23 appeared only 66th in the list of endogenous OGFOD1 interacting proteins in HEK293 cells.

Aside from ribosomal proteins, STRING analysis did not show clustering of interacting proteins in other functional categories. A list of the top 30 endogenous OGFOD1 interacting partners ranked by peptide level abundance and enrichment ratio is presented in Table 5.3. 23 proteins were identified as specific OGFOD1 interacting proteins as they were not identified following immunoprecipitation with the control antibody in either biological replicate. Within the top 30 OGFOD1 interacting proteins, a number of ribosomal proteins

showed significant enrichment relative to the control immunoprecipitation (>500 fold) including RPS7, RPL22, and RPS10 suggesting that they are high stoichiometric associations. The reasons for these contrasting results achieved with different antibodies and expression systems is currently unclear. However, it was noted that THAP11, which was identified from the FLAG-OGFOD1 proteomic experiments was also identified as one of the the top 30 endogenous OGFOD1 interacting proteins (Table 5.3).

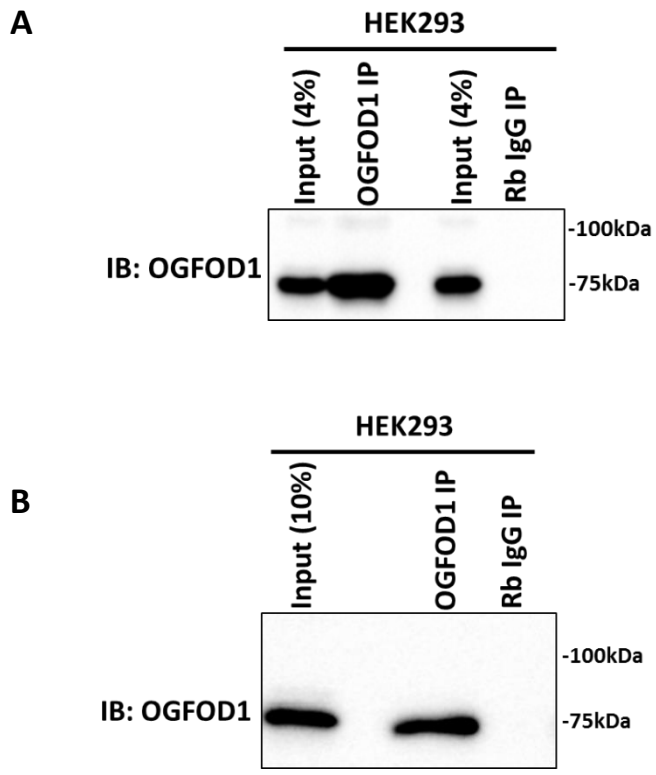


Figure 5.3: Validation of endogenous OGFOD1 immunoprecipitation in HEK293 cells. Confirmation of OGFOD1 immunoprecipitation in HEK239 cells in biological replicate (**A** and **B**). Immunoblotting using an anti-OGFOD1 antibody (Sigma) demonstrates immunoprecipitation of OGFOD1 using a full length anti-OGFOD1 antibody (Generon) at 75 kDa. A weak signal corresponding to the 100 kDa OGFOD1:RPS23 complex was observed in replicate 1 **(A)**, which was not detected in replicate 2 **(B)** and may reflect reduced immunoprecipitation efficiency relative to **(A)**. An anti-rabbit control antibody (Rb IgG) failed to immunoprecipitate OGFOD1 at 75 kDa or the 100 kDa complex. Inputs correspond to cell extracts before immunoprecipitation.

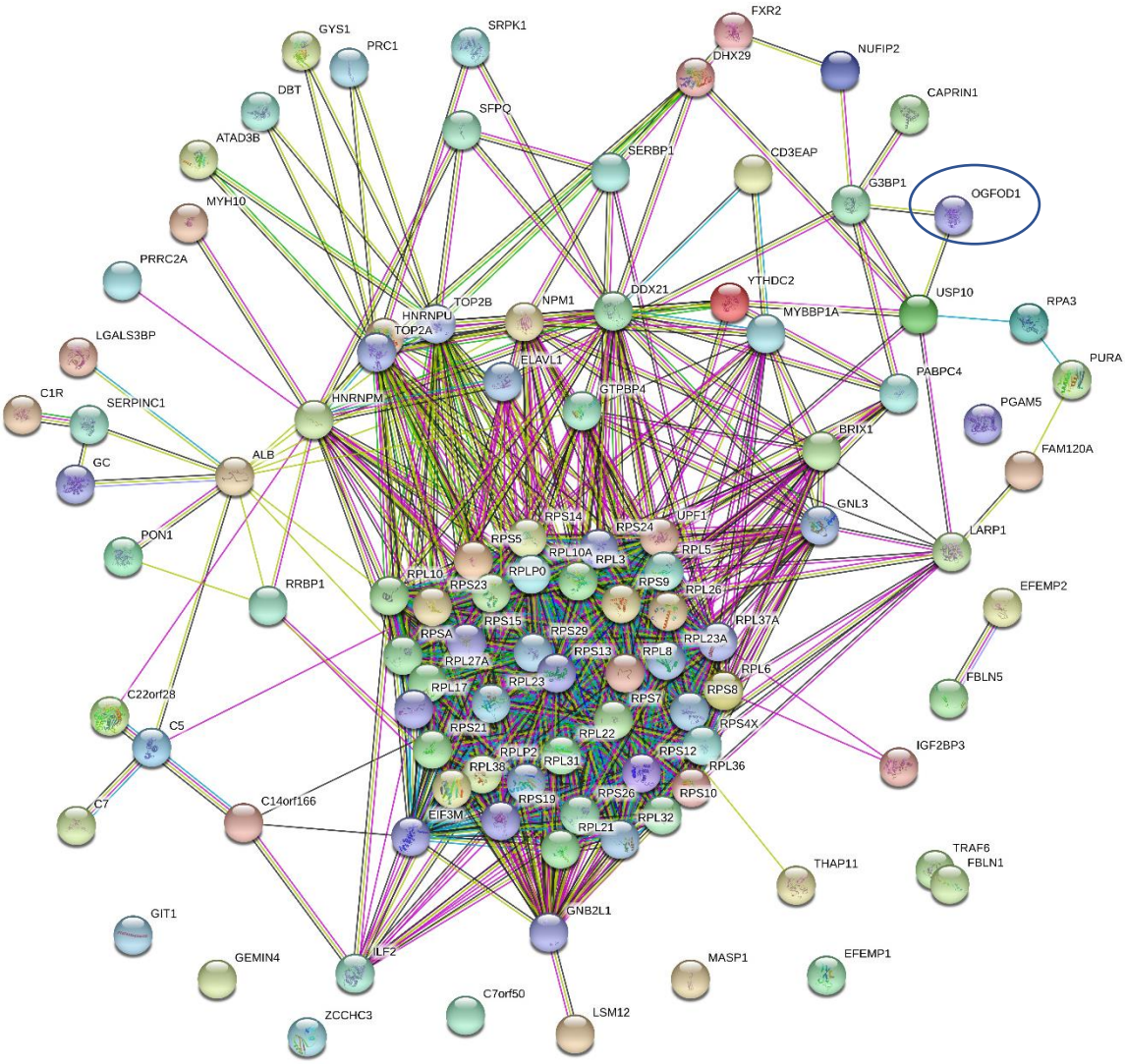


Figure 5.4: STRING analysis of the top 100 endogenous OGFOD1 interacting proteins in HEK293 cells. The top 100 endogenous OGFOD1 interacting proteins defined by peptide level abundance and meeting significance threshold (Peaks score >20 -10lgP) and 10-fold enrichment ratio were subject to functional categorisation by STRING analysis. The position of OGFOD1 within its interacting proteins as assigned by STRING analysis is highlighted.

Gene ID	Significance	Coverage (%)	#Unique	#1 Rb IgG Area	#2 Rb IgG Area	#1 OGFOD1 IP Area	#2 OGFOD1 IP Area	Mean Control IP Area	Mean OGFOD1 IP Area	Ratio: OGF/Con	Description
OGFOD1	**73.09**	**50**	**11**	**0**	**0**	**88000000**	**57500000**	**0**	**72800000**	**DIV/0**	**Prolyl 3-hydroxylase OGFOD1**
EFEMP1	49.94	20	5	0	0	43200000	17600000	0	30400000	DIV/0	Isoform 2 of EGF-containing fibulin-like extracellular matrix protein 1
PON1	27.37	8	2	0	0	18900000	9870000	0	14400000	DIV/0	Serum paraoxonase/arylesterase 1
C5	51.13	7	9	0	0	13600000	11800000	0	12700000	DIV/0	Complement C5
GC	48.95	5	2	0	0	13800000	10700000	0	12200000	DIV/0	Vitamin D-binding protein
FXR2	46.57	27	6	0	0	10300000	6610000	0	8460000	DIV/0	Fragile X mental retardation syndrome-related protein 2
RPA3	42.34	35	2	0	0	6960000	6990000	0	6970000	DIV/0	Replication protein A 14 kDa subunit
C7orf50	44.44	29	3	0	0	7710000	4900000	0	6300000	DIV/0	Uncharacterized protein C7orf50 (Fragment) O
FBLN1	45.25	16	2	0	0	9190000	3360000	0	6270000	DIV/0	Isoform C of Fibulin-1
C1R	31.68	5	2	0	0	7750000	4690000	0	6220000	DIV/0	Complement C1r subcomponent
TRAF6	41.74	16	4	0	0	5930000	4400000	0	5160000	DIV/0	TNF receptor-associated factor 6
LSM12	43	23	3	0	0	4920000	4730000	0	4820000	DIV/0	Protein LSM12 homolog
C7	24.7	4	2	0	0	5100000	2830000	0	3960000	DIV/0	Complement component C7
PRC1	41.95	6	2	0	0	4840000	1830000	0	3330000	DIV/0	Isoform 4 of Protein regulator of cytokinesis 1
MASP1	24.09	4	2	0	0	3560000	3070000	0	3310000	DIV/0	Isoform 2 of Mannan-binding lectin serine protease 1
ZCCHC3	36.17	14	3	0	0	3700000	2730000	0	3220000	DIV/0	Zinc finger CCHC domain-containing protein 3
CD3EAP	41.71	18	3	0	0	3790000	2100000	0	2950000	DIV/0	DNA-directed RNA polymerase I subunit RPA34
GEMIN4	37.79	6	3	0	0	3740000	2150000	0	2940000	DIV/0	Gem-associated protein 4
SRPK1	34.71	6	2	0	0	3870000	1820000	0	2840000	DIV/0	Isoform 3 of SRSF protein kinase 1
FBLN5	41.61	12	2	0	0	3870000	1610000	0	2740000	DIV/0	Fibulin-5
BRIX1	24.1	15	2	0	0	3660000	1620000	0	2640000	DIV/0	Ribosome biogenesis protein BRX1 homolog
TOP2B	33.71	4	2	0	0	3110000	1960000	0	2530000	DIV/0	Isoform Beta-1 of DNA topoisomerase 2-beta
YTHDC2	29.51	4	3	0	0	3140000	1810000	0	2470000	DIV/0	Probable ATP-dependent RNA helicase YTHDC2
DHX29	33.67	2	2	0	0	3150000	951000	0	2050000	DIV/0	ATP-dependent RNA helicase DHX29
SERPINC1	60.88	21	6	0	18800	46500000	53400000	9420	49900000	5297.24	Antithrombin-III
RPS7	53.32	44	5	0	83700	79000000	18600000	33500	48800000	1456.72	40S ribosomal protein S7
THAP11	39.92	8	2	0	16000	7280000	7130000	8020	7200000	897.76	THAP domain-containing protein 11
RPL22	23.01	30	2	0	69400	28800000	18300000	34700	23600000	680.12	60S ribosomal protein L22
ALB	55.53	7	3	0	110000	31700000	34500000	54800	33100000	604.01	Serum albumin
RPS10	32.75	37	6	0	91900	40300000	20400000	55100	30400000	551.72	40S ribosomal protein S10

Table 5.3: Top 30 endogenous OGFOD1 interacting proteins in HEK293 cells. OGFOD1 interacting proteins were identified using PEAKS software and were ranked according to the mean intensity of two unique identifying peptides that were present in both biological replicates. The enrichment of proteins co-immunoprecipitating with OGFOD1 relative to the control antibody were expressed as a ratio (Ratio: OGF/Con). The top 30 interacting proteins are presented and ranked according to enrichiment ratio and mean peptide level abundance. The "Significance", "Coverage" and "Unique" column are as described in Table 5.1.

5.2.3 Identification of common OGFOD1 interacting proteins

A comparison was made between the different proteomic experiments considering interacting proteins that showed a 3-fold enrichment relative to control immunoprecipitates (Table 5.4). All 166 proteins identified from the endogenous proteomics had an enrichement ratio greater than 3-fold and, therefore were compared. Surprisingly, based on the list of FLAG-OGFOD1 interacting proteins, only two proteins, namely RPS23 and THAP11, showed consistent enrichment across all proteomic experiments. *Th*anatos-*a*ssociated *p*rotein (THAP) 11 possesses a zinc finger motif that has sequence specific DNA binding activity and functions as a transcriptional regulator in a number of cell types (Dejosez et al., 2010; Parker et al., 2012). These observations provide a platform for the study of a potentially novel signalling mechanism, analogous to Ofd1 and TPA1, linking OGFOD1 to transcriptional regulation.

	Enrichment ratio >3		
IP:	**FLAG-OGFOD1**	**FLAG-OGFOD1**	**Endogenous OGFOD1**
Cell line:	**HEK293**	**SW620**	**HEK293**
Gene			
RPS23	✓	✓	✓
THAP11	✓	✓	✓
PKMYT1	✓	✓	
C2CD2L	✓	✓	
FAM207A	✓	✓	
MORC3		✓	
PURB	✓		
EXD2	✓		
MEST		✓	
NET1	✓		
KRT2		✓	
PTPN14	✓		
PHLPP2	✓		
SP4	✓		
MRPL11	✓		
MRPS9	✓		
KRT9	✓		
RBM27	✓		

Table 5.4: Common interacting proteins in FLAG-OGFOD1 and endogenous OGFOD1 proteomic studies. OGFOD1 interacting proteins were defined from the FLAG-OGFOD1 interactomes in HEK293 and SW620 cells that showed a 3-fold enrichment relative to control immunoprecipitates. The presence of these proteins in the interactomes of FLAG-OGFOD1 HEK293 cells, FLAG-OGFOD1 SW620 cells or endogenous OGFOD1 HEK293 cells is indicated.

5.2.4 Validation of THAP11 as a novel OGFOD1 interacting partner

In order to validate the proteomic assignments and demonstrate that the OGFOD1 and THAP11 association occurs in cells, a number of immunoprecipitation experiments were performed. An expression vector encoding FLAG-tagged THAP11 was transfected into 293T cells and immunoprecipitation with anti-FLAG beads confirmed the existence of an association with OGFOD1 by immunoblotting (Figure 5.5A). Similarly, anti-FLAG immunoprecipitation of extracts from SW620 FLAG-OGFOD1 cells demonstrated capture of THAP11, and supported results from the SW620 FLAG-OGFOD1 proteomic screen (Figure 5.5B).

In order to determine the physiological existence of the association, the OGFOD1-THAP11 interaction was assayed by immunoprecipitation of endogenous proteins in a panel of four cell lines (Figure 5.5C). Immunoblotting anti-OGFOD1 immunoprecipitates with a THAP11 antibody revealed a robust association between the two proteins in the steady state. The capture of THAP11 by OGFOD1 was broadly similar across the cell panel ranging from ~10% in U2OS to ~20% in SW620 cells.

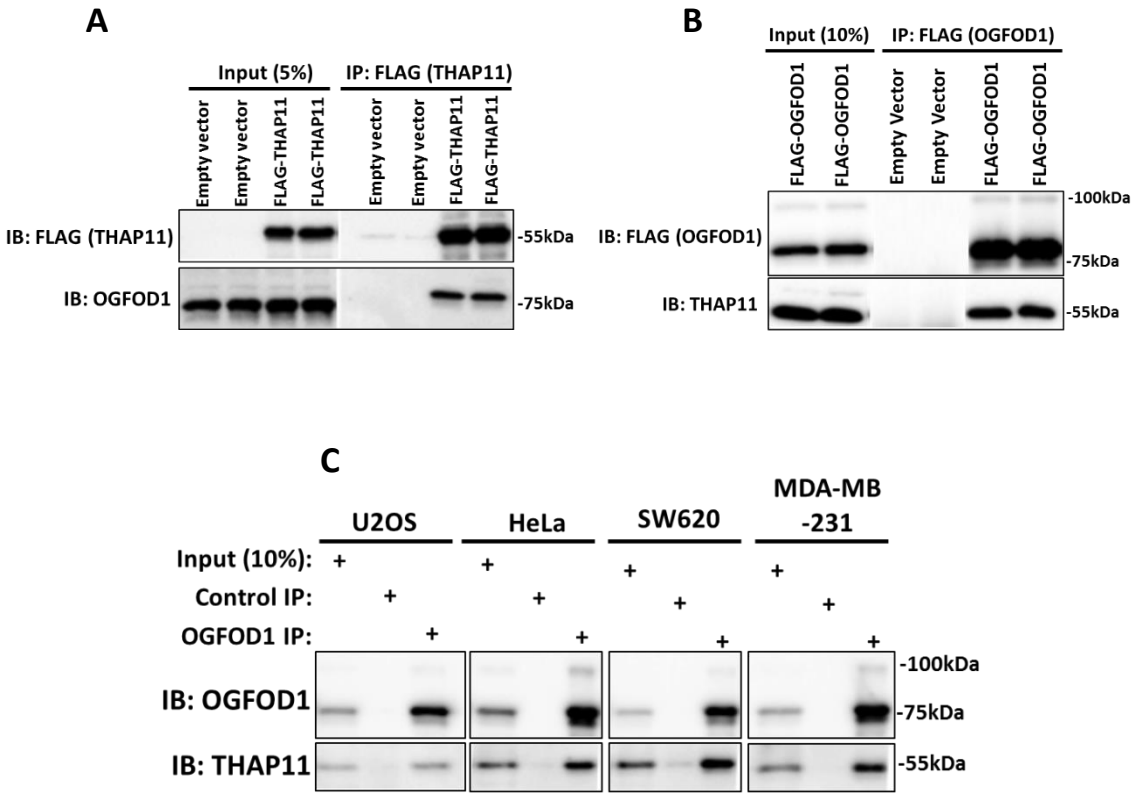


Figure 5.5: Identification of THAP11 as a novel interaction partner for OGFOD1. A) Immunoblot demonstrating co-immunoprecipitation of OGFOD1 following FLAG (THAP11) IP in 293T cells transiently transfected with empty vector or FLAG-THAP11, samples are displayed as technical replicates. **B)** Immunoblot demonstrating co-immunoprecipitation of THAP11 following FLAG (OGFOD1) IP in SW620 cells transduced with lentiviral plasmids expressing empty vector or encoding FLAG-OGFOD1, samples are displayed as technical replicates **C)** Anti-OGFOD1 antibody, and not control (Rabbit IgG), co-precipitates THAP11. Inputs corresponds to cell extracts before immunoprecipitation.

To further define the association between OGFOD1 and THAP11, the interaction was interrogated using recombinant proteins that were received as a kind gift from by Dr. Phebee Liu-Yia, University of Oxford. Purified recombinant OGFOD1, THAP11 and RPS23 proteins were mixed together for one hour before performing an OGFOD1 IP (Figure 5.6). RPS23 served as the control and confirmed that the OGFOD1 and RPS23 association is direct. The results indicated that the OGFOD1 and THAP11 interaction was also direct.

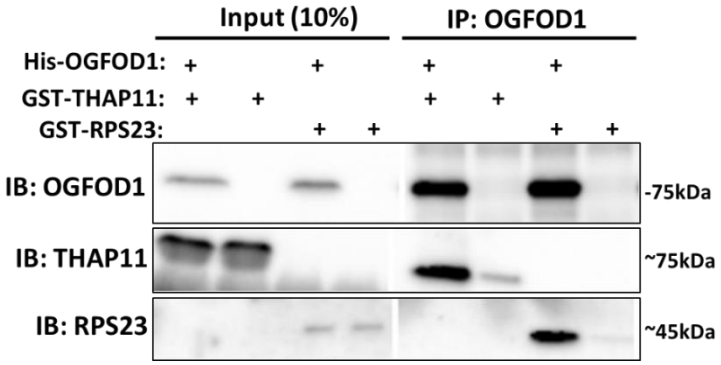


Figure 5.6: OGFOD1 interacts directly with THAP11 and RPS23. pET His-OGFOD1, pGEX GST-RPS23, or pGEX GST-THAP11 were transfected into *E. coli* and recombinant protein was produced by isopropyl β-D-1-thiogalactopyranoside (IPTG) induction. Recombinant proteins were then mixed in JIES complete in the presence of 1 mg/ml BSA and incubated at 4°C for 1 hour followed by anti-OGFOD1 immunoprecipitation. Immunoblot showing THAP11 and RPS23 co-immunoprecipitation in the presence of OGFOD1. THAP11 and RPS23 are detected at ~75 kDa and 45 kDa respectively (GST = +26 kDa). Input corresponds to 10% of starting material.

5.2.5 Mapping the OGFOD1 binding domain in THAP11

The THAP family form a large group of sequence specific DNA binding factors, and despite their conserved DNA binding domain they vary in length and differ in the remaining portion of their sequences (Cukier et al., 2015). THAP11 forms a complex on chromatin with the co-activator Host Cell Factor 1 (HCF-1) that is required for THAP11 mediated transcriptional regulation (Parker et al., 2014). The domain architecture of THAP11 comprises the following structural and functional sequences: a tetrapeptide HCF-1 binding motif (HBM); a coiled-coil domain (CC) which is thought to be important for protein function; a predicted nuclear localisation signal (NLS); and a 29 residue polyglutamine stretch (Q) (Figure 5.7A) (Cukier et al., 2015).

In order to determine if there are any sequence similarities between THAP11 and OGFOD1-binding homologues, a BlastP search was performed on known Ofd1 interactors. Surprisingly, by performing a BlastP human database search with the *S. pombe* Nro1 yeast

consensus, that interacts with Ofd1, there is significant sequence alignment with THAP11 (Figure 5.7B) (Yeh et al., 2011). Furthermore, THAP11 also shares some sequence homology to Sre1N with the region bound by Ofd1 (Figure 5.7B) (Lee et al., 2011). This finding indicates that the binding domains targeted by Ofd1 might be similarly targeted by OGFOD1 and support the hypothesis that OGFOD1 may modulate an alternative transcriptional regulator in mammalian cells. The homology between THAP11 and Nro1/Sre1 exists in the region between the nuclear localisation signal and polyglutamine tract of THAP11 (Figure 5.7A).

As THAP11 shares homology to the Nro1/Sre1 yeast consensus it would be predicated that deletion of this shared domain in THAP11 would prevent OGFOD1 binding. In order to delineate the OGFOD1 and THAP11 interaction domain, a series of THAP11 mutants were created in a mammalian expression vector harbouring a *C*-terminal FLAG-tag. The transient expression of FLAG-THAP11 is capable of co-immunoprecipitating OGFOD1 (Figure 5.5A). Therefore, FLAG-THAP11 mutants were transiently transfected into 293T cells and the interaction with OGFOD1 was determined by immunoblotting following FLAG immunoprecipitation (Figure 5.7C). Despite some differences in the expression of the mutants, it was evident that assaying wild-type (WT) FLAG-THAP11 binding to OGFOD1 generated only a relatively weak association. Deletion of either the *N* or *C* terminus (DNA binding domain or HCF-1 binding motif/coiled-coil domain respectively) enhanced THAP11 association (2-3 fold) with OGFOD1 over WT FLAG-THAP11. One possible explanation is that limiting the association of THAP11 with DNA liberates a greater pool of THAP11 that is able to associate with OGFOD1.

In support of the hypothesis that THAP11 could be binding similarly to Nro1/Sre1, deletion of the Nro1/Sre1 consensus prevented THAP11 binding to OGFOD1 (Figure 5.7C). The differential binding between THAP11 and OGFOD1 was supported by the observation that

THAP11 co-immunoprecipitation of HCF-1 appeared unchanged when transfected with WT-FLAG-THAP11, deletion of the Nro1/Sre1 consensus, or deletion of the DNA binding domain (Figure 5.7C). As a positive control for HCF-1 binding to THAP11, deletion of the *C*-terminal HCF-1 binding domain prevented HCF-1 co-immunoprecipitation by THAP11, and removal of the *C*-terminal coiled-coil domain reduced the ability of THAP11 to capture HCF-1 (Figure 5.7C).

To extend these observations and further define the minimal OGFOD1 binding domain of THAP11, additional mutants were generated surrounding the central region of THAP11 (adjacent to the Sre1/Nro1 consensus). Despite high levels of overexpression, the newly generated mutants (102-end and 132-end) together with the Nro1/Sre1 mutant were unable to associate with OGFOD1 (Figure 5.7D). Overall, these data suggest that a region between 92-102 in THAP11 is critical for OGFOD1 binding and additionally raise the hypothesis that THAP11 has a conserved function to Ofd1 interacting proteins.

5.2.6 The subcellular localisation of OGFOD1 and THAP11

Endogenous OGFOD1 is primarily localised to the nucleus (Singleton et al., 2014), and given that THAP11 is a transcriptional regulator it would be predicted that the interaction occurs in the nucleus. To investigate the subcellular localisation of the OGFOD1 and THAP11 interaction, FLAG-tagged OGFOD1 or FLAG-tagged THAP11 constructs were transiently transfected into U2OS cells and their localisation was visualised by confocal immunofluorescence following anti-FLAG immunostaining. The results demonstrated a predominant OGFOD1 signal in the nucleus with some diffuse cytoplasmic staining (Figure 5.8A). For OGFOD1, increased signal was noted at the nuclear membrane suggesting potential shuttling of OGFOD1 between the nucleus and cytosol or a function in nuclear transport. FLAG-THAP11 expression was also predominantly nuclear with some cytosolic staining, and suggested a likely nuclear interaction between OGFOD1 and THAP11.

To test this hypothesis, an immunofluorescence based assay for detecting protein-protein interactions was utilised, termed proximity ligation assay (PLA). This method utilises species-specific antibodies directed to each component of the putative protein complex that are conjugated with a short DNA strand. When the PLA probes are in close proximity (<40nm) the DNA strands interact and can be ligated together. Rolling circle DNA synthesis can be initiated to amplify the DNA, which fluorescent probes subsequently bind to. The amplified DNA can then be visualised by confocal immunofluorescence revealing the location of the interaction. U2OS cells were transiently transfected with either pcDNA EV or FLAG-THAP11 variants. OGFOD1 (Rabbit pAb) and FLAG (Mouse mAb) primary antibodies were used to detect the association. WT FLAG-THAP11 and OGFOD1 gave rise to a predominantly nuclear PLA signal with only weak non-specific background stain present in the empty vector control (Figure 5.8B). The heterogenous PLA signal is likely due to incomplete transfection efficiency. Truncated forms of THAP11 that displayed either enhanced OGFOD1 binding (Figure 5.7C; 91-end) or no appreciable association with OGFOD1 (Figure 5.7D; 132-end) were tested using the PLA method to corroborate these findings. Consistent with the interaction and subcellular localisation data, marked PLA signal was discernible around the nuclear membrane when assaying the interaction between FLAG-THAP11 (91-End) and endogenous OGFOD1. Accordingly, no detectable PLA signal was observed in co-transfection assays with THAP11 (132-End) which failed to co-precipitate OGFOD1.

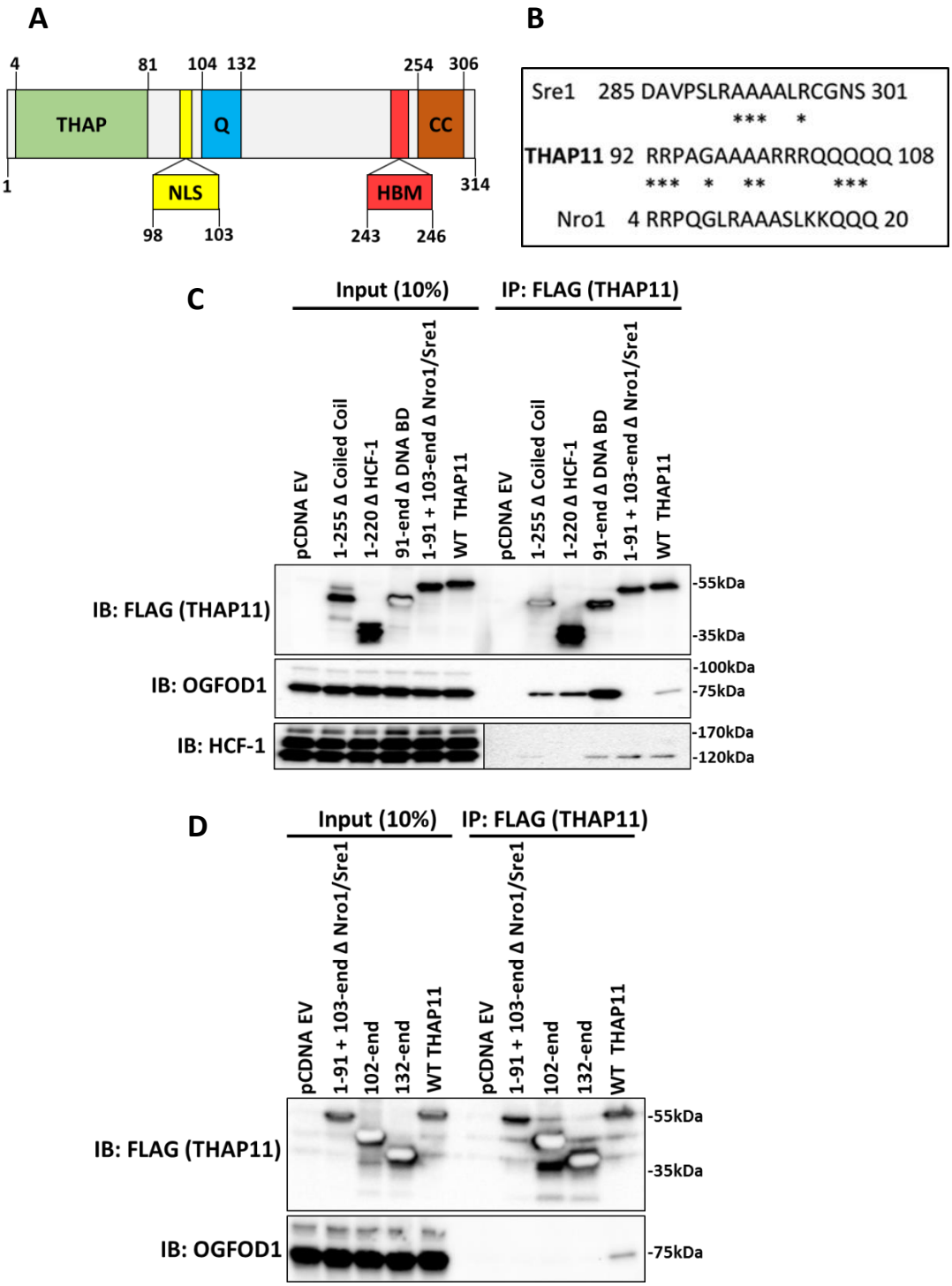


Figure 5.7: Binding determinants: delineation of interaction domains. A) Schematic of the THAP11 domain structure. The THAP11 DNA binding domain (THAP), Nuclear localisation signal (NLS), Polyglutamine tract (Q), HCF-1 binding motif (HBM), Coiled-coil domain (CC) are depicted. Adapted from Cukier et al., 2016. **B)** Sequence homology between THAP11 and Ofd1 interacting proteins: Nro1 and Sre1. **C)** Immunoblot showing delineation of the OGFOD1 and THAP11 binding site following anti-FLAG IP of FLAG-THAP11 constructs transfected into 293T cells. **D)** Further delineation of the OGFOD1 and THAP11 binding site transfecting 293T cells with FLAG-THAP11 mutants surrounding the Nro1/Sre1 like consensus. Transfected cells were subject to anti-FLAG IP and immunoblotted to determine the association with OGFOD1.

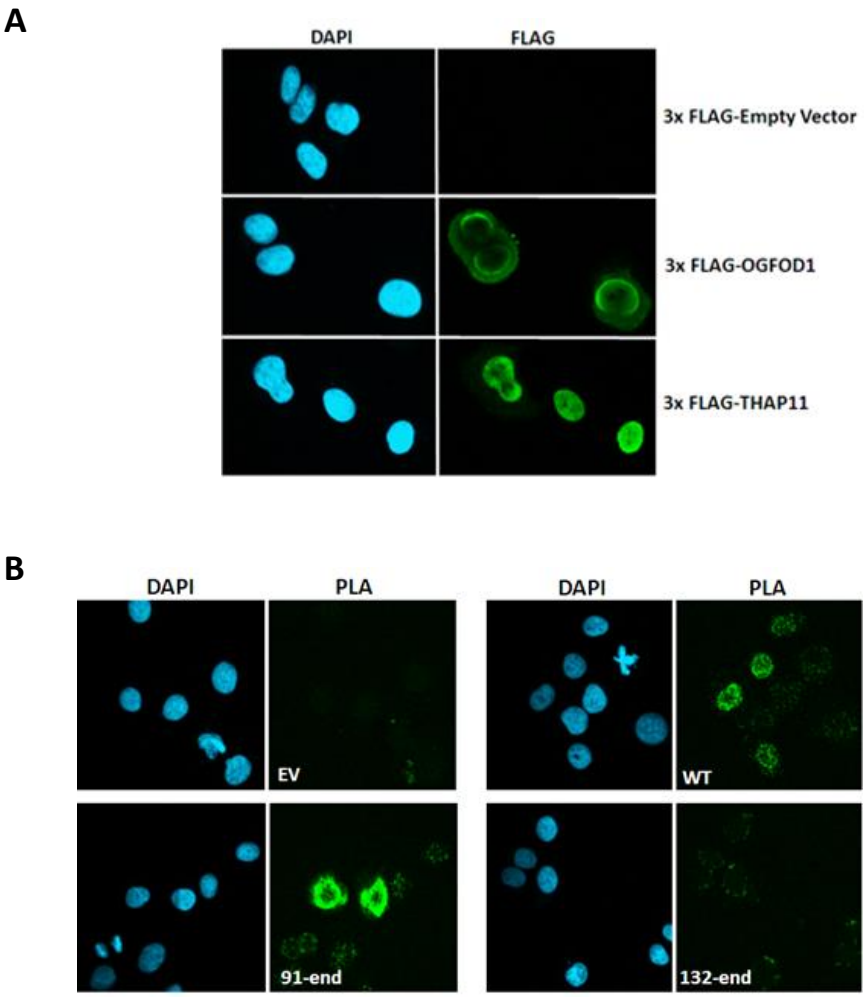


Figure 5.8: Wild-type THAP11 associates with OGFOD1 in the nucleus. A) U2OS cells transiently transfected with an empty vector, FLAG-OGFOD1, or FLAG-THAP11 and were immunostained for FLAG (Green) and nuclei were stained with DAPI (Blue). Confocal immunofluorescence showing dominant expression of THAP11 and OGFOD1 in the nucleus, with some cytosolic staining. **B)** U2OS cells transiently transfected with empty vector (EV) or FLAG-THAP11 constructs (WT, 91-end, 132-end). Representative confocal images using FLAG (Mouse) and OGFOD1 (Rabbit) primary antibodies to detect OGFOD1 and THAP11 association with species specific secondary antibody PLA probes (Green).

5.3 Discussion

This chapter sought to identify robust OGFOD1-interacting proteins using affinity purification coupled to mass spectrometry. The hypothesis underpinning this approach was that if OGFOD1 possessed a signalling function akin to Ofd1 in *S. pombe*, then a proteomic display of OGFOD1-interacting proteins could be highly informative.

Preparative OGFOD1 immunoprecipitations were performed using anti-FLAG resin in HEK293 and SW620 cells stably-expressing FLAG-tagged OGFOD1. As expected, in both cells lines OGFOD1 was the most abundant species (Table 5.1 and 5.2). Similarities in OGFOD1 interacting proteins were observed between the two cell lines, including RPS23, which readily co-purified with FLAG-OGFOD1 irrespective of the differing levels of ectopic FLAG-OGFOD1 expression (Figure 5.2). In addition, a subset of functionally diverse proteins co-purified with OGFOD1 in both HEK293 and SW620 FLAG-OGFOD1 cells (Figure 5.2) that did not appear to be spurious given their enrichment in two different cellular backgrounds. Furthermore, in support that FLAG-OGFOD1 is not aberrantly expressed, confocal immunofluorescence indicated its predominant localisation in the nucleus following transient transfection (Figure 5.8A).

In contrast, replicate endogenous OGFOD1 interaction screens performed in HEK293 cells defined a much larger set of putative interacting proteins, including numerous ribosomal proteins (Table 5.3; Figure 5.4). In addition, very little overlap was observed between FLAG-OGFOD1 and endogenous OGFOD1 pull downs, with the exception of RPS23 and THAP11 (Table 5.4). The discrepancies between FLAG-OGFOD1 and endogenous OGFOD1 pull downs are unclear, however, it is possible that the OGFOD1 polyclonal antibody exhibits a level of non-specific capture. To test this possibility, OGFOD1-defective cells that were generated using CRISPR-Cas9 could be used as a control to test for non-specific antibody binding.

Despite these uncertainties, the four immunoprecipitation experiments identified the OGFOD1 substrate, RPS23, suggesting that common interacting proteins captured in several independent experiments should be of functional interest. THAP11 was identified as a novel interacting protein that was present across all of the OGFOD1 immunoprecipitation experiments and, therefore, further analysis of this association was performed.

The association between OGFOD1 and THAP11 was confirmed by a series of immunoprecipitation experiments in a range of cell lines (Figure 5.5). Furthermore, purified recombinant OGFOD1 and THAP11 proteins supported a direct interaction (Figure 5.6). The rationale to study THAP11 was reinforced given the sequence similarity with Nro1 and Sre1N, components that are bound by Ofd1 in *S. pombe* (Figure 5.7B) (Lee et al., 2011; Yeh et al., 2011). Domain mapping within THAP11 demonstrated that the region bound by Ofd1 in Nro1 and Sre1N is required for OGFOD1 binding to THAP11 (Figure 5.7C and D). These findings support the hypothesis that OGFOD1 may share functional homology to the yeast homolog Ofd1. The subcellular localisation of the OGFOD1 and THAP11 interaction was visualised by confocal immunofluorescence and indicated that they are both predominantly nuclear proteins (Figure 5.8A). Furthermore, a nuclear association between OGFOD1 and THAP11 was supported by proximity ligation assays, suggesting that OGFOD1 may regulate a nuclear function of THAP11 (Figure 5.8B).

Though neither Nro1 nor Sre1N have been proposed to be substrates of Ofd1 in *S.pombe* (Hughes and Espenshade, 2008; Lee et al., 2011), given that RPS23 was identified using proteomic screens, it remained a possibility that THAP11 might be a substrate of OGFOD1. In collaboration with the Department of Chemistry (C. Schofield Lab, University of Oxford) attempts were made to generate soluble recombinant THAP11 protein that could be used to determine if THAP11 was an OGFOD1 substrate. Full length THAP11 was expressed in *E.coli* and was reacted with recombinant OGFOD1 in the presence of 2-OG and ferrous sulphate.

The reaction mix was resolved by SDS-PAGE and the species corresponding to THAP11 was purified and subject to elastase digestion followed by analysis using LC-MS/MS analysis. Mass spectrometry coverage of full length THAP11 was obtained, however, proline oxidation was not assigned by LC-MS/MS suggesting that THAP11 is not a substrate for OGFOD1 (data not shown).

Overall, in defining a novel association between OGFOD1 and THAP11, that is both direct and mediated by sequences with homology to Ofd1 signalling components, this work has provided a focus for the remainder of the work described in this thesis. THAP11 is a transcriptional regulator that possesses a zinc finger motif with sequence specific DNA binding activity (Dejosez et al., 2010; Parker et al., 2012). Therefore, this supports a potentially novel signalling mechanism, analogous to Ofd1 (Lee et al., 2011), linking OGFOD1 to transcriptional regulation and ribosome hydroxylation.

Chapter 6: Characterisation of THAP11 cellular complexes

6.1 Introduction and aims of the chapter

THAP11 is a zinc-dependent DNA binding factor that was identified as an OGFOD1-interacting protein across multiple cell lines (chapter 5). THAP11 has largely been characterised with respect to its DNA binding capabilities, mediated by a zinc finger motif that has sequence specific DNA binding activity (Dejosez et al., 2010; Parker et al., 2012). However, in addition to this relatively well described function, there is evidence to suggest involvement in non-transcriptional processes. For instance, a yeast two-hybrid screen identified Poly-C binding protein (PCBP1) as an interacting protein for THAP11 (Lian et al., 2012). Poly-C binding proteins possess post-transcriptional functions, such as the control of mRNA stability and splicing (Chaudhury et al., 2010; Zhang et al., 2010). Indeed, Lian et al., subsequently demonstrated THAP11-regulated splicing of the CD44 cell surface marker, in a hepatoma cell line that supports an endogenous interaction between THAP11 and PCBP1. These data raise the possibility that THAP11 has other roles that have not been explored in detail and led me to consider that an unprejudiced biochemical characterisation of THAP11 protein could inform upon OGFOD1-regulated functions.

This chapter sought to determine the effect of OGFOD1 modulation on THAP11 protein behaviour in established OGFOD1-defective cell lines, including doxycycline-inducible re-expression cell lines. To consider whether OGFOD1 might modulate RPS23 in a similar manner to THAP11, the cellular properties of RPS23 were assayed in parallel. The effect of

OGFOD1 modulation on THAP11 and RPS23 protein levels and their subcellular distribution were determined by immunoblotting and confocal immunofluorescence, respectively. Affinity-purification of THAP11 was performed in wild-type and OGFOD1-defective cells, and alterations in the THAP11 interactome were investigated by mass spectrometry. In addition, biochemical fractionation techniques were used to identify differences in THAP11 and RPS23 cellular complexes.

6.2 Results

6.2.1 The effect of OGFOD1 on THAP11 and RPS23 protein levels

To investigate effects of OGFOD1 loss on THAP11 (and RPS23), previously established OGFOD1-defective and OGFOD1-inducible re-expressing HEK293 clonal cell lines were utilised; these cell lines were initially characterised in chapters 2 and 3. To broaden the cellular context, OGFOD1-defective cell lines were also generated in HeLa and SW620 cell backgrounds by CRISPR-Cas9 gene editing using the double-nickase methodology. These cell contexts were selected on the basis of observed high stoichiometry endogenous OGFOD1-THAP11 associations (chapter 5: Figure 5.5C). A comparison between three independent OGFOD1-defective cell lines was made to consider the possibility that effects might be specific to different cell types. Accordingly, OGFOD1-defective cell lines that were derived in HEK293, SW620 and HeLa backgrounds were investigated. To assay the effect of OGFOD1 loss on total protein levels, lysates from wild-type and OGFOD1-defective cell lines were prepared. A highly denaturing lysis buffer containing 9M urea was used to extract total protein including chromatin-associated proteins. The amount of protein solubilised by this extraction method was referenced to non-denaturing (JIES) lysis buffer, which was subsequently used to define THAP11 associations and complex composition (see section 6.2.4). Immunoblotting for OGFOD1 indicated an apparent loss of OGFOD1 protein in

OGFOD1-defective cells irrespective of protein extraction method (Figure 6.1). Consequent with OGFOD1 loss, immunoblotting with an antibody specific to the non-hydroxylated form of RPS23 demonstrated clear signal enrichment in CRISPR-defective lines relative to wild-type counterparts, indicating that functional inactivation of the OGFOD1 gene had been achieved in SW620 and HeLa backgrounds. When comparing across the cell panel, no clear differences in THAP11 or RPS23 levels were observed in response to OGFOD1 loss. These findings were independent of cell lysis protocol, with the immunoprecipitation-compatible (JIES) buffer extracting and solubilising similar amounts of assayed protein. THAP11 and RPS23 levels appeared lower in HeLa cells, however, this may in part be due to differences in protein loading between the different cell lines.

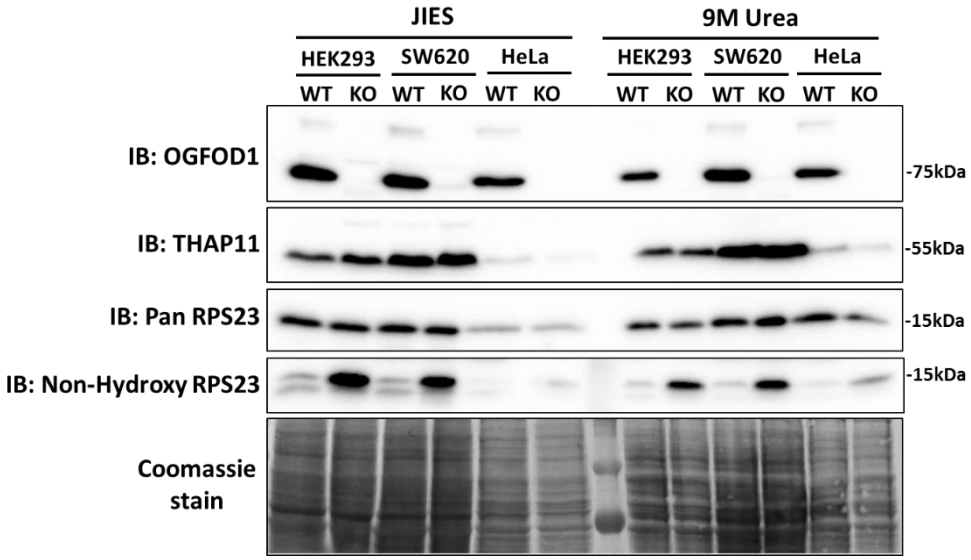


Figure 6.1: Characterisation of the effect of OGFOD1 loss on THAP11 and RPS23 protein levels with different protein extraction methods (JIES and 9M urea lysis buffers). Immunoblot demonstrating the effect of OGFOD1 loss on THAP11 and RPS23 protein levels using wild-type (WT) and OGFOD1 knockout (KO) HEK293 (clone DN2), SW620 and HeLa cells. Immunoblotting with an anti-OGFOD1 antibody demonstrated loss of OGFOD1 protein in the knockout cells and immunoblotting for non-hydroxylated RPS23 revealed a commensurate induction of the non-hydroxylated form in knockout cells. No clear effect on RPS23 or THAP11 protein levels were observed in response to OGFOD1 loss. Cells were harvested with different lysis buffers: JIES - used for IP experiments, and 9M urea - used for whole cell extraction.

Taking a similar approach, the protein levels of THAP11 and RPS23 were assessed in response to OGFOD1 inducible re-expression. Cell lysates were prepared with JIES lysis buffer from two independent OGFOD1 inducible re-expressing HEK293 clones ('e' and 'f'), that were derived from OGFOD1 knockout 'DSB' clone (chapter 3: Figure 3.4A). OGFOD1 inducible re-expressing HEK293 clones were treated with doxycycline for the indicated timepoints (Figure 6.2). OGFOD1 Immunoblotting indicated a clear induction of OGFOD1 in response to doxycycline treatment. A reduction in non-hydroxylated RPS23 was observed in response to doxycycline treatment with suppression achieved in both clones by day 3. However, no significant effect on RPS23 or THAP11 levels was observed with OGFOD1 re-expression, replicating observations in paired, non-isogenic OGFOD1-defective and wild-type HEK293 cells (Figure 6.1).

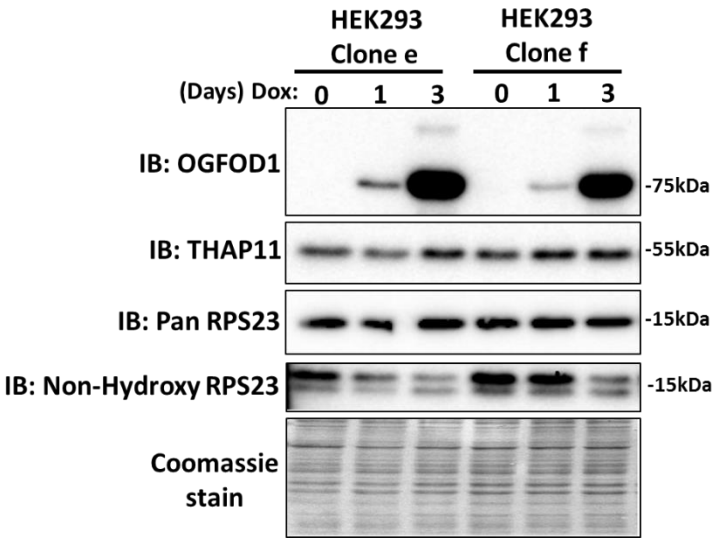


Figure 6.2: Characterising the effect of OGFOD1 re-expression on THAP11 and RPS23 protein levels. Immunoblotting for OGFOD1 demonstrates re-expression in HEK293 OGFOD1 knockout clones 'e' and 'f' (derived from OGFOD1 knockout 'DSB' clone) in response to doxycycline treatment (1 µg/ml) for the indicated times. Immunoblotting with anti-non-hydroxylated RPS23 antibody demonstrates suppression of the non-hydroxylated form in response to doxycycline treatment. No clear effect on RPS23 or THAP11 protein levels were observed in response to OGFOD1 overexpression over the 3-day time course.

6.2.2 The effect of OGFOD1 on the subcellular localisation of THAP11 and RPS23

Although no alterations in total protein levels were observed, it remained possible that OGFOD1 inactivation had an effect on the subcellular distribution of THAP11 or RPS23. As a first assessment of this, the localisation of THAP11 and RPS23 following OGFOD1 loss was determined by confocal immunofluorescence (Figure 6.3). Immunostaining for OGFOD1 demonstrated that a homogeneous population of OGFOD1-defective cells had been isolated following CRISPR-mediated gene targeting. THAP11 Immunofluorescence was predominantly nuclear with discernible cytosolic staining. Similar observations were made for ectopic FLAG-THAP11 (chapter 5: Figure 5.8A) and furthermore, are consistent with published reports (Parker et al., 2012). No clear difference in THAP11 staining was observed between wild-type and OGFOD1 knockout HEK293 cells (Figure 6.3). Total RPS23 levels were

immunostained using an anti-RPS23 antibody and indicated a predominantly cytosolic stain. No clear effect of OGFOD1 loss on RPS23 localisation was observed in wild-type versus OGFOD1 knockout cells.

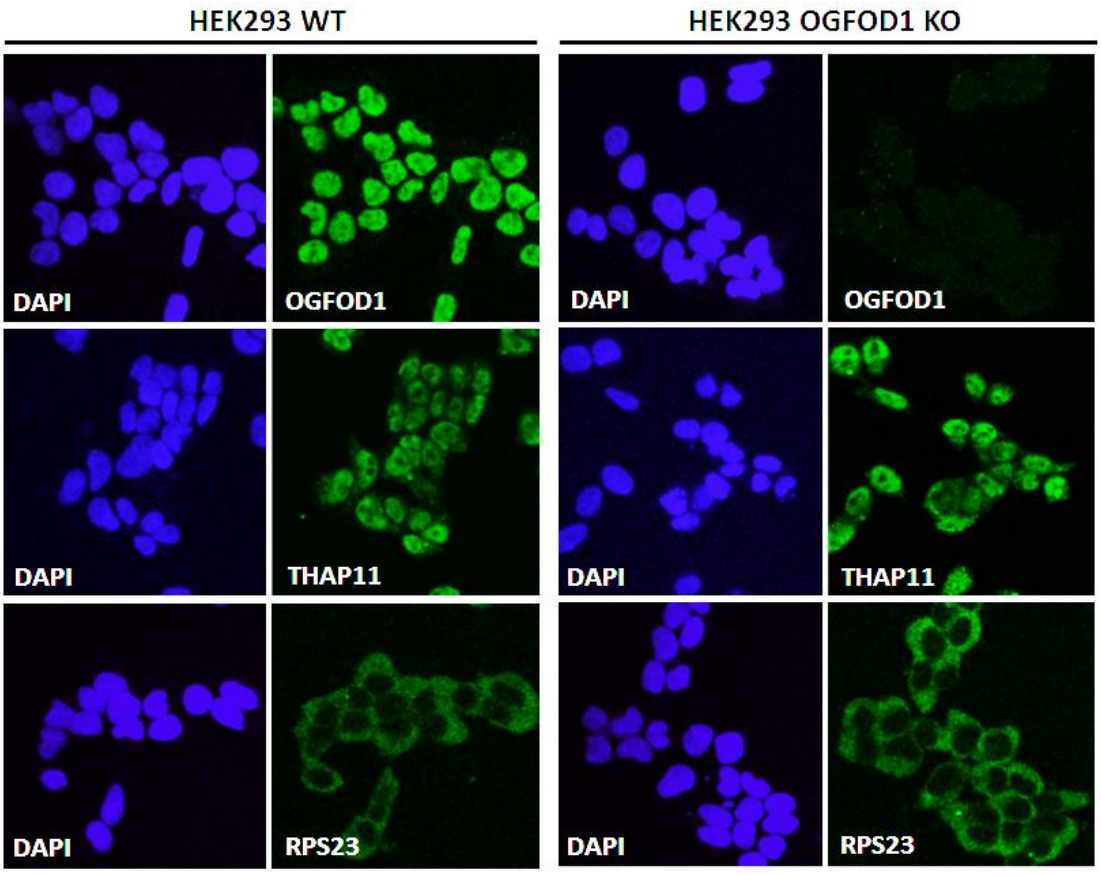


Figure 6.3: Characterisation of the effect of OGFOD1 loss on the subcellular localisation of THAP11 and RPS23. Confocal immunofluorescence in wild-type and OGFOD1 knockout (KO) (clone DN2) HEK293 cells. Anti-OGFOD1 antibody demonstrates loss of OGFOD1 protein in the knockout cells. A predominant THAP11 nuclear stain is observed with some cytosolic staining in both wild-type and OGFOD1 knockout cells using anti-THAP11 antibody. A predominant cytosolic RPS23 signal is observed in both wild-type and OGFOD1 knockout cells using anti- (pan) RPS23 antibody. Nuclei are counterstained with DAPI (blue).

To assess the effect of acute changes in OGFOD1 on the subcellular localisation of THAP11 and RPS23, OGFOD1 inducible re-expressing HEK93 cells (clone 'f') were utilised. OGFOD1 re-expressing HEK293 cells were treated with doxycycline for 3 days before co-staining with either, anti-OGFOD1 and anti-(pan) RPS23 (Figure 6.4A), or anti-FLAG (OGFOD1) and anti-THAP11 antibodies (Figure 6.4B). The results demonstrate that ectopically expressed FLAG-

OGFOD1 predominantly localises to the nucleus. Surprisingly, it was noted that the re-expression level of OGFOD1 had markedly declined from early passage cultures used in proliferation assays (>80% high re-expression; chapter 3: Figure 3.4B) to those described here (<50% high OGFOD1 re-expressing cells; Figure 6.4). Importantly, immunoblotting with an antibody specific to non-hydroxylated RPS23 demonstrated a level of functional restoration within the cell population (Figure 6.2). This finding would argue that the shift in OGFOD1 expression likely reflects a downregulation of OGFOD1 expression, rather than outgrowth of OGFOD1-defective cells. Regardless of how the phenomena originated, the heterogenous population of OGFOD1 expressing cells enabled a direct comparison between OGFOD1 expression levels and the subcellular localisation of RPS23 and THAP11 within the same field of view. In this way, a striking correlation between OGFOD1 expression and enhanced nuclear RPS23 signal was observed that titrated with expression of ectopic OGFOD1 (Figure 6.4A). Similar associations were observed between OGFOD1 and THAP11, although the dynamic range was less owing to the basal nuclear expression of THAP11 (Figure 6.4B). Collectively, these results indicate that OGFOD1 is capable of sequestering RPS23 and THAP11 in the nucleus when overexpressed. These data are consistent with OGFOD1-dependent nuclear partitioning of RPS23 and THAP11 independent of protein stability (Figure 6.2). However, since the minority of cells express FLAG-OGFOD1 at a level sufficient to observe the effect, there are caveats to this interpretation.

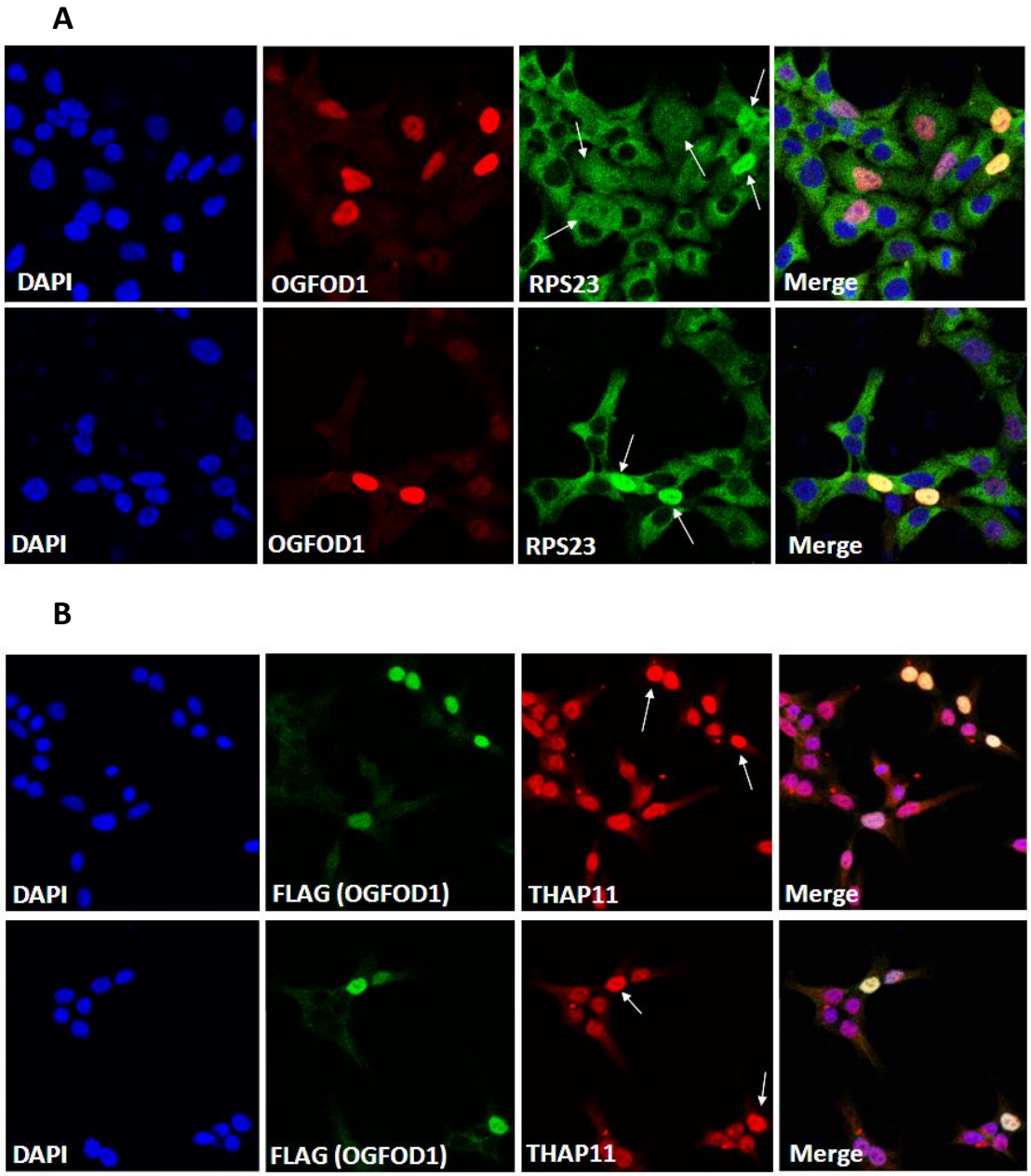


Figure 6.4: Characterising the effect of OGFOD1 re-expression on the subcellular localisation of RPS23 and THAP11. OGFOD1 inducible re-expressing HEK293 cells (clone 'f') were pre-treated with doxycycline (1 µg/ml) for 3 days prior to confocal immunofluorescence**.** Cells were co-stained with anti-OGFOD1 antibody and anti-RPS23 antibody **(A)**, or anti-FLAG (OGFOD1) antibody and anti-THAP11 antibody **(B)**. Heterogeneous OGFOD1 re-expression was observed that upon co-staining correlated with enhanced nuclear expression of RPS23 and THAP11 (indicated by arrow). Two representative fields of view per antibody couple are presented.

6.2.3 The effect of OGFOD1 loss on the THAP11 interactome

In considering the observation that THAP11 is potentially sequestered into a nuclear-OGFOD1 containing complex, I decided to investigate the THAP11 interactome by proteomic analysis in wild-type and OGFOD1-defective cells. In addition to providing a better definition of the effect of OGFOD1 on THAP11, this approach could also uncover potentially novel THAP11 function(s).

Endogenous THAP11 immunoprecipitations were favoured as a physiological context in which to observe potential OGFOD1-depedent shifts in protein associations. Preparative-scale THAP11 immunoprecipitations were performed in wild-type and OGFOD1-defective HEK293 cells. Control (THAP11 IP/IB) immunoblots indicated clear enrichment of THAP11 protein in THAP11 immunoprecipitates (and reciprocal loss of signal in the post IP "depleted" lysate) derived from both wild-type and OGFOD1-defective cell lysate (Figure 6.5). Proteomic analysis was performed on the isolated endogenous THAP11 complexes following in-solution trypsinolysis. THAP11 interacting proteins were identified and relative label-free quantitation was performed with the PEAKS software package (as described in chapter 5: section 5.2.1). In order to perform a robust analysis of the OGFOD1 dependence on the THAP11 interactome, proteins present in the rabbit IgG IP from either wild-type or OGFOD1 knockout cells were excluded. I initially focussed on the top 30 THAP11 interacting proteins in wild-type HEK293 cells to determine the effect of OGFOD1 loss on the highly abundant and high stoichiometry associations. Interacting proteins in wild-type HEK293 cells were ranked according to peptide-level abundance (mean intensity of two unique peptides against the identifying protein (Table 6.1: 'THAP11 IP WT OGFOD1 area' column). The data supported the efficiency of the THAP11 IP/IB (Figure 6.5) as THAP11 was a highly abundant species. Furthermore, the level of THAP11 capture between wild-type and OGFOD1

knockout cells was nearly equivalent (wild-type: OGFOD1 knockout; 1:0.91) (Table 6.1: 'Ratio' column).

Based on the ratios of the top 30 THAP11 interacting proteins between wild-type and OGFOD1 knockout cells and within the limitations of a single experiment (Table 6.1: 'Ratio' column) it was evident that OGFOD1 loss did not have a significant impact on the THAP11 interactome. However, associations between THAP11 and a number of novel proteins were observed that remained of interest. A number of ribosomal proteins including both large and small ribosomal subunits co-purified with THAP11. Furthermore, an association between THAP11 and G3BP1 was noted given the proposed roles for OGFOD1 in stress granule assembly (Wehner et al., 2010; Singleton et al, 2014). Although no large OGFOD1-dependent effects were observed between THAP11 and these complexes, further work would be required to understand whether THAP11 possesses a functional role in translational control.

To further explore the effect of OGFOD1 loss on the THAP11 interactome, I next considered the top 100 THAP11 interacting proteins in wild-type HEK293 cells. Proteins that showed a 2-fold difference in enrichment ratio between wild-type and OGFOD1 knockout cells were determined. Surprisingly, OGFOD1 loss did not appear to have a large effect on the THAP11 interactome in this larger data set. Only 7 proteins out of the top 100 THAP11 interacting proteins showed a 2-fold difference in enrichment ratios between wild-type and OGFOD1 knockout cells (Table 6.2: 'Ratio' column). Furthermore, a number of the differentially regulated proteins appear to be low stoichiometry (Table 6.2: 'Rank' column) suggesting the effects are unlikely to be biologically significant.

Whilst OGFOD1 loss did not appear to have a significant impact on the THAP11 interactome, it was noted that OGFOD1 or HCF-1 was not detected in the proteomic datasets in either wild-type or OGFOD1 knockout cells. The absence of known THAP11 interacting proteins

suggests that a proportion of the THAP11 interactome has not been captured. Although the reasons for this remain unclear, this highlights a potential technical caveat to the work presented.

Despite this, I sought to investigate THAP11 function further and I considered the enrichment between the identified THAP11 associations. The top 100 THAP11 interacting proteins were subject to STRING analysis as described in chapter 5 (Figure 6.6). Functional enrichment between THAP11 and the mediator complex, a transcriptional co-activator that associates with RNA polymerase II, supports its predominant role as a transcriptional regulator (Taatjes et al., 2010). It was also noted that a large number of other ribosomal proteins interacted specifically with THAP11. As too did the eIF3 complex, a large protein scaffold involved in the formation of translation initiation complexes and with a role in regulating specific mRNAs linked to cell proliferation (Lee et al., 2015). Finally, an association between THAP11 and a number of other stress granule proteins, including G3BP2 and USP10 were observed. Stress granules are largely comprised of stalled translation initiation complexes, 40S ribosomal subunits and mRNA (Kedersha et al., 2016). Collectively these findings point to an interesting and potentially novel role for THAP11 in translational control through its association with eIF3, ribosomal proteins, and stress granule proteins.

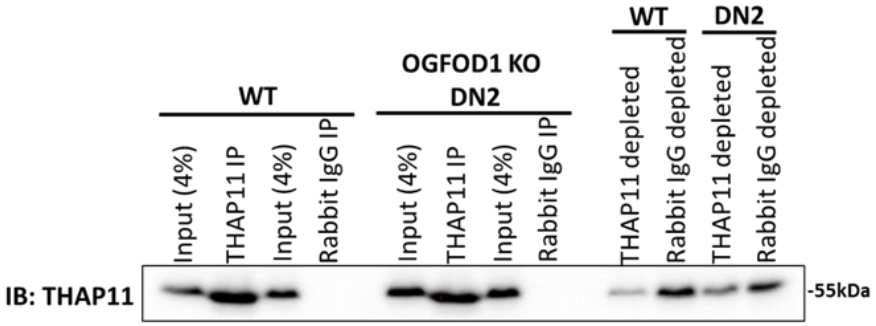


Figure 6.5: Confirming the efficacy of preparative scale THAP11 pulldowns. THAP11 immunoblot of preparative-scale THAP11 pulldowns in wild-type and OGFOD1-defective (DN2 clone) HEK293 cell lines. Anti-THAP11 antibody, and not control (normal Rabbit IgG) immunoprecipitates THAP11. The level of THAP11 capture is similar in wild-type and OGFOD1 knockout cells. Depletion of THAP11 within the lysates is similar between the wild-type and OGFOD1 knockout cells as indicated in the 'depleted' fractions.

Gene ID	Significance	Coverage (%)	#Unique	THAP11 IP OGF KO Area	THAP11 IP OGF WT Area	Ratio (OGF KO/OGF WT)	Description
RPSA	200	71	27	97500000	169000000	0.58	40S ribosomal protein SA (Fragment)
RPL8	200	58	24	65200000	99800000	0.65	60S ribosomal protein L8
THAP11	200	26	9	44500000	49100000	0.91	THAP domain-containing protein 11
RPL3	200	52	6	3240000	29000000	0.11	60S ribosomal protein L3
RPS15A	200	62	9	48500000	27900000	1.74	40S ribosomal protein S15a
G3BP1	200	57	16	29900000	23500000	1.27	Ras GTPase-activating protein-binding protein 1
RPL10	200	46	2	37200000	20500000	1.81	60S ribosomal protein L10
RPA1	200	62	25	58500000	20200000	2.90	Replication protein A 70 kDa DNA-binding subunit
DHX9	200	50	47	28700000	17700000	1.62	ATP-dependent RNA helicase A
SSBP1	200	48	7	7940000	14600000	0.54	Single-stranded DNA-binding protein mitochondrial
RPL13A	200	41	13	3730000	13800000	0.27	60S ribosomal protein L13a
SERBP1	200	50	4	19300000	13400000	1.44	Plasminogen activator inhibitor 1 RNA-binding protein
PRPF19	200	67	15	12300000	12400000	0.99	Pre-mRNA-processing factor 19
ILF2	200	75	19	13800000	12200000	1.13	Interleukin enhancer-binding factor 2
EMD	200	48	9	11100000	11300000	0.98	Emerin
HNRNPM	200	26	11	14500000	9660000	1.50	Isoform 2 of Heterogeneous nuclear ribonucleoprotein M
FAM98A	200	29	8	5550000	9660000	0.57	Isoform 2 of Protein FAM98A
FXR2	200	51	18	7410000	8590000	0.86	Fragile X mental retardation syndrome-related protein 2
RBBP4	200	59	8	6190000	8370000	0.74	Isoform 3 of Histone-binding protein RBBP4
NONO	200	38	14	12500000	8300000	1.51	Non-POU domain-containing octamer-binding protein
TOP2A	200	39	39	10200000	7860000	1.30	DNA topoisomerase 2-alpha
C14orf166	200	48	8	6720000	7730000	0.87	UPF0568 protein C14orf166
LARP1	200	43	27	10200000	7340000	1.39	La-related protein 1
DDX21	200	45	25	17000000	7300000	2.33	Isoform 2 of Nucleolar RNA helicase 2
MYBBP1A	200	39	40	11500000	6810000	1.69	Myb-binding protein 1A
DDX1	200	42	18	10200000	6570000	1.55	Isoform 3 of ATP-dependent RNA helicase DDX1
UPF1	200	47	35	5690000	6410000	0.89	Regulator of nonsense transcripts 1
RTCB	200	49	17	7200000	6360000	1.13	tRNA-splicing ligase RtcB homolog
SRP9	200	26	2	8430000	6240000	1.35	Signal recognition particle 9 kDa protein
TOP1	200	20	12	7130000	5980000	1.19	DNA topoisomerase 1

Table 6.1. Top 30 endogenous THAP11 interacting proteins in HEK293 cells in both wild-type and OGFOD1 knockout cells. Anti-THAP11 antibody or Rabbit IgG control antibody was used for immunoprecipitation in wild-type (OGF WT) and OGFOD1 knockout (OGF KO) HEK293 cells. THAP11 interacting proteins were identified using PEAKS software and were ranked according to the mean intensity of two unique peptides against the identifying protein in wild-type HEK293 cells (THAP11 IP WT OGFOD1 area column). Interacting proteins that were present in Rabbit IgG control IPs from both wild-type and OGFOD1 knockout cells were excluded in order to derive a list of robust THAP11 interacting proteins. The effect from OGFOD1 loss on the top 30 proteins is indicated in the “ratio”, values are normalised to “THAP11 IP OGF WT Area”.

Gene ID	Significance	Coverage (%)	#Unique	THAP11 IP OGF KO Area	THAP11 IP OGF WT Area	Ratio (OGF KO/OGF WT)	Rank (from top 100 THAP11 OGF WT Area)	Description
RPL22	200	38	5	36200000	2800000	12.93	84	60S ribosomal protein L22
RPA1	200	62	25	58500000	20200000	2.90	8	Replication protein A 70 kDa DNA-binding subunit
EIF3D	200	41	13	6430000	2480000	2.59	100	Isoform 3 of Eukaryotic translation initiation factor 3 subunit D
YBX3	200	54	3	6460000	2730000	2.37	90	Isoform 3 of Y-box-binding protein 3
DDX21	200	45	25	17000000	7300000	2.33	24	Isoform 2 of Nucleolar RNA helicase 2
C1QBP	200	19	4	1760000	3640000	0.48	59	Complement component 1 Q subcomponent-binding protein mitochondrial
RPL13A	200	41	13	3730000	13800000	0.27	11	60S ribosomal protein L13a

Table 6.2. THAP11 interacting proteins with a 2-fold difference in enrichment ratio between wild-type and OGFOD1 knockout HEK293 cells. Anti-THAP11 antibody or Rabbit IgG control antibody was used for immunoprecipitation in wild-type (OGF WT) and OGFOD1 knockout (OGF KO) HEK293 cells. THAP11 interacting proteins were identified using PEAKS software and were ranked according to the mean intensity of two unique peptides against the identifying protein in wild-type HEK293 cells (THAP11 IP WT OGFOD1 area column). Interacting proteins that were present in Rabbit IgG control IPs from both wild-type and OGFOD1 knockout cells were excluded. A list of the top 100 THAP11 interacting proteins were derived in wild-type HEK293 cells and proteins with a 2-fold difference in enrichment ratio between wild-type and OGFOD1 knockout cells are presented. The effect from OGFOD1 loss is indicated in the "ratio", values are normalised to "THAP11 IP OGF WT Area". Position in the list of top 100 THAP11 interacting proteins in wild-type HEK293 cells is indicated by the "Rank (from top 100 THAP11 OGF WT Area)".

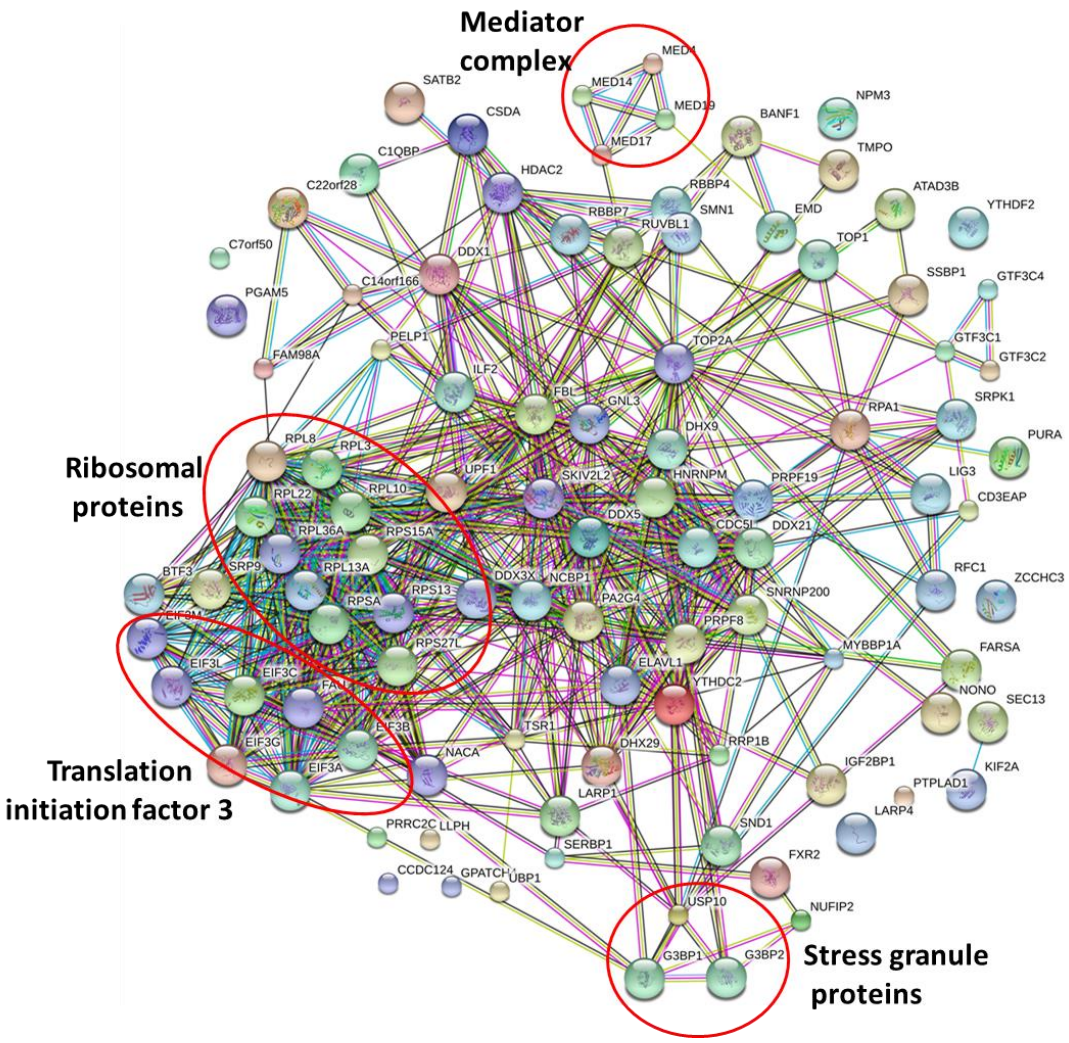


Figure 6.6 STRING analysis of the top 100 endogenous THAP11 interacting proteins in HEK293 cells. The top 100 endogenous THAP11 interacting proteins in wild-type HEK293 cells defined by peptide level abundance and meeting significance threshold (Peaks score >20 -10lgP) and an enrichiment ratio of over 10-fold relative to control antibody were subject to functional categorisation by STRING analysis.

6.2.4 The effect of OGFOD1 on THAP11 and RPS23 complexes

The interpretation of the THAP11 interactome in wild-type and OGFOD1 knockout cells was limited given the absence of OGFOD1 in the THAP11 pull-down (Figure 6.6). To better understand the OGFOD1 and THAP11 interaction I wished to determine the composition of THAP11 protein complexes. To this end, a biochemical fractionation technique was utilised termed sucrose gradient sedimentation. This technique separates proteins by centrifugation based on their size, typically through a sucrose gradient. An outline of this technique is highlighted in Figure 6.7.

To consider whether OGFOD1 inactivation modulates THAP11 protein complex composition, lysates from wild-type and OGFOD1 knockout HEK293 cells were prepared and passed through a 10-40% sucrose gradient by ultracentrifugation. Twenty fractions within the sucrose gradient were collected, desalted by methanol chloroform extraction and subject to SDS-PAGE immunoblot analysis of OGFOD1-related components and/or reference proteins. In addition to OGFOD1, THAP11 and RPS23, I considered the following proteins: (i) G3BP1 - reported as an OGFOD1-interacting protein by Wehner et al., 2010 and a THAP11 interacting protein (Table 6.1) and; (ii) RPL13A - identified as a specific THAP11 interacting protein (Table 6.1) and used to define fractions containing 60S ribosomal protein complexes. To help identify clonal artefacts unrelated to OGFOD1, I compared sucrose sedimentation profiles of wild-type HEK293 cells with two independent OGFOD1-defective clones ('DN2' and 'DSB') derived by CRISPR. Pre-fractionated input levels were also assessed - which included the use of a reference wild-type input lysate to facilitate cross-blot comparisons (i.e., normalisation of immunoblot exposures).

Immunoblotting fractionated lysates indicated that OGFOD1 existed exclusively in low molecular weight complexes in wild-type cells (Fractions 1-4, Figure 6.8). The sucrose sedimentation profile revealed by THAP11 immunoblotting indicated the existence of three

discrete protein complexes: a low molecular weight complex overlapping with OGFOD1 (Fractions 1-4), and two higher molecular weight complexes overlapping with RPS23, which likely represent the position of 40S (Fractions 11-13) and 80S ribosomes (Fractions 16-18) complexes within the gradient. In support of this, prior incubation of lysate with ribonuclease A redistributed ribosomal proteins to low density fractions (Dr. Matthew Cockman, personal communication). Pre-ribosomal RPS23 signal (complexed to OGFOD1; fractions 1-4) was not detected in wild-type lysate, perhaps reflecting the low steady state levels of non-ribosomal RPS23. In this setting, OGFOD1 inactivation did not measurably alter the sedimentation of RPS23 or THAP11 with similar profiles observed between wild-type and OGFOD1 knockout cells (Figure 6.8). Nonetheless, the striking overlap between THAP11 and RPS23 sedimentation profiles and the finding that these complexes are discrete from OGFOD1 was of considerable interest. Taken together, these data corroborate the findings of the THAP11 interactome screen and establish a novel interface between THAP11 and the protein synthesis machinery (Figure 6.6).

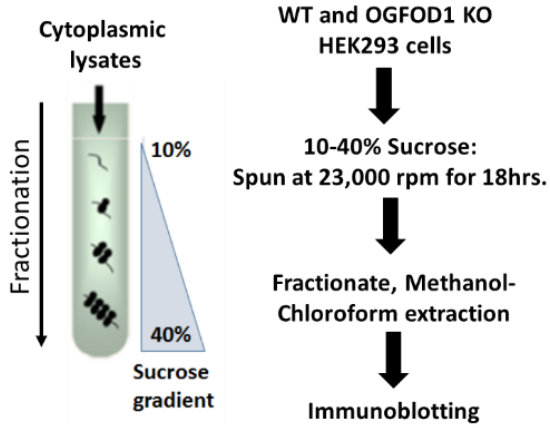


Figure 6.7: Schematic of sucrose gradient sedimentation technique. Lysates from WT and OGFOD1 CRISPR-derived knockout HEK293 clones were passed through a sucrose gradient (10-40%) by ultracentrifugation (at 23,000 rpm for 18 hours). Fractions collected from the top of the gradient represent low molecular weight complexes and fractions from the bottom of the gradient represent high molecular weight complexes. Following collection, samples were precipitated by addition of methanol and chloroform and re-suspended in 9M urea before immunoblotting.

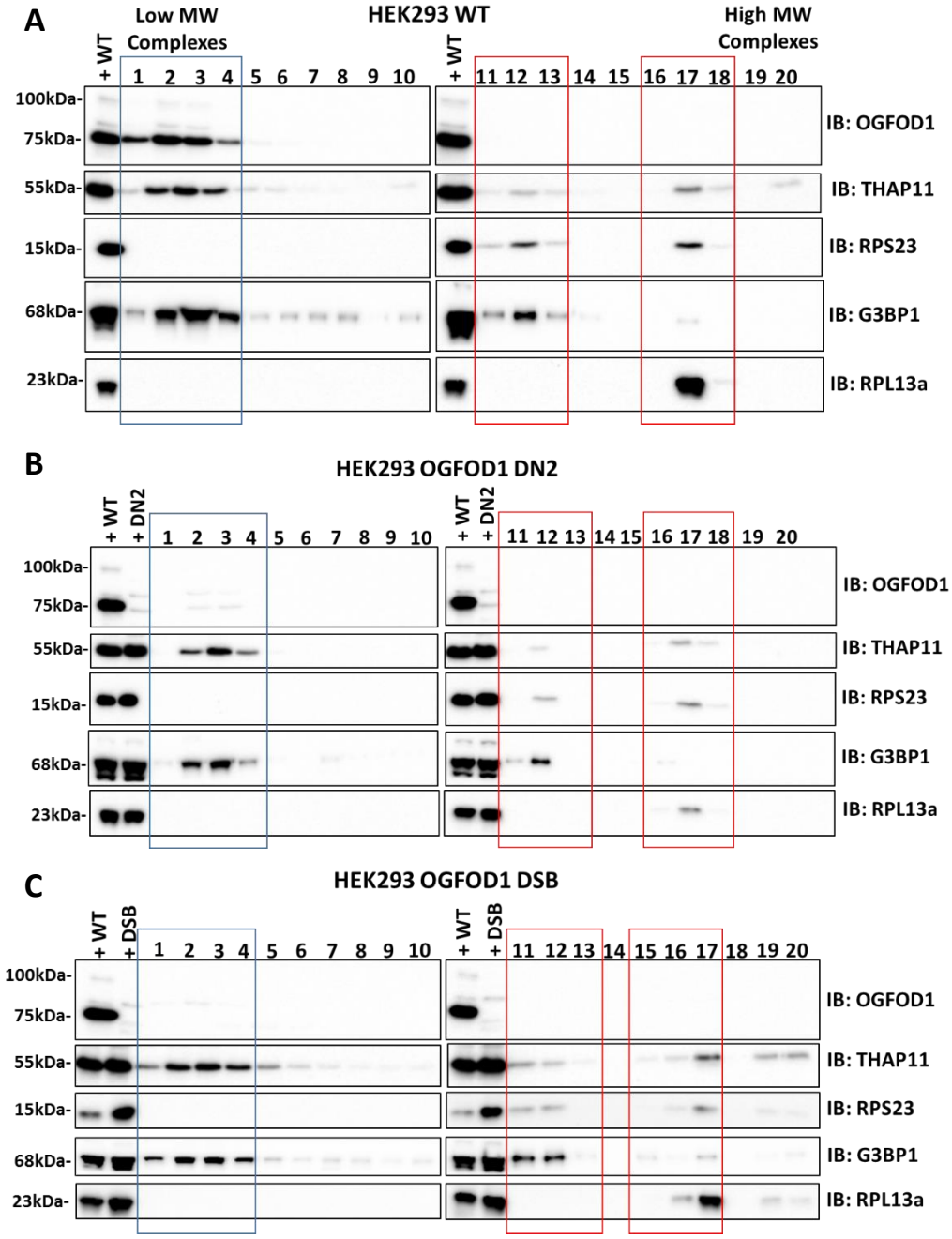


Figure 6.8 Protein complex fractionation in wild-type and OGFOD1 knockout HEK293 cells. **A)** Wild-type HEK293 cells were subject to sucrose gradient sedimentation. 20 fractions across the sucrose gradient were immunoblotted against the respective antibodies. **B) and C)** OGFOD1 knockout cells (DN2 and DSB clone, respectively) were subject to sucrose gradient sedimentation. +WT represents input of wild-type HEK293 lysate prior to ultracentrifugation. +DN2 and +DSB represents input of the OGFOD1 knockout cell lysates prior to ultracentrifugation. Blue box indicates the OGFOD1 low-molecular weight complex that overlaps with THAP11 and G3BP1. Red boxes represent two THAP11 high-molecular weight complexes that predominantly overlap with RPS23 and G3BP1 or RPS23 and RPL13a. To note, effects on total RPS23 levels between WT and DSB inputs were not observed in independent immunoblotting experiments.

The confocal immunofluorescence results indicated that changes in OGFOD1 expression can alter the subcellular distribution of its interacting partners: RPS23 and THAP11 (Figure 6.4). Therefore, it was hypothesised that effects on the distribution of their protein complexes would also be observed. The confocal immunofluorescent results indicated that OGFOD1 expression was not homogenous in the re-expressing cell line (Figure 6.4). Further assessment of this sub-line by immunofluorescence using an anti-OGFOD1 antibody indicated that a relatively large proportion of cells were unable to re-express OGFOD1 to the same extent as observed in earlier passage cultures (Figure 6.9 versus chapter 3: Figure 3.4B). As the cells were maintained in the absence of doxycycline and the presence of antibiotic selection, this highlights a technical caveat of this inducible re-expressing cell line. Therefore, an alternative cellular model was sought in which OGFOD1 re-expression could be better correlated with effects on THAP11 complexes.

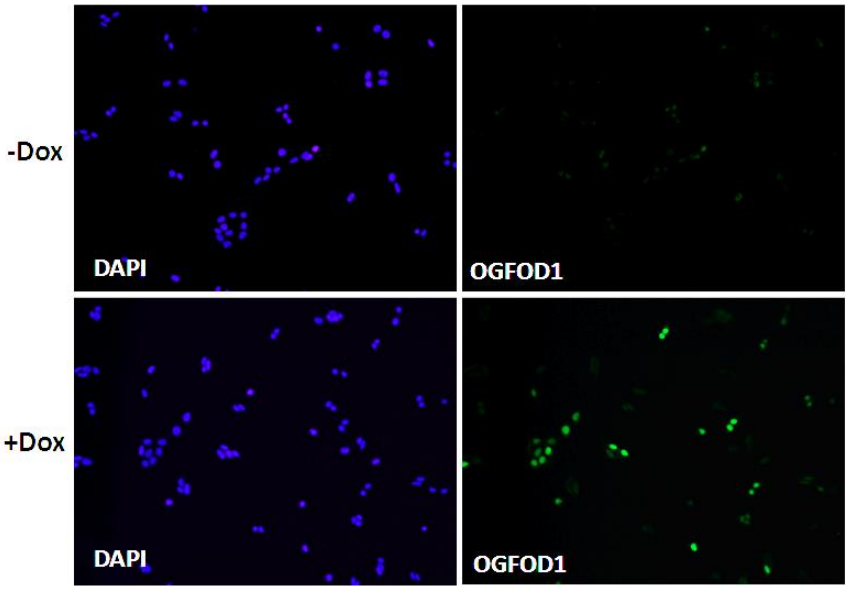


Figure 6.9: OGFOD1 re-expressing cells lose their ability to re-express OGFOD1 over time. Late passage clone 'f' was subject to confocal immunofluorescence using anti-OGFOD1 antibody following treatment with doxycycline (1 µg/ml) for 3 days. Relative to chapter 3: Figure 3.4B, immunofluorescence indicates a reduced number of cells that can re-express OGFOD1 in the presence of doxycycline.

To assess the effect on THAP11 complexes across a larger range of OGFOD1 expression a previously established cell model was utilised in mouse embryonic fibroblasts (MEFs). Sucrose gradient sedimentation was performed in OGFOD1 -/- MEFs and OGFOD1 -/- MEFs stably re-expressing FLAG-OGFOD1. These cell lines were obtained as a kind gift from Dr. Rachelle Singleton, University of Oxford. Although a different cell setting, this model may provide a more homogenous OGFOD1 re-expressing cell line and help to corroborate the confocal immunofluorescence data. Consistent with the sedimentation profile of endogenous OGFOD1 in HEK293 cells (Figure 6.8A), immunoblotting for OGFOD1 indicated that ectopic FLAG-OGFOD1 exists in low molecular weight fractions when it is re-expressed in MEFs (Figure 6.10A). RPS23 and THAP11 immunoblots also demonstrated a level of reproducibility, co-sedimenting in discrete high molecular weight fractions presumed to contain 40S and 80S ribosomal complexes in OGFOD1 -/- MEFs (Figure 6.10B). However, in the setting of OGFOD1 overexpression, clear OGFOD1-dependent shifts in RPS23 distribution and to a lesser extent THAP11 were observed (Figure 6.10A). In FLAG-OGFOD1 expressing MEFs, a striking redistribution of RPS23 was observed with RPS23 signal shifted from high molecular fractions into low molecular weight fractions that overlap with OGFOD1. Consistent with these being mediated by OGFOD1, ectopic FLAG-OGFOD1 forms a high stoichiometry association with RPS23 and is capable of sequestering RPS23 in the nucleus (Chapter 5: Figure 5.1; Chapter 6: Figure 6.4). These findings are further underscored by the appearance of the ~100 kDa OGFOD1:RPS23 adduct in the relevant low molecular weight fractions. A similar, albeit more modest, redistribution of THAP11 was also noted in the FLAG-OGFOD1 overexpressing cells. Overall, the results indicate that changes in OGFOD1 expression can impact on the cellular distribution of its interacting proteins. However, given the absence of a clear effect on cellular growth, further work may be required to understand the setting in which OGFOD1 modulation can mediate a phenotype.

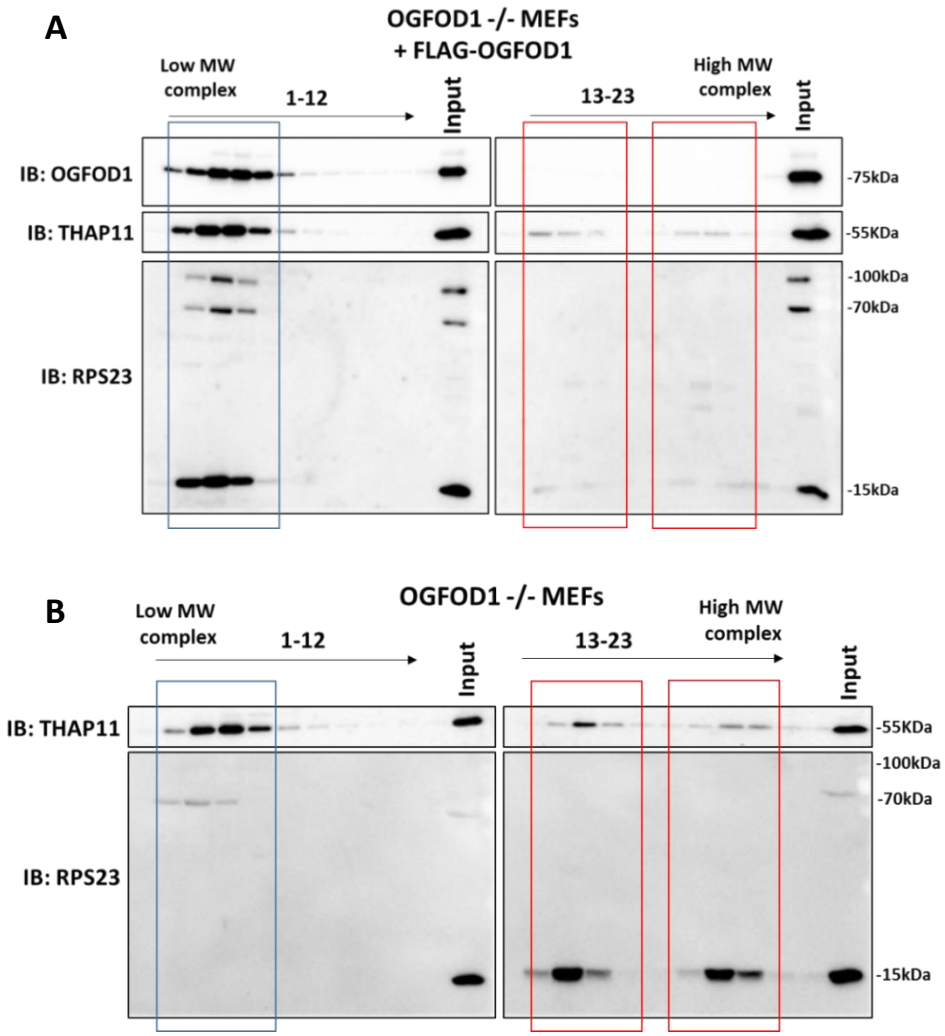


Figure 6.10: Protein complex fractionation in OGFOD1 -/- and OGFOD1 re-expressing mouse embryonic fibroblasts. OGFOD1 -/- MEFs transduced with FLAG-OGFOD1 and OGFOD1 -/- MEFs were subject to sucrose gradient sedimentation. 23 fractions across the sucrose gradient were collected and subject to methanol chloroform precipitation and re-suspension in 9M urea before immunoblotting. **A)** Immunoblotting of OGFOD1 -/- MEFs transduced with FLAG-OGFOD1 with anti-OGFOD1 antibody indicates that OGFOD1 exists in a low molecular weight complex when it is re-expressed. Immunoblotting using anti-THAP11 antibody demonstrates that THAP11 exists in a low molecular weight complex and two high molecular weight complexes when OGFOD1 is re-expressed. Immunoblotting using an anti-RPS23 antibody demonstrates that RPS23 exists in a low molecular weight complex at 100 kDa (OGFOD1:RPS23 adduct) and 15 kDa. **B)** Immunoblotting of OGFOD1 -/- MEFs using anti-THAP11 antibody demonstrates that THAP11 high molecular weight complexes are moderately increased and a subtle decrease in its high molecular weight complex is observed (relative to A). Immunoblotting using an anti-RPS23 antibody demonstrates that RPS23 exists in two high molecular weight complexes in OGFOD1 -/- MEFs. RPS23 bands at 70 kDa appear as cross-reactive species. Input represents lysate from the OGFOD1 re-expressing MEFs prior to ultracentrifugation.

6.2.5 Investigating the role of THAP11 in translational control

The novel association between THAP11 and the translational machinery (including ribosomal proteins) was supported by the endogenous THAP11 interactome together with protein complex fractionation experiments (Figure 6.6; Figure 6.8; Figure 6.10). These data indicated that THAP11 may possess a role in global translational control that warranted further investigation.

The effect of THAP11 knockdown on ribosome biogenesis and protein translation was assessed by polysome profiling. This technique employs sucrose gradient centrifugation to separate individual subunits of the ribosome; 40S, 60S, 80S subunits, and polyribosomes; consisting of a cluster of ribosomes bound to mRNA in the act of translation. To identify potential OGFOD1 dependence in the role of THAP11 in translational control, THAP11 knockdown was performed in wild-type and two OGFOD1 knockout HEK293 clones (DN2 and DSB). Immunoblotting demonstrated the loss of OGFOD1 in the two knockout clones (DN2 and DSB) and confirmed that THAP11 knockdown had been achieved (>60% at the protein level) (Figure 6.11A). Analysis of polysome traces did not reveal any clear defects following THAP11 knockdown in either wild-type or OGFOD1 knockout cells, nor were there any noticeable differences in response to OGFOD1 loss compared to the wild-type cells (Figure 6.11B). Surprisingly, the results did not support a large effect from OGFOD1 or THAP11 modulation on global translation under steady state conditions in this cell type.

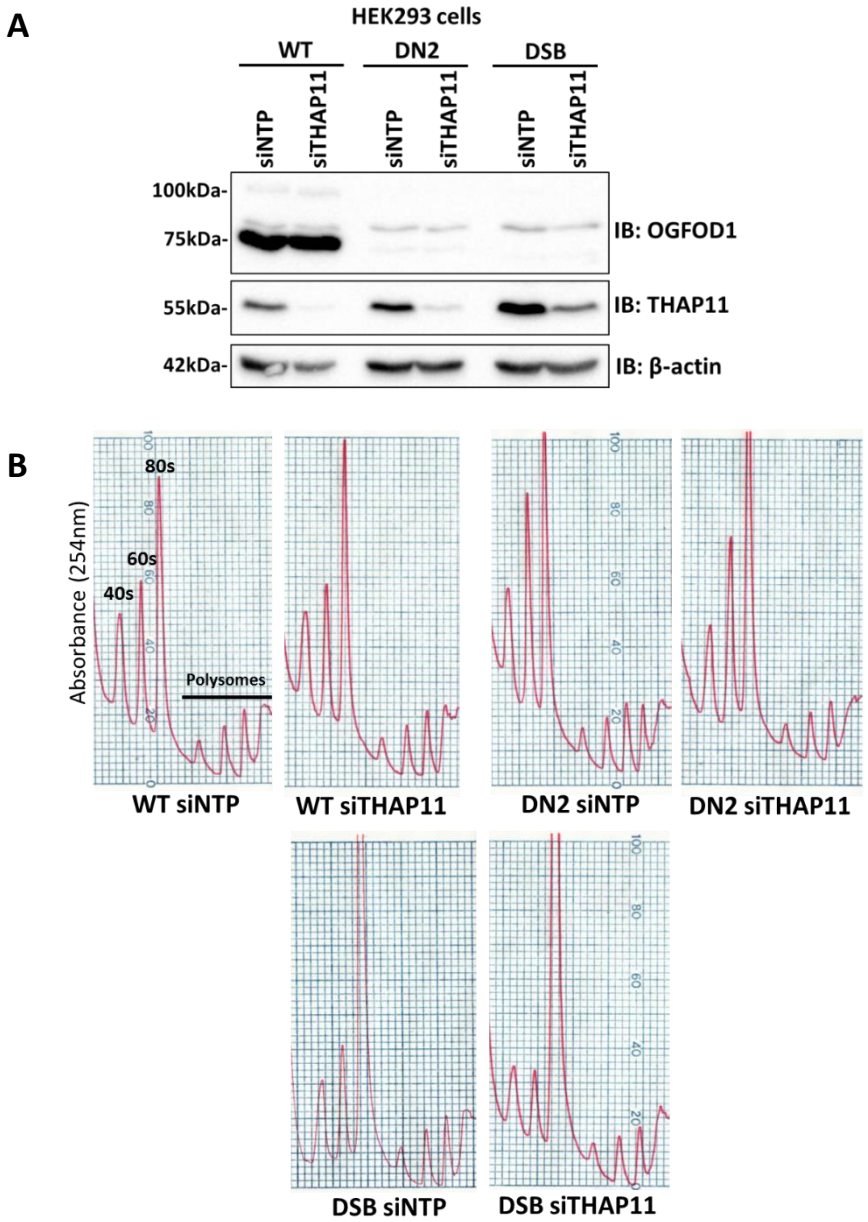


Figure 6.11: Investigating the role of THAP11 and OGFOD1 in translational control by polysome profiling. A) Immunoblot demonstrating THAP11 knockdown in wild-type and OGFOD1 knockout (DN2 and DSB) HEK293 cells. Cells were treated with pooled siRNA directed against THAP11 or equivalent control (non-targeting pool; NTP). Immunoblot analysis indicated >60% knockdown of THAP11 in wild-type and OGFOD1 defective cells. Control OGFOD1 immunoblots were also performed. **B)** Polysome profiles of wild-type and OGFOD1 knockout HEK293 cells treated with THAP11 siRNA. Lysates from **(A)** were normalised to 1-A260 before centrifugation through a sucrose gradient (17-50% w/v). Peaks corresponding to 40s, 60s, 80s and polysomes are annotated.

6.3 Discussion

The results presented in this chapter comprise a detailed analysis of THAP11 protein complexes in response to OGFOD1 modulation. As a first assessment, the effect on the total protein levels of THAP11 (and in parallel RPS23) was assayed by comparing wild-type and OGFOD1 knockout cells and inducible OGFOD1 re-expressing HEK293 cells, however, no clear differences were observed (Figure 6.1 and 6.2). This suggests that OGFOD1 is not functioning to regulate the synthesis, stability or degradation of THAP11 or RPS23 in these cellular contexts. In relation to THAP11, these findings also contrast with the effect of Ofd1 inactivation in *S. pombe* on the stability of the Sre1N transcription factor (Lee et al., 2009).

Subsequent analysis of the protein complexes by confocal immunofluorescence revealed that acute re-expression of OGFOD1 was associated with enhanced nuclear retention of THAP11 and RPS23 (Figure 6.4). These results were also consistent with effects on the protein complexes as assessed by sucrose gradient sedimentation in OGFOD1 re-expressing MEFs (Figure 6.10). A clear redistribution of RPS23 into a low molecular weight complex, that overlapped with OGFOD1, was observed in OGFOD1 re-expressing cells. Alterations in THAP11 protein complexes, although less pronounced, were also observed in response to OGFOD1 re-expressing MEFs. No clear effects on the subcellular distribution of THAP11 or RPS23 or their protein complexes were observed between wild-type and OGFOD1 knockout cells (Figure 6.3 and 6.8). This suggests that in the context of the described assays, only ectopic OGFOD1 expression appears to mediate a regulatory function on THAP11 and RPS23 complexes. These effects are likely to be directed through enhanced OGFOD1 sequestration of THAP11 and RPS23, although further work using OGFOD1 mutants (that are unable to bind THAP11 or RPS23) would be required to confirm this hypothesis. In addition, given the striking redistribution of RPS23 in response to OGFOD1 re-expression, further investigation

would be required to determine whether there is a compensatory mechanism that exists to help maintain the composition of a functioning ribosome. Also, further work would be required to establish whether overexpressed OGFOD1 could alter a nuclear function of THAP11.

An effect from OGFOD1 inactivation on THAP11 complexes was not evident following a detailed analysis of the THAP11 interactome in wild-type and OGFOD1 knockout HEK293 cells (Table 6.1. and 6.2). However, the absence of OGFOD1 in the proteomic datasets, which could reflect occlusion of the antibody epitope upon complexation with OGFOD1, highlights a caveat of this data. Despite this, mass spectrometry analysis identified an interesting association between THAP11 and the ribosome, the eIF3 complex and stress granule proteins in wild-type HEK293 cells (Figure 6.6). This data was also supported by the co-sedimentation of THAP11 with RPS23, RPL13A and G3BP1, suggesting a novel non-nuclear role for THAP11 in translational control. Individual or combined loss of OGFOD1 or THAP11 did not have a significant impact on polysome profiles (Figure 6.11). Whether there was a cell context in which OGFOD1 or THAP11 could regulate global translation, or whether they exerted regulation on a specific subset of mRNAs would require further investigation.

The association between THAP11 and the translational machinery remains of interest, especially given the overlap between the co-sedimentation of THAP11 and RPS23. However, studies indicate that THAP11 is predominantly a nuclear transcriptional regulator (Dejosez et al., 2010; Parker et al., 2012). Based on the apparent nuclear sequestration of THAP11 following OGFOD1 overexpression (Figure 6.4B and 6.10) and given the sequence homology between THAP11 and Sre1N (chapter 5: Figure 5.7B), it is possible that OGFOD1 has a regulatory function on THAP11 transcription that operates in an analogous manner to Ofd1-dependent inhibition of Sre1N DNA binding (Lee et al., 2011).

Chapter 7: Investigating a regulatory role for OGFOD1 on the THAP11 transcriptional programme

7.1 Introduction and aims of the chapter

Work presented in chapter 6 established novel links between THAP11 and the protein synthesis machinery. Despite significant effort, however, I was not able to define a physiological effect of OGFOD1 intervention on a range of THAP11 properties, including protein abundance, sub-cellular disposition and protein complex association. In light of these results, I shifted focus to consider the possibility that OGFOD1 might regulate THAP11 transcription. In relation to this work, an interesting connection between THAP11 and the sterol responsive transcription factors (SREBPs) had emerged. Specifically, the DNA-binding determinants of THAP11 (defined by pan-genomic chromatin immunoprecipitation) closely resembled a promoter consensus (termed the M4 motif) that was also linked to SREBP DNA-binding (Xie et al., 2005; Seo et al., 2009; Dejosez et al., 2010). This finding raised the interesting possibility that the OGFOD1-THAP11 axis might be an evolutionary re-wiring of Ofd1-Sre1 signalling in *S. pombe*.

The THAP11-dependent transcriptional response has been characterised in a number of settings ranging from transgenic mouse models and cultured murine embryonic stem (ES) cells to human cancer cell lines (Dejosez et al., 2008 and 2010; Parker et al., 2012; Poche et al., 2016)[1]. Genome-wide assessment of THAP11 DNA binding and transcript level profiling indicate a diverse cohort of largely non-overlapping transcriptional targets. The THAP11 transcriptional program in mouse embryonic stem cells was of particular interest, with

[1] To note THAP11 is commonly termed 'Ronin' in the mouse.

significant enrichment reported for genes involved in protein biosynthesis. Exemplifying this, THAP11 was bound to the promoters and positively regulated the expression of multiple genes that encode ribosomal proteins, including RPS23 (Dejosez et al., 2010). Prominent nucleoli were characteristic of THAP11-overexpressing mouse ES cells, reinforcing the link between THAP11 transcription and augmented ribosome biogenesis. The transcriptional signature associated with THAP11 knockdown in SW620 human colon cancer cells was different to that observed in ES cells with no obvious connection to the protein synthesis machinery (Parker et al., 2012).

THAP11 functions as a transcriptional coregulator; it can either activate or repress its transcriptional targets. The mechanism(s) underlying the different dimensions of THAP11 target gene regulation remain obscure. However, a requirement for Host Cell Factor-1 (HCF-1), a ubiquitously expressed transcriptional regulator, is well established (Dejosez at al., 2008 and 2010; Parker et al., 2012). Association with HCF-1 is mediated by a tetrapeptide binding sequence E/DHXY (where X is any amino acid) in the *C*-terminus of THAP11. This consensus, which is present in other THAP family members, is commonly referred to as the HCF-1-binding motif (HBM) (Mazars et al., 2010). Extrapolations from related systems suggest that HCF-1 serves as a scaffold, linking THAP11 DNA-binding activity to enzymes capable of modulating the local histone and/or chromatin environment (Michaud et al., 2013).

In addition to the obligatory recruitment of HCF-1, a third component of the THAP11 transcriptional network, Zinc Finger Protein 143 (ZNF143) has recently been identified (Michaud et al., 2013; Ngondo-Mbongo et al., 2013; Parker et al., 2014). The significance of this binding event is less clear, however, with conflicting reports describing either co-factor function or mutually exclusive (competitive) binding with THAP11 (Ngondo-Mbongo et al., 2013; Parker et al., 2014).

The work presented in this chapter describes my attempts to define a functional role for OGFOD1 in THAP11-dependent gene expression. I used aforementioned ES and SW620 cell models in which to manipulate OGFOD1 levels and assay for effects on known THAP11 target genes.

7.2 Results

7.2.1 OGFOD1 does not associate with the THAP11 transcriptional co-activator HCF-1

THAP11 forms a mutually dependent complex on chromatin with HCF-1, a transcriptional co-regulator that is essential for cell-cycle progression and cell proliferation (Parker et al., 2014). Having established that a large proportion of THAP11 is bound by OGFOD1 in chapter 5 (Figure 5.5), I wished to gain further insight into the relationship between OGFOD1, THAP11 and HCF-1 binding. Thus, endogenous components were isolated by immunoprecipitation and co-precipitating partners were identified by immunoblotting in HeLa and SW620 cell lines. For THAP11, two independent polyclonal antibodies raised to different immunogens were used. Despite efficient retrieval of THAP11, neither OGFOD1 nor HCF-1 was detected in THAP11 immunoprecipitates (Figure 7.1). These findings contrast with FLAG-THAP11 pulldowns and suggest that (THAP11 antibody) epitope occlusion is the likely basis for these results (Chapter 5: Figure 5.7C). However, using reciprocal immunoprecipitating antibodies to OGFOD1 and HCF-1 associations with THAP11 were noted (Figure 7.1). Importantly, an association between OGFOD1 and THAP11 was detected in the absence of discernible HCF-1 co-precipitation and similarly an association between HCF1 and THAP11 was detected in the absence of any co-purifying OGFOD1. Taken together, these findings suggest that OGFOD1:THAP11 and THAP11:HCF-1 exist in mutually

exclusive complexes, and raise the possibility that OGFOD1 might limit THAP11 availability to HCF-1.

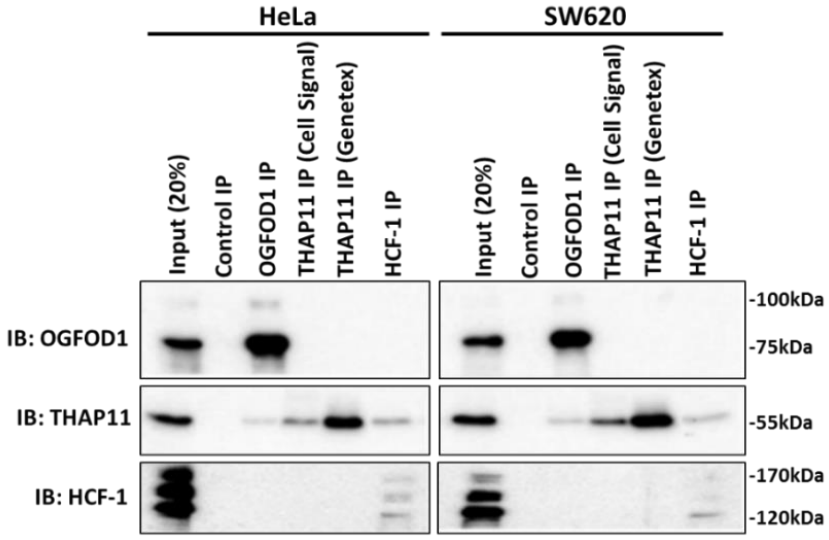


Figure 7.1: Characterisation of OGFOD1, THAP11 and HCF-1 protein complexes. In support of mutually-exclusive OGFOD1:THAP11 and THAP11:HCF-1 complexes; anti-OGFOD1 and anti-HCF-1 antibody, but not control (Rabbit IgG), co-precipitate THAP11 in the absence of either component in HeLa and SW620 cells.

7.2.2 Does OGFOD1 modulate the THAP11 transcriptional program in SW620 colon cancer cells?

To assay for effects of OGFOD1 modulation, I used the colon cancer cell line, SW620, which had previously been characterised with respect to its THAP11-dependent gene signature (Parker et al., 2012). In support of this being an appropriate cell context, a robust association between the OGFOD1 and THAP11 had been previously noted in SW620 cells (Figure 5.5C, and 7.1).

In the first instance, I sought to determine the effect of OGFOD1 overexpression on THAP11 dependent gene expression. SW620 cells were transduced with lentiviral plasmids encoding untagged OGFOD1 or empty vector (EV). Immunoblot analysis revealed supraphysiological expression of OGFOD1 protein and mRNA (Figure 7.2A and B). As a control for THAP11-

dependent gene expression changes (and to corroborate the findings of Parker et al.), THAP11 knockdown was performed in the untransduced (NT), EV and OGFOD1 overexpressing cells (Parker et al., 2012). The results indicated that ~60% knockdown of THAP11 protein and mRNA had been achieved (Figure 7.2A and C).

I assayed the effect of OGFOD1 overexpression on the most significantly regulated THAP11 target genes as determined by Parker et al (Parker et al., 2012). Accordingly, gene expression analysis was performed on the following targets by qPCR: THAP11 repressed (siTHAP11 upregulated) - ALG14, FBXL19; and THAP11 activated (siTHAP11 downregulated) - OPHN1. The expression of both THAP11-repressed (ALG14; Figure 7.2D, FBXL19; Figure 7.2E) and THAP11-activated (OPHN1; Figure 7.2F) target genes were modulated in OGFOD1 overexpressing cells relative to those expressing the empty vector (cf. columns 3 with 5). Notably, the highly repressed THAP11 transcript, FBXL19 - a member of the long non-coding RNA class, showed clear (4-fold) up-regulation by OGFOD1 overexpression. The effect of OGFOD1 overexpression on target gene expression was similar in magnitude to that observed when EV SW620 control cells were treated with THAP11 siRNA (cf. column 4 with 5). Target gene expression was further augmented in OGFOD1 overexpressing cells treated with THAP11 siRNA, presumably reflecting the combined potency of OGFOD1 overexpression under conditions of incomplete (~60%) THAP11 knockdown. Concordant effects of OGFOD1 overexpression with THAP11 knockdown on the expression of THAP11 target genes suggested that OGFOD1 can inhibit THAP11 activity when it is overexpressed in cells.

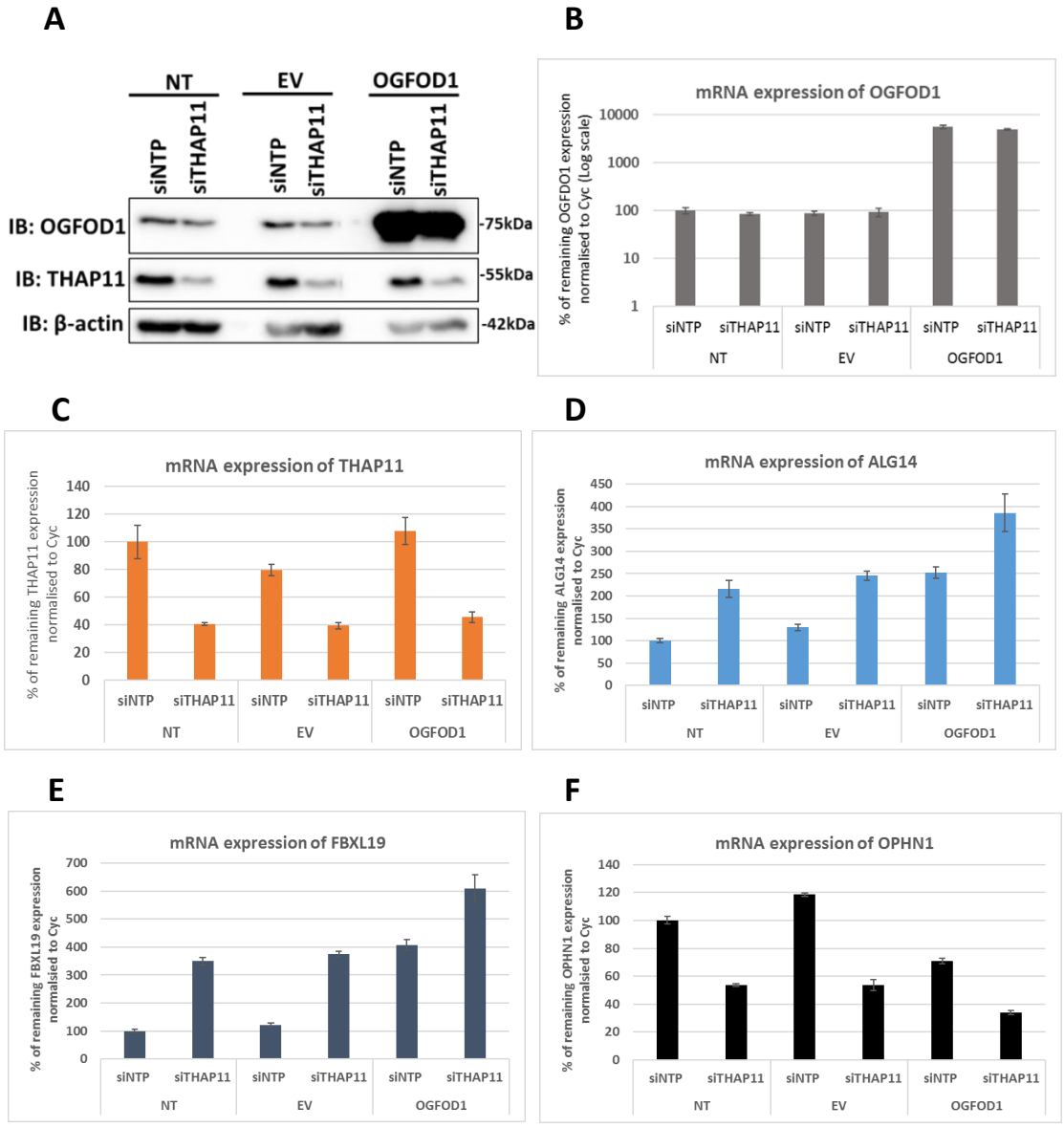


Figure 7.2: Characterisation of THAP11 transcriptional targets in response to OGFOD1 overexpression in SW620 cells. A) Immunoblot of OGFOD1 and THAP11 in untransduced SW620 cells (NT) or cells transduced with either empty vector (EV) or OGFOD1. Cell populations were transfected each at a concentration of 10 nM with non-targeting siRNA (siNTP) or THAP11 siRNA (siTHAP11) and harvested after 48 hours. Target gene mRNA expression was assessed by qPCR: OGFOD1 **(B)**, THAP11 **(C)**, ALG14 **(D)**, FBXL19 **(E)** and OPHN1 **(F)**. qPCR data represent the normalised mean expression between technical triplicates ± standard deviation.

I next sought to determine if there was a relationship between the level of OGFOD1 overexpression, the ability to capture/sequester THAP11, and effects on THAP11-dependent target gene expression. SW620 cells were transduced with lentiviral transfer plasmids encoding FLAG-tagged OGFOD1 (FLAG-OGFOD1) or EV upstream of an IRES-driven GFP reporter. Transduced cells were selected by GFP and flow-sorted into fractions representing the lowest 20% (low), the median (mid), and the top 20% (high) of GFP-positive cells, generating discrete populations with different levels of OGFOD1 expression.

FLAG immunoblotting revealed the expected correlation between GFP fluorescence and FLAG-OGFOD1 protein and mRNA levels (Figure 7.3A and B). Despite efficient retrieval of FLAG-OGFOD1 across all populations, THAP11 was not detected in FLAG IPs from the low-expressing OGFOD1 cells. These immunoprecipitates also showed only modest capture of RPS23. However, increased levels of OGFOD1 (mid and high fractions) was associated with a titratable increase in both THAP11 and RPS23 binding. It was also noted that OGFOD1 overexpression appeared to cause a modest stabilisation of RPS23 in the inputs of the FLAG-OGFOD1 in 'high' expressing cells, as had been observed with FLAG-OGFOD1 HA-RPS23 co-transfection experiments in chapter 4 (Figure 4.1).

THAP11 target gene expression was analysed in the different pools of OGFOD1 overexpressing cells. Expression of ALG14 and OPHN1, showed a modest response to OGFOD1 in 'high' expressing cells (Figure 7.3C and E). This could reflect differences in the levels of OGFOD1 overexpression in comparison to the untagged lentiviral construct (Figure 7.2A). FBXL19 was the most highly induced THAP11 target in the untagged OGFOD1 overexpressing cells. For this highly induced target, increased expression was observed when titrating OGFOD1 expression levels from 'low' to 'high' (Figure 7.3D), supporting an OGFOD1-regulatory effect on selected THAP11 target genes.

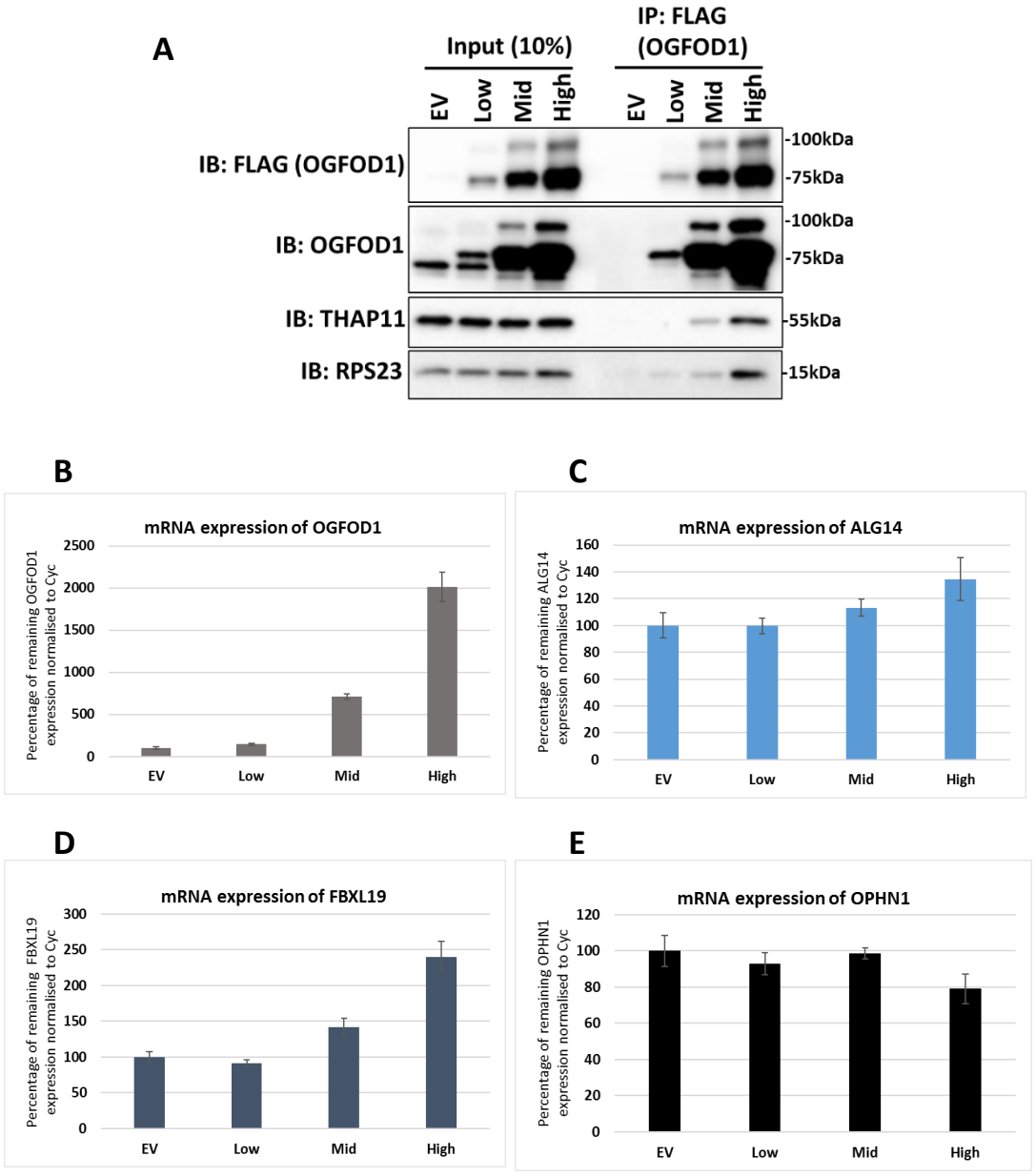


Figure 7.3: Characterisation of THAP11 transcriptional targets in response to differing levels of OGFOD1 overexpression in SW620 cells. A) Immunoblot of FLAG immunoprecipitates following FLAG IP in SW620 cells transduced with either empty vector (EV) or FLAG-OGFOD1 and GFP sorted (empty vector – top 20%; FLAG-OGFOD1 Low – lowest 20%; FLAG OGFOD1 Mid – median; and FLAG-OGFOD1 High – top 20%). Input corresponds to 10% of starting material. Target gene mRNA expression was assessed in response to OGFOD1 overexpression by qPCR: OGFOD1 **(B)**, ALG14 **(C)**, FBXL19 **(D)** and OPHN1 **(E).** mRNA expression is normalised to empty vector transduced cells. qPCR data represent the normalised mean expression between technical triplicates ± standard deviation.

In order to determine if the response to OGFOD1 overexpression could be negated by alterations to OGFOD1's catalytic activity or its ability to bind THAP11, two OGFOD1 variants were selected for further investigation. Namely, the catalytically inactive variant D157A and the variant F287A, which is unable to bind THAP11 yet retains hydroxylase activity (Dr. Matthew Cockman, Unpublished data). As before, OGFOD1 mutants were introduced into SW620 cells by lentiviral delivery and transduced cells were enriched by GFP sorting. FLAG IP was performed with a suboptimal FLAG affinity gel that did not efficiently immunopurify FLAG-OGFOD1 from the overexpressing cells. Exemplifying this, I observed equivalent capture of THAP11 between median and high-expressing wild-type OGFOD1 populations, which differs from Figure 7.3A when using excess FLAG affinity gel (~10-fold more per IP). Regardless of the quantitative aspects of the IP, the OGFOD1 variant F287A did not associate with THAP11, whilst the catalytically inactive variant D157A retained affinity for THAP11 (Figure 7.4A). On a separate note, D157A and F287A did not form the previously characterised 100 kDa OGFOD1-RPS23 SDS-PAGE resistant complex (Singleton et al., 2014).

Gene expression analysis of FBXL19 indicates reproducible effects of OGFOD1 overexpression with a titratable induction observed with 'mid' and 'high' OGFOD1 expressing cells relative to EV (Figure 7.4B). Importantly, FBXL19 expression is unchanged in cells overexpressing the F287A variant of OGFOD1 that is unable to bind THAP11, suggesting that gene expression changes are dependent on the association between OGFOD1 and THAP11. Cells overexpressing the D157A variant show a clear increase in FBXL19 expression, consistent with the robust THAP11 interaction data, and indicate that OGFOD1 catalytic activity is not required to exert THAP11-dependent gene expression changes. As stated previously, the D157A variant has a reduced affinity toward RPS23 (Singleton et al., 2014), but interestingly show a modest enhancement in FBXL19 expression relative to wild-type OGFOD1 cells. Whether this reflects cross talk with RPS23 (i.e., a more potent inhibitory

function for D157A by virtue of its reduced affinity or catalytic activity for RPS23), will be of interest to determine.

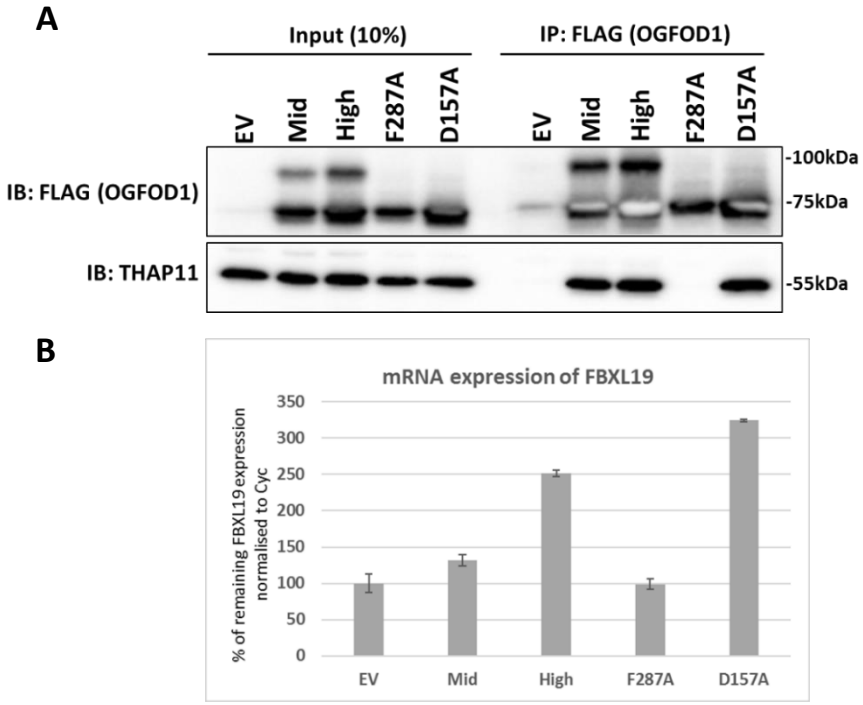


Figure 7.4 Characterisation of THAP11 transcriptional targets in response to overexpression of OGFOD1 mutants in SW620 cells. A) Immunoblot following FLAG IP of FLAG-OGFOD1 and FLAG-OGFOD1 mutants. Transduced cells were enriched by GFP sorting (top 20% for: 'EV', 'High', 'F287A' and 'D157A'; median value for 'Mid' FLAG-OGFOD1). **B)** mRNA expression of FBXL19 by qPCR in FLAG-OGFOD1 and FLAG-OGFOD1 mutant sorted cells. FBXL19 expression is normalised to EV transduced cells. qPCR data represent the normalised mean expression between technical triplicates ± standard deviation.

Parker et al. had performed ChIP-PCR of both repressed and activated THAP11 target genes and identified THAP11 binding within 500 bp of the annotated transcriptional start site of each target gene (Parker et al., 2012). The authors demonstrated THAP11 binding to both activated and repressed genes. OGFOD1 overexpression modulated THAP11 targets in a manner that was consistent with the effect of THAP11 knockdown. Therefore, it was hypothesised that OGFOD1 was acting upstream of THAP11 by preventing THAP11 from binding to DNA. To explore this further, THAP11 ChIP was performed in SW620 cells, transduced with either empty vector (EV) or an untagged OGFOD1 construct (Figure 7.5A

and B)**.** Results showed that OGFOD1 overexpression consistently reduced enrichment of immunoprecipitated chromatin across all four targets - up to around 50%. Despite differences in the amount of chromatin enrichment between two independent experiments the trend supports the hypothesis that OGFOD1 can sequester THAP11 and reduce its ability to bind DNA.

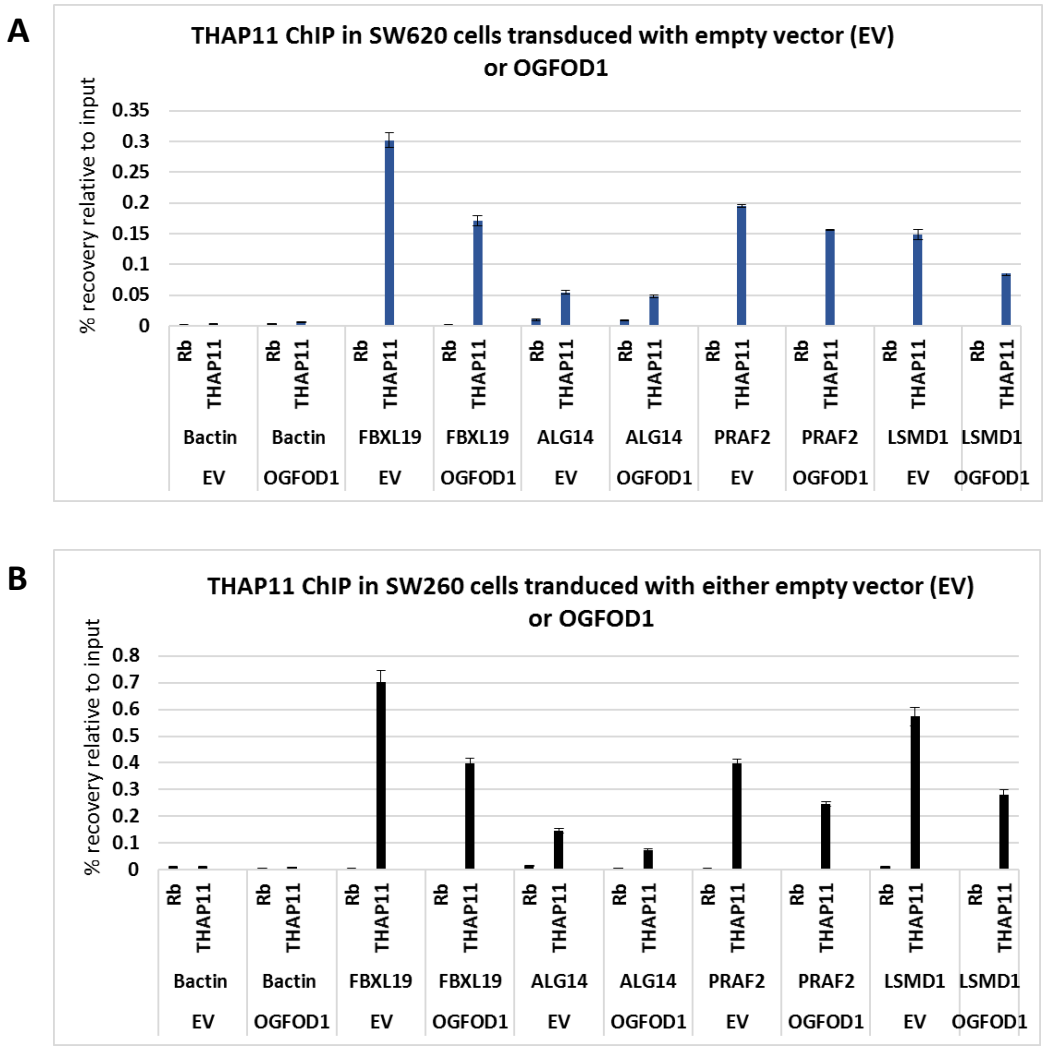


Figure 7.5: Characterisation of THAP11 DNA binding in response to OGFOD1 overexpression in SW620 cells. (A and B) THAP11 ChIP assay in SW620 cells transduced with either empty vector (EV) or OGFOD1 overexpression (using an untagged construct). Transduced cells were enriched by GFP sorting and the top 20% of GFP positive cells were retained. Standard methods were used for ChIP and DNA was immunoprecipitated by anti-THAP11 antibody or Rb IgG and amplified by real-time PCR. Primer pairs for qPCR analysis were selected from four THAP11 targets described by Parker et al., 2012. Chromatin enrichment at the four target sites: FBXL19, ALG14, PRAF2, and LSMD1 is expressed as a percentage of recovery relative to input. Results are from two independent experiments. Each target showed a consistent reduction in enrichment with OGFOD1 overexpression across the two experiments. Data represent the normalised mean expression between technical triplicates ± standard deviation.

In order to determine whether endogenous levels of OGFOD1 regulate the THAP11 transcriptional program in SW620 cells, siRNA mediated knockdown of OGFOD1 was performed. As a positive control for gene expression changes, THAP11 knockdown was performed in parallel. Transcript and protein expression analyses indicated efficient knockdown of both OGFOD1 and THAP11 (Figure 7.6A and B). No significant effect of OGFOD1 knockdown on THAP11 protein expression was observed or vice versa. It was also noted that THAP11 knockdown did not alter the OGFOD1:RPS23 100 kDa adduct, suggesting that THAP11 does not affect the formation of this species in this context.

The effect of OGFOD1 knockdown on the expression of THAP11 target genes was determined and representative qPCR analysis is shown for: LSMD1, ALG14 and OPHN1 (Figure 7.6C-E). Consistent with Parker et al., THAP11 knockdown was associated with a 3-fold increased expression of LSMD1 and ALG14, and a 3-fold reduction in OPHN1 expression relative to control siRNA (Parker et al., 2012). No effect of OGFOD1 knockdown was observed on any of the targets over the 96-hour time course. Independent siRNA knockdown experiments were performed with gene expression analysis carried out 48 hours after a second siRNA transfection. The mRNA levels of OGFOD1 and THAP11 indicated relatively efficient knockdown (Figure 7.7A and B). Effects of THAP11 knockdown were observed at this timepoint for FBXL19 and ALG14 (Figure 7.7C and D). However, no effect of OGFOD1 knockdown was observed on the same set of targets.

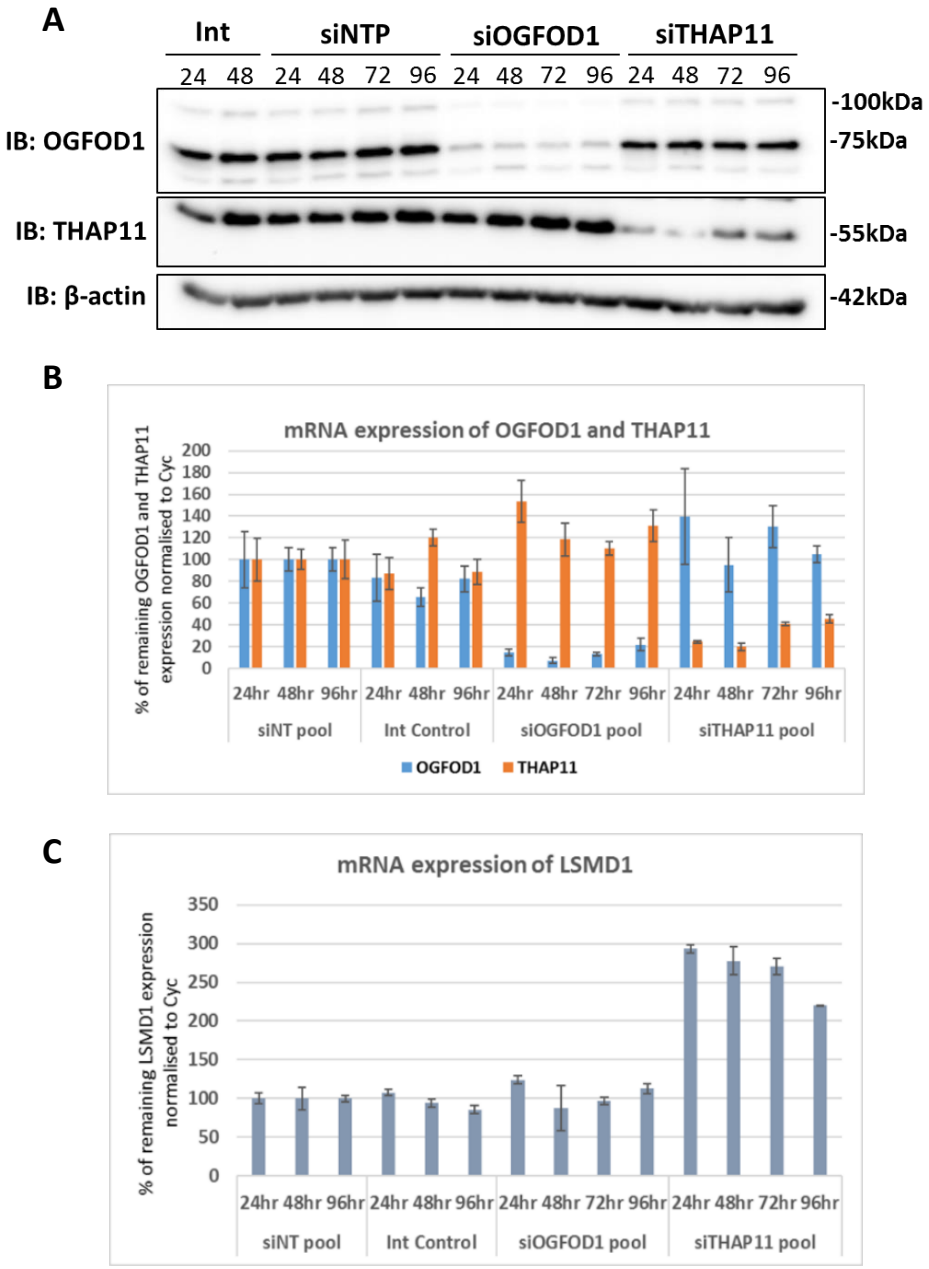


Figure 7.6: Characterisation of THAP11 transcriptional targets in response to OGFOD1 siRNA in SW620 cells. Time course of OGFOD1 and THAP11 knockdown using siRNA in SW620 cells. Cells were treated with a pool of four siRNAs directed against either OGFOD1 or THAP11. Two transfections of 10 nM siRNA were performed by both forward and reverse methods. Protein and RNA samples were collected over a 24-hour to 96-hour period. A non-targeting siRNA pool ('siNTP') and transfection reagent alone ('Int') served as negative controls. Data shows OGFOD1 and THAP11 immunoblot **(A)** and qPCR results of OGFOD1 and THAP11 mRNA **(B)**, and mRNA of THAP11 target gene LSMD1 **(C)**, following siRNA at 24, 48, 72, 96 hour timepoints, taken 24 hours after the second siRNA transfection. qPCR data represent the normalised mean expression between technical triplicates ± standard deviation.

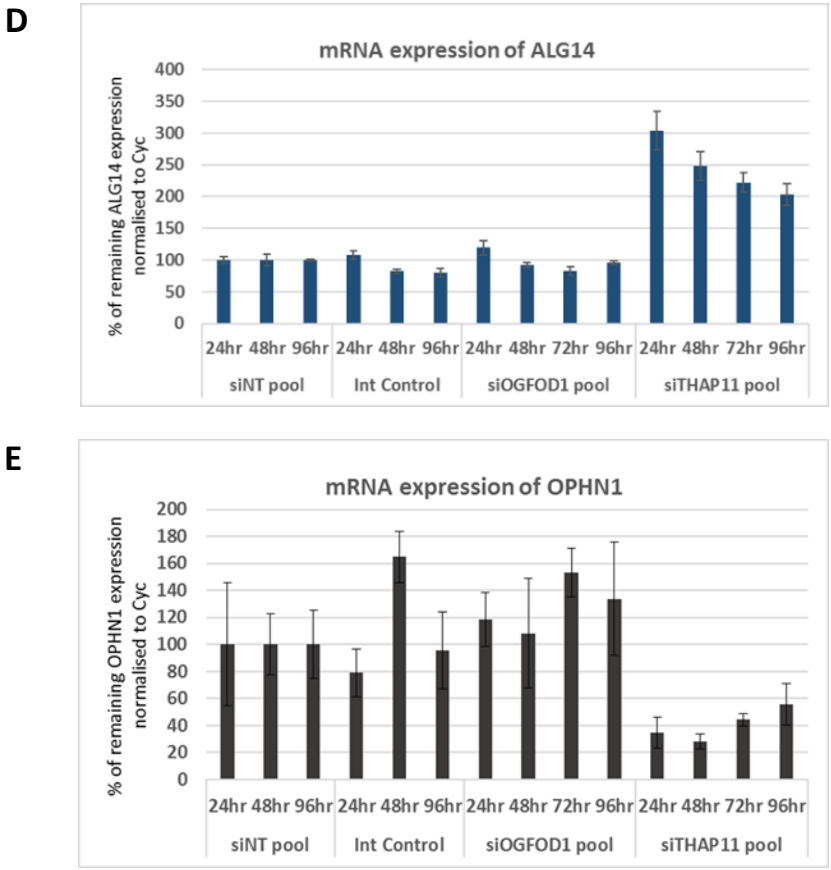


Figure 7.6 (Continued): Characterisation of THAP11 transcriptional targets in response to OGFOD1 siRNA in SW620 cells. Data shows qPCR results of THAP11 target genes ALG14 **(D)**, and OPHN1 **(E)** following OGFOD1 or THAP11 siRNA at 24, 48, 72, 96-hour timepoints, taken 24 hours after the second siRNA transfection.

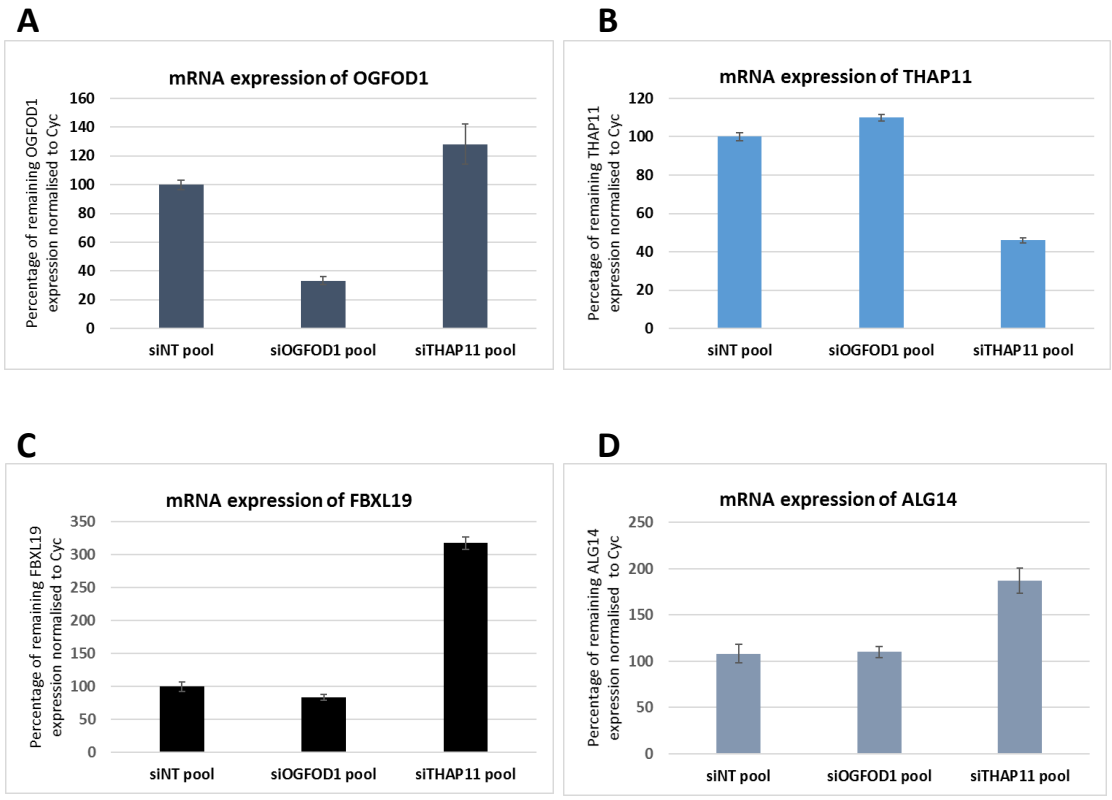


Figure 7.7: Characterisation of THAP11 transcriptional targets in response to OGFOD1 siRNA in SW620 cells. An independent siRNA experiment was performed using a pool of four siRNAs directed against either OGFOD1 or THAP11. Two transfections of 10 nM siRNA were performed by both forward and reverse methods. RNA samples were collected 48 hours after the second siRNA transfection. qPCR results for OGFOD1 **(A)**, THAP11 **(B)**, and THAP11 target genes FBXL19 **(C)** and ALG14 **(D)** are shown. Data represent the normalised mean expression between technical triplicates ± standard deviation.

Despite achieving considerable knockdown of OGFOD1 at the protein and mRNA levels (Figure 7.6 and 7.7), it was conceivable that the level of knockdown was not sufficient to modulate THAP11 gene expression changes. To address this, an OGFOD1 knockout cell line in the SW620 background was utilised that had been generated by CRISPR-Cas9 gene editing using the double-nickase methodology. Clonal isolation of SW620 cells transfected with OGFOD1 targeting CRISPR vectors proved difficult owing to the non-adherent nature of this cell line, and required sub-cloning from a mixed population of cells by limiting dilution

(Figure 7.8A). The transcriptional data in SW620 CRISPR cells are, therefore, derived from sub-clones of a single OGFOD1 knockout clone (DN9). Efficacy of the re-cloning was assessed by immunoblotting for OGFOD1 and then performing immunofluorescence to confirm a pure population had been achieved (Figure 7.8B and C). To note, the SW620 OGFOD1 knockout cell line used in chapter 6: Figure 6.1 is also a subline derivative from DN9. Consistent with data from chapter 6, THAP11 or RPS23 protein expression was unchanged in the SW620 OGFOD1-defective cells (Figure 7.8C). THAP11 dependent genes were assayed (namely ALG14, LSMD1, OPHN1 and FBXL19), however, no clear effect on gene expression across the OGFOD1 knockout sublines (DN2- A9; B2; B7) was observed relative to an empty vector (EV) transfected clone or wild-type (WT) SW620 cells, representative qPCR analysis is shown for FBXL19 (Figure 7.8D).

Although the work potentially implicates OGFOD1 in the regulation of the THAP11 transcriptional response, it appeared that OGFOD1 was not exerting a 'tonic' effect on the response as manifest by effects on this limited set of genes under conditions of OGFOD1 overexpression. As only a restricted number of targets have been assayed, it was hypothesised that genome wide transcript analyses using an OGFOD1 overexpressing cell line or OGFOD1-defective cell line would demonstrate if there are global transcriptional effects on THAP11 that are attributed to OGFOD1 function.

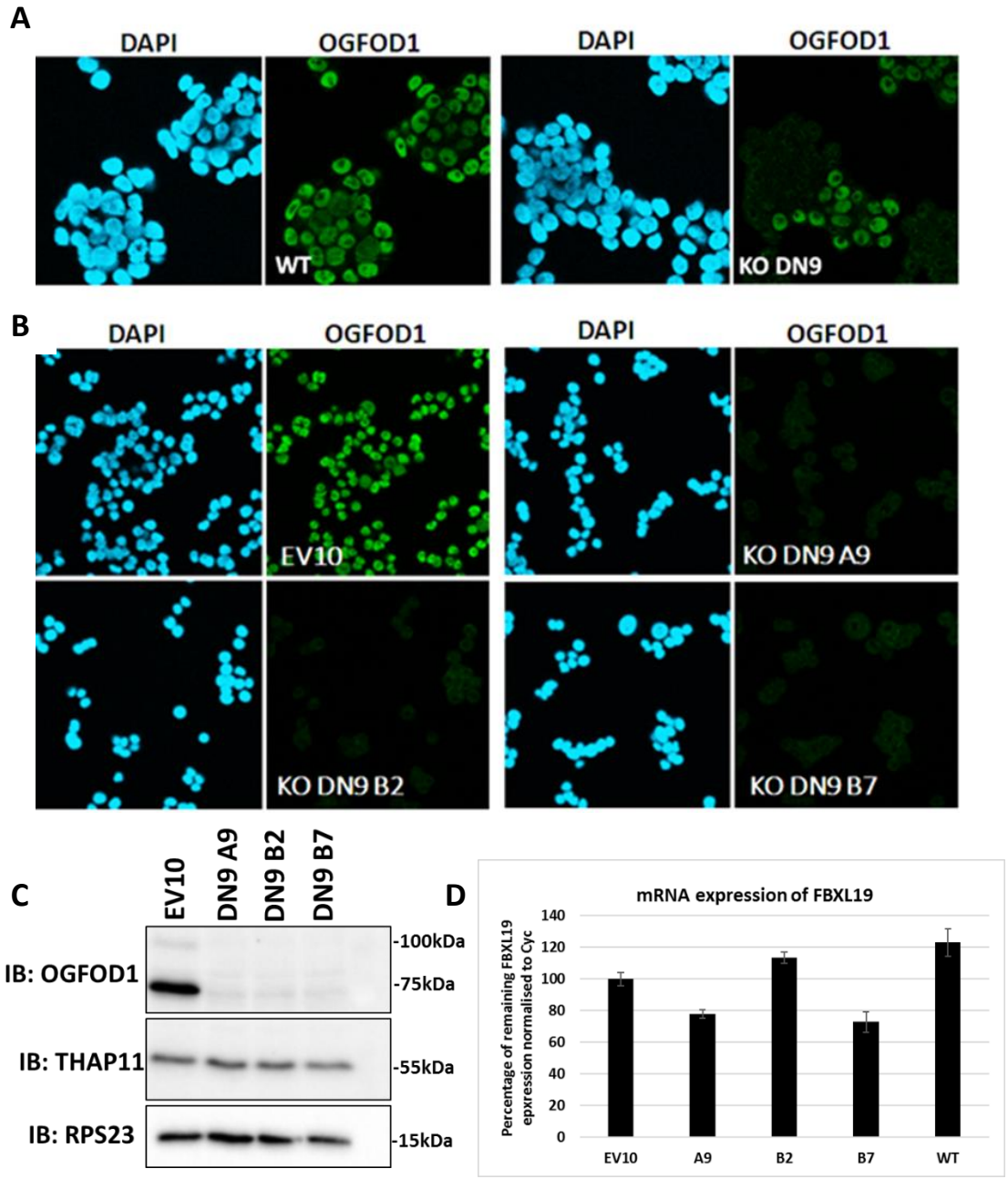


Figure 7.8: Generation and characterisation of OGFOD1 knockout SW620 cells. A) Confocal immunofluorescence of OGFOD1 CRISPR SW620 cells using anti-OGFOD1 antibody demonstrating a mixed population of OGFOD1 wild-type and OGFOD1-defective cells (DN9). **B)** Confocal immunofluorescence of OGFOD1 CRISPR clones (A9, B2, B7) derived from DN9 demonstrates a homogenous population of OGFOD1-defective cells. **C)** Immunoblot confirming generated OGFOD1 CRISPR knockout clones in SW620 cells using anti-OGFOD1 antibody. **D)** Representative qPCR showing the effect of OGFOD1 knockout in SW620 cells on THAP11 repressed gene, FBXL19. Expression is relative to an empty vector transfected clone (EV10) and expression in the parental SW620 cell line is also represented (WT). qPCR data represent the normalised mean expression between technical triplicates ± standard deviation.

7.2.3 Does OGFOD1 modulate the THAP11 transcriptional program in mouse embryonic stem (ES) cells?

Outside of the SW620 colon cancer setting, the transcriptional role of THAP11 has been defined in embryonic stem (ES) cells. THAP11 and has been shown to sustain the growth of ES cells through the regulation of a transcriptional program involved in key metabolic processes (Dejosez et al., 2008 and 2010). Interestingly, OGFOD1 mRNA is highly enriched in ES cells as indicated in data derived from a publicly available microarray (Figure 7.9A). This suggests that ES cells might provide a cell context where OGFOD1 is able to exert a greater effect on THAP11 transcription under physiological conditions. Furthermore, the essential role of THAP11 in the maintenance of ES cell self-renewal highlights a potentially important function for OGFOD1 in this cell type (Dejosez et al., 2008 and 2010).

In order to determine if OGFOD1 could be regulating a global transcriptional effect on THAP11, OGFOD1-defective ES cells were generated. In a collaborative project with Dr. Ben Davies (Wellcome Trust Centre for Human Genetics, University of Oxford), OGFOD1 knockout sub-lines were derived using CRISPR-Cas9 in JM8F6 ES cells. Complete loss of OGFOD1 protein was confirmed by immunoblotting in five independent CRISPR sub-lines (Figure 7.9B).

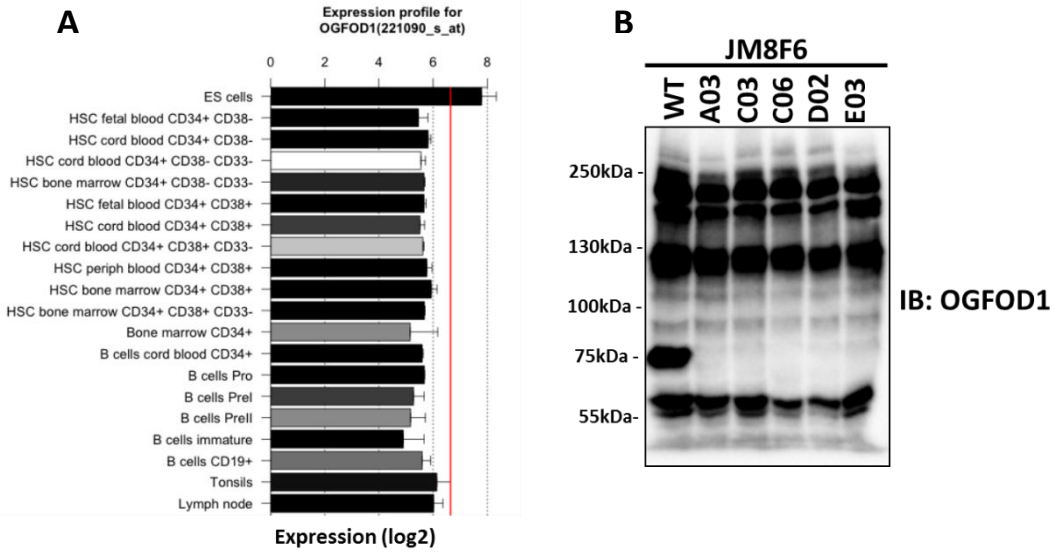


Figure 7.9: Generation of OGFOD1-defective mouse embryonic stem cells. A) mRNA expression profile of OGFOD1 in various tissues derived from publicly available results of microarray experiments (www.ebi.ac.uk). **B)** Immunoblot showing loss of OGFOD1 protein in five independent OGFOD1-defective mouse ES clones derived through CRISPR-Cas9 ('A03', 'C03', 'C06', 'D02', 'E03') relative to wild-type ES cells (WT).

If OGFOD1 was acting as a negative regulator of THAP11 function, then it was hypothesised that THAP11 target gene expression would be de-repressed in the context of an OGFOD1 knockout. The aim was therefore to identify whether OGFOD1 loss could alter THAP11 target genes on a genome-wide scale. The experimental rationale was to perform THAP11 knockdown (by siRNA) in a wild-type and an OGFOD1 knockout ES clone to identify THAP11 regulated genes and to demonstrate the potential OGFOD1 dependence on the THAP11 gene signature.

Kumar et al. demonstrated that culturing ES cells in 2i medium (MEK inhibitor (ERK pathway) and GSK3 inhibitor) in the presence of Leukaemia inhibitory factor (LIF) (downstream mediator Stat3) enables the cells to maintain optimal pluripotency (Kumar et al., 2014). To investigate the THAP11 transcriptional program, ES cells were plated on gelatin-coated

dishes and cultured in 2i medium to derive homogenous ES cells in the undifferentiated state. The ES cells grow as aggregates to form colonies making forward siRNA transfection methods highly ineffective, however, by dispersing the colonies into single cells after plating the transfection efficiency is greatly improved. THAP11 knockdown was optimised in the ES cells, and over 80% knockdown of THAP11 protein levels was achieved using 30 nM of THAP11 siRNA (Figure 7.10A).

It was noted that THAP11 siRNA appeared to enhance OGFOD1 protein expression by ~2-fold in wild-type ES cells treated with 10 nM and 30 nM THAP11 siRNA (Figure 7.10A), suggesting a potential non-transcriptional role of THAP11 in the regulation of OGFOD1. To confirm these observations, an independent THAP11 siRNA experiment was performed using wild-type and OGFOD1-defective ES cells (Figure 7.10B). However, no effect of THAP11 knockdown was observed in wild-type ES cells on OGFOD1 protein level. Furthermore, in previous THAP11 siRNA knockdown experiments performed in SW620 cells, the induction of OGFOD1 was not observed (Figure 7.6A), and the reasons for these discrepant results remain unclear.

The OGFOD1-defective ES cells displayed clear loss of OGFOD1 protein implying that functional OGFOD1 knockout sub-lines had been obtained (Figure 7.9B). The hydroxylation specific antibodies were used to confirm that RPS23 hydroxylation was impaired in the OGFOD1-defective ES cells (Figure 7.10B). Immunoblotting for the hydroxylated form of RPS23 demonstrated clear signal in the wild-type cells that was absent in the OGFOD1-defective clone (D02). As expected, immunoblotting for the non-hydroxylated form of RPS23 demonstrated signal enrichment in OGFOD1 defective cells. These results support that an OGFOD1 functional knockout cell line had been derived in ES cells. Interestingly, a modest reduction in hydroxylated RPS23 was observed in the wild-type ES cells following THAP11 siRNA. Despite this, no detectable increase in the non-hydroxylated RPS23 signal was

observed and the effect on hydroxylated RPS23 was not reproduced in SW620 cells (data not shown). The definitive assessment of whether THAP11 has any role in regulating RPS23 hydroxylation will require further investigation.

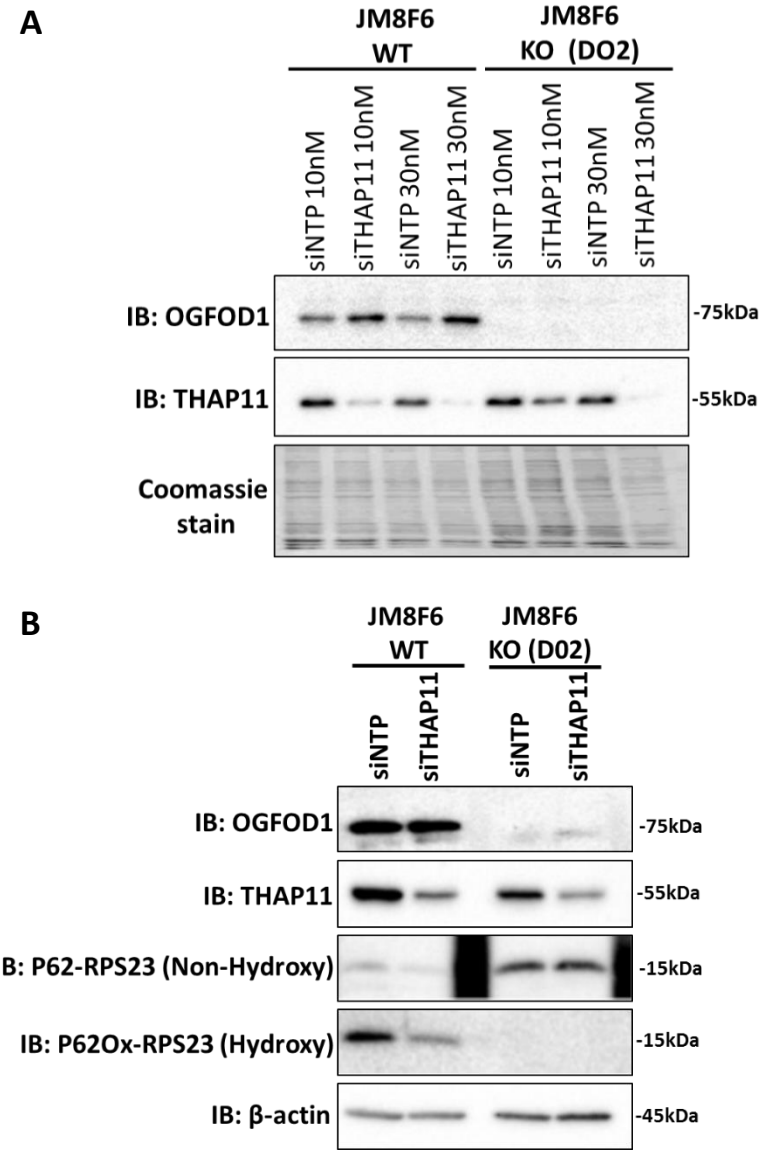
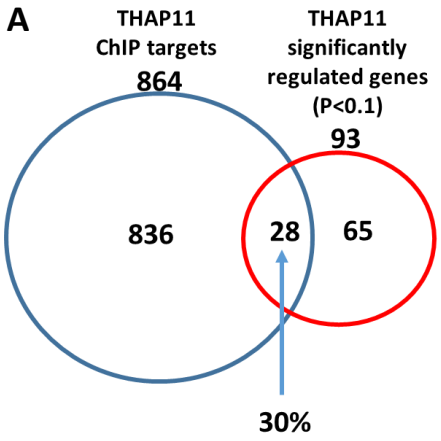


Figure 7.10: Optimisation of THAP11 knockdown in wild-type and OGFOD1 knockout mouse ES cells. A) Immunoblot of OGFOD1 and THAP11 protein levels in wild-type and OGFOD1 knockout ES cells. Optimisation of THAP11 knockdown was performed in wild-type and OGFOD1 knockout ES cells (clone D02). Cells were subject to a forward and reverse transfection (24 hours apart) at a concentration of 30 nM siRNA. Cells were harvested 48-hours after the second transfection. **B)** Immunoblot showing loss of OGFOD1 and induction of non-hydroxylated RPS23 in OGFOD1 knockout ES cells (clone D02). Wild-type and OGFOD1 knockout cells were subject to a forward and reverse transfection (24 hours apart) at a concentration of 30 nM siRNA. Cells were harvested 48 hours after the second transfection.

To consider the potential regulation of OGFOD1 genome wide on the THAP11 transcriptional program in ES cells, a gene expression microarray was performed using Illumina Mouse WG-6 arrays. THAP11 knockdown was performed in a wild-type and an OGFOD1 knockout ES cell clone (D02) in biological triplicate.

By performing THAP11 knockdown in wild-type ES cells, 93 genes were significantly regulated (adjusted p-value <0.1). Of these significantly regulated genes 30% overlapped with previously reported THAP11 binding loci as determined by ChIP-seq (Dejosez et al., 2010) (Figure 7.11A). Dejosez et al. identified 864 THAP11 targets of which included a proportion of ribosomal proteins, however, the results did not reveal regulation of mRNAs encoding ribosomal proteins. Taking the most stringent analysis of top THAP11 significantly regulated genes (adjusted p-value <0.01) an increase in correlation between these THAP11 regulated genes and the reported THAP11 ChIP targets were observed (Figure 7.11B). These data are supportive that THAP11 regulated genes have been defined following THAP11 siRNA.



B

Top THAP11 regulated genes (p<0.01)	THAP11 ChIP
Ccdc22	-
Thap11	Thap11
Gpnmb	-
Trmt10a	-
Tfpi	-
Bckdk	Bckdk
Lysmd1	-
Rabl3	Rabl3
Pdia5	Pdia5
Fsd1	Fsd1
Vamp7	-
Enox2	-
Lmnb2	Lmnb2
Zc4h2	-
Ctns	Ctns
Pus3	-
Pdia5	Pdia5
Josd2	Josd2
Zfp446	-
Rasip1	-

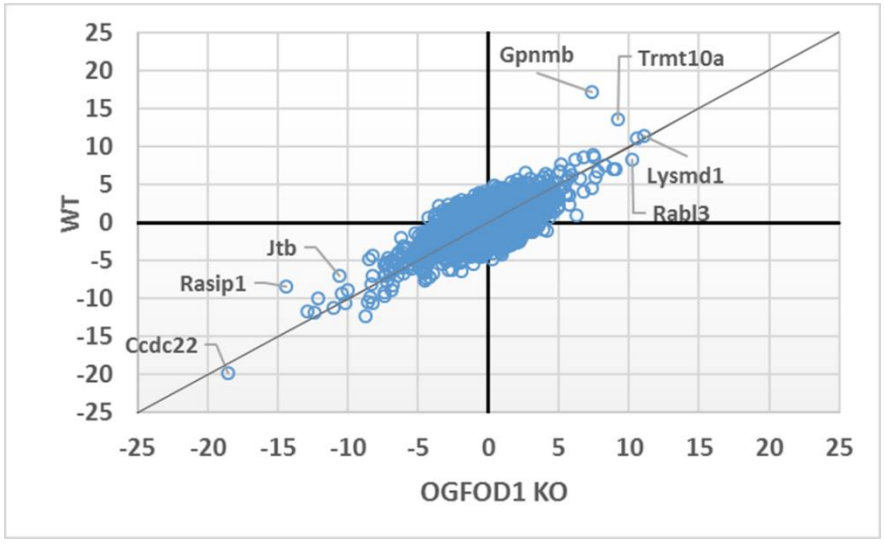
Figure 7.11: Overlap between THAP11 gene targets in ES cells identified by ChIP-seq and THAP11 regulated genes following THAP11 siRNA. A) Schematic of overlapping THAP11 targets identified by previously published ChIP-seq (Dejosez et al., 2010) and THAP11 regulated genes derived from the microarray following THAP11 siRNA. **B)** Correlation between the top 20 most significantly regulated genes following THAP11 siRNA and published THAP11 ChIP-seq targets. '-'denotes that this target was not reported as a THAP11 bound target gene as determined by ChIP-seq.

To determine the global effect of OGFOD1 on THAP11 dependent gene expression, the entire gene expression array was analysed by comparing the effect of THAP11 knockdown in wild-type and OGFOD1-defective cells. Importantly, the level of THAP11 knockdown was similar between wild-type and OGFOD1 knockout cells with an average knockdown of approximately 50-60% achieved in wild-type and OGFOD1 knockout cells across the three biological replicates (data not shown).

Microarray analysis was performed by Dr. Rafik Salama (University of Oxford) using R. The T-Statistic, a normalised change accounting for differences in the biological triplicate experiments, was used to measure the change in gene expression due to THAP11 on the wild-type background and compare it with the change observed on the OGFOD1 knockout background. Accordingly, for every gene assayed in the microarray, the change in gene expression was plotted following THAP11 knockdown on the wild-type background versus the change in gene expression following THAP11 knockdown on OGFOD1 knockout background (Figure 7.12A). The lower left quadrant shows highly repressed genes by THAP11 knockdown (including Ccdc22) and the upper right quadrant highly induced genes by THAP11 knockdown (including Lysmd1). The diagonal line in this case represents equal changes in gene expression associated with the wild-type and the OGFOD1 knockout background. Genes deviating from the diagonal line would represent a difference whose THAP11-dependent gene expression was affected by the presence or absence of OGFOD1. It is seen that the majority of genes change in a similar manner irrespective of OGFOD1.

If OGFOD1 were functioning upstream of THAP11 then changes in the basal expression of the THAP11 regulated genes might also be expected when comparing wild-type versus OGFOD1 knockout cells (independent of THAP11 siRNA). A robust set of THAP11 dependent targets was identified by looking at the most significantly regulated genes (upregulated and downregulated) following THAP11 siRNA in wild-type ES cells (Figure 7.12B). Based on the model discussed earlier in this chapter, in the OGFOD1 knockout cells greater availability of THAP11 would be predicted to further downregulate its repressed targets and upregulate its induced targets. However, OGFOD1 knockout had little effect on THAP11 target gene expression, with ‘Gpnmb’ the only target that showed significant ($p<0.05$) downregulation in the OGFOD1 knockout cells (Figure 7.12C and D). Thus, the data overall do not support large effects of OGFOD1 on THAP11-dependent gene expression.

A



B

Upregulated (P<0.05)	Downregulated (P<0.05)
Gpnmb	Gm21974;Vkorc1
Trmt10a	Syde1
Rabl3	Bola1
Foxd1	Kdelc1;Gm29247
Lysmd1	Mtrf1
Lamtor2	Galm
Josd2	Mrpl54
Elp6	Zc4h2
Mib2	Letm1
1700003M02Rik	Jtb
Dync1i2	Pus3
Zfp446	Zbtb8b
Acadvl	Ctns
Zmat5	Lmnb2
	Fsd1
	Asb13
	Bckdk
	Rasip1
	Pdia5
	Enox2
	Tfpi
	Vamp7
	Thap11
	Ccdc22

Figure 7.12: Characterising the effect of OGFOD1 loss on the THAP11 transcriptional program in mouse ES cells. A) To determine the global gene expression differences between non-targeting siRNA and THAP11 siRNA on the background of wild-type ES cells versus OGFOD1 knockout ES cells a T-statistic was performed. The T-statistic provides a normalised change in gene expression and accounts for variation in the biological triplicate experiments. The lower left quadrant represents repressed genes by THAP11 knockdown and the upper right quadrant represents induced genes by THAP11 knockdown. The diagonal line represents equal changes in gene expression associated with the wild-type and the OGFOD1 knockout background. **B)** The most robust (p<0.05) THAP11 regulated genes were determined in wild-type ES cells comparing siNTP against siTHAP11. THAP11 target genes are separated into upregulated and downregulated genes following THAP11 siRNA.

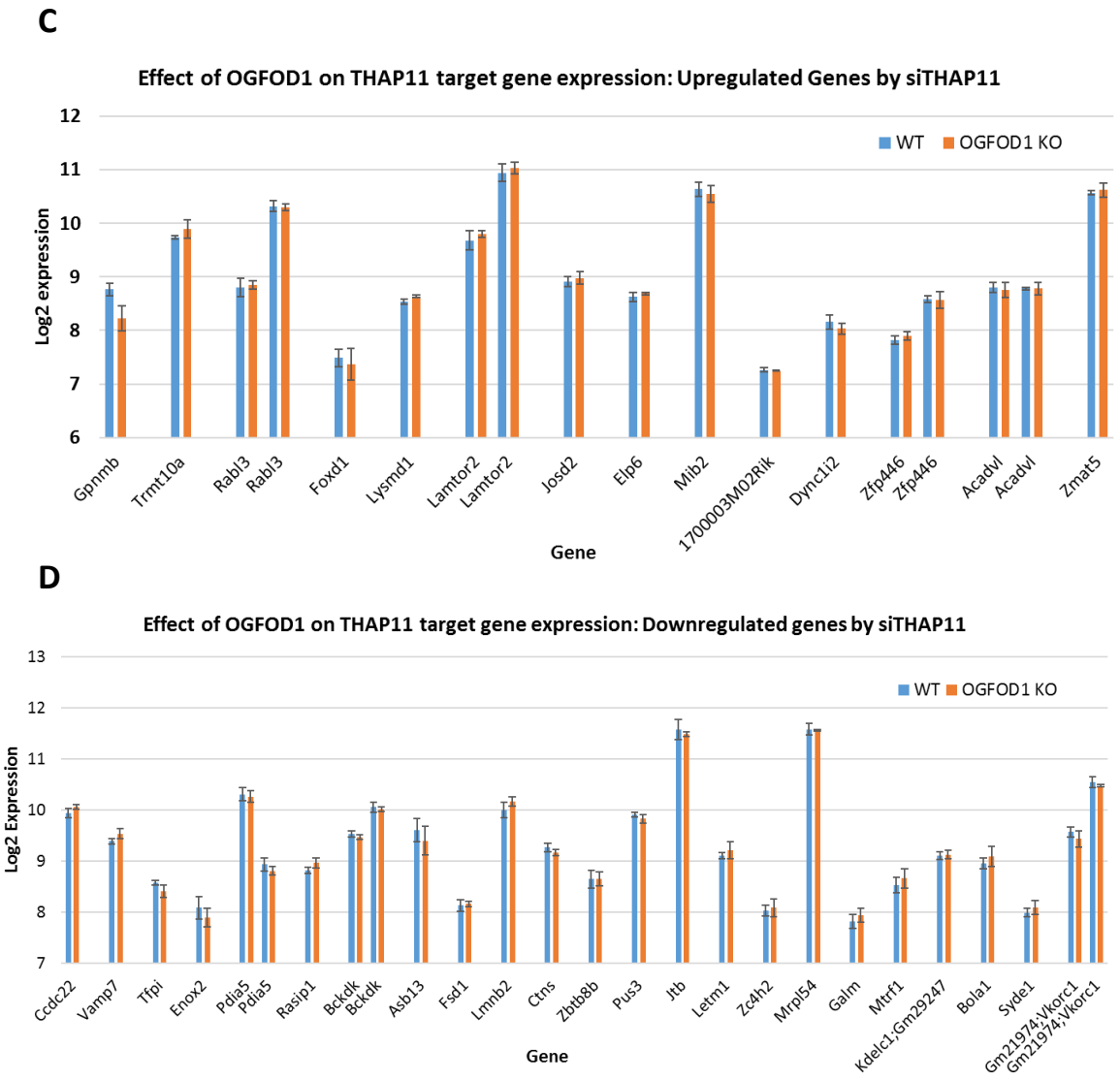


Figure 7.12 (Continued): Characterising the effect of OGFOD1 loss on the THAP11 transcriptional program in mouse ES cells. THAP11 significantly regulated genes ($p<0.05$) were separated into repressed targets (upregulated by siTHAP11) **(C)** and induced targets (downregulated by siTHAP11) **(D)**. A comparison of gene expression (log2) was made between wild-type (with non-targeting siRNA) and OGFOD1 knockout (with non-targeting siRNA) ES cells on these THAP11 dependent genes. Data represent the normalised mean expression between biological triplicates ± standard deviation.

Independent of THAP11, the gene expression patterns when comparing wild-type and OGFOD1 knockout ES cells (under conditions of a non-targeting siRNA) were also surprisingly similar. The fold change effects between wild-type and OGFOD1 knockout ES cells are small as illustrated by the volcano plot (Figure 7.13A). Three genes were downregulated by ~3 fold in the OGFOD1 knockout cells and achieve significance (by adjusted p-value). These genes namely: Rian, Meg3 and 1110006E14RIK localise to an imprinted region on chromosome 12qF1 which is critical for the pluripotency of stem cells. Interestingly, Stadtfeld et al. compared genetically identical mouse ES cells and iPSCs and showed that overall messenger RNA and microRNA expression patterns are indistinguishable with the exception of a few transcripts, Rian and Meg3, that are encoded within the imprinted Dlk1–Dio3 gene cluster that are silenced in iPSCs (Stadtfeld et al., 2010). Further experiments were performed using qPCR to validate the OGFOD1 dependence on the expression of Meg3 and Rian (Figure 7.13B). However, although qPCR assays replicated the differences between wild-type ES cells and clone D02, opposing effects were observed in two further OGFOD1 knockout clones (A03 and C06) relative to clone D02, suggesting that Rian and Meg3 manifest large clonal differences in expression unrelated to OGFOD1. Overall, the data do not support global gene expression changes or effects on THAP11-dependent gene expression in response to OGFOD1 loss in mouse embryonic stem cells.

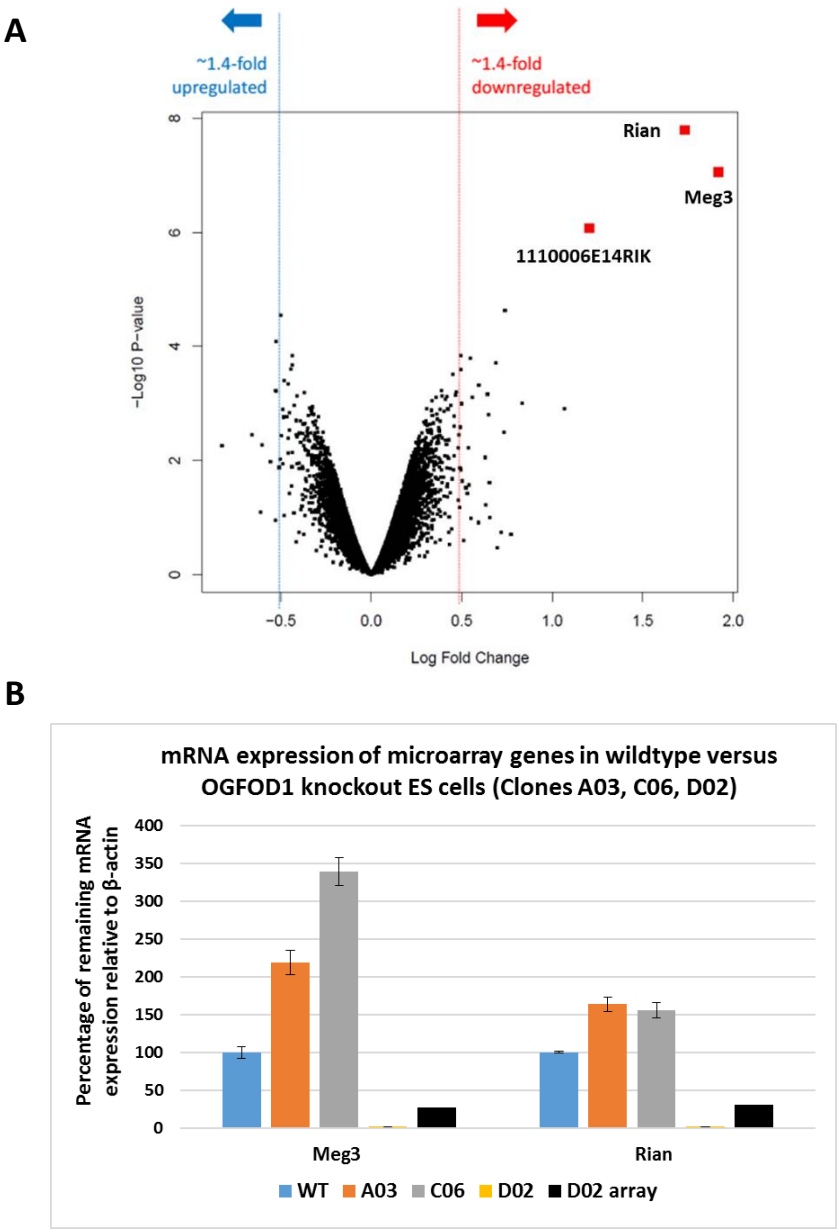


Figure 7.13: Characterisation of OGFOD1-dependent genes in mouse embryonic stem cells. **A)** Volcano plot of log2 fold change versus –Log10 p-value for wild-type (with siNTP)/OGFOD1 knockout (with siNTP) ES cells. Three imprinted genes: Rian, Meg3 and 1110006E14RIK were shown to be significantly downregulated in OGFOD1 knockout ES cells. **B)** qPCR analysis of OGFOD1 dependent genes in wild-type ES cells and 3 independent OGFOD1 knockout ES cells. qPCR assays replicated the differences between wild-type ES cells and clone 'D02' for two genes: Meg3 and Rian. However, opposing effects were observed in OGFOD1 knockout clones: 'A03' and 'C06'. For reference the fold change of Meg3 and Rian was calculated from the microarray 'D02 array' (comparing wild-type + siNTP versus OGFOD1 knockout (clone 'D02') + siNTP). qPCR data represent the normalised mean expression between technical triplicates ± standard deviation.

7.3 Discussion

Work described in this chapter sought to determine if OGFOD1 could regulate a transcriptional function of THAP11 as assayed in SW620 colon cancer cells and mouse ES cells. The association between OGFOD1 and THAP11 in the absence of an interaction between OGFOD1 and the transcriptional co-activator HCF-1 indicated that OGFOD1 might have the potential to restrict the THAP11 transcriptional complex through a competitive interaction (Figure 7.1).

In support of OGFOD1-dependent regulation on THAP11 transcription, reproducible effects on THAP11 induced and repressed target genes were demonstrated following OGFOD1 overexpression in SW620 cells (Figure 7.2). OGFOD1-dependent effects correlate directly with OGFOD1 expression and subsequent capture of THAP11 (Figure 7.3). The effects were not seen with an OGFOD1 mutant that was unable to bind THAP11 (F287A), suggesting that modulation of the THAP11 transcriptional response is mediated through direct sequestration of THAP11 (Figure 7.4). Furthermore, THAP11 target genes are regulated by both wild-type OGFOD1 and a catalytically inactive OGFOD1 mutant (D157A), suggesting that regulation of the THAP11 transcriptional programme does not require enzymatic activity (Figure 7.4). This finding is also consistent with work on the yeast homolog, Ofd1, which showed that dioxygenase activity was not required for degradation of Sre1N (Hughes et al., 2008). Interestingly, a greater effect on the THAP11 transcriptional programme was observed upon expression of a catalytically inactive OGFOD1 mutant, relative to that observed with wild-type OGFOD1 (Figure 7.4), indicating that reduced catalytic activity or reduced affinity for RPS23 may promote a more potent inhibitory effect of OGFOD1. The results were also consistent with an inhibitory effect of OGFOD1 on THAP11 function as assessed by ChIP-qPCR which indicated that OGFOD1 overexpression sequesters THAP11

from the DNA (Figure 7.5). These findings are also consistent with work on the OGFOD1 yeast homolog, in which Ofd1 inhibits Sre1N-dependent transcription by blocking DNA binding (Lee et al., 2011).

In contrast to the inhibitory effects observed following OGFOD1 overexpression, no effect was observed following suppression of OGFOD1 in SW620 cells by siRNA or by inactivation in OGFOD1 CRISPR derived cells (Figure 7.6-7.8). In order to explore the effect of OGFOD1 loss in a different cell context, OGFOD1 knockout cells were generated in mouse ES cells, in which a transcriptional function of THAP11 had also been described (Dejosez et al., 2008 and 2010). THAP11 target genes were defined using THAP11 siRNA and the effect of OGFOD1 inactivation on the defined THAP11 target genes were investigated. However, similar to the SW620 knockout cells, no clear effect from OGFOD1 loss was observed on the THAP11 transcriptional program (Figure 7.12). Surprisingly, in the absence of THAP1 siRNA, direct comparison of wild-type and OGFOD1 knockout ES cells revealed very few changes in gene expression. Furthermore, the few gene expression changes that were observed appeared to be independent of the OGFOD1 genotype as they were not observed in other OGFOD1 knockout ES cell sublines (Figure 7.13).

One possible explanation is that THAP11 is not limiting in either SW620 cells or ES cells. In support of this, Parker et al. demonstrated that overexpression of THAP11 in SW620 cells had only a modest effect (in contrast to THAP11 knockdown) on gene expression (~0.7-fold) despite increasing THAP11 expression by over 15-fold (Parker et al., 2012). Therefore, based on the OGFOD1 immunoprecipitation data in SW620 cells, which captures around 10-20% of THAP11 (chapter 5: Figure 5.5C), liberating the pool of OGFOD1 bound by THAP11 may not have substantial effects on THAP11 target gene expression. It is also possible that the THAP11 transcriptional output is restricted in these cellular settings, by other mechanisms. In relation to this hypothesis, the levels of the transcriptional co-activator HCF-1 appear

relatively low in SW620 cells (Figure 7.1). A cell context in which more THAP11 is bound to the transcriptional co-activator HCF-1, may provide a setting in which the transcriptional output is greater, such that alterations in endogenous OGFOD1 levels can impact on THAP11 transcription under physiological conditions.

The SW620 and ES models provided two contexts in which to determine the role of OGFOD1 on the THAP11 transcriptional program. Other cell contexts may provide a setting in which there is more THAP11 bound by OGFOD1 providing a greater potential for OGFOD1 to exert physiological regulation on THAP11 transcription. Initial screening across a panel of four cell lines indicated that the interaction appears to remain at around 10-20% (chapter 5: Figure 5.5C). A similar level of association between OGFOD1 and THAP11 in mouse ES cells might also occur, however, the absence of immunoprecipitating antibodies precluded examination of the stoichiometry (data not shown). Future work might be directed at exploring alternative cellular settings in which a higher stoichiometric interaction occurs between OGFOD1 and THAP11.

Previous studies have shown that RPS23 hydroxylation is complete in a range of cell lines (Singleton et al., 2014). It is hypothesised that conditions which limit RPS23 availability or reduce the rate of RPS23 hydroxylation may enhance the inhibitory effect of OGFOD1 on the THAP11 transcriptional programme. This hypothesis is also supported by the observation that the catalytically inactive OGFOD1 mutant (D157A) appeared to have a more potent inhibitory function on the THAP11 transcriptional programme (Figure 7.4). Future work might therefore focus on assaying the availability of free (pre-ribosomal) RPS23 and on modulating RPS23 production in cellular settings in which there is more THAP11 bound by OGFOD1 and/or where HCF-1 is not limiting.

Chapter 8: Final Discussion

8.1 Overview

The work described in this thesis sought to illuminate the function of mammalian OGFOD1, a highly conserved 2-OG dependent oxygenase that belongs to the family of ribosomal oxygenases that includes MINA53 and NO66 (Singleton et al., 2014; Ge et al., 2012). The work was conducted against a background literature encompassing a number of studies on OGFOD1 in mammalian cells, invertebrates (Sud1 in *D. melanogaster*) and yeast (TPA1 in *S. cerevisiae* and Ofd1 in *S. pombe*) (Singleton et al., 2014; Katz et al., 2014; Loenarz et al., 2014; Lee et al., 2011). These studies pointed to two types of function for OGFOD1 in both translation and transcription. However, it was not known whether these functions are conserved in mammalian cells or if they are linked.

Prior to the commencement of the work described in this thesis, the principal finding was the identification of RPS23 as an evolutionarily conserved substrate for OGFOD1 and its orthologs: Sud1, TPA1 and Ofd1 (Singleton et al., 2014; Katz et al., 2014; Loenarz et al., 2014). The hydroxylated residue, equivalent to Proline-62 in humans, is located within the decoding centre of the ribosome. Consistent with a role in translational control, effects on stop codon readthrough had been reported in response to OGFOD1 and TPA1 modulation (Keeling et al., 2006; Singleton et al., 2014; Loenarz et al., 2014). However, bidirectional effects on the efficacy of decoding stop codons were reported and, therefore, the precise effect on translation termination efficiency or other recoding events is unclear. Interventions on OGFOD1, predominantly using siRNA and shRNA-based knockdown, had

been associated with abnormalities in cellular proliferation across a range of cell types (Singleton et al., 2014; Katz et al., 2014; Kustatscher et al., 2014; Kim et al., 2015). However, in some contexts, cells did not display a proliferative defect in response to OGFOD1 intervention despite inhibitory effects on RPS23 hydroxylation. Whilst the majority of studies did not measure effects of OGFOD1 suppression on RPS23 hydroxylation and hence could not correlate altered hydroxylation with cellular growth rates, these data suggest that alterations in cellular growth may not be directly mediated via RPS23 hydroxylation. In some situations, sensitivity to, or resistance to, cellular 'stresses', including sodium arsenite-induced translational stress and oxygen-glucose deprivation, was observed following OGFOD1 intervention (Wehner et al., 2010; Saito et al., 2010). However, the relationships between these observations were also unclear.

Equally, the relationship between these properties and nuclear functions of OGFOD1 were poorly understood. The OGFOD1 ortholog in fission yeast (Ofd1) had been extensively studied as an oxygen-dependent regulator of the transcriptional response to low sterol availability (Lee et al., 2009; Lee et al., 2011). In this setting, Ofd1 acts as an antagonist of Sre1N in the presence of oxygen. In human cells the stability of orthologous SREBP transcription factors is not, apparently, regulated by oxygen. However, a discrete interface with oxygen is conferred by the HIF system, which indirectly suppresses SREBP transcripts via the upregulation of the transcriptional repressors DEC1 and DEC2, which are HIF target genes (Choi et al., 2008). Nevertheless, human OGFOD1 is largely a nuclear protein suggesting a possible signalling function, analogous to Ofd1-mediated regulation of the Sre1N transcription factor in *S. pombe.* The work described in this thesis aimed to shed light on these enigmatic findings using a combination of cell biological and biochemical methods.

8.2 Cellular phenotypes associated with genetic interventions on OGFOD1

Given the above uncertainties, it was considered that better definition of the phenotypes associated with OGFOD1 might provide guidance as to the best context to explore the underlying mechanistic biochemistry.

The studies utilising RNAi-mediated knockdown of OGFOD1 implied that differences in the severity of the phenotypes may be due to variation in suppression of OGFOD1 levels. To address this, a number of OGFOD1 defective cells were generated by genome editing using the CRISPR methodology. However, genetic inactivation of OGFOD1 did not appear to mimic the reported growth phenotypes observed by RNAi (chapter 2: Figure 2.1). Furthermore, no clear evidence for activation of translational stress phenotypes, including eIF2α phosphorylation, formation of G3BP1-containing stress granules or altered polysome profiles, was observed in OGFOD1 defective cells (chapter 2: Figures 2.2-2.3; chapter 6: Figure 6.11). These findings were unexpected given the literature and the proposed role for OGFOD1 in cellular growth and translational control. As a potential explanation it was hypothesised that a rapid change in OGFOD1 status, mirroring that achieved by RNAi-mediated knockdown of OGFOD1, might have generated the reported abnormalities of growth. Therefore, effects on cellular growth were further explored using OGFOD1 shRNA and inducible re-expression systems (chapter 3: Figures 3.2-3.5). However only modest effects were observed, which did not conform to a consistent pattern of response.

As these inconsistencies might be explained by contextual effects on the function of OGFOD1, the role of OGFOD1 in the response to a range of stresses was examined, including: serum starvation, low glutamine, low glucose and hypoxia. However, no clear effect of OGFOD1 status was observed, even when stresses were applied that closely mimic those associated with OGFOD1-dependent responses in previous studies (chapter 3: Figures 3.6-3.8). It is possible that further exploration of other stresses would reveal an OGFOD1-

dependent phenotype, although the tested conditions were diverse, encompassing many different types of cellular stress.

The reasons for the discordance between my findings and the phenotypes reported by others remain unclear. In respect of the RNAi-associated phenotypes it is possible that off-target effects or insufficient knockdown underlies some of the variability. In relation to the reported OGFOD1-associated proliferative defect, however, it is important to note that independent groups drew broadly similar conclusions with different siRNA and shRNA sequences (Singleton et al., 2014; Katz et al., 2014; Kustatscher et al., 2014; Kim et al., 2015).

Another possibility is that the cellular context was not correct or that some aspects of the cellular phenotype were particularly dependent on culture conditions, for example: transfection protocol, cell density or serum formulation. In relation to the first point, this would appear unlikely as OGFOD1 was inactivated in a number of cell types, including, HEK293, HeLa, SW620 and mouse embryonic stem cells. Moreover, some of these cell lines (HEK293 and SW620) had previously been shown to be sensitive to RNAi-mediated knockdown of OGFOD1 (Singleton et al., 2014). For cells engineered by CRISPR, a plausible explanation is that during the expansion and isolation of clones, OGFOD1-defective cells come under strong selection pressure and "lose" the pathways connecting aberrant OGFOD1 functions to reduced growth and translational stress phenotypes. This is a well-recognized problem with the long-term maintenance of cultured cells (Esquenet et al., 1997; O'Driscoll et al., 2006).

Taken together, these data suggest that there is no clear and direct relationship between hydroxylation of RPS23 and growth or translational stress phenotypes in human cells. These findings were unexpected given the number of independent studies describing large phenotypes in response to OGFOD1 modulation. Antibodies were produced to facilitate the

measurement of levels of RPS23 hydroxylation in cells (chapter 3: Figure 3.1). These studies confirmed that large changes in the hydroxylation of RPS23 were produced by interventions on OGFOD1 and proved that preserved growth and other normal cellular phenotypes could exist even in the face of complete loss of RPS23 hydroxylation.

Aside from the cellular phenotypes described in cultured cells, phenotypes associated with OGFOD1 inactivation in the mouse have been reported by the International Mouse Phenotyping Consortium. These phenotypes, including an abnormal femoral morphology and an abnormal skin condition, reinforce that in certain contexts OGFOD1 has important non-redundant functions. My own studies on a patient with numerous dysmorphic features bearing a mutation in RSP23 that impaired OGFOD1-dependent hydroxylation were consistent with this, though difficult to pursue mechanistically (chapter 4).

In view of the difficulty in defining a consistent OGFOD1-dependent cellular phenotype, it was decided to pursue a more biochemical approach, on the basis that this might ultimately provide a better focus for cellular studies.

8.3 Identification of novel OGFOD1 binding proteins by mass spectrometry

To provide new insight into OGFOD1 cellular function(s), OGFOD1-containing protein complexes were affinity purified from cells and analysed by tandem mass spectrometry (chapter 5: Figures 5.1-5.4). A wide range of proteins co-purified with endogenous OGFOD1 and ectopically expressed FLAG-OGFOD1, though surprisingly the overlap between the two settings was limited. THAP11 was identified as a novel interacting protein that, along with RPS23, was detected in all OGFOD1 affinity-purification mass spectrometry experiments. A robust association between endogenous OGFOD1 and THAP11 was observed across a range of cell lines, suggesting that the interaction was of functional relevance (chapter 5: Figure 5.5). Further analysis of this association was performed and sequence homology was identified between the OGFOD1 binding site in THAP11 and the Ofd1 binding site in both

Sre1N and in the nuclear importer and antagonist of Sre1N, Nro1 (chapter 5: Figure 5.7). Given that THAP11 is a transcriptional regulator this was suggestive of a relationship analogous to Ofd1, most likely in the regulation on Sre1N.

To investigate the physiological significance of the OGFOD1:THAP11 association, the interactions and potential functions of THAP11 properties were analysed in response to OGFOD1 modulation (chapter 6). These analyses included comparative displays of THAP11 interacting partners by mass spectrometry in wild-type and OGFOD1-defective cells. These studies did not define an effect of OGFOD1 status on the THAP11 interactome, as displayed by immunoprecipitation and analysis of complexes by density gradient centrifugation. However, such studies do not exclude the existence of OGFOD1-dependent interactions of THAP11, particularly as OGFOD1 itself was not captured, possibly due to antibody mediated occlusion of the binding site. Nevertheless, the experiments did reveal novel and interesting associations of THAP11. In particular, THAP11 was associated with components of the protein synthesis machinery including ribosomal proteins and eIF3 complex components, ribonucleoproteins and stress granule-associated proteins. These interactions were demonstrated by affinity-purification mass spectrometry and supported by sucrose density separation of complexes (chapter 6: Figure 6.5-6.10). With regards to a role in global translation and ribosome biogenesis, the polysome profiles of wild-type and OGFOD1-defective cells were broadly similar, irrespective of THAP11 gene knockdown (chapter 6: Figure 6.11). Despite no clear functional output on the polysome profiles following THAP11 intervention, the association between THAP11 and the translational machinery remained of interest, especially given the striking overlap between THAP11 and RPS23 protein complexes. Thus, it remains to be determined if THAP11 has additional roles in the post-transcriptional regulation of gene expression beyond the transcriptional functions that have been described (Dejosez et al., 2010; Parker et al., 2012). The observations on THAP11

associations with the translational machinery also raise the possibility that the associations between OGFOD1:THAP11:RPS23 are in some way interactive; specifically, that competition may exist between a nuclear transcriptional association (THAP11) and a ribosomal association (RPS23) for OGFOD1. Such a possibility has also been suggested by work on Ofd1 with respect to regulation of Sre1N and the potential interaction of this process with RPS23 hydroxylation in *S. Pombe* (Lee et al., 2011; Loenarz et al., 2014).

8.4 The transcriptional interaction between OGFOD1 and THAP11

The body of scientific knowledge relating to THAP11 gene function is predominantly focused on its role as a transcriptional regulator. Accordingly, I considered the possibility that OGFOD1 might modulate the THAP11 transcriptional programme (chapter 7) (Dejosez et al., 2010; Parker et al., 2012). This was of particular interest as THAP11 transcription has been reported to target biosynthetic processes including ribosome biogenesis (Dejosez et al., 2010). My studies defined an action of OGFOD1 overexpression to restrain THAP11-mediated transcription (chapter 7: Figure 7.2-7.5). Inhibition of THAP11-mediated transcriptional responses was titratable with respect to the level of OGFOD1 expression. In contrast, I was not able to demonstrate an effect of OGFOD1 suppression by RNAi or in OGFOD1-defective cells on THAP11-mediated transcription in different systems including SW620 cells and ES cells, suggesting that OGFOD1 restraint of THAP11 is not “tonic” under the conditions examined (chapter 7: Figure 7.6-7.12). One possibility is that THAP11 is not limited in these cellular contexts and, therefore, liberating the pool of THAP11 bound by OGFOD1 may not have substantial or measurable effects on THAP11 target gene expression. Furthermore, since THAP11 transcriptional activity is dependent on recruitment of HCF-1, and for some target genes the zinc finger transcription factor ZNF143, the levels and availability of these co-factors will also shape the transcriptional output and might have

been rate limiting under the conditions of the experiments (Dejosez et al., 2010; Ngondo-Mbongo et al., 2013; Vinckevicius et al., 2015).

Failure to demonstrate a regulatory function of THAP11 by modulating endogenous OGFOD1 expression might also indicate that the interaction between OGFOD1 and THAP11 is more complex. In respect of this, the role of RPS23 in the OGFOD1:THAP11 axis has not been explored. One possibility is that the availability of free (pre-ribosomal) RPS23 affects a physical or functional interaction of OGFOD1 with THAP11 and that the conditions of these experiments were such that OGFOD1 levels did not influence THAP11. For instance, high availability of RPS23 might restrict functional effects of OGFOD1 which might otherwise exist under conditions of low availability of free RPS23.

In considering the role of RPS23 in this process, better definition of the relevant protein complexes would be insightful. My attempts to address OGFOD1 complex composition were hampered by an inability to co-precipitate OGFOD1 with antibodies to endogenous THAP11 and RPS23 (chapter 7: Figure 7.1 and data not shown). A fundamental question that exists therefore, is whether OGFOD1 exists in a trimeric complex with RPS23 and THAP11 or in mutually exclusive OGFOD1:RPS23 and OGFOD1:THAP11 complexes. If the latter, then a competitive interaction between RPS23 and THAP11 would be predicted. A corollary to this is that the affinity (stability) of the RPS23 interaction with OGFOD1 is likely to increase under conditions that inhibit OGFOD1 catalytic activity which in turn might have a THAP11-dependent transcriptional reflection.

Pertinent to this, formation of the 100 kDa OGFOD1:RPS23 adduct that is suppressed by catalytic inhibitors is also inhibited under moderate hypoxia (1% oxygen; Dr. Matthew Cockman, unpublished) (Singleton et al., 2014). Thus, although hydroxylation of RPS23 in the mature ribosome appears to be complete except under severe hypoxia (Singleton et al.,

2014), it is possible that the catalytic rate of OGFOD1 is reduced by modest hypoxia and that physiological sequestration by OGFOD1 is relayed as a transcriptional signal via THAP11.

A separate finding that could add a further layer of control is the observation that THAP11 and RPS23 form a discrete and likely large macromolecular complex with other translation factors in cells (chapter 6: Figure 6.6; Figure 6.8). The significance of this association is currently unclear and it remains to be determined if this association is direct and/or regulated by hydroxylation. Arguing against the latter, I did not observe striking differences in THAP11 co-sedimentation with ribosomal components or the co-precipitation of ribosomal components with THAP11 immunoprecipitation in wild-type and OGFOD1-defective cells (chapter 6). Nevertheless, there is an intriguing connection between THAP11 - a transcription factor with a role in ribosome biogenesis and the observed association with components of the protein synthesis machinery that has the potential for a regulatory role.

The signalling mechanism that regulates Sre1N in *S. pombe* is directed through competitive binding between Sre1N and Nro1 to Ofd1 (Lee et al., 2009). The Nro1 protein has been reported as a nuclear import adapter protein for Ofd1 (Yeh et al., 2011). I showed that the binding of THAP11 to OGFOD1 involved a binding site on THAP11 that shows a high degree of homology to Nro1 and well as Sre1N (chapter 5: Figure 5.7). It is, therefore, not clear whether in mammalian cells THAP11 is involved primarily as a transcriptional regulator (like Sre1N) or whether it may possess alternative functions (like Nro1), or both. Future work should address whether THAP11 can regulate the subcellular localisation of OGFOD1 and RPS23, and/or the availability of RPS23 for OGFOD1-dependent hydroxylation.

If THAP11 served as both a nuclear transcriptional regulator (like Sre1N) and a nuclear import adapter (like Nro1) but with complexed ribosomal components, including RPS23, then its nuclear transcriptional role could be regulated by RPS23. For example, as argued above, under conditions in which RPS23 levels were constrained, the transcriptional

capacity of THAP11 may be enhanced due to the consequent reduction in affinity between THAP11 and the ribosome. Interestingly, in unpublished work (presented by P. Espenshade at Keystone, 2014), it has been proposed that reducing the levels of RPS23 in fission yeast can inhibit the Sre1N transcriptional response, supporting the possibility that RPS23 is a regulator of THAP11 function. Singleton et al. demonstrated that RPS23 hydroxylation is complete in a range of cell lines suggesting that RPS23 may in fact be the restraining factor for other OGFOD1-dependent functions (Singleton et al., 2014). Under conditions in which RPS23 is restricted, OGFOD1 may have the capacity to exert greater regulation on THAP11 in a physiological setting. This model is also supported by the observation that overexpression of a catalytically inactive OGFOD1 mutant appears to be a more potent inhibitor of the THAP11 transcriptional programme (chapter 7: Figure 7.4). An important future line of inquiry therefore, is to establish the effect of RPS23 modulation on the THAP11 transcriptional programme.

Taken together, the work has highlighted complexities in the cell biology of OGFOD1. However, identification of THAP11 as a binding partner for OGFOD1 and the demonstration of a transcriptional interaction between OGFOD1 and THAP11 suggests that similarities to the Ofd1:Sre1N:Nro1 system exist in mammalian cells and provide a framework for future work.

Chapter 9: Materials and Methods

9.1 Reagents and Solutions

Chemical regents were obtained through Sigma-Aldrich unless otherwise specified. An index of general solutions used in this thesis, prepared as 1x stock solutions is indicated in Table 9.1.

Solution	Description
Luria-Bertani (LB) medium	25 g of LB powder was diluted in 1 L of MilliQ water prior to sterilisation.
LB Agar	15 g of agar was diluted in 1 L of LB medium and autoclaved. The solution was cooled to 50°C before addition of ampicillin (100 µg/ml); agar plates were then poured and allowed to set.
Phosphate buffered saline (PBS)	137 mM NaCl; 2.7 mM KCl; 4.3 mM $Na_2HPO_4.7H_2O$; 1.4 mM KH_2PO_4 at pH 7.3.
Tris buffered saline (TBS)	20 mM Tris; 150 mM NaCl at pH 7.6.
Immunoblot Tris-Glycine SDS-PAGE running buffer	25 mM Tris base, 190 mM Glycine, 0.1% (w/v) SDS.
Immunoblot Transfer buffer	10 mM Tris base, 100 mM Glycine, 10 % (v/v) Methanol.
SDS-PAGE resolving gel buffer	375 mM Tris-HCl (pH 8.8), 0.1% SDS.
SDS-PAGE stacking gel buffer	125 mM Tris-HCl (pH 6.8), 0.1% SDS.
Polysome gradient buffer	110 mM potassium acetate, 20 mM magnesium acetate, 10 mM HEPES pH 7.6.
Ribosome lysis buffer (A1)	5% (w/v) sucrose, 20 mM Tris-HCl pH 8, 100 mM NaCl, 20 mM KCl, 10 mM $MgCl_2$, 6 mM 2-Mercaptoethanol, 1% Triton X-100, 1x protease inhibitor cocktail.
Ribosome sucrose cushion buffer (A2)	20 mM Tris-HCl pH 8, 100 mM NaCl, 20 mM KCl, 10 mM $MgCl_2$ 6 mM 2-Mercaptoethanol.
Ribosome resuspension buffer (C)	50 mM Tris pH 7.5, 5 mM $MgCl_2$, 25 mM KCl.

Table 9.1: Index of solutions used in this study.

9.2 Plasmids

A list of plasmids used in this study is indicated in Table 9.2.

Name	Application	Source	Derivatives
pRRL-IRES-EGFP	Lentiviral cDNA expression	K. Kranc, The University of Edinburgh	Untagged OGFOD1, *N*-terminal FLAG-tagged OGFOD1 and OGFOD1 mutants (F287A and D157A) were inserted into pRRL-IRES-EGFP via BamHI–SnaBI sites. OGFOD1 mutants were generated by Quikchange PCR-based mutagenesis (Agilent Technologies). From Dr. M. Cockman, University of Oxford.
pTRIBZ	Doxycycline-inducible lentiviral cDNA expression	T. Tenev, ICR, London	*N*-terminal FLAG-tagged OGFOD1 was inserted into pTRIBZ vector. From Dr. M. Cockman.
pZIP-shERWOOD UltramiR	Lentiviral shRNA	Transomic Technologies Inc.	pZIP vectors containing OGFOD1 shRNA targeting sequences “88”, “89”, and “90”.
pCMV-VSV-G and pCMV-dR8.91	Lentiviral production	Addgene	Envelope (pCMV-VSV-G) and packaging (pCMV-dR8.91) plasmids were used in conjunction with pRRL, pTRIBZ and pZIP vectors.
p3xFLAG CMV10	Constitutive cDNA expression	Sigma-Aldrich	Expression of 3xFLAG-OGFOD1 were obtained by inserting into NotI-BamHI sites of p3xFLAG CMV10. From Dr. M. Cockman.
PCDNA3	Constitutive cDNA expression	Invitrogen	Expression of full length RPS23 with an *N*-terminal FLAG-tag. Expression of full length THAP11 or THAP11 mutants (1-255; 1-220; 91-314; 1-91,103-314; 102-314; 132-314) with an *C*-terminal FLAG-tag. FLAG-THAP11 mutants were generated by PCR directed mutagenesis. From Dr. M. Cockman.

Table 9.2: List of plasmids used in this study.

Name	Application	Source	Derivatives
pCS2+	Constitutive cDNA expression	Addgene	Wild-type and Arg67Lys human RPS23 gene fragments (NCBI CCDS47241) with a *C*-terminal HA tag (Eurofins Genomics) were inserted into pCS2+ via BamHI-XbaI sites. Phe120Ile was introduced using Quickchange II Site Directed Mutagenesis kit (Agilent). From Dr. Alyson MacInnes, Academic Medical Centre, Amsterdam, the Netherlands.
pET, pGEX	Recombinant protein production in *E. coli*	Addgene	pET His-OGFOD1, pGEX GST-RPS23, or pGEX GST- THAP11 plasmids were obtained from Dr. Phebee Liu-Yia, University of Oxford.
pSpCas9(BB)-2A-GFP (wild-type: PX458) and (D10A mutant: PX461)	CRISPR-Cas9 human knockout cell lines	Addgene	OGFOD1 guide RNA sequences targeting exon 1 were annealed by heating to 95°C and then cooled to room temperature, and ligated into BbsI digested CRISPR-Cas9 plasmids.
pX335-puro (D10A mutant)	CRISPR-Cas9 mouse knockout cell lines	Addgene	OGFOD1 guide sequences targeting exon 2 were annealed by heating to 95°C and then cooled to room temperature, and ligated into BbsI digested CRISPR-Cas9 plasmids. From Dr. Ben Davies, Wellcome Trust Centre for Human Genetics, University of Oxford.

Table 9.2 (Continued): List of plasmids used in this study.

A list of OGFOD1 CRISPR targeting sequences together with their respective plasmids are highlighted in Table 9.3.

Plasmid	Targeted Exon	OGFOD1 guide Sequences (5'-3')	
PX458 (WT Cas9)	1	**F:** CACCGGAGTTTTCGGACGCTGTTA **R:** AAACTAACAGCGTCCGAAAACTCC	
PX461 (D10A Cas9)	1	**F:** CACCGGAGTTTTCGGACGCTGTTA **R:** AAACTAACAGCGTCCGAAAACTCC	**F:** CACCGTTTCCCACCCGGGCTGGGCC **R:** AAACGGCCCAGCCCGGGTGGGAAAC
pX335 (D10A Cas9)	2	**F:** CACCGCATCCAAAGCCAAGACTTCT **R:** AAACAGAAGTCTTGGCTTTGGATGC	**F:** CACCGAGTTTGGGATCACACAGTGA **R:** AAACTCACTGTGTGATCCCAAACTC

Table 9.3: OGFOD1 CRISPR guide sequences and plasmids.

9.3 Bacterial techniques

9.3.1 Transformation

Chemically competent DH5α *E. coli* (NEB) were thawed on ice and incubated with plasmid DNA (~500 ng) for 15 minutes prior to heat shock at 42°C for 30 seconds in a water bath. The bacterial suspension was incubated on ice for a further 5 minutes before inoculating onto LB agar plates or into LB medium (Table 9.1) supplemented with ampicillin for 16 hours at 37°C.

9.3.2 Plasmid DNA purification

Plasmid DNA was isolated using commercially available kits (Miniprep/Midiprep; Qiagen) in accordance with manufacturer's instructions. The purity and concentration of the retrieved plasmid was determined using a spectrophotometer (ND-1000; NanoDrop). Plasmid preparations with an absorbance ratio (determined by the values of 260 nm over 280 nm) of between 1.75-1.95 were of sufficient purity for experimental work.

9.4 Nucleic acid techniques

9.4.1 Restriction enzyme digestion

3 µg of plasmid DNA was digested with 10 units of the appropriate restriction enzyme and 1x reaction buffer (NEB) in a 30 µl reaction volume. Digestion was carried out at 37°C for 90 minutes.

9.4.2 Ligation

Ligation reactions were performed using the Quick Ligation Kit (NEB). Ligation mixtures containing a molar ratio of 5:1 insert to vector (30 ng of vector) were prepared in ligation

buffer and 1 µl of Quick ligase made up to a final volume of 20 µl with nuclease free water. The reaction mixture was incubated for 5 minutes at room temperature.

9.4.3 DNA sequencing

Plasmid sequence integrity was confirmed by the Sanger sequencing method (Source Bioscience). Plasmids were supplied at a concentration of 100 ng/µl and primers were supplied at 3.2 pmol/µl. The following primer was used for sequencing of OGFOD1 CRISPR-Cas9 plasmids: (5'-3') **F:** TTCCCATGATTCCTTCATATTTGCA.

9.4.4 Agarose gel electrophoresis

Agarose (2% w/v) gels were prepared in Tris-Borate-EDTA (TBE) buffer (89 mM Tris (pH 7.6), 89 mM boric acid and 2 mM EDTA) supplemented with ethidium bromide to a final concentration of 1 µg /ml. Samples were pre-mixed with loading dye (NEB) prior to horizontal electrophoresis; typically performed at 100 V for 30 minutes. Sizing of DNA fragments was by reference to a DNA ladder mix (100 bp/1 kb DNA ladder; NEB). Nucleic acid was visualised by UV transillumination (Chemi doc; Bio-Rad).

9.4.5 Genomic DNA extraction

For purification of genomic DNA, 1 x 10^6 cells were lysed in 400 µl DNA extraction buffer (100 mM EDTA (pH 8.0), 50 mM Tris-HCl (pH 8.0), 100 mM NaCl, 1% SDS) supplemented with proteinase K at a final concentration of 1 mg/ml and incubated overnight at 55°C. To facilitate precipitation, 160 µl of 5 M NaCl solution was added to the lysate with constant agitation for 2 minutes (Thermomixer; Eppendorf). Samples were microcentrifuged at maximum speed to pellet insoluble material and supernatant was transferred to a clean microfuge tube containing 300 µl of iso-propanol. After mixing, the samples were microfuged for 10 minutes at maximum speed to pellet the DNA. The DNA pellet was bathed in 75% ethanol before a final microfugation step (maximum speed; two minutes).

The supernatant was removed and the pellet was dried by heating in a 55°C heat block before resuspension in 50 µl of nuclease free water.

9.4.6 Polymerase chain reaction (PCR)

PCR was typically performed in 20 µl reaction volumes, containing 100 ng of DNA template, 10 pM of forward and reverse primers, 1.5 mM $MgCl_2$, 200 µM dNTPs and 1 U of Phusion polymerase in 1x reaction buffer (NEB). Amplification of DNA was performed using a Veriti Thermal Cycler (Thermo Scientific) and the following parameters: 30 seconds at 98°C for initial denaturation, 35 cycles of 98°C for 10 seconds, 65°C for 30 seconds, 72°C for 30 seconds per kb and final extension at 72°C for 10 minutes.

9.4.7 SURVEYOR mutation detection assay

The SURVEYOR mutation detection assay (Transgenomic) was used to test the efficiency of human OGFOD1 CRISPR targeting sequences (Table 9.3). This assay uses a mismatch-specific DNA endonuclease to identify mutations in heteroduplex DNA. 293T cells were transfected with 2 µg of OGFOD1 CRISPR-Cas9 constructs by cationic polymer transfection (as described in 9.5.2). Genomic DNA was extracted 48 hours post transfection (as described in 9.4.5) and PCR amplified (as described in 9.4.6) from the region surrounding the CRISPR guide target site using primers as highlighted in Table 9.4. Two plasmids were supplied with the SURVEYOR mutation assay that differed by a single base pair and served as the positive and negative controls when hybridised together. To detect a mutation in the test sample, the heterogenous DNA is hybridised to generate mismatches for SURVEYOR nuclease cleavage. To form heteroduplexes 450 ng of PCR product was heated to 95°C for 10 minutes and allowed to cool to 25°C using a thermocycler (with samples held at intervals of 10°C for 1 minute). The hybridized DNA is then subject to SURVEYOR nuclease treatment: 450 ng of hybridized DNA is mixed with $MgCl_2$ (0.15M), SURVEYOR Enhancer (1 µl) and SURVEYOR

nuclease (1 µl) to a total volume of 16 µl. The mixture was incubated at 42°C for 60 minutes after which 1.6 µl of Stop Solution was added. Samples were mixed with DNA loading dye and subject to agarose gel electrophoresis as described in 9.4.4. This assay is referred to in Appendix 1: Validation of OGFOD1 CRISPR guide sequences by SURVEYOR Mutation detection assay.

	Sequences (5'-3')
OGFOD1 CRISPR site	**F:** CGCCTTCTCTTACTTTGGTGCTT **R:** TCCATTTCTCCCTCTTCTCACGT

Table 9.4 Oligonucleotide primers used for PCR of OGFOD1 CRISPR target site in SURVEYOR mutation detection assay.

9.4.8 RNA extraction using TRIzol

Unless otherwise stated, total RNA was purified from cells using TRIzol reagent (Life Technologies) in accordance with the manufacturer's instructions. RNA extractions were typically performed in 6-well plate format; ~1 x 10^6 cells harvested in 1 ml of TRIzol. RNA was separated into the aqueous phase by addition of 200 µl of chloroform. 1 µl of glycogen (25 mg/ml) was added to aid pellet visualisation and the RNA was precipitated using isopropanol and 75% ethanol. RNA concentration and purity was determined using a spectrophotometer (ND-1000; NanoDrop). RNA preparations with an absorbance ratio (determined by the values of 260 nm over 280 nm) of between 1.8-2.1 were of sufficient purity for experimental work.

9.4.9 RNA extraction for microarray using mirVana isolation kit

Total RNA for the ES cell microarray (n=12 samples; wild-type Vs OGFOD1 knockout, ± siTHAP11, independent triplicates) was purified using a commercially available miRNA isolation kit (MirVana; Life Technologies) according to the manufacturer's protocol. The kit employs an organic extraction using acid-phenol: chloroform followed by immobilization of RNA on glass-fibre filters to purify total RNA. RNA purity and concentration were rigorously

determined using UV spectrophotometric (Nanodrop) and fluorometric devices (Qubit 2.0; Life Technologies). RNA from each sample (400 µg) was submitted to Oxford Genomics Core (Wellcome Trust Centre for Human Genetics) whereupon additional quality checks using a chip-based capillary instrument (Bioanalyzer 2100; Agilent) were performed. All RNA samples gave an RNA integrity number (RIN) of over 9.7 which is indicative of pure and intact RNA.

9.4.10 Reverse transcription

First-strand complementary DNA (cDNA) was prepared from TRIzol-extracted RNA using the High Capacity cDNA Reverse Transcription kit (Applied Biosystems). Reverse transcription (RT) was performed in 20 µl reaction volumes, with 1 µg RNA as input and supplemented with the proprietary master mix containing RT buffer, RT random primers, dNTP mix, RNase inhibitor and reverse transcriptase. A brief incubation step of 10 minutes at 25°C was performed to enable priming through the length of the RNA. This preceded cDNA strand synthesis, which took place at 37°C for 120 minutes and was followed by a 5 minute heat inactivation step at 85°C.

9.4.11 Quantitative polymerase chain reaction (qPCR)

Quantitative real-time PCR assays employed TaqMan (Thermo Scientific) chemistry methods. Gene expression assays were performed as duplex PCR using validated probes with different reporter dyes. A typical 10 µl reaction mix comprised: 10 ng cDNA template, 0.5 µl FAM-probe (Gene of Interest), 0.5 µl VIC-probe (endogenous control: Cyclophilin A or β-actin) and 1x Gene Expression Master Mix. Each sample was analysed in triplicate and normalised to the endogenous control. A non-template control (no cDNA) was used as a negative control for each Taqman probe mix. qPCR was performed using a Step One Plus thermocycler (Applied Biosystems) and the conditions were as follows: 2 minutes at 50°C,

10 minutes at 95°C, 40 cycles of 95°C for 15 seconds, and 60°C for 1 minute. Expression was evaluated through quantification of mRNA using a comparative delta-delta cycle threshold (ΔΔCT) method (Livak et al., 2001). The Taqman probes used in this study are highlighted in Table 9.5.

Gene	Species	Probe	Product reference
OGFOD1	Human	FAM	Hs00250914_m1
THAP11	Human	FAM	Hs00740885_s1
LSMD1	Human	FAM	Hs00414732_g1
ALG14	Human	FAM	Hs00293655_m1
FBXL19	Human	FAM	Hs00703308_s1
OPHN1	Human	FAM	Hs00609994_m1
Cyclophilin A	Human	VIC	4326316E
Meg3	Mouse	FAM	Mm00522599_m1
Rian	Mouse	FAM	Mm01325842_g1
β-actin	Mouse	VIC	4352341E

Table 9.5 List of Taqman probes used in this study.

9.4.12 Chromatin immunoprecipitation (ChIP)- qPCR

SW620 cells (5 x 10^7 cells per condition) were cross-linked by addition of 1% formaldehyde to the cell media for 12 minutes on ice. To prevent excessive crosslinking, exogenous glycine (125 mM) was added for 5 minutes at room temperature, prior to cell harvest (by scraping) in ice cold PBS (Table 9.1), and recovery by centrifugation (1500 x g for 10 minutes 4°C). Cell pellets were resuspended in 1 ml SDS lysis buffer (1% SDS, 10 mM EDTA, 50 mM Tris-HCl (pH 8.1), 1x protease inhibitors) before 3 sonication cycles of 5 minutes (15 seconds on, 15 seconds off) in an ice-water bath (Bioruptor; Diagenode) to fragment the DNA. Cellular debris was removed by centrifugation (20,000 x g for 10 minutes 4°C) and the remaining supernatant split into equal fractions for THAP11 and control (normal rabbit IgG) immunoprecipitations after removal of the input (10%) fraction. Samples were incubated overnight with 5 µg of anti-THAP11 antibody (Genetex) or control (normal rabbit IgG) antibody at 4°C following addition of ChIP dilution buffer (0.01% SDS, 1.1% Triton X-100, 1.2 mM EDTA, 16.7 mM Tris-HCl (pH 8.1)) at a ratio of 1:10 supernatant lysate: ChIP dilution

buffer. Protein A agarose beads (90 µl per IP) were incubated on an end-over-end rotator for a further 2 hours at 4°C. Sequential bead washes (1 ml volume) followed agarose binding with: (i) Low salt buffer (0.1% SDS, 1% Triton X-100, 2 mM EDTA, 20 mM Tris-HCl (pH 8.1) 150 mM NaCl); (ii) High salt buffer (0.1% SDS 1% Triton X-100, 2 mM EDTA, 20 mM Tris-HCl (pH 8.1) 500 mM NaCl); (iii) Lithium buffer (0.25 M LiCl, 1% NP-40, 1% Sodium Deoxycholate, 1 mM EDTA, 10 mM Tris-HCl (pH 8.1) and (iv) TE buffer (10 mM Tris-HCl (pH 8.0), 1 mM EDTA). Following the final wash, DNA was recovered by addition of 500 µl heated elution buffer (1% SDS, 0.1 M $NaHCO_3$). Formaldehyde crosslinks from input and eluted immunoprecipitated DNA were reversed to aid DNA purification by incubating samples overnight on a heated (65°C) shaker with proteinase K (0.2 mg/ml). 1 µl of RNase A (10 mg/ml) was then added to the eluted bead mixture for 30 minutes at 37°C to remove RNA that could interfere in subsequent DNA purification steps. Beads were removed by centrifugation at 1000 x g for 3 minutes and DNA was purified by PCR purification kit (Qiagen) and eluted in 50 µl nuclease free water. ChIP-enriched DNA was analysed by PCR using a Step One Plus thermocycler (Applied Biosystems) using SYBR green master mix (Applied Biosystems) and primers (Table 9.6) flanking putative THAP11 binding sites (Parker et al., 2012). Thermocycling conditions were as follows: 95°C for 20 seconds followed by 40 cycles of 95°C for 3 seconds and 60°C for 30 seconds, and a melt-curve analysis performed at 95°C for 15 seconds, 60°C for 1 minute and heated at a rate of 0.3°C/second to 95°C for 15 seconds. Threshold cycle (CT) values of ChIP-enriched DNA were expressed as percent recovery relative to the input DNA analysed in parallel.

Gene	Sequences (5'-3')
LSMD1	**F:** CCCAACCTGAAAGGTGCTTA **R:** CGACTGCAACAGCCATTCT
ALG14	**F:** TTGTGACTGGGACCTCAGC **R:** GTCTTGGTGGGCTGGTCTT
FBXL19	**F:** CTTAAGAATGGCGGAACCAG **R:** AGACCGGGAGAGGCTAGGTA
PRAF2	**F:** CTGGTCCAGCCACATTAACC **R:** CCCAGAACAAAGTCGTCCAG
β-actin	**F:** AAACTGGAACGGTGAAGGTG **R:** TGGACTTGGGAGAGGACTGG

Table 9.6 Primers used for ChIP-qPCR.

9.4.13 Microarray

Mouse WG-6 v2.0 Expression BeadChip arrays (Illumina) were used for gene expression analysis of wild-type and CRISPR-Cas9-derived OGFOD1 knockout mouse embryonic stem (ES) cells. The BeadChip content encompassing 45,200 transcripts is derived from the National Center for Biotechnology Information Reference Sequence (NCBI RefSeq) database and, supplemented with probes from the Mouse Exonic Evidence Based Oligonucliotide (MEEBO) and protein-coding sequences described in the RIKEN FANTOM2 database. RNA samples were amplified and hybridised to two Mouse WG-6 v2.0 Expression BeadChip arrays (Oxford Genomics Core, Wellcome Trust Centre for Human Genetics). Microarray analysis was performed by Dr. Rafik Salama (University of Oxford) using R. Data were $\log_2$ transformed and normalised using cyclic loess to account for differences in signal intensity between the two arrays. The T-Statistic (normalised change accounting for differences in the replicate experiments) was used to measure the change in gene expression due to THAP11 knockdown in wild-type ES cells and compare it with the change observed in the OGFOD1 knockout ES cells.

9.5 Tissue culture techniques

9.5.1 Cell lines

Cell lines used in this study are as outlined in Table 9.7 and unless otherwise stated, were maintained in Dulbecco's Modified Eagle's Medium (DMEM) containing 4500 mg/L glucose supplemented with 10% foetal bovine serum (FBS), 2 mM L-glutamine, 50 IU/ml penicillin, 50 µg/ml streptomycin, to yield a 'complete' medium. Lymphocytes were maintained in RPMI medium supplemented with 10% heat inactivated foetal bovine serum (FBS), 2 mM L-glutamine, 50 IU/ml penicillin, 50 µg/ml streptomycin.

JM8.F6 embryonic stem (ES) cells use Murine Embryonic Fibroblasts (MEFs) as feeder layers. Mitotic inactivation of MEFs was performed using Mitomycin C treatment (carried out by B. Davies Group, Wellcome Trust Centre for Human Genetics, Oxford). ES cells were expanded on MEFs and maintained in Knockout DMEM; complete DMEM supplemented with 1 mM non-essential amino acids, 0.1 mM 2-Mercaptoethanol, 200 U/ml Leukaemia Inhibitory Factor (LIF). For THAP11 knockdown and microarray analysis, MEFs were omitted and ES cells were cultured on gelatinised (0.1% v/v) plates in Knockout DMEM supplemented with 2i reagents: MEK inhibitor: PD0325901 (1 µM), and GSK-3 inhibitor: CHIR99021 (3 µM). This media has been formulated to maintain ES cell pluripotency in the absence of a feeder layer. Separation of ES cells from MEFs was achieved through serial re-plating: MEFs displayed enhanced attachment rates that enabled removal of the less-adherent ES cells shortly after plating. Cells were cultured at 37°C in a humidified atmosphere containing 5% CO_2. Cells were passaged by washing with sterile PBS and dissociated using trypsin-EDTA solution. Cells counts were performed using a haemocytometer and Zeiss Primovert inverted microscope.

To induce expression of the transgene within doxycycline-regulable cell lines (T-REx FLAG-OGFOD1 and pTRIBZ FLAG-OGFOD1), cells were treated with doxycycline at a dosage of 1 µg/ml for the indicated period. For experiments requiring long-term treatment, doxycycline dosage was replenished every 3-4 days.

Cell line	Species	Description	Source	Derivatives
HEK293	Human	Embryonic kidney	ATCC	- OGFOD1 knockout (CRISPR) - OGFOD1 knockout re-expressing cells (FLAG-OGFOD1) - T-REx FLAG-OGFOD1
293T	Human	Embryonic kidney transformed with SV40 T-antigen.	ATCC	-
SW620	Human	Adenocarcinoma colon; derived from metastatic site: lymph node	ATCC	- OGFOD1 knockout (CRISPR) - OGFOD1 overexpressing cells (Untagged; FLAG-OGFOD1: WT, F287A, D157A)
HeLa	Human	Adenocarcinoma; cervix	ATCC	- OGFOD1 knockout (CRISPR)
U2OS	Human	Osteosarcoma; bone	ATCC	-
MDA -MB-231	Human	Adenocarcinoma; mammary gland/breast; derived from metastatic site: pleural effusion	ATCC	-
Healthy control Lymphocytes	Human	EBV-immortalization of peripheral mononuclear cells isolated from whole blood	A. MacInnes	-
RPS23 Arg67Lys Lymphocytes	Human	EBV-immortalization of peripheral mononuclear cells isolated from whole blood	A. MacInnes	-
JM8.F6	Mouse	C57BL/6N Mouse embryonic stem cells	B. Davies	- OGFOD1 knockout (CRISPR)
Murine embryonic fibroblasts (MEF)	Mouse	Embryonic fibroblasts generated from dissected embryos (E13.5)	B. Davies	-
OGFOD1$^{Fl/Fl}$ Murine embryonic fibroblasts (MEF)	Mouse	Embryonic fibroblasts generated from OGFOD1$^{Fl/Fl}$ dissected embryos (E14.5) and transformed with SV40 T-antigen	M. Cockman	- OGFOD1 knockout (Cre recombinase) - OGFOD1 knockout re-expressing cells (FLAG-OGFOD1)

Table 9.7 Parental human and mouse cell lines used in this study and their derivatives.

9.5.2 Plasmid transfection

Plasmid transfection used a commercial cationic polymer formulation (Turbofect; Thermo Fisher) in accordance with manufacturer's recommendations. For a typical experiment, sub-confluent cells (~2 x 10^6) were transfected with 4 µg of plasmid that was prepared as a cationic-DNA complex; 15 minute incubation of plasmid with 8 µl Turbofect in 400 µl of Opti-MEM (Thermo Scientific). Downstream analyses were performed up to 48 hours post transfection.

9.5.3 Generation of OGFOD1 CRISPR-Cas9 knockout cells

Human OGFOD1 CRISPR targeting sequences were designed at crispr.mit.edu targeting exon 1 and selected based on their on-target specificity. The SURVEYOR mutation detection assay (Transgenomic) was used to test the efficiency of the selected guides (Table 9.3; Section 9.4.7; Appendix I). For the generation of OGFOD1 human knockout sublines CRISPR-Cas9 plasmids (PX458 and PX461) bearing OGFOD1-directed guide RNAs were transfected into cells as described (Section 9.5.2). Transfected cells were enriched by fluorescence-activated cell sorting (FACS) for green fluorescent protein (GFP) – a selectable marker encoded on the CRISPR-Cas9 plasmids. The most highly fluorescent cell populations (top 20%) were collected (Dr. Andrew Worth; FACS manager, Jenner Institute, University of Oxford) and plated by serial dilution into 150 mm culture dishes at a concentration of 2000 cells/ml to 20 cells/ml. Macroscopically-visible individual clones were isolated approximately two weeks later using cloning cylinders, and expanded prior to screening by OGFOD1 immunoblotting (Section 9.6.2).

The generation of OGFOD1 knockout ES cells was performed by B. Davies Group (Wellcome Trust Centre for Human Genetics, Oxford). To derive OGFOD1 knockout ES cells, JM8F6 ES cells (1x10^6) were electroporated with 2.5 µg of pX335-OGFOD1 constructs (Table 9.3) using

the Neon transfection system (Life technologies) (3×1400 V, 10 ms). To select for transfected cells, a 48-hour pulse of puromycin selection (600 ng/ml) was applied 24 hours post-electroporation. Independent clones were isolated and screened by immunoblotting (Section 9.6.2).

9.5.4 Lentiviral production and creation of stable cell lines

Stable cell lines were derived by lentiviral mediated delivery of plasmids detailed in Table 9.2 For lentiviral production, 5 μg of lentiviral transfer vector (namely, pRRL, pTRIBZ, pZIP-shERWOOD UltramiR) was co-transfected with 1 μg of packaging plasmid (pCMV-dR8.91) and 5 μg glycoprotein envelope plasmid (pCMV-VSV-G) into $3x10^6$ 293T cells using Turbofect reagent (section 9.5.2). Media containing lentivirus was collected 72 hours post-transfection and syringe filtered (0.45 μm), to remove cellular debris. Target cell lines were transduced with viral supernatant diluted (1:3) in complete media containing 4 μg/ml polybrene to enhance transduction efficiency. After 24 hours, media was replenished with complete medium. Transductions were performed over 24 hours, after which time media was replenished and cells selected with antibiotic (pTRIBZ, blasticidin 10 μg/ml; pZIP-shERWOOD, puromycin 2 μg/ml) or FACS (pRRL; Section 9.5.3) and, where appropriate, subject to clonal isolation (Section 9.5.3).

pZIP-shERWOOD UltramiR vectors targeting OGFOD1 were purchased from Transomic Technologies Inc. and shRNA product information is presented in Table 9.8.

Target	Product reference	Reference in this thesis	Sequence
Non-targeting (Pool)	-	NT	TGCTGTTGACAGTGAGCGAAGGCAGAAGTATGCAAAGCAT TAGTGAAGCCACAGATGTAATGCTTTGCATACTTCTGCCTG TGCCTACTGCCTCGGA
OGFOD1	ULTRA-3439088	"88"	TGCTGTTGACAGTGAGCGAAGACAGAGAGACTCTGAAATA TAGTGAAGCCACAGATGTATATTTCAGAGTCTCTCTGTCTC TGCCTACTGCCTCGGA
OGFOD1	ULTRA-3439089	"89"	TGCTGTTGACAGTGAGCGCAGAAAAGTCACGTTTGTCTAA TAGTGAAGCCACAGATGTATTAGACAAACGTGACTTTTCTT TGCCTACTGCCTCGGA
OGFOD1	ULTRA-3439090	"90"	TGCTGTTGACAGTGAGCGAGATTACCAAGTTCAAATTCAA TAGTGAAGCCACAGATGTATTGAATTTGAACTTGGTAATCC TGCCTACTGCCTCGGA

Table 9.8 shRNA product information from Transomic Technologies Inc. used in this study, targeting sequences are underlined.

9.5.5 siRNA transfection

siRNA transfection was performed either using INTERFERin (Polyplus Transfection) or Lipofectamine RNAiMAX (Thermo Scientific) transfection reagents in accordance with the manufacturer's recommendations. For a typical experiment, sub-confluent cells (~1 x 10^6) were transfected by preparing two separate mixtures in which siRNAs were diluted in 150 µl Opti-MEM and ~9 µl transfection reagent was diluted in 150 µl Opti-MEM. The two mixtures were combined and incubated at room temperature for 5-10 minutes before addition of the siRNA and transfection reagent mix to the cells. Optimal protein knockdown of OGFOD1 and THAP11 was achieved using two transfections: forward (addition of siRNA and transfection reagent mix to the media of adherent cells) and reverse (addition of siRNA and transfection reagent mix to the media of cells whilst in suspension during re-plating); performed 24 hours apart. Cells were typically harvested 48 hours after the second transfection. siRNA product information is presented in Table 9.9.

Target	Species	Product reference	Supplier
Non-targeting (Pool)	-	D-001810-10-20	GE Healthcare
OGFOD1 (Pool)	Human	L-021197-01-0005	GE Healthcare
THAP11 (Pool)	Human	L-021450-01-0005	GE Healthcare
THAP11 (Pool)	Mouse	L-048713-01-0005	GE Healthcare

Table 9.9 siRNA product information used in this study.

9.5.6 Exposure of cells to test stimuli

Sodium arsenite: For induction of translational stress, cells were treated with sodium arsenite at a working concentration of 0.05 M to 1 M. For recovery experiments, arsenite was removed by gentle washing in pre-warmed media as described by Wehner et al., 2010.

Methyl methane sulfonate (MMS): For induction of DNA damage, cells were treated with the alkylating agent MMS. MMS solution (11.8 M) was serially-diluted in complete growth medium to a working concentration of 0.05 mM to 3 mM. Cell medium was aspirated and the MMS medium was applied to the cells at the indicated concentration and time.

Hypoxia: For ischemic stress, cells were subject to hypoxia and medium containing low glucose (1 g/L). Cells were placed in hypoxic chambers (In vivo$_2$ 400 Baker Ruskinn) set at 21%, 1% or 0.1% O_2, 5% CO_2 and 37°C. Standard incubators were used for the normoxic (21% O_2) controls.

9.5.7 Preparation of cell lysate

Urea lysis buffer: Where appropriate, whole cell lysates for SDS-PAGE immunoblotting were prepared with Urea lysis buffer (9 M urea, 75 mM Tris-HCl pH 7.5, 0.15 M 2-Mercaptoethanol). Cells were washed and sedimented (2000 rpm for 4 minutes) with ice-cold PBS prior to resuspension in Urea lysis buffer (typically 200 µl for a 60 -mm dish). To reduce viscosity (and shear genomic DNA), lysates were sonicated in an iced-water bath for 15 seconds (Bioruptor; Diagenode). Insoluble material was pelleted by microfugation

(13,000 rpm for 10 minutes) and clarified lysate supernatant was mixed with an equal volume of 2x sample buffer (3.3% SDS, 6 M urea, 17 mM Tris-HCl pH 7.5, 0.07 M 2-Mercaptoethanol, 0.01% bromophenol blue prior to SDS-PAGE electrophoresis (Section 9.6.2).

JIES' lysis buffer: Non-denaturing lysis immunoprecipitation, rate-zonal centrifugation in sucrose gradient and immunoblotting procedures using extracts prepared in JIES lysis buffer (100 mM NaCl, 20 mM Tris-HCl pH 7.4, 5 mM $MgCl_2$, 0.5% (v/v) NP40, Protease Inhibitors (HALT; Thermo Scientific). Briefly, cell monolayers were washed in ice-cold PBS, scraped in JIES lysis buffer (typically 300 µl per 60 -mm dish) and incubated at 4°C with agitation for 10 minutes. Crude lysate was clarified by microfugation (13,000 rpm for 10 min) and used accordingly. Samples for direct immunoblot were mixed with the appropriate volume of 6x SDS sample buffer (0.375 M Tris-HCl pH 6.8, 10% (w/v) SDS, 30% (v/v) glycerol, 0.6 M dithiothreitol (DTT), 0.05% (w/v) bromophenol blue) prior to heat denaturation (5 minutes at 95°C) and SDS-PAGE.

9.5.8 Cell proliferation assays

Cell viability was determined by MTS [3-(4,5-dimethylthiazol-2-yl)-5-(3-carboxymethoxyphenyl)-2-(4-sulfophenyl)-2H-tetrazolium) assay. MTS is reduced by metabolically active cells into a formazan product. The quantity of formazan product as measured by absorbance at 490 nm is directly proportional to the number of living cells in culture. Standardised conditions were applied to MTS assays that were performed in 96-well culture plates. Briefly, HEK293 cells were plated at 1.5 x 10^4 cells/well (in 100 µl) with a minimum of 4 replicates per cell line and/or condition. Replicate plates were prepared for interval timepoints that extended from Day 1 to Day 5 timepoints. The absorbance at 490 nm was recorded following 1 hour incubation at 37°C with 20 µl MTS reagent (CellTiter 96

Aqueous One; Promega) using a FLUOstar Omega plate reader (BMG Labtech). The mean absorbance was calculated from the replicates and subtracted from control (media alone) values.

9.5.9 Colony survival assays

Colony survival assays were performed as described by Franken et al., 2006. In brief, cells were plated into 6-well plates at 150 cells/well and stained with crystal violet solution (6% glutaraldehyde (v/v), 0.5% crystal violet (w/v) in water) approximately 10 days later. Cells were stained at room temperature for 30 minutes, washed with water and air-dried prior to visualisation.

9.5.10 Immunofluorescence

Where appropriate (e.g. for HEK293 cells), 8-well chamber slides (BD Falcon) were pre-coated with 5 µg/ml Poly-D-lysine to enhance attachment and prevent dissociation during procedural wash steps. Cells were seeded (1.5×10^4 cells per well) into chamber slides and allowed to attach overnight. Medium was aspirated and cells were washed twice with PBS prior to 30 minute fixation in 400 µl (per well) of paraformaldehyde (PFA) 4% (w/v) at room temperature. PFA was aspirated and slides were washed twice with PBS before permeabilisation with 0.5% (v/v) Triton-X 100 in PBS; 3 cycles of 5 minutes. To prevent non-specific antibody binding, blocking solution (0.5% (v/v) Triton-X 100, 1% (w/v) Bovine Serum Albumin in PBS) was applied in two 15 minute intervals. Antibody incubation was performed at the indicated dilution (Table 9.10) in blocking solution overnight. The following day, slides were washed twice in blocking solution and incubated for 1 hour with the appropriate species-specific fluorophore-conjugated antibody (Table 9.10). Following final wash steps in permeabilisation buffer (2 cycles) and additional PBS (2 cycles), slides were mounted with Vectashield containing DAPI (Vector Laboratories).

Antigen	Antibody	Dilution	Product reference	Source
OGFOD1	Rb pAb	1/250	HPA003215	Sigma-Aldrich
THAP11	Rb pAb	1/200	GTX119804	Genetex
RPS23	Ms mAb	1/200	Ab57644	Abcam
G3BP1	Ms mAb	1/250	611127	BD Transduction Laboratories
FLAG	Ms mAb	1/500	F1804	Sigma-Aldrich
Anti-Mouse Alexa-Fluor 488	Dk pAb	1/1000	A21202	Life Technologies
Anti-Rabbit Alexa-Fluor 488	Dk pAb	1/1000	A21206	Life Technologies
Anti-Rabbit Alexa-Fluor 555	Dk pAb	1/1000	A31572	Life Technologies

Table 9.10 Antibodies used for immunofluorescence in this study (Rb: Rabbit; Ms: Mouse; Dk: Donkey).

9.5.11 Proximity ligation assays (PLA)

For visualisation of protein interactions in situ, proximity ligation assays (Duolink; Sigma-Aldrich) were performed. Cell plating, fixation and permeabilization steps were as described in section 9.5.10. Blocking (30 minutes) and primary antibody incubations (overnight, 4°C) at specified concentration (Table 9.10) were performed in proprietary Duolink In Situ blocking solution. Primary antibody solution was aspirated and chamber partitions were removed. Reaction areas were defined with a grease pen before proceeding with the remaining Duolink In Situ protocol in accordance with manufacturer's recommendations. This method utilises species specific antibodies directed to components of the protein complex that are conjugated with a short DNA strand – the PLA probes ('minus' and 'plus'). When the PLA probes are in close proximity (<40 nm) the DNA strands interact and can be ligated together. Cells were gently washed in Duolink Wash Buffer A (2 cycles of 5 minutes) prior to application of species-specific antibody-conjugated PLA probes ('minus' and 'plus'). PLA Probe solution (100 µl) was diluted 1:5 with PLA antibody diluent, applied to defined areas and incubated at 37°C for 30 minutes. Cells were then washed twice in Duolink Wash Buffer

A for 5 minutes before addition of ligation solution (37°C, 30 minutes) and further washing (2 cycles of 2 minutes). The proprietary polymerase solution was added to the slides and incubated for 100 minutes at 37°C before the final wash procedure in 1x Duolink Wash Buffer B for (2 cycles, 10 minutes) and in 0.01x Duolink Wash Buffer B for 1 minute. Slides were mounted with a coverslip using Vectashield containing DAPI (Vector Laboratories).

9.5.12 Microscopy

Confocal immunofluorescence images were obtained using either a Zeiss LSM510 confocal microscope with LSM510 software, or Zeiss LSM710 confocal microscope with Zen software. Visualisation of DAPI was performed using a Violet Diode laser (405 nm), visualisation of Alexa-Fluor-488 conjugated antibodies was performed using a blue argon laser (488 nm), and visualisation of Alexa-Fluor-555 and PLA- conjugated antibodies was performed using a green laser (543 nm). Either 20x, 40x or 60x (oil) objectives were used and image analysis and processing were performed using LSM image viewer software.

9.5.13 Polysome profile analysis

Sucrose gradients were prepared in 5 ml SW 55 ultracentrifuge tubes (Beckman Coulter). In brief, 2.25 ml of 50% sucrose solution in 1x polysome gradient buffer (Table 9.1) was layered beneath an equivalent volume of 17% sucrose also diluted in 1x polysome gradient buffer. Tubes were sealed with Parafilm and positioned horizontally to facilitate sucrose diffusion. The following day, sucrose gradients were carefully upended and balanced to 0.01g with 17% sucrose solution.

Cells were washed in ice-cold PBS, harvested in polysome lysis buffer (300 µl per 60- mm dish; (100 mM potassium chloride**,** 10 mM magnesium chloride**,** 0.1% NP-40 in 1x polysome gradient buffer**.** 2 mM DTT and 40 U/mL RNase inhibitor was added on the day of use). The lysates were passed ten times though a 21-gauge needle and were incubated on ice for 10

minutes and insoluble material was pelleted by microfugation (13,000 rpm, 10 minutes). The concentration of RNA in the clarified lysate was determined by measuring the absorbance at 260 nm with a spectrophotometer (NanoDrop; Thermo Fisher). Samples were normalised and 1 ODU260 from each sample/condition was applied to the top of the sucrose gradient. Tubes were centrifuged at 55,000 rpm for 55 minutes at 4°C using an SW 55 Ti swinging bucket rotor in an L60 ultracentrifuge (Beckman Coulter). Resolved sucrose gradients were subject to polysome analysis using a Density Gradient Fractionation System (Teledyne Isco). A continuous UV absorbance (254 nm) profile was monitored as the gradient was displaced by injection of Fluorinert FC-40, dense chase solution.

9.6 Protein techniques

9.6.1 Production of custom antibodies used in this study

Generation of rabbit polyclonal RPS23 hydroxylation-specific antibodies: A custom antibody project was undertaken with Dundee Cell Products to obtain antibodies specific to both hydroxylated and non-hydroxylated forms of RPS23. Peptide immunogens were used that were specific to the hydroxylated and non-hydroxylated forms of RPS23 (Peptide sequence: VGVEAKQPNSAIRKC (non-hydroxylated); VGVEAKQP(OH)NSAIRKC (hydroxylated)). The peptides were synthesised as KLH (keyhole limpet haemocyanin) conjugates. To enhance specificity, cross-adsorption with reciprocal peptide was performed prior to affinity purification. Affinity purification was performed using antigenic peptide coupled to BSA.

Generation of a rabbit polyclonal OGFOD1 antibody: Full-length OGFOD1 protein was used as the immunogen and was provided in collaboration with the Department of Chemistry (C. Schofield Lab, University of Oxford). Immunization of OGFOD1 protein (2x 200 μg) and

affinity purification was performed as a service by Generon, and initial antibody specificity was carried out by dot blot analysis.

9.6.2 Immunoblotting

Denaturing polyacrylamide gel electrophoresis (PAGE) was performed using Mini-Protean apparatus (Bio-Rad). Resolving gels were prepared by mixing 30% acrylamide: bis-acrylamide (37.5:1) to the desired final concentration (typically: 7.5%, 10%, 15%) in SDS-PAGE resolving gel buffer (Table 9.1). The stacking layer comprised 3.9% acrylamide in SDS-PAGE stacking gel buffer (Table 9.1). Gel polymerisation was performed using ammonium persulphate (0.1% w/v) and Tetramethylethylenediamine (TEMED) (0.1% v/v). For some applications pre-cast 8-16% gradient gels (NuSep) were preferred. Gel electrophoresis of cell extracts diluted in SDS-sample buffer (Section 9.5.7) was performed at 20 mA/gel for ~1 hour in Tris-Glycine SDS-PAGE running buffer (Table 9.1). A pre-stained protein ladder (PageRuler Plus, Thermo Scientific) was used to determine the molecular weight of proteins resolved by SDS-PAGE. Proteins were electroblotted (100 V, 1 hour) in transfer buffer (Table 9.1) on to PDVF membrane by tank/wet transfer method (Mini Trans-Blot; BioRad). Membranes were incubated for 1 hour in blocking buffer (PBS-T (1x PBS (Table 9.1) containing 0.1% (v/v) Tween-20), supplemented with 5% (w/v) dried skimmed milk) to minimise non-specific antibody binding. Blocking buffer served as the diluent for primary and secondary antibody incubations. For detection of phosphorylated proteins, 1% (w/v) BSA served as the non-specific blocking agent in TBS-T diluent (1x TBS (Table 9.1), containing 0.1% (v/v) Tween-20.

Membranes were incubated with primary antibodies (see Table 9.11 for antibody information) overnight at 4°C. After extensive washing in PBS-T (3 cycles, 5 minute intervals), membranes were incubated with species-specific HRP-conjugated secondary antibodies (Dako) for 1 hour at room temperature. Following an identical wash regimen,

membranes were treated with Chemiluminsecent substrate (Supersignal West Dura or Femto; Thermo Scientific) and HRP activity was visualised using a Bio-Rad Chemi Doc MP imaging system. Protein loading equivalence was confirmed after chemiluminescent detection by staining membranes in 0.1% Coomassie Brilliant Blue, 50% methanol for 30 minutes prior to destain (50% methanol 10% glacial acetic acid) and drying.

Antigen	Antibody	Dilution	Product reference	Source
OGFOD1	Rb pAb	1/1000	HPA003215	Sigma-Aldrich
OGFOD1	Rb pAb	1/1000	In house (See section 9.6.1)	Generon
THAP11	Rb pAb	1/1000	12305	Cell Signalling
THAP11	Rb pAb	1/1000	GTX119804	Genetex
THAP11	Ms mAb	1/1000	562548	BD Pharmingen
RPS23	Ms mAb	1/1000	ab57644	Abcam
Hydroxylated RPS23	Rb pAB	1/250	In house - 15.1.4 (See section 9.6.1)	Dundee cell products
Non-hydroxylated RPS23	Rb pAB	1/500	In house - 14.1.6 (See section 9.6.1)	Dundee cell products
G3BP1	Ms mAB	1/1000	611127	BD Transduction Laboratories
RPL13a	Rb pAB	1/1000	2765	Cell signalling
HCF-1	Rb pAB	1/1000	A301-399A	Bethyl Laboratories
eIF-2α	Ms mAb	1/1000	2103	Cell signalling
P-eIF-2α	Rb pAB	1/1000	9721	Cell signalling
HA	Rt mAb	1/1000	11867423001	Sigma-Aldrich
FLAG-HRP	Ms mAb	1/1000	A8592	Sigma-Aldrich
β-actin-HRP	Ms mAb	1/25000	ab8226	Abcam
Anti-Mouse-HRP	Gt pAb	1/1000	P0447	Dako
Anti-Rabbit-HRP	Gt pAb	1/1000	P0448	Dako
Anti-Rat-HRP	Gt pAb	1/1000	P0450	Dako
Anti-Rabbit-True blot-HRP	Ms mAb	1/1000	18-8816-31	Rockland

Table 9.11 Antibodies used for immunoblotting in this study.

9.6.3 Rate zonal centrifugation of protein complexes in sucrose gradients

Sucrose gradients were prepared as previously described (section 9.5.13) with the following modifications: (i) Low density (10%) and high density (40%) sucrose (w/v) solutions were

diluted in 20 mM HEPES, 150 mM NaCl and 0.05% (v/v) Triton X-100; and (ii) large-scale gradients in 38.5 ml ultracentrifuge tubes were prepared; 17.5 ml of each layer. Preparative scale cultures (~5 x 10^7 cells) were lysed in 3 ml of JIES lysis buffer (section 9.5.7). Normalised input lysate was layered onto the sucrose gradients and centrifuged at 23,000 rpm for 18 hours at 4°C in an L60 ultracentrifuge using an SW 28 Ti swinging bucket rotor (Beckman Coulter). Fractions (1.4 ml) of resolved lysate were collected using a Density Gradient Fractionation System (Teledyne Isco), subject to methanol chloroform extraction (Section 9.6.4), prior to resuspension in 100 µl 6M urea (in 100 mM Tris-HCl pH7.8) and immunoblotting.

9.6.4 Methanol chloroform precipitation of proteins

Samples derived from rate zonal sedimentation experiments or preparative-scale immunoprecipitations were subject to methanol-chloroform precipitation. In brief, 600 µl of methanol was added to 200 µl of sample and mixed thoroughly by vortexing. Successive additions of chloroform (150 µl) and MilliQ water (450 µl) were performed with thorough mixing. After microcentrifugation (13,000 rpm for 5 minutes), the upper aqueous phase was removed and 450 µl of methanol was added the organic phase containing the protein precipitate. This mixture was vortexed and microfuged (13,000 rpm for 2 minutes) in order to sediment the protein pellet that was air-dried before resuspension in 6 M urea in 100 mM Tris-HCl pH 7.8.

9.7 Proteomic techniques

9.7.1 Immunoprecipitation

Immunoprecipitation for immunoblot: Antibodies were pre-bound to magnetic beads coated with anti-Rabbit IgG (Dynabeads M-280; Life Technologies) by rotation overnight at

4°C in JIES buffer; for 5 x 10^6 cells, 1 µg of antibody was pre-bound to 20 µl of Dynabead suspension. Cells were harvested in 1 ml JIES buffer (Section 9.5.7); ~10% lysate was retained for input and the remaining lysate was incubated overnight at 4°C with the antibody matrix on an end-over-end rotator. Beads were washed four times by magnetic separation in JIES buffer and eluted by boiling in SDS-PAGE sample buffer. For FLAG and HA immunoprecipitation, antibody-coupled agarose was used; 10 µl bed volume on equivalent cell volume. Four washes were performed by bead sedimentation in a microfuge (2,000 rpm for 1 min) prior to elution in SDS-PAGE sample buffer or, where appropriate, FLAG peptide (100 µg/ml). For immunoblotting of the immunoprecipitated lysates True-Blot antibodies (Table 9.11) were used following elution with SDS-PAGE sample buffer to prevent detection of heavy and light chains from the immunoprecipitating antibody.

Preparative scale immunoprecipitation for mass spectrometry: Preparative immunoprecipitations used magnetic separation as per IP/IB procedures but were typically performed on 5 x 10^7 cells. To minimise IgG contamination of pulldowns, THAP11 (Genetex) and OGFOD1 (Generon) antibodies were covalently coupled to M-270 epoxy resin (Dynabeads antibody coupling kit; Thermo Fisher) according to the manufacturer's recommendations and, where appropriate, commercial preparations of FLAG magnetic resin (Sigma) were used. Preparative immunoprecipitations used the following amount of antibody/resin: 8 µg THAP11; 14 µg OGFOD1; and 30 µl bed volume of FLAG resin. Immunoprecipitates were eluted at high pH with 0.5 M ammonium hydroxide, 0.5 mM EDTA and eluted material was subject to methanol-chloroform extraction (Section 9.6.4) prior to in-solution trypsinolysis (Section 9.7.2).

9.7.2 In-solution tryptic digestion

Samples (typically 50 µl volume) in 6 M Urea 100 mM Tris-HCl pH 7.8 were reduced by treatment with 5 mM DTT for 1 hour at room temperature. Reduced cysteines were

alkylated by addition of Iodoacetamide (200 mM, 60 minutes at room temperature) prior to 5-fold dilution in MilliQ water. Lyophilised Trypsin Singles (1 µg) were resuspended in 30 µl of 50 mM ammonium bicarbonate and digestion was performed overnight at 37°C. Purification and concentration of peptide samples was performed using C-18 spin columns (PepClean; Thermo Scientific) according to the manufacturer's protocol. Samples were dried by vacuum centrifugation (Concentrator plus; Eppendorf) and resuspended in 15 µl of Buffer A, containing 0.1% (v/v) formic acid and 2% (v/v) acetonitrile before transfer to conical bottomed glass vials (Waters) that were compatible with the mass spectrometry instrument.

9.7.3 Purification of ribosomal proteins

For quantification of RPS23 hydroxylation, ribosomal purification was performed on control and patient R67K lymphocytes. Approximately 2 x 10^8 cells were harvested in 10 ml of ribosome lysis buffer (A1) (Table 9.1) incubated at 4°C for 1 hour with end-over-end rotation. Lysate was clarified by microfugation (15,000 rpm for 30 minutes at 4°C) and the supernatant was passed through a 0.45 µM syringe filter before layering over a sucrose cushion of 25% (w/v) for isolation of > 80S ribosomes in ribosome sucrose cushion buffer (A2) (Table 9.1) in 38 ml ultracentrifuge tubes. Ribosomes were sedimented by ultracentrifugation at 28,000 rpm for 3 hours at 4°C in an L60 ultracentrifuge with SW-28 swinging bucket rotor (Beckman Coulter). The sedimented pellet was resuspended in 1 ml of ribosome resuspension buffer C (Table 9.1). Proteins were precipitated upon addition of 5 µl of 1M magnesium chloride and 700 µl ethanol and sedimented by microfugation (14,000 rpm for 2 minutes). Pellets were resuspended in 250 µl ribosome resuspension buffer C and contaminating rRNA was precipitated by addition of 25 µl 1 M magnesium chloride and 550 µl glacial acetic acid with end-over-end rotation for 1 hour at 4°C. Following removal of the rRNA, proteins in the clarified supernatant (microfugation; 14,000 rpm for 10 minutes) were

precipitated by incubation with 4 volumes of ice cold acetone at -20°C for 16 hours and sedimented by microfugation (14,000 rpm for 10 minutes). Pellets were lyophilised by vacuum centrifugation (Concentrator plus; Eppendorf) and resuspended in 300 µl of HPLC sample buffer (2% acetic acid, 10% acetonitrile). RPS23 was isolated by reverse phase HPLC using a mobile phase of buffer A (0.1% trifluoroacetic acid in water) and buffer B (0.08% trifluoroacetic acid in acetonitrile) on an Agilent 1200 system with C4 column (Vydac 214TP 250 x 4.6 mm, particle size 5 µM; Grace). Flow rate was 1 ml/minute with the following gradient: 0.01 min-10% B; 10 min-10% B; 25 min-20% B; 180 min-43% B; 185 min-95% B. Protein absorbance was measured at 214 nm. Fractions collected between 90 and 120 minutes (RPS23 elution window) were lyophilised by vacuum centrifugation, resuspended in 6 M Urea, 100 mM Tris-HCl pH 7.8, and immunoblotted for RPS23. Specific RPS23 fraction(s) were resolved by SDS-PAGE and corresponding gel slices, visualised by Coomassie stain (Imperial protein Stain; Thermo Scientific), were excised and subject to in-gel trypsinolysis (Section 9.7.4).

9.7.4 In-gel tryptic digestion

Excised gel fragments were washed extensively in 50% methanol, 5% acetic acid on an end-over-end rotator (4°C, overnight). Gel pieces were dehydrated by addition of 200 µl acetonitrile (5 minutes, room temperature) and rehydrated in buffer containing DTT for cysteine reduction (50 µl of 10 mM DTT, 100 mM ammonium bicarbonate; 1 hour at room temperature). Cysteine alkylation was achieved by addition of iodoacetamide (50 µl of 50 mM iodoacetamide in 100 mM ammonium bicarbonate) over 60 minutes, with gentle agitation at room temperature. Gel pieces were “washed” by successive rounds of dehydration (200 µl acetonitrile, 5 minutes), rehydration (200 µl of 100 mM ammonium bicarbonate, 5 minutes and dehydration (as previously described). Lyophilised Trypsin Singles (1 µg) were resuspended in 30 µl of 50 mM ammonium bicarbonate and added to

dehydrated gel pieces and incubated overnight at 37°C. Soluble tryptic peptides were recovered from the gel matrix by 10 minute additions of: (i) 50 µl of 50 mM ammonium bicarbonate; (ii) 50 µl of extraction buffer I (50% acetonitrile, 5% formic acid); and (ii) and 50 µl of extraction buffer II (85% acetonitrile, 5% formic acid). Eluates were pooled, lyophilised by vacuum centrifugation and resuspended in 15 µl of buffer containing 0.1% (v/v) formic acid and 2% (v/v) acetonitrile.

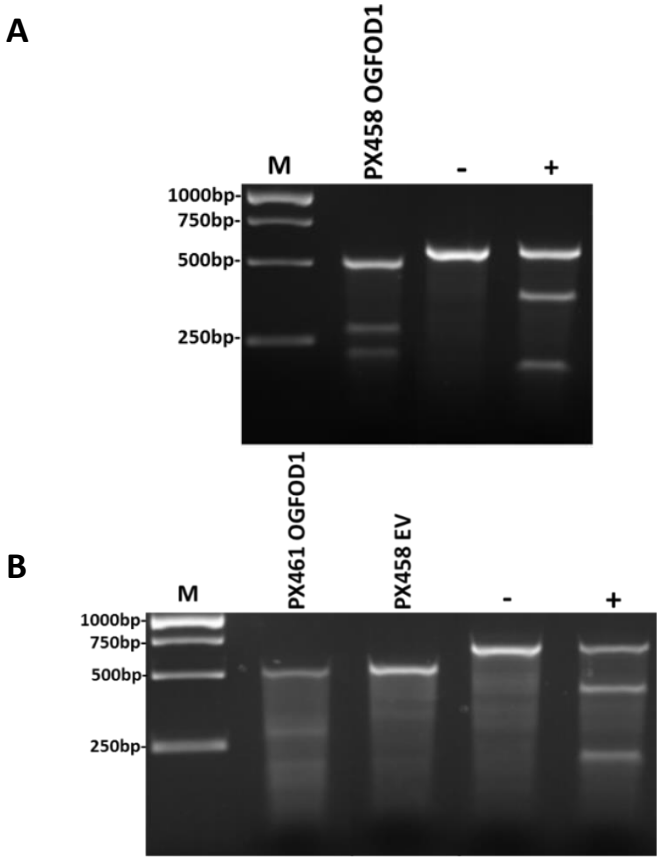
9.7.5 LC-MS/MS

LC-MS/MS of patient samples used a Dionex Ultimate 3000 nanoLC Orbitrap Fusion Lumos mass spectrometer (MS laboratory, Target Discovery Institute, University of Oxford) using standardised MS acquisition parameters. Data processing was performed with PEAKS 7 software (Bioinformatics Solutions) with the following parameters: full tryptic specificity with two missed cleavages; mass tolerance set at 5ppm for precursor and 0.5Da for product ions; cysteine carbamidomethylation as a fixed modification; methionine oxidation, hydroxylation, deamidation (Asn/Gln) and Pyro-glu (Gln) were specified as variable modifications; and a maximum of 3 PTMs per peptide. Data files were searched against the human Uniprot database supplemented with the RPS23 Arg67Lys protein sequence. Peptide assignments were filtered to a false discovery rate (FDR) of <1%. PEAKS searches assigned a number of modifications associated with sample handing to Pro-62 containing peptides, including: conversion of *N*-terminal Gln to pyro-Glu, deamidation of Gln/Asn and carbamylation and carbamidomethylation of Lys. Because detection of these artefactual modifications varied between samples, the most frequently detected peptide variants were aggregated to derive a robust quantitation (For summary of quantitated peptides and counts see chapter 4: Table 4.1). Relative peptide quantitation was performed using precursor ion signal intensity. Abundance measurements (peak area integrations of

extracted ion chromatograms) were obtained using the Genesis peak detection algorithm in Qual Browser (Xcalibur, Thermo Fisher).

For interactome studies, LC-MS was performed on a Dionex Ultimate 3000 nanoLC system coupled to a QExactive HF mass spectrometer (MS laboratory, Target Discovery Institute, University of Oxford) using standardised MS acquisition parameters. Data processing used PEAKS 8 software (Bioinformatics Solutions) with the following parameters: full tryptic specificity with two missed cleavages; mass tolerance set at 5ppm for precursor and 0.02Da for product ions; cysteine carbamidomethylation as a fixed modification; methionine oxidation, hydroxylation, acetylation, and deamidation were specified as variable modifications; and a maximum of 2 PTMs per peptide. Data files were searched against human Uniprot database (version February 2016) and peptide assignments were filtered to a false discovery rate (FDR) of <1%. Label-free protein level quantitation used the integrated Q module; at least 2 unique peptides were required (peptide feature thresholds: significance ≥ 20, quality ≥ 0.5) and sample normalisation was performed with reference to Total Ion Current (TIC).

Appendix 1: Validation of OGFOD1 CRISPR guide sequences by SURVEYOR Mutation detection assay



293T cells were transfected with 2 µg of OGFOD1 targeting CRISPR-Cas9 plasmids (chapter 9: Table 9.3) using Turbofect transfection reagent according to the manufacturers protocol (chapter 9: Section 9.5.2). DNA was extracted 48 hours after transfection (chapter 9: section 9.4.5) and PCR amplified (chapter 9: section 9.4.6) from the region surrounding the CRISPR guide target site. The SURVEYOR nuclease is an endonuclease that cleaves DNA at sites of base-substitution mismatch. The heterogenous DNA is hybridised to generate mismatches and then subject to SURVEYOR nuclease treatment (chapter 9: Section 9.4.7). Two plasmids were supplied with the SURVEYOR mutation assay that differed by a single base pair. Hybridisation of a single plasmid was used to yield homoduplex DNA (negative control, '-') and hybridisation of the two plasmids would generate mismatches that could be used to control for SURVEYOR nuclease activity (positive control, '+'). Agarose gel electrophoresis of the DNA indicates mutations have been introduced as nuclease cleavage has occurred in cells transfected with the wild-type CRISPR-Cas9 plasmid containing OGFOD1 guide RNA targeting sequences (**Figure A**: PX458 OGFOD1) relative to negative control (-). Similarly, nuclease cleavage is detected in cells transfected with D10A mutant CRISPR-Cas9 plasmids containing OGFOD1 guide RNA targeting sequences (**Figure B**: PX461 OGFOD1) relative to PX461 plasmid alone (PX461 EV) and the negative control (-). Sizing of DNA fragments was by reference to a 100 bp DNA ladder 'M'.

Appendix 2: Abbreviations

2-OG	2-oxoglutarate
BSA	Bovine serum albumin
cDNA	Complementary DNA
ChIP	Chromatin immunoprecipitation
CRISPR	Clustered Regularly Interspaced Short Palindromic Repeats
CTD	*C*-terminal domain
DAPI	4',6-diamidino-2-phenylindole
Dk	Donkey
DMEM	Dulbecco's Modified Eagle's Medium
DMOG	Dimethyloxalylglycine
DN	Double nickase
DNA	Deoxyribonucleic acid
Dox	Doxycycline
DSB	Double strand break
DTT	Dithiothreitol
EDTA	Ethylenediamine tetra-acetic acid
eIF2α	Eukaryotic translation Initiation Factor 2 alpha
ES cell	Embryonic stem cell
ETT1	Enhancer of translation termination 1
EV	Empty vector
FACS	Fluorescence activated cell sorting
FBS	Foetal bovine serum
FIH	Factor inhibiting HIF
g	Gravitational acceleration
G3BP1	Ras GTPase-activating protein-binding protein 1
GFP	Green fluorescent protein
GST	Glutathione S-transferase
HA	Haemagglutinin
HAP1	Heme-responsive zinc finger transcription factor 1
HCF-1	Host cell factor 1
HIF	Hypoxia inducible factor
His	Polyhistidine
HRE	Hypoxia response element
HRP	Horse-radish peroxidase
IB	Immunoblot
IgG	Immunoglobulin G
IP	Immunoprecipitation
IPTG	Isopropyl β-D-1-thiogalactopyranoside
IRES	Internal ribosome entry site
kDa	Kilodalton

KO	Knockout
LB	Luria-Bertani
LCLs	Lymphocytes
LC-MS/MS	Liquid chromatography coupled with tandem mass spectrometry
M	Molar
mAb	Monoclonal antibody
MEF	Mouse embryonic fibroblast
mM	Milimolar
MMS	Methyl methane sulfonate
mRNA	Messenger RNA
Ms	Mouse
MTS	3-(4,5-dimethylthiazol-2-yl)-5-(3-carboxymethoxyphenyl)-2-(4-sulfophenyl)-2H-tetrazolium
nM	Nanomolar
Nro1	Negative regulator of Ofd1
NT	Non-targeting
NTD	*N*-terminal domain
NTP	Non-targeting pool
Ofd1	2-oxoglutarate and Fe(II) dioxygenase 1
OGFOD1	2-oxoglutarate and iron-dependent oxygenase domain containing protein 1
pAb	Polyclonal antibody
PAGE	Polyacrylamide gel electrophoresis
PFA	Paraformaldehyde
PHD	Prolyl hydroxylase domain
PLA	Proximity ligation assay
qPCR	Quantitative polymerase chain reaction
Rb	Rabbit
RNA	Ribonucleic acid
RNAi	RNA interference
RNase	Ribonuclease
ROX	Ribosomal oxygenase
RP	Ribosomal protein
RPL13a	Large ribosomal subunit protein L13a
rpm	Revolutions per minute
RPMI	Roswell Park Memorial Institute
RPS23	Small ribosomal subunit protein S23
SDS	Sodium dodecyl sulfate
shRNA	short hairpin RNA
siRNA	short interfering RNA
Sre1N	Sterol regulatory element-binding protein 1 *N*-terminal region
SREBP	Sterol regulatory element-binding protein
Sud1	Sudestada1
Tet	Tetracycline
THAP11	Thanatos associated protein 11

TIC	Total ion current
TPA1	Termination and polyadenylation protein 1
T-REx	Tetracycline Regulated expression
tRNA	Transfer RNA
UV	Ultraviolet
WT	Wild-type

Appendix 3: Published Material

Nahuel A. Paolini, **Martin Attwood**, Samuel B. Sondalle, Carolina Marques dos Santos Vieira, Anita M. van Adrichem, Franca M. di Summa, Marie-Francoise O'Donohue, Pierre-Emmanuel Gleizes, Swaksha Rachuri, Joseph W. Briggs, Roman Fischer, Peter J. Ratcliffe, Marcin W. Wlodarski, Riekelt H. Houtkooper, Marieke von Lindern, Taco W. Kuijpers, Jonathan D. Dinman, Susan J. Baserga, Matthew E. Cockman, and Alyson W. MacInnes. (2017). A Ribosomopathy Reveals Decoding Defective Ribosomes Driving Human Dysmorphism. Am J Hum Genet *100*, 506-522.

Bibliography

Aik, W., McDonough, M.A., Thalhammer, A., Chowdhury, R., and Schofield, C.J. (2012). Role of the jelly-roll fold in substrate binding by 2-oxoglutarate oxygenases. Curr Opin Struct Biol *22*, 691-700.

Anderson, P., Kedersha, N., and Ivanov, P. (2015). Stress granules, P-bodies and cancer. Biochim Biophys Acta *1849*, 861-870.

Aulas, A., Fay, M.M., Lyons, S.M., Achorn, C.A., Kedersha, N., Anderson, P., and Ivanov, P. (2017). Stress-specific differences in assembly and composition of stress granules and related foci. J Cell Sci *130*, 927-937.

Auyeung, V.C., Ulitsky, I., McGeary, S.E., and Bartel, D.P. (2013). Beyond secondary structure: primary-sequence determinants license pri-miRNA hairpins for processing. Cell *152*, 844-858.

Ban, N., Beckmann, R., Cate, J., Dinman, J., Dragon, F., Ellis, R., Lafontaine, D., Lindahl, L., Liljas, A., Lipton, J., McAlear, M., Moore, P., Noller, H., Ortega, J., Panse, V., Ramakrishnan, V., Spahn, C., Steitz, T., Tchorzewski, M., Tollervey, D., Warren, A., Williamson, J., Wilson, D., Yonath, A., and Yusupov, M. (2014). A new system for naming ribosomal proteins. Curr Opin Struct Biol. 24: 165–169.

Bien, C.M., and Espenshade, P.J. (2010). Sterol regulatory element binding proteins in fungi: hypoxic transcription factors linked to pathogenesis. Eukaryot Cell *9*, 352-359.

Bishop, T., and Ratcliffe, P.J. (2014). Signaling hypoxia by hypoxia-inducible factor protein hydroxylases: a historical overview and future perspectives. Hypoxia (Auckl) *2*, 197-213.

Bordeleau, M.E., Matthews, J., Wojnar, J.M., Lindqvist, L., Novac, O., Jankowsky, E., Sonenberg, N., Northcote, P., Teesdale-Spittle, P., and Pelletier, J. (2005). Stimulation of mammalian translation initiation factor eIF4A activity by a small molecule inhibitor of eukaryotic translation. Proc Natl Acad Sci U S A *102*, 10460-10465.

Boukhettala, N., Claeyssens, S., Bensifi, M., Maurer, B., Abed, J., Lavoinne, A., Dechelotte, P., and Coeffier, M. (2012). Effects of essential amino acids or glutamine deprivation on intestinal permeability and protein synthesis in HCT-8 cells: involvement of GCN2 and mTOR pathways. Amino Acids *42*, 375-383.

Breker, M., and Schuldiner, M. (2014). The emergence of proteome-wide technologies: systematic analysis of proteins comes of age. Nat Rev Mol Cell Biol *15*, 453-464.

Brown, M.S., Ye, J., Rawson, R.B., and Goldstein, J.L. (2000). Regulated intramembrane proteolysis: a control mechanism conserved from bacteria to humans. Cell *100*, 391-398.

Bruick, R.K., and McKnight, S.L. (2001). A conserved family of prolyl-4-hydroxylases that modify HIF. Science *294*, 1337-1340.

Burma, S., Chen, B.P., Murphy, M., Kurimasa, A., and Chen, D.J. (2001). ATM phosphorylates histone H2AX in response to DNA double-strand breaks. J Biol Chem *276*, 42462-42467.

Campagnoli, M.F., Ramenghi, U., Armiraglio, M., Quarello, P., Garelli, E., Carando, A., Avondo, F., Pavesi, E., Fribourg, S., Gleizes, P.E.*, et al.* (2008). RPS19 mutations in patients with Diamond-Blackfan anemia. Hum Mutat *29*, 911-920.

Chan, D.A., Sutphin, P.D., Yen, S.E., and Giaccia, A.J. (2005). Coordinate regulation of the oxygen-dependent degradation domains of hypoxia-inducible factor 1 alpha. Mol Cell Biol *25*, 6415-6426.

Chaudhury, A., Chander, P., and Howe, P.H. (2010). Heterogeneous nuclear ribonucleoproteins (hnRNPs) in cellular processes: Focus on hnRNP E1's multifunctional regulatory roles. RNA *16*, 1449-1462.

Chavatte, L., Seit-Nebi, A., Dubovaya, V., and Favre, A. (2002). The invariant uridine of stop codons contacts the conserved NIKSR loop of human eRF1 in the ribosome. EMBO J *21*, 5302-5311.

Choi, S.M., Cho, H.J., Cho, H., Kim, K.H., Kim, J.B., and Park, H. (2008). Stra13/DEC1 and DEC2 inhibit sterol regulatory element binding protein-1c in a hypoxia-inducible factor-dependent mechanism. Nucleic Acids Res *36*, 6372-6385.

Choudhary, C., and Mann, M. (2010). Decoding signalling networks by mass spectrometry-based proteomics. Nat Rev Mol Cell Biol *11*, 427-439.

Chowdhury, R., Sekirnik, R., Brissett, N.C., Krojer, T., Ho, C.H., Ng, S.S., Clifton, I.J., Ge, W., Kershaw, N.J., Fox, G.C.*, et al.* (2014). Ribosomal oxygenases are structurally conserved from prokaryotes to humans. Nature *510*, 422-426.

Clifton, I.J., McDonough, M.A., Ehrismann, D., Kershaw, N.J., Granatino, N., and Schofield, C.J. (2006). Structural studies on 2-oxoglutarate oxygenases and related double-stranded beta-helix fold proteins. J Inorg Biochem *100*, 644-669.

Cukier, C.D., Maveyraud, L., Saurel, O., Guillet, V., Milon, A., and Gervais, V. (2016). The C-terminal region of the transcriptional regulator THAP11 forms a parallel coiled-coil domain involved in protein dimerization. J Struct Biol *194*, 337-346.

Dang, Y., Kedersha, N., Low, W.K., Romo, D., Gorospe, M., Kaufman, R., Anderson, P., and Liu, J.O. (2006). Eukaryotic initiation factor 2alpha-independent pathway of stress granule induction by the natural product pateamine A. J Biol Chem *281*, 32870-32878.

Dejosez, M., Krumenacker, J.S., Zitur, L.J., Passeri, M., Chu, L.F., Songyang, Z., Thomson, J.A., and Zwaka, T.P. (2008). Ronin is essential for embryogenesis and the pluripotency of mouse embryonic stem cells. Cell *133*, 1162-1174.

Dejosez, M., Levine, S.S., Frampton, G.M., Whyte, W.A., Stratton, S.A., Barton, M.C., Gunaratne, P.H., Young, R.A., and Zwaka, T.P. (2010). Ronin/Hcf-1 binds to a hyperconserved enhancer element and regulates genes involved in the growth of embryonic stem cells. Genes Dev *24*, 1479-1484.

Eilbracht, J., Reichenzeller, M., Hergt, M., Schnolzer, M., Heid, H., Stohr, M., Franke, W.W., and Schmidt-Zachmann, M.S. (2004). NO66, a highly conserved dual location protein in the nucleolus and in a special type of synchronously replicating chromatin. Mol Biol Cell *15*, 1816-1832.

Epstein, A.C., Gleadle, J.M., McNeill, L.A., Hewitson, K.S., O'Rourke, J., Mole, D.R., Mukherji, M., Metzen, E., Wilson, M.I., Dhanda, A.*, et al.* (2001). C. elegans EGL-9 and mammalian homologs define a family of dioxygenases that regulate HIF by prolyl hydroxylation. Cell *107*, 43-54.

Esquenet, M., Swinnen, J.V., Heyns, W., and Verhoeven, G. (1997). LNCaP prostatic adenocarcinoma cells derived from low and high passage numbers display divergent responses not only to androgens but also to retinoids. J Steroid Biochem Mol Biol *62*, 391-399.

Falnes, P.O., Johansen, R.F., and Seeberg, E. (2002). AlkB-mediated oxidative demethylation reverses DNA damage in Escherichia coli. Nature *419*, 178-182.

Fedorov, Y., Anderson, E.M., Birmingham, A., Reynolds, A., Karpilow, J., Robinson, K., Leake, D., Marshall, W.S., and Khvorova, A. (2006). Off-target effects by siRNA can induce toxic phenotype. RNA *12*, 1188-1196.

Feng, T., Yamamoto, A., Wilkins, S.E., Sokolova, E., Yates, L.A., Munzel, M., Singh, P., Hopkinson, R.J., Fischer, R., Cockman, M.E.*, et al.* (2014). Optimal translational termination requires C4 lysyl hydroxylation of eRF1. Mol Cell *53*, 645-654.

Franken, N.A., Rodermond, H.M., Stap, J., Haveman, J., and van Bree, C. (2006). Clonogenic assay of cells in vitro. Nat Protoc *1*, 2315-2319.

Fu, Y., Dai, Q., Zhang, W., Ren, J., Pan, T., and He, C. (2010). The AlkB domain of mammalian ABH8 catalyzes hydroxylation of 5-methoxycarbonylmethyluridine at the wobble position of tRNA. Angew Chem Int Ed Engl *49*, 8885-8888.

Ge, W., Wolf, A., Feng, T., Ho, C.H., Sekirnik, R., Zayer, A., Granatino, N., Cockman, M.E., Loenarz, C., Loik, N.D.*, et al.* (2012). Oxygenase-catalyzed ribosome hydroxylation occurs in prokaryotes and humans. Nat Chem Biol *8*, 960-962.

Gu, L., Gao, W., Yang, H.M., Wang, B.B., Wang, X.N., Xu, J., and Zhang, H. (2016). Control of Trx1 redox state modulates protection against methyl methanesulfonate-induced DNA damage via stabilization of p21. J Biochem *159*, 101-110.

Gu, Y.Z., Moran, S.M., Hogenesch, J.B., Wartman, L., and Bradfield, C.A. (1998). Molecular characterization and chromosomal localization of a third alpha-class hypoxia inducible factor subunit, HIF3alpha. Gene Expr *7*, 205-213.

Hanway, D., Chin, J.K., Xia, G., Oshiro, G., Winzeler, E.A., and Romesberg, F.E. (2002). Previously uncharacterized genes in the UV- and MMS-induced DNA damage response in yeast. Proc Natl Acad Sci U S A *99*, 10605-10610.

Harding, H.P., Zhang, Y., Zeng, H., Novoa, I., Lu, P.D., Calfon, M., Sadri, N., Yun, C., Popko, B., Paules, R.*, et al.* (2003). An integrated stress response regulates amino acid metabolism and resistance to oxidative stress. Mol Cell *11*, 619-633.

Helm, M. (2006). Post-transcriptional nucleotide modification and alternative folding of RNA. Nucleic Acids Res *34*, 721-733.

Henri, J., Rispal, D., Bayart, E., van Tilbeurgh, H., Seraphin, B., and Graille, M. (2010). Structural and functional insights into Saccharomyces cerevisiae Tpa1, a putative prolylhydroxylase influencing translation termination and transcription. J Biol Chem *285*, 30767-30778.

Hetz, C. (2012). The unfolded protein response: controlling cell fate decisions under ER stress and beyond. Nat Rev Mol Cell Biol *13*, 89-102.

Horita, S., Scotti, J.S., Thinnes, C., Mottaghi-Taromsari, Y.S., Thalhammer, A., Ge, W., Aik, W., Loenarz, C., Schofield, C.J., and McDonough, M.A. (2015). Structure of the ribosomal oxygenase OGFOD1 provides insights into the regio- and stereoselectivity of prolyl hydroxylases. Structure *23*, 639-652.

Hornung, V., Guenthner-Biller, M., Bourquin, C., Ablasser, A., Schlee, M., Uematsu, S., Noronha, A., Manoharan, M., Akira, S., de Fougerolles, A.*, et al.* (2005). Sequence-specific potent induction of IFN-alpha by short interfering RNA in plasmacytoid dendritic cells through TLR7. Nat Med *11*, 263-270.

Hughes, B.T., and Espenshade, P.J. (2008). Oxygen-regulated degradation of fission yeast SREBP by Ofd1, a prolyl hydroxylase family member. EMBO J *27*, 1491-1501.

Hutton, J.J., Tappel, A.L., and Udenfreind, S. (1967). Cofactor and substrate requirements of collagen proline hydroxylase. Arch Biochem Biophys *118*, 231-240.

Ingolia, N.T., Brar, G.A., Rouskin, S., McGeachy, A.M., and Weissman, J.S. (2012). The ribosome profiling strategy for monitoring translation in vivo by deep sequencing of ribosome-protected mRNA fragments. Nat Protoc *7*, 1534-1550.

Ivan, M., Kondo, K., Yang, H., Kim, W., Valiando, J., Ohh, M., Salic, A., Asara, J.M., Lane, W.S., and Kaelin, W.G., Jr. (2001). HIFalpha targeted for VHL-mediated destruction by proline hydroxylation: implications for O2 sensing. Science *292*, 464-468.

Jaakkola, P., Mole, D.R., Tian, Y.M., Wilson, M.I., Gielbert, J., Gaskell, S.J., von Kriegsheim, A., Hebestreit, H.F., Mukherji, M., Schofield, C.J.*, et al.* (2001). Targeting of HIF-alpha to the von Hippel-Lindau ubiquitylation complex by O2-regulated prolyl hydroxylation. Science *292*, 468-472.

Jackson, A.L., and Linsley, P.S. (2010). Recognizing and avoiding siRNA off-target effects for target identification and therapeutic application. Nat Rev Drug Discov *9*, 57-67.

Jackson, S.P., and Bartek, J. (2009). The DNA-damage response in human biology and disease. Nature *461*, 1071-1078.

Johansson, C., Tumber, A., Che, K., Cain, P., Nowak, R., Gileadi, C., and Oppermann, U. (2014). The roles of Jumonji-type oxygenases in human disease. Epigenomics *6*, 89-120.

Julien, E., and Herr, W. (2003). Proteolytic processing is necessary to separate and ensure proper cell growth and cytokinesis functions of HCF-1. EMBO J *22*, 2360-2369.

Katz, M.J., Acevedo, J.M., Loenarz, C., Galagovsky, D., Liu-Yi, P., Perez-Pepe, M., Thalhammer, A., Sekirnik, R., Ge, W., Melani, M.*, et al.* (2014). Sudestada1, a Drosophila ribosomal prolyl-hydroxylase required for mRNA translation, cell homeostasis, and organ growth. Proc Natl Acad Sci U S A *111*, 4025-4030.

Kedersha, N., Panas, M.D., Achorn, C.A., Lyons, S., Tisdale, S., Hickman, T., Thomas, M., Lieberman, J., McInerney, G.M., Ivanov, P.*, et al.* (2016). G3BP-Caprin1-USP10 complexes mediate stress granule condensation and associate with 40S subunits. J Cell Biol *212*, 845-860.

Keeling, K.M., Salas-Marco, J., Osherovich, L.Z., and Bedwell, D.M. (2006). Tpa1p is part of an mRNP complex that influences translation termination, mRNA deadenylation, and mRNA turnover in Saccharomyces cerevisiae. Mol Cell Biol *26*, 5237-5248.

Khatter, H., Myasnikov, A.G., Natchiar, S.K., and Klaholz, B.P. (2015). Structure of the human 80S ribosome. Nature *520*, 640-645.

Kim, H.S., Kim, H.L., Kim, K.H., Kim, D.J., Lee, S.J., Yoon, J.Y., Yoon, H.J., Lee, H.Y., Park, S.B., Kim, S.J.*, et al.* (2010). Crystal structure of Tpa1 from Saccharomyces cerevisiae, a component of the messenger ribonucleoprotein complex. Nucleic Acids Res *38*, 2099-2110.

Kim, J.H., Lee, S.M., Lee, J.H., Chun, S., Kang, B.H., Kwak, S., Roe, J.S., Kim, T.W., Kim, H., Kim, W.H.*, et al.* (2015). OGFOD1 is required for breast cancer cell proliferation and is associated with poor prognosis in breast cancer. Oncotarget *6*, 19528-19541.

Klose, R.J., Kallin, E.M., and Zhang, Y. (2006). JmjC-domain-containing proteins and histone demethylation. Nat Rev Genet *7*, 715-727.

Knott, S.R.V., Maceli, A., Erard, N., Chang, K., Marran, K., Zhou, X., Gordon, A., Demerdash, O.E., Wagenblast, E., Kim, S.*, et al.* (2014). A computational algorithm to predict shRNA potency. Mol Cell *56*, 796-807.

Kooistra, S.M., and Helin, K. (2012). Molecular mechanisms and potential functions of histone demethylases. Nat Rev Mol Cell Biol *13*, 297-311.

Krogan, N.J., Cagney, G., Yu, H., Zhong, G., Guo, X., Ignatchenko, A., Li, J., Pu, S., Datta, N., Tikuisis, A.P.*, et al.* (2006). Global landscape of protein complexes in the yeast Saccharomyces cerevisiae. Nature *440*, 637-643.

Kumar, R.M., Cahan, P., Shalek, A.K., Satija, R., DaleyKeyser, A., Li, H., Zhang, J., Pardee, K., Gennert, D., Trombetta, J.J.*, et al.* (2014). Deconstructing transcriptional heterogeneity in pluripotent stem cells. Nature *516*, 56-61.

Kustatscher, G., Hegarat, N., Wills, K.L., Furlan, C., Bukowski-Wills, J.C., Hochegger, H., and Rappsilber, J. (2014). Proteomics of a fuzzy organelle: interphase chromatin. EMBO J *33*, 648-664.

Lando, D., Peet, D.J., Gorman, J.J., Whelan, D.A., Whitelaw, M.L., and Bruick, R.K. (2002). FIH-1 is an asparaginyl hydroxylase enzyme that regulates the transcriptional activity of hypoxia-inducible factor. Genes Dev *16*, 1466-1471.

Lee, A.S., Kranzusch, P.J., and Cate, J.H. (2015). eIF3 targets cell-proliferation messenger RNAs for translational activation or repression. Nature *522*, 111-114.

Lee, C.Y., Stewart, E.V., Hughes, B.T., and Espenshade, P.J. (2009). Oxygen-dependent binding of Nro1 to the prolyl hydroxylase Ofd1 regulates SREBP degradation in yeast. EMBO J *28*, 135-143.

Lee, C.Y., Yeh, T.L., Hughes, B.T., and Espenshade, P.J. (2011). Regulation of the Sre1 hypoxic transcription factor by oxygen-dependent control of DNA binding. Mol Cell *44*, 225-234.

Lian, W.X., Yin, R.H., Kong, X.Z., Zhang, T., Huang, X.H., Zheng, W.W., Yang, Y., Zhan, Y.Q., Xu, W.X., Yu, M.*, et al.* (2012). THAP11, a novel binding protein of PCBP1, negatively regulates CD44 alternative splicing and cell invasion in a human hepatoma cell line. FEBS Lett *586*, 1431-1438.

Livak, K.J., and Schmittgen, T.D. (2001). Analysis of relative gene expression data using real-time quantitative PCR and the 2(-Delta Delta C(T)) Method. Methods *25*, 402-408.

Loenarz, C., Coleman, M.L., Boleininger, A., Schierwater, B., Holland, P.W., Ratcliffe, P.J., and Schofield, C.J. (2011). The hypoxia-inducible transcription factor pathway regulates oxygen sensing in the simplest animal, Trichoplax adhaerens. EMBO Rep *12*, 63-70.

Loenarz, C., and Schofield, C.J. (2008). Expanding chemical biology of 2-oxoglutarate oxygenases. Nat Chem Biol *4*, 152-156.

Loenarz, C., and Schofield, C.J. (2011). Physiological and biochemical aspects of hydroxylations and demethylations catalyzed by human 2-oxoglutarate oxygenases. Trends Biochem Sci *36*, 7-18.

Loenarz, C., Sekirnik, R., Thalhammer, A., Ge, W., Spivakovsky, E., Mackeen, M.M., McDonough, M.A., Cockman, M.E., Kessler, B.M., Ratcliffe, P.J.*, et al.* (2014). Hydroxylation of the eukaryotic ribosomal decoding center affects translational accuracy. Proc Natl Acad Sci U S A *111*, 4019-4024.

Lu, L., Han, A.P., and Chen, J.J. (2001). Translation initiation control by heme-regulated eukaryotic initiation factor 2alpha kinase in erythroid cells under cytoplasmic stresses. Mol Cell Biol *21*, 7971-7980.

Lu, Y., Chang, Q., Zhang, Y., Beezhold, K., Rojanasakul, Y., Zhao, H., Castranova, V., Shi, X., and Chen, F. (2009). Lung cancer-associated JmjC domain protein mdig suppresses formation of tri-methyl lysine 9 of histone H3. Cell Cycle *8*, 2101-2109.

Lundin, C., North, M., Erixon, K., Walters, K., Jenssen, D., Goldman, A.S., and Helleday, T. (2005). Methyl methanesulfonate (MMS) produces heat-labile DNA damage but no detectable in vivo DNA double-strand breaks. Nucleic Acids Res *33*, 3799-3811.

Mahon, P.C., Hirota, K., and Semenza, G.L. (2001). FIH-1: a novel protein that interacts with HIF-1alpha and VHL to mediate repression of HIF-1 transcriptional activity. Genes Dev *15*, 2675-2686.

Markolovic, S., Wilkins, S.E., and Schofield, C.J. (2015). Protein Hydroxylation Catalyzed by 2-Oxoglutarate-dependent Oxygenases. J Biol Chem *290*, 20712-20722.

Masson, N., and Ratcliffe, P.J. (2014). Hypoxia signaling pathways in cancer metabolism: the importance of co-selecting interconnected physiological pathways. Cancer Metab *2*, 3.

Masson, N., Willam, C., Maxwell, P.H., Pugh, C.W., and Ratcliffe, P.J. (2001). Independent function of two destruction domains in hypoxia-inducible factor-alpha chains activated by prolyl hydroxylation. EMBO J *20*, 5197-5206.

Maxwell, P.H., Wiesener, M.S., Chang, G.W., Clifford, S.C., Vaux, E.C., Cockman, M.E., Wykoff, C.C., Pugh, C.W., Maher, E.R., and Ratcliffe, P.J. (1999). The tumour suppressor protein VHL targets hypoxia-inducible factors for oxygen-dependent proteolysis. Nature *399*, 271-275.

Mazars, R., Gonzalez-de-Peredo, A., Cayrol, C., Lavigne, A.C., Vogel, J.L., Ortega, N., Lacroix, C., Gautier, V., Huet, G., Ray, A.*, et al.* (2010). The THAP-zinc finger protein THAP1 associates with coactivator HCF-1 and O-GlcNAc transferase: a link between DYT6 and DYT3 dystonias. J Biol Chem *285*, 13364-13371.

McEwen, E., Kedersha, N., Song, B., Scheuner, D., Gilks, N., Han, A., Chen, J.J., Anderson, P., and Kaufman, R.J. (2005). Heme-regulated inhibitor kinase-mediated phosphorylation of eukaryotic translation initiation factor 2 inhibits translation, induces stress granule formation, and mediates survival upon arsenite exposure. J Biol Chem *280*, 16925-16933.

Michaud, J., Praz, V., James Faresse, N., Jnbaptiste, C.K., Tyagi, S., Schutz, F., and Herr, W. (2013). HCFC1 is a common component of active human CpG-island promoters and coincides with ZNF143, THAP11, YY1, and GABP transcription factor occupancy. Genome Res *23*, 907-916.

Minguez, P., Parca, L., Diella, F., Mende, D.R., Kumar, R., Helmer-Citterich, M., Gavin, A.C., van Noort, V., and Bork, P. (2012). Deciphering a global network of functionally associated post-translational modifications. Mol Syst Biol *8*, 599.

Myllyharju, J., and Kivirikko, K.I. (2004). Collagens, modifying enzymes and their mutations in humans, flies and worms. Trends Genet *20*, 33-43.

Nakhoul, H., Ke, J., Zhou, X., Liao, W., Zeng, S.X., and Lu, H. (2014). Ribosomopathies: mechanisms of disease. Clin Med Insights Blood Disord *7*, 7-16.

Ngondo-Mbongo, R.P., Myslinski, E., Aster, J.C., and Carbon, P. (2013). Modulation of gene expression via overlapping binding sites exerted by ZNF143, Notch1 and THAP11. Nucleic Acids Res *41*, 4000-4014.

Noma, A., Ishitani, R., Kato, M., Nagao, A., Nureki, O., and Suzuki, T. (2010). Expanding role of the jumonji C domain as an RNA hydroxylase. J Biol Chem *285*, 34503-34507.

O'Driscoll, L., Gammell, P., McKiernan, E., Ryan, E., Jeppesen, P.B., Rani, S., and Clynes, M. (2006). Phenotypic and global gene expression profile changes between low passage and high passage MIN-6 cells. J Endocrinol *191*, 665-676.

O'Gorman, S., Fox, D.T., and Wahl, G.M. (1991). Recombinase-mediated gene activation and site-specific integration in mammalian cells. Science *251*, 1351-1355.

Olcina, M.M., Foskolou, I.P., Anbalagan, S., Senra, J.M., Pires, I.M., Jiang, Y., Ryan, A.J., and Hammond, E.M. (2013). Replication stress and chromatin context link ATM activation to a role in DNA replication. Mol Cell *52*, 758-766.

Pakos-Zebrucka, K., Koryga, I., Mnich, K., Ljujic, M., Samali, A., and Gorman, A.M. (2016). The integrated stress response. EMBO Rep *17*, 1374-1395.

Paolini, N.A., Attwood, M., Sondalle, S.B., Vieira, C.M., van Adrichem, A.M., di Summa, F.M., O'Donohue, M.F., Gleizes, P.E., Rachuri, S., Briggs, J.W*., et al.* (2017). A Ribosomopathy Reveals Decoding Defective Ribosomes Driving Human Dysmorphism. Am J Hum Genet *100*, 506-522.

Paquet, D., Kwart, D., Chen, A., Sproul, A., Jacob, S., Teo, S., Olsen, K.M., Gregg, A., Noggle, S., and Tessier-Lavigne, M. (2016). Efficient introduction of specific homozygous and heterozygous mutations using CRISPR/Cas9. Nature *533*, 125-129.

Parker, J.B., Palchaudhuri, S., Yin, H., Wei, J., and Chakravarti, D. (2012). A transcriptional regulatory role of the THAP11-HCF-1 complex in colon cancer cell function. Mol Cell Biol *32*, 1654-1670.

Parker, J.B., Yin, H., Vinckevicius, A., and Chakravarti, D. (2014). Host cell factor-1 recruitment to E2F-bound and cell-cycle-control genes is mediated by THAP11 and ZNF143. Cell Rep *9*, 967-982.

Pirkmajer, S., and Chibalin, A.V. (2011). Serum starvation: caveat emptor. Am J Physiol Cell Physiol *301*, C272-279.

Ploumakis, A., and Coleman, M.L. (2015). OH, the Places You'll Go! Hydroxylation, Gene Expression, and Cancer. Mol Cell *58*, 729-741.

Porter, J.R., Lee, C.Y., Espenshade, P.J., and Iglesias, P.A. (2012). Regulation of SREBP during hypoxia requires Ofd1-mediated control of both DNA binding and degradation. Mol Biol Cell *23*, 3764-3774.

Ran, F.A., Hsu, P.D., Lin, C.Y., Gootenberg, J.S., Konermann, S., Trevino, A.E., Scott, D.A., Inoue, A., Matoba, S., Zhang, Y.*, et al.* (2013). Double nicking by RNA-guided CRISPR Cas9 for enhanced genome editing specificity. Cell *154*, 1380-1389.

Rozpedek, W., Pytel, D., Mucha, B., Leszczynska, H., Diehl, J.A., and Majsterek, I. (2016). The Role of the PERK/eIF2alpha/ATF4/CHOP Signaling Pathway in Tumor Progression During Endoplasmic Reticulum Stress. Curr Mol Med *16*, 533-544.

Saito, K., Adachi, N., Koyama, H., and Matsushita, M. (2010). OGFOD1, a member of the 2-oxoglutarate and iron dependent dioxygenase family, functions in ischemic signaling. FEBS Lett *584*, 3340-3347.

Schofield, C.J., and Ratcliffe, P.J. (2004). Oxygen sensing by HIF hydroxylases. Nat Rev Mol Cell Biol *5*, 343-354.

Scotti, J.S., Leung, I.K., Ge, W., Bentley, M.A., Paps, J., Kramer, H.B., Lee, J., Aik, W., Choi, H., Paulsen, S.M.*, et al.* (2014). Human oxygen sensing may have origins in prokaryotic elongation factor Tu prolyl-hydroxylation. Proc Natl Acad Sci U S A *111*, 13331-13336.

Sedgwick, B., Bates, P.A., Paik, J., Jacobs, S.C., and Lindahl, T. (2007). Repair of alkylated DNA: recent advances. DNA Repair (Amst) *6*, 429-442.

Seo, Y.K., Chong, H.K., Infante, A.M., Im, S.S., Xie, X., and Osborne, T.F. (2009). Genome-wide analysis of SREBP-1 binding in mouse liver chromatin reveals a preference for promoter proximal binding to a new motif. Proc Natl Acad Sci U S A *106*, 13765-13769.

Shanware, N.P., Bray, K., Eng, C.H., Wang, F., Follettie, M., Myers, J., Fantin, V.R., and Abraham, R.T. (2014). Glutamine deprivation stimulates mTOR-JNK-dependent chemokine secretion. Nat Commun *5*, 4900.

Sharma, D., Cukras, A.R., Rogers, E.J., Southworth, D.R., and Green, R. (2007). Mutational analysis of S12 protein and implications for the accuracy of decoding by the ribosome. J Mol Biol *374*, 1065-1076.

Shivange, G., Kodipelli, N., Monisha, M., and Anindya, R. (2014). A role for Saccharomyces cerevisiae Tpa1 protein in direct alkylation repair. J Biol Chem *289*, 35939-35952.

Shohet, R.V., and Garcia, J.A. (2007). Keeping the engine primed: HIF factors as key regulators of cardiac metabolism and angiogenesis during ischemia. J Mol Med (Berl) *85*, 1309-1315.

Singleton, R.S., Liu-Yi, P., Formenti, F., Ge, W., Sekirnik, R., Fischer, R., Adam, J., Pollard, P.J., Wolf, A., Thalhammer, A.*, et al.* (2014). OGFOD1 catalyzes prolyl hydroxylation of RPS23 and is involved in translation control and stress granule formation. Proc Natl Acad Sci U S A *111*, 4031-4036.

Sinha, K.M., Yasuda, H., Coombes, M.M., Dent, S.Y., and de Crombrugghe, B. (2010). Regulation of the osteoblast-specific transcription factor Osterix by NO66, a Jumonji family histone demethylase. EMBO J *29*, 68-79.

Son, J., Lyssiotis, C.A., Ying, H., Wang, X., Hua, S., Ligorio, M., Perera, R.M., Ferrone, C.R., Mullarky, E., Shyh-Chang, N.*, et al.* (2013). Glutamine supports pancreatic cancer growth through a KRAS-regulated metabolic pathway. Nature *496*, 101-105.

Song, H., Mugnier, P., Das, A.K., Webb, H.M., Evans, D.R., Tuite, M.F., Hemmings, B.A., and Barford, D. (2000). The crystal structure of human eukaryotic release factor eRF1--mechanism of stop codon recognition and peptidyl-tRNA hydrolysis. Cell *100*, 311-321.

Songe-Moller, L., van den Born, E., Leihne, V., Vagbo, C.B., Kristoffersen, T., Krokan, H.E., Kirpekar, F., Falnes, P.O., and Klungland, A. (2010). Mammalian ALKBH8 possesses tRNA methyltransferase activity required for the biogenesis of multiple wobble uridine modifications implicated in translational decoding. Mol Cell Biol *30*, 1814-1827.

Stadtfeld, M., Apostolou, E., Akutsu, H., Fukuda, A., Follett, P., Natesan, S., Kono, T., Shioda, T., and Hochedlinger, K. (2010). Aberrant silencing of imprinted genes on chromosome 12qF1 in mouse induced pluripotent stem cells. Nature *465*, 175-181.

Stark, H., Rodnina, M.V., Wieden, H.J., Zemlin, F., Wintermeyer, W., and van Heel, M. (2002). Ribosome interactions of aminoacyl-tRNA and elongation factor Tu in the codon-recognition complex. Nat Struct Biol *9*, 849-854.

Stewart, E.V., Nwosu, C.C., Tong, Z., Roguev, A., Cummins, T.D., Kim, D.U., Hayles, J., Park, H.O., Hoe, K.L., Powell, D.W.*, et al.* (2011). Yeast SREBP cleavage activation requires the Golgi Dsc E3 ligase complex. Mol Cell *42*, 160-171.

Stolze, I.P., Tian, Y.M., Appelhoff, R.J., Turley, H., Wykoff, C.C., Gleadle, J.M., and Ratcliffe, P.J. (2004). Genetic analysis of the role of the asparaginyl hydroxylase factor inhibiting hypoxia-inducible factor (FIH) in regulating hypoxia-inducible factor (HIF) transcriptional target genes [corrected]. J Biol Chem *279*, 42719-42725.

Suzuki, C., Takahashi, K., Hayama, S., Ishikawa, N., Kato, T., Ito, T., Tsuchiya, E., Nakamura, Y., and Daigo, Y. (2007). Identification of Myc-associated protein with JmjC domain as a novel therapeutic target oncogene for lung cancer. Mol Cancer Ther *6*, 542-551.

Taatjes, D.J. (2010). The human Mediator complex: a versatile, genome-wide regulator of transcription. Trends Biochem Sci *35*, 315-322.

Tian, H., McKnight, S.L., and Russell, D.W. (1997). Endothelial PAS domain protein 1 (EPAS1), a transcription factor selectively expressed in endothelial cells. Genes Dev *11*, 72-82.

Tian, Y.M., Yeoh, K.K., Lee, M.K., Eriksson, T., Kessler, B.M., Kramer, H.B., Edelmann, M.J., Willam, C., Pugh, C.W., Schofield, C.J.*, et al.* (2011). Differential sensitivity of hypoxia inducible factor hydroxylation sites to hypoxia and hydroxylase inhibitors. J Biol Chem *286*, 13041-13051.

Todd, B.L., Stewart, E.V., Burg, J.S., Hughes, A.L., and Espenshade, P.J. (2006). Sterol regulatory element binding protein is a principal regulator of anaerobic gene expression in fission yeast. Mol Cell Biol *26*, 2817-2831.

Trewick, S.C., Henshaw, T.F., Hausinger, R.P., Lindahl, T., and Sedgwick, B. (2002). Oxidative demethylation by Escherichia coli AlkB directly reverts DNA base damage. Nature *419*, 174-178.

Tsuneoka, M., Koda, Y., Soejima, M., Teye, K., and Kimura, H. (2002). A novel myc target gene, mina53, that is involved in cell proliferation. J Biol Chem *277*, 35450-35459.

van den Born, E., Vagbo, C.B., Songe-Moller, L., Leihne, V., Lien, G.F., Leszczynska, G., Malkiewicz, A., Krokan, H.E., Kirpekar, F., Klungland, A*., et al.* (2011). ALKBH8-mediated formation of a novel diastereomeric pair of wobble nucleosides in mammalian tRNA. Nat Commun *2*, 172.

van der Valk, J., Brunner, D., De Smet, K., Fex Svenningsen, A., Honegger, P., Knudsen, L.E., Lindl, T., Noraberg, J., Price, A., Scarino, M.L*., et al.* (2010). Optimization of chemically defined cell culture media--replacing fetal bovine serum in mammalian in vitro methods. Toxicol In Vitro *24*, 1053-1063.

Vinckevicius, A., Parker, J.B., and Chakravarti, D. (2015). Genomic Determinants of THAP11/ZNF143/HCFC1 Complex Recruitment to Chromatin. Mol Cell Biol *35*, 4135-4146.

Waas, W.F., Druzina, Z., Hanan, M., and Schimmel, P. (2007). Role of a tRNA base modification and its precursors in frameshifting in eukaryotes. J Biol Chem *282*, 26026-26034.

Wang, G.L., Jiang, B.H., Rue, E.A., and Semenza, G.L. (1995). Hypoxia-inducible factor 1 is a basic-helix-loop-helix-PAS heterodimer regulated by cellular O2 tension. Proc Natl Acad Sci U S A *92*, 5510-5514.

Wang, G.L., and Semenza, G.L. (1995). Purification and characterization of hypoxia-inducible factor 1. J Biol Chem *270*, 1230-1237.

Ward, I.M., and Chen, J. (2001). Histone H2AX is phosphorylated in an ATR-dependent manner in response to replicational stress. J Biol Chem *276*, 47759-47762.

Wehner, K.A., Schutz, S., and Sarnow, P. (2010). OGFOD1, a novel modulator of eukaryotic translation initiation factor 2alpha phosphorylation and the cellular response to stress. Mol Cell Biol *30*, 2006-2016.

Xie, X., Lu, J., Kulbokas, E.J., Golub, T.R., Mootha, V., Lindblad-Toh, K., Lander, E.S., and Kellis, M. (2005). Systematic discovery of regulatory motifs in human promoters and 3' UTRs by comparison of several mammals. Nature *434*, 338-345.

Yeh, T.L., Lee, C.Y., Amzel, L.M., Espenshade, P.J., and Bianchet, M.A. (2011). The hypoxic regulator of sterol synthesis nro1 is a nuclear import adaptor. Structure *19*, 503-514.

Zhang, T., Huang, X.H., Dong, L., Hu, D., Ge, C., Zhan, Y.Q., Xu, W.X., Yu, M., Li, W., Wang, X*., et al.* (2010). PCBP-1 regulates alternative splicing of the CD44 gene and inhibits invasion in human hepatoma cell line HepG2 cells. Mol Cancer *9*, 72.

Ziv, Y., Bielopolski, D., Galanty, Y., Lukas, C., Taya, Y., Schultz, D.C., Lukas, J., Bekker-Jensen, S., Bartek, J., and Shiloh, Y. (2006). Chromatin relaxation in response to DNA double-strand breaks is modulated by a novel ATM- and KAP-1 dependent pathway. Nat Cell Biol *8*, 870-876.

Acknowledgements

I would like to thank my supervisors Peter Ratcliffe and Matthew Cockman for conceiving a very interesting project and providing me with the opportunity to conduct this research. I would like to thank Peter who has provided insightful discussions and scientific critique that has helped to shape this project and provide direction, and Matthew who has given assiduous encouragement and provided immeasurable support both academically and in the lab. I would like to thank the Ludwig Institute for Cancer Research for funding this project and providing a community with an ethos of scientific rigour.

I would like to acknowledge Chris Pugh whose experience and scientific dedication provides an invaluable perspective. I would like to thank members of the lab, past and present, who have also provided me with advice, ideas, reagents and useful discussions including: but not limited to: Norma Masson, David Mole, James Platt, Rafik Salama, Peter Simpson, James Smythies, Min Sun, Ya-Min Tian, Atsushi Yammamoto, Tzu-Lan Yeh. I would also like to thank Catherine King for her support and empathy, especially over the last few months.

A special thank you to Ben Davies and his lab for teaching me the art of embryonic stem cell culture, and I am also grateful to Alyson MacInnes who I was fortunate to work with as part of a collaboration. I would also like to thank my College, St. Edmund Hall, for providing a sense of community outside of the lab, together with my College advisor, Paul Matthews, for introducing me to College life and for his scientific enthusiasm.

Finally, I would like to thank my parents and my brother, Simon, for providing relentless support throughout, and to Inhye, for always being there for me.